JOURNAL OF FLUID MECHANICS

THE UNIVERSITY
OF MICHIGAN
FEB 12 1960
ENGINEERING
LIBRARY

VOLUME 7 PART 1

JANUARY 1960

THE UNIVERSITY
OF MICHIGAN
FEB [illegible] 0
ENG[illegible]G

PUBLISHED BY

CAMBRIDGE UNIVERSITY PRESS

BENTLEY HOUSE, 200 EUSTON ROAD, LONDON, N.W.1
AMERICAN BRANCH: 32 EAST 57TH STREET, NEW YORK 22, N.Y.

Price 30*s.* (*U.S.A.* $5.00)

The JOURNAL OF FLUID MECHANICS exists for the publication of theoretical and experimental investigations of all aspects of the mechanics of fluids, and is issued in four parts per volume.

EDITOR

DR G. K. BATCHELOR

Department of Applied Mathematics and Theoretical Physics, University of Cambridge, Free School Lane, Cambridge, England

ASSISTANT EDITORS

DR T. B. BENJAMIN, DR I. PROUDMAN, DR P. G. SAFFMAN

Department of Applied Mathematics and Theoretical Physics, University of Cambridge, Free School Lane, Cambridge, England

ASSOCIATE EDITORS

PROF. G. F. CARRIER

Pierce Hall, Harvard University, Cambridge 38, *Massachusetts, U.S.A.*

DR W. C. GRIFFITH

Research and Development Laboratory, Missile Systems Division, Lockheed Aircraft Corporation, Palo Alto, California, U.S.A.

M. J. LIGHTHILL

Royal Aircraft Establishment, Farnborough, Hampshire, England

PROF. R. R. LONG

School of Engineering, The Johns Hopkins University, Baltimore 18, *Maryland, U.S.A.*

Authors wishing to have papers published in the JOURNAL should communicate them to any one of the persons named above, choosing one in their own country where possible.

Authors are urged to ensure that their papers are written clearly and attractively, in order that their work will be readily accessible to readers.

Manuscripts should be typed in double spacing on one side of the paper only, with references listed at the end in alphabetical order of authors. Drawings should be done on a large scale in Indian ink on tracing cloth or drawing paper, the lettering being shown clearly in pencil for reproduction by the printer; the list of captions should be typed at the end of the manuscript. Proofs of papers from overseas will usually be despatched to authors by airmail. There is no charge for publication. Authors are entitled to receive 50 offprints of a paper in the JOURNAL free of charge, and additional offprints can be purchased if ordered in advance.

SUBSCRIPTIONS

The subscription price for a volume of four parts is £5. 10*s*. net, post free, payable in advance; separate parts 30*s*. net, plus postage. Subscriptions may be sent to any bookseller, or to the Cambridge University Press, Bentley House, 200 Euston Road, London, N.W.1.

Subscribers in the United States should send their orders to the Cambridge University Press, American Branch, 32 East 57th Street, New York 22. The subscription price per volume is $18.50, post free, payable in advance; separate parts $5.00, plus postage.

On the flow past a quarter infinite plate using Oseen's equations

By K. STEWARTSON
Department of Mathematics, University of Durham, Durham

AND L. HOWARTH
Department of Mathematics, University of Bristol

(Received 29 April 1959)

This paper is concerned with the determination, on the basis of Oseen's equations, of the flow past a quarter-plane with its leading edge normal to, and its side edge parallel to, a uniform incident stream. The solution is completed, except for a region in the vicinity of the corner, correct to order $\nu^{\frac{1}{2}}$ for small kinematic viscosity ν.

Away from the vicinity of the side edge the flow will approximate to the two-dimensional flow past a semi-infinite plate. This two-dimensional flow can be built up successively, if we like to think in terms of boundary conditions at the plate rather than at the edge of the boundary layer, from the potential flow associated with the uniform stream, a shear layer introduced to remove the tangential slip and a potential flow to remove the normal velocity at the plate associated with the shear layer. In the vicinity of the plate the three together give the usual boundary-layer solution.

We start our solution from this same basis, namely, the potential flow associated with the uniform stream and the shear layer to restore the no-slip condition. As a first approximation, neglecting the effects of the edges, this will be the same as for the two-dimensional problem. The normal velocity introduced by this shear layer has to be compensated by a potential flow (see §4). This potential flow in turn (and here our problem diverges significantly from the two-dimensional problem) introduces tangential velocities with components parallel to both leading and side edges which require the introduction of a further shear layer. Over the main body of the plate this secondary shear layer is of a conventional form (§5) but requires special examination near the edges. In §6 it is shown how Carrier & Lewis's (1949) solution can be modified to give the flow near the leading edge away from the tip and in §7, the core of the paper, the flow near the side edge is determined.

In the vicinity of the side edge the extra potential flow has no component in the direction of that edge and so the solution given by Howarth (1950) for the corresponding unsteady problem is applicable. What emerges from the present calculations, however, is that Howarth's application of Rayleigh's analogy to give the excess skin friction is seriously incomplete. For, whilst this argument gives correctly the local increase of order ν in skin friction in the immediate vicinity of the side edge, it omits the widespread effects of the secondary shear layer. These are found to be of the same order in ν as the local effects.

The cross-flow in the side edge region has features of special interest. Its determination depends on a knowledge of the potential flow associated with the primary shear layer and so it depends, for instance, on the shape of the leading edge and is not, as appears to have been assumed up to now, determined completely by local conditions. This is further exemplified by the fact that it cannot be expressed in terms of what would be regarded as the natural boundary-layer variables but involves quite separately the distance from the leading edge.

1. Introduction

The Blasius solution for the flow past a semi-infinite flat plate has been shown to be capable of generalization to flat plates with curved leading edges provided that there are no discontinuities in the slopes of the leading edges. The flow in any plane parallel to the direction of the incident stream and containing a normal to the plate is then in fact the same as that given by the Blasius solution.

This generalization breaks down when a discontinuity of slope occurs in the leading edge for then the solution would imply discontinuities in velocity derivatives, and an extreme case is provided by a quarter infinite plate with its leading edge normal to, and its side edge parallel to, the incident stream. Though little has been published about this problem the interest it has created has been rather more perhaps than the actual problem would at first sight appear to warrant. This is because it raises problems of fundamental importance in the interplay between boundary layer and external flow and contributes to our knowledge of the role played by boundary-layer theory in obtaining solutions of the full equations of flow. One remark about the novelty of the problem is sufficient to convey the importance of it in boundary-layer theory. Calculations of the effect of the edge in increasing the skin frictional force on the plate are, as will be shown below for the Oseen equations, quite incomplete until one includes the effect of the boundary layer on the potential flow outside.

Although the essential ideas underlying the solution are simple some of the details are complicated, and all the present paper sets out to do is to attempt, on the basis of Oseen's linearization of the flow equations, to obtain as much as possible of the flow field correct to order $\nu^{\frac{1}{2}}$ for small kinematic viscosity ν. It is necessary to work to this order if the effect of the edge on the skin friction is to be estimated and it has been found possible to determine the whole of the field to this order apart from a small region near the corner. Of course with the Navier–Stokes equations as basis rather than the Oseen linearization of them the problem is more difficult, but the effects discussed here will have their counterpart there and that is the prime justification for the present paper. Some discussion of the differences to be expected with the exact equations is given at the end of the paper.

2. The Blasius problem

Some of the ideas for the present solution are contained in the two-dimensional problem of the flow past a semi-infinite plate, and as we shall require to make use of the solution of this problem anyway some discussion of it is a useful intro-

duction. The exact solution of the Oseen equations for this problem is known;* for small ν it comprises a potential flow together with a conventional boundary layer. With U as the speed of the incident stream, the origin at the leading edge, the x-axis parallel to the incident stream and the y-axis normal to the plate, Oseen's equations may be split into the forms

$$p = -\rho U \frac{\partial \phi}{\partial x}, \quad \mathbf{v} = \operatorname{grad} \phi + \mathbf{v}', \tag{2.1}$$

$$\nabla^2 \phi = 0, \tag{2.2}$$

$$U \frac{\partial \mathbf{v}'}{\partial x} = \nu \nabla^2 \mathbf{v}', \tag{2.3}$$

$$\operatorname{div} \mathbf{v}' = 0, \tag{2.4}$$

where $\mathbf{v} = (u, v)$ is the velocity of flow. At infinity we must have $u \to U$, $v \to 0$ and at the plate $u = v = 0$.

Looking at the solution from the boundary-layer point of view in the co-ordinates x, y, the first approximation for ϕ is Ux. This would be a complete solution with $\mathbf{v}' = 0$ except that the boundary condition $u = 0$ at the plate would be violated. We remove this difficulty by introducing a shear layer outside of which $\mathbf{v}' = (u_1', v_1')$ tends to zero and in which u_1' is determined by the approximate form

$$U \frac{\partial u_1'}{\partial x} = \nu \frac{\partial^2 u_1'}{\partial y^2} \tag{2.5}$$

of the first component of (2.3), and the condition $u_1' = -U$ at the plate. This gives

$$u_1' = -U \operatorname{erfc} \eta, \quad \text{where} \quad \eta = \frac{y}{2} \left(\frac{U}{\nu x} \right)^{\frac{1}{2}}, \tag{2.6}$$

and (2.4) then implies

$$v_1' = \int_y^\infty \frac{\partial u_1'}{\partial x} dy. \tag{2.7}$$

(It is worth noting that (2.7) satisfies the shear layer form

$$U \frac{\partial v_1'}{\partial x} = \nu \frac{\partial^2 v_1'}{\partial y^2}$$

of the second component of (2.3).)

Equation (2.7) gives a non-zero value for

$$[v_1']_0 = \int_0^\infty \frac{\partial u_1'}{\partial y} dy = -U \left(\frac{\nu}{U \pi x} \right)^{\frac{1}{2}} \operatorname{sgn} y \tag{2.8}$$

on the two sides of the plate, where suffix 0 refers to values at $y = 0$. This in turn means that the boundary condition $v = 0$ must be satisfied by writing

$$\phi = Ux + \phi_1, \tag{2.9}$$

where ϕ_1 is defined by $\nabla^2 \phi_1 = 0$ and

$$\frac{\partial \phi_1}{\partial y} = -[v_1']_0 = U \left(\frac{\nu}{U \pi x} \right)^{\frac{1}{2}} \operatorname{sgn} y$$

on the two sides of the plate.

* Carrier & Lewis (1949) were the first to obtain the skin friction and a formal solution of the flow field. Kaplun (1954) and others have shown that the solution takes on a relatively simple form in parabolic co-ordinates.

One might expect that the associated value $(\partial\phi_1/\partial x)_0$ would be $O(\nu^{\frac{1}{2}})$ and different from zero; if this were so it would lead to the necessity for another shear layer type solution to remove it. In fact $(\partial\phi_1/\partial x)_0$ turns out to be zero and shear layer and potential flow are completely matched by the forms $\phi = Ux + \phi_1$ and $\mathbf{v}'$.

Two further points are worth making. First of all the conventional boundary-layer solution is $u = u_1' + U$, $v = v_1' - [v_1']_0$, and so gives $v = 0$ at the plate and $v \neq 0$ at infinity as expected. (The term $-[v_1']_0$ arises from $\partial\phi_1/\partial y$ since *inside the shear layer* $\nabla^2\phi_1 = 0$ is approximated to by $\partial^2\phi_1/\partial y^2 = 0$ which in turn implies $\partial\phi_1/\partial y = (\partial\phi_1/\partial y)_0 = -[v_1']_0$.) The velocities inside the boundary layer are then determined correct to $O(\nu^{\frac{1}{2}})$ except possibly in the vicinity of the leading edge. Secondly, in that vicinity nothing short of the full equations (2.2)–(2.4) is useful; the analysis of Carrier & Lewis (1949) solves the problem completely and shows that the skin friction determined by the boundary-layer approximation is in fact exact.

3. The quarter-plate problem: general considerations

With the origin at the corner, the x-axis parallel to the stream, the z-axis along the leading edge and the y-axis perpendicular to the plate, Oseen's equations are equivalent to

$$p = -\rho U\frac{\partial\phi}{\partial x}, \quad \mathbf{v} = \operatorname{grad}\phi + \mathbf{v}', \tag{3.1}$$

$$\nabla^2\phi = 0, \tag{3.2}$$

$$U\frac{\partial\mathbf{v}'}{\partial x} = \nu\nabla^2\mathbf{v}', \tag{3.3}$$

$$\operatorname{div}\mathbf{v}' = 0. \tag{3.4}$$

For small ν we shall now have small exceptional regions near both leading and side edges, but elsewhere on the plate we must expect a conventional type shear layer in which $\partial/\partial y \gg \partial/\partial x$ and $\partial/\partial z$.

Thus we start as before by taking $\phi = Ux$ and then removing the tangential slip by a shear layer defined by

$$U\frac{\partial u_1'}{\partial x} = \nu\frac{\partial^2 u_1'}{\partial y^2}, \tag{3.5}$$

$$\frac{\partial u_1'}{\partial x} + \frac{\partial v_1'}{\partial y} = 0, \tag{3.6}$$

$$w_1' = 0, \tag{3.7}$$

where $\mathbf{v}' = \mathbf{v}_1' = (u_1', v_1', w_1')$ and the boundary conditions are $u_1' = -U$ at the plate and $\mathbf{v}_1' \to 0$ at infinity. Equations (3.5) and (3.6) are precisely those (equations (2.4) and (2.5)) for the Blasius problem and the solution is given in (2.6) and (2.7). We may note as before that with this solution the approximate form

$$U\frac{\partial v_1'}{\partial x} = \nu\frac{\partial^2 v_1'}{\partial y^2} \tag{3.8}$$

of the second component of (3.3) is also satisfied. Again, as before, we have a velocity $[v_1']_0$ at the plate given by (2.8) for $z > 0$. We shall refer to this as the primary shear layer. We therefore require to introduce a term ϕ_1 where

$$\phi = Ux + \phi_1$$

and

$$\left.\begin{aligned} \left(\frac{\partial \phi_1}{\partial y}\right)_0 &= U\left(\frac{\nu}{U\pi x}\right)^{\frac{1}{2}} \operatorname{sgn} y \quad \text{for} \quad x > 0, z > 0 \\ &= 0 \text{ elsewhere.} \end{aligned}\right\} \tag{3.9}$$

Thus the first impact of the three-dimensional nature of the flow is felt at this stage. We now have a three-dimensional potential problem different from the corresponding two-dimensional one. Not least of these differences is, as we shall see below in §4, that $(\partial\phi_1/\partial x)_0$ and $(\partial\phi_1/\partial z)_0$ are different from zero on the plate; both are $O(\nu^{\frac{1}{2}})$. Hence to get u and w correct to order $\nu^{\frac{1}{2}}$ we have to introduce shear layers with velocity $\mathbf{v}_2' = (u_2', v_2', w_2')$ such that

$$U\frac{\partial u_2'}{\partial x} = \nu\frac{\partial^2 u_2'}{\partial y^2}, \tag{3.10}$$

$$U\frac{\partial w_2'}{\partial x} = \nu\frac{\partial^2 w_2'}{\partial y^2}, \tag{3.11}$$

$$\frac{\partial u_2'}{\partial x} + \frac{\partial v_2'}{\partial y} + \frac{\partial w_2'}{\partial z} = 0, \tag{3.12}$$

where $\mathbf{v}_2' \to 0$ at infinity and

$$u_2' = -\left(\frac{\partial \phi_1}{\partial x}\right)_0, \quad w_2' = -\left(\frac{\partial \phi_1}{\partial z}\right)_0$$

at the plate. Thus

$$v_2' = \int_y^\infty \left\{\frac{\partial u_2'}{\partial x} + \frac{\partial w_2'}{\partial z}\right\} dy \tag{3.13}$$

and again we may note that this satisfies the approximate form

$$U\frac{\partial v_2'}{\partial x} = \nu\frac{\partial^2 v_2'}{\partial y^2}, \tag{3.14}$$

for the second component.

Equation (3.13) gives a value of $[v_2']_0$ different from zero and the next step for a complete solution would be to introduce a potential ϕ_2 to restore the boundary condition at the plate by putting $(\partial\phi_2/\partial y)_0 = -[v_2']_0$ at the plate. Inside the shear layer the appropriate form of $\nabla^2\phi_2 = 0$ is $\partial^2\phi_2/\partial y^2 = 0$ and so inside the layer we should simply have to add a velocity $\partial\phi_2/\partial y = (\partial\phi_2/\partial y)_0 = -[v_2']_0$. However, v_2' and ϕ_2 are both of order ν and we need not determine them with our limited objective of obtaining the velocities correct to order $\nu^{\frac{1}{2}}$.

Thus equations (3.10) and (3.11) with their boundary conditions complete the solution correct to order $\nu^{\frac{1}{2}}$ except near the leading and side edges. We shall refer to the corresponding flow as the secondary shear layer. Outside the primary and secondary shear layers, as can be verified *a posteriori* from the detailed solutions in §§6 and 7, the error in the potential solution $\phi = Ux + \phi_1$ arising from the neglect of these edge regions in the determination of ϕ_1 is fortunately of higher order than $\nu^{\frac{1}{2}}$. Hence we can limit further attention to the shear type flows near the edges.

It is convenient in dealing with Oseen's equations in the simplest way to work with the shear layers introduced above rather than the actual boundary layers. The latter can easily be obtained from the former. Thus the primary boundary layer is obtained from the primary shear layer by superposing a velocity U in the x-direction and $-[v_1']_0$ in the y-direction. The secondary boundary layer is derived from the secondary shear layer by superposing velocities $(\partial\phi_1/\partial x)_0$ and $(\partial\phi_1/\partial z)_0$ in the x- and z-directions and $-[v_2']_0$ in the y-direction (though the latter is negligible to order ν). Similarly, in the discussions below of the edge regions the shear layer results can be translated immediately into standard boundary-layer forms.

One could say that the difference between the shear layer and boundary-layer approach lay in the difference between 'matching' at the boundary and matching at the edge of the boundary layer. In the Oseen equations to the order of accuracy of this paper the two approaches produce identical results. With the full (non-linear) boundary-layer equations standard practice is to match at the edge of the boundary layer, but it is for consideration here too whether matching at the boundary might be advantageous as suggested by Latta (1951) and Kaplun (1954) in another, though not unrelated, connexion.

Turning now to the shear layer near the leading edge and away from the vicinity of the tip, we can therein no longer neglect $\partial/\partial x$ in comparison with $\partial/\partial y$ but we can still neglect $\partial/\partial z$ and this is true *within* the layer for the potential contribution to the flow inside it. Thus the equations determining this layer with $\phi = Ux + \phi_1 + \phi'$ are

$$\frac{\partial^2\phi'}{\partial x^2} + \frac{\partial^2\phi'}{\partial y^2} = 0, \tag{3.15}$$

$$U\frac{\partial \mathbf{v}'}{\partial x} = \nu\left(\frac{\partial^2\mathbf{v}'}{\partial x^2} + \frac{\partial^2\mathbf{v}'}{\partial y^2}\right), \tag{3.16}$$

$$\operatorname{div}\mathbf{v}' = 0. \tag{3.17}$$

In this region, however, $w' = O(\nu^{\frac{1}{2}})$ and $\partial w'/\partial z = O(\nu^{\frac{1}{2}})$, and the effect of this term in (3.16) would be to give contributions of higher order than $O(\nu^{\frac{1}{2}})$ to u' and v', since the extent of the region in x and y is $O(\nu^{\frac{1}{2}})$. Hence we may take (3.17) in the approximate form

$$\frac{\partial u'}{\partial x} + \frac{\partial v'}{\partial y} = 0. \tag{3.18}$$

The boundary conditions are

$$u' = -U - \frac{\partial\phi_1}{\partial x} - \frac{\partial\phi'}{\partial x}, \quad v' = -\frac{\partial\phi_1}{\partial y} - \frac{\partial\phi'}{\partial y}, \quad w' = -\frac{\partial\phi_1}{\partial z} - \frac{\partial\phi'}{\partial z}$$

at the plate, and u', v', w' and grad $\phi' \to 0$ at infinity. The solution is considered in §6 below.

Near the side edge and away from the vicinity of the tip we may neglect $\partial/\partial x$ in comparison with $\partial/\partial y$ but must now retain $\partial/\partial z$. Thus inside the side edge shear layer the potential equation can be written

$$\frac{\partial^2\phi'}{\partial y^2} + \frac{\partial^2\phi'}{\partial z^2} = 0, \tag{3.19}$$

where $\phi = Ux + \phi_1 + \phi'$ and the equation for the shear layer velocity is

$$U\frac{\partial \mathbf{v}'}{\partial x} = \nu\left(\frac{\partial^2 \mathbf{v}'}{\partial y^2} + \frac{\partial^2 \mathbf{v}'}{\partial z^2}\right). \tag{3.20}$$

In this region, since $\partial u'/\partial x$ is $O(1)$, we have to retain the full equation of continuity

$$\frac{\partial u'}{\partial x} + \frac{\partial v'}{\partial y} + \frac{\partial w'}{\partial z} = 0. \tag{3.21}$$

The boundary conditions are $\mathbf{v}' \to 0$ and grad $\phi' \to 0$ at infinity, whilst at the plate

$$u' = -U - \frac{\partial \phi_1}{\partial x} - \frac{\partial \phi'}{\partial x}, \quad v' = -\frac{\partial \phi_1}{\partial y} - \frac{\partial \phi'}{\partial y} \quad w' = -\frac{\partial \phi_1}{\partial z} - \frac{\partial \phi'}{\partial z}.$$

We shall find it convenient, when we consider the solution in detail in § 7 below, to introduce the two-dimensional harmonic ψ conjugate to ϕ' so that we shall have

$$\frac{\partial^2 \psi}{\partial y^2} + \frac{\partial^2 \psi}{\partial z^2} = 0 \tag{3.22}$$

and boundary conditions at the plate of the form

$$u' = -U - \frac{\partial \phi_1}{\partial x} - \frac{\partial \phi'}{\partial x}, \quad v' = -\frac{\partial \phi_1}{\partial y} - \frac{\partial \psi}{\partial z}, \quad w' = -\frac{\partial \phi_1}{\partial z} + \frac{\partial \psi}{\partial y}.$$

4. The potential solution

The potential problem posed by (3.9) has the solution

$$2\pi\phi_1(x,y,z) = -\left(\frac{U\nu}{\pi}\right)^{\frac{1}{2}} \int_0^\infty \int_0^\infty \frac{dX\,dZ}{X^{\frac{1}{2}}\{(X-x)^2+y^2+(Z-z)^2\}^{\frac{1}{2}}}, \tag{4.1}$$

so that

$$2\pi\frac{\partial \phi_1}{\partial x} = \left(\frac{U\nu}{\pi}\right)^{\frac{1}{2}} \int_0^\infty \int_0^\infty \frac{(x-X)\,dX\,dZ}{X^{\frac{1}{2}}\{(X-x)^2+y^2+(Z-z)^2\}^{\frac{3}{2}}}, \tag{4.2}$$

$$2\pi\frac{\partial \phi_1}{\partial z} = \left(\frac{U\nu}{\pi}\right)^{\frac{1}{2}} \int_0^\infty \int_0^\infty \frac{(z-Z)\,dX\,dZ}{X^{\frac{1}{2}}\{(X-x)^2+y^2+(Z-z)^2\}^{\frac{3}{2}}}. \tag{4.3}$$

It follows that

$$2\pi\frac{\partial \phi_1}{\partial x} = \left(\frac{U\nu}{\pi}\right)^{\frac{1}{2}} \left\{\int_0^\infty \frac{(x-X)\,dX}{X^{\frac{1}{2}}[(x-X)^2+y^2]} + \int_0^\infty \frac{z(x-X)\,dX}{X^{\frac{1}{2}}[(x-X)^2+y^2]\,[(x-X)^2+y^2+z^2]^{\frac{1}{2}}}\right\} \tag{4.4}$$

and

$$2\pi\frac{\partial \phi_1}{\partial z} = -\left(\frac{U\nu}{\pi}\right)^{\frac{1}{2}} \int_0^\infty \frac{dX}{X^{\frac{1}{2}}[(X-x)^2+y^2+z^2]^{\frac{1}{2}}}. \tag{4.5}$$

Hence

$$\frac{\partial \phi_1}{\partial x} = \left(\frac{U\nu}{\pi x}\right)^{\frac{1}{2}} U_1(\xi,\chi), \quad \frac{\partial \phi_1}{\partial z} = \left(\frac{U\nu}{\pi x}\right)^{\frac{1}{2}} W_1[\sqrt{(\xi^2+\chi^2)}], \tag{4.6}$$

where

$$\chi = y/x, \quad \xi = z/x, \tag{4.7}$$

$$U_1(\xi,\chi) = -\frac{1}{2\pi}\int_0^\infty \frac{(t-1)\,dt}{t^{\frac{1}{2}}[(t-1)^2+\chi^2]} - \frac{\xi}{2\pi}\int_0^\infty \frac{(t-1)\,dt}{t^{\frac{1}{2}}[(t-1)^2+\chi^2]\,[(t-1)^2+\xi^2+\chi^2]^{\frac{1}{2}}} \tag{4.8}$$

and

$$W_1(s) = -\frac{1}{2\pi}\int_0^\infty \frac{dt}{t^{\frac{1}{2}}[(t-1)^2+s^2]^{\frac{1}{2}}}. \tag{4.9}$$

On the quarter-plane itself we have

$$U_1(\xi,0) = -\frac{\xi}{2\pi}\lim_{\chi\to 0}\int_0^\infty \frac{(t-1)\,dt}{t^{\frac{1}{2}}[(t-1)^2+\chi^2]\,[(t-1)^2+\xi^2]^{\frac{1}{2}}}, \tag{4.10}$$

$$W_1(\xi) = -\frac{1}{2\pi}\int_0^\infty \frac{dt}{t^{\frac{1}{2}}[(t-1)^2+\xi^2]^{\frac{1}{2}}}. \tag{4.11}$$

When ξ is large

$$U_1(\xi,0) \sim -\frac{1}{2\pi\xi^{\frac{1}{2}}}\int_0^\infty \left\{1-\frac{1}{(1+t^4)^{\frac{1}{2}}}\right\}\frac{dt}{t^2} = \frac{0{\cdot}848}{\pi\xi^{\frac{1}{2}}} \tag{4.12}$$

and

$$W_1(\xi) \sim -\frac{1}{\pi\xi^{\frac{1}{2}}}\int_0^\infty \frac{dt}{(1+t^4)^{\frac{1}{2}}} = -\frac{1{\cdot}854}{\pi\xi^{\frac{1}{2}}}, \tag{4.13}$$

while when ξ is small

$$U_1(\xi,0) \sim -\frac{\xi}{2\pi}\left(\log\frac{\xi}{8}+1\right) \tag{4.14}$$

and

$$W_1(\xi) \sim \frac{1}{\pi}\log\frac{\xi}{8} + O(\xi\log\xi). \tag{4.15}$$

Finally, we shall need W_1 when $y \neq 0$ but $y^2+z^2 \ll x^2$. It follows immediately from (4.6), (4.9), (4.11) and (4.15) that

$$W_1 \sim \frac{1}{2\pi}\log\frac{y^2+z^2}{64x^2}. \tag{4.16}$$

If instead of considering the quarter infinite plane $x > 0$, $y = 0$, $z > 0$ we had supposed that the leading edge was a curve of arbitrary shape but that the side edge was unaltered, the flow v_1' determined from (3.6) would be different and so would the potential problem corresponding to (3.9). In fact the logarithmic singularity in W_1 shown by (4.16) would be unchanged but it would be necessary to add to (4.16) a term $c(x)\,x^{\frac{1}{2}}$, where $c(x)$ depends on the shape of the leading edge. A corresponding addition would be necessary for U_1. In particular if the plate is the semi-infinite strip $y = 0$, $x > 0$, $R > z > 0$ where R is large, then

$$c(x) = -\frac{1{\cdot}854}{\pi R^{\frac{1}{2}}}.$$

5. The secondary shear layer

The secondary shear layer problem is posed in equations (3.10), (3.11), together with the boundary conditions

$$u_2' = U_2 = -\left(\frac{Uv}{\pi x}\right)^{\frac{1}{2}} U_1(\xi,0), \quad w_2' = W_2 = -\left(\frac{Uv}{\pi x}\right)^{\frac{1}{2}} W_1(\xi) \tag{5.1}$$

at $y = 0$, $x > 0$, $z > 0$, and

$$u_2' = w_2' = 0 \quad \text{at} \quad x = 0, \quad (y > 0, z > 0).$$

We solve the problem for the whole of the quarter-plane realizing that there will be errors near the leading and side edges. These regions will be dealt with in detail below.

We see that z appears in the equations and boundary conditions entirely as a parameter and we have essentially equations to solve in two independent variables. Introducing Laplace transforms with respect to x with parameter s^2 and using Gothic type to denote transforms we have

$$\mathfrak{U}_2(s) = -\left(\frac{U\nu}{\pi}\right)^{\frac{1}{2}} \int_0^\infty x^{-\frac{1}{2}} U_1\left(\frac{z}{x}, 0\right) e^{-s^2 x}\, dx, \tag{5.2}$$

$$\mathfrak{W}_2(s) = -\left(\frac{U\nu}{\pi}\right)^{\frac{1}{2}} \int_0^\infty x^{-\frac{1}{2}} W_1\left(\frac{z}{x}\right) e^{-s^2 x}\, dx, \tag{5.3}$$

$$Us^2\mathfrak{u}_2 = \nu \frac{\partial^2 \mathfrak{u}_2}{\partial y^2}, \quad Us^2\mathfrak{w}_2 = \nu \frac{\partial^2 \mathfrak{w}_2}{\partial y^2}, \tag{5.4}$$

so that

$$u_2 = \mathfrak{U}_2 e^{-(U/\nu)^{\frac{1}{2}} sy}, \quad w_2 = \mathfrak{W}_2 e^{-(U/\nu)^{\frac{1}{2}} sy}, \tag{5.5}$$

which give the solution in operational form.

It will be sufficient for our purpose to comment on the asymptotic form of the results when ξ is either large or small. When ξ is large we find immediately that

$$u_2' = -\frac{0{\cdot}848}{\pi}\left(\frac{\nu U}{\pi z}\right)^{\frac{1}{2}} \operatorname{erfc} \eta, \quad w_2' = \frac{1{\cdot}854}{\pi}\left(\frac{\nu U}{\pi z}\right)^{\frac{1}{2}} \operatorname{erfc} \eta, \tag{5.6}$$

whilst when ξ is small

$$u_2' = \left(\frac{\nu U}{\pi x}\right)^{\frac{1}{2}} \left\{\frac{\xi}{2\pi}\left(\log\frac{\xi}{8} + 1\right)(1 - 2\eta^2) e^{-\eta^2} + \frac{\xi}{2\pi} A(\eta)\right\}, \tag{5.7}$$

$$w_2' = \left(\frac{\nu U}{\pi x}\right)^{\frac{1}{2}} \left\{\frac{1}{\pi} e^{-\eta^2} \log\frac{\xi}{8} + \frac{1}{\pi} B(\eta)\right\}, \tag{5.8}$$

where $A(\eta)$ and $B(\eta)$ are functions of η only, with

$$A(0) = B(0) = 0, \quad A'(0) = 4\pi^{\frac{1}{2}}, \quad B'(0) = -2\pi^{\frac{1}{2}}.$$

It will be seen that in the region on the plate where (5.6) is valid

$$\frac{\partial u_2'}{\partial y} = \frac{0{\cdot}848}{\pi^2} \frac{U}{(zx)^{\frac{1}{2}}}, \quad \frac{\partial w_2'}{\partial y} = -\frac{1{\cdot}854}{\pi^2} \frac{U}{(zx)^{\frac{1}{2}}}. \tag{5.9}$$

Therefore the contribution to the skin friction in the direction of the incident stream from the part of the plane defined by

$$0 < x < x_1,\ z_1 < z < z_2,\ z_1 \gg x_1 \text{ is } (3{\cdot}390/\pi^2)\,\mu U[x_1(z_2 - z_1)]^{\frac{1}{2}}.$$

The corresponding sideways force is $-(7{\cdot}416/\pi^2)\,\mu U[x_1(z_2 - z_1)]^{\frac{1}{2}}$. The former must be compared with the excess skin friction $\frac{1}{2}\mu U x_1$ for the rectangular strip $0 < x < x_1$, $0 < z < \infty$ found by Howarth (1950) using Rayleigh's analogy and determined by considerations in the vicinity of the edge of a type to be discussed below. In Howarth's time-variable problem of the flow engendered by a semi-infinite plane started to move parallel to its (straight) side edge the velocity is everywhere parallel to the side edge. Rayleigh's (1911) analogy as applied by Howarth to determine the flow past a quarter-plane leads to results which are seriously incomplete, since the values just quoted show that the contribution to the skin friction from the induced potential flow via the secondary shear layer are at least as important as the contribution to the skin friction from the immediate neighbourhood of the side edge. In fact the contribution from the induced potential flow tends to infinity with $|z_2 - z_1|$.

6. The flow near the leading edge excluding the corner region

Near the leading edge the flow is determined by the equations (3.15), (3.16), (3.18); again z appears only as a parameter. The solution is therefore of the type found by Carrier & Lewis (1949). Thus with parabolic co-ordinates ζ_1, ζ_2, where

$$x+iy = (\zeta_1+i\zeta_2)^2, \tag{6.1}$$

we find that ϕ' is negligible to order $\nu^{\frac{1}{2}}$ and that correct to this order

$$u' = U\left(\frac{\nu}{U\pi}\right)^{\frac{1}{2}}\frac{\zeta_2 e^{-(U\zeta_2^2/\nu)}}{\zeta_1^2+\zeta_2^2} - U\left[1+\frac{0{\cdot}848}{\pi}\left(\frac{\nu}{\pi Uz}\right)^{\frac{1}{2}}\right]\operatorname{erfc}\left(\frac{U}{\nu}\right)^{\frac{1}{2}}\zeta_2, \tag{6.2}$$

$$v' = -U\left(\frac{\nu}{U\pi}\right)^{\frac{1}{2}}\frac{\zeta_1 e^{-(U\zeta_1^2/\nu)}}{\zeta_1^2+\zeta_2^2}, \tag{6.3}$$

$$w' = \frac{1{\cdot}854}{\pi}\left(\frac{\nu}{\pi Uz}\right)^{\frac{1}{2}}\operatorname{erfc}\left(\frac{U}{\nu}\right)^{\frac{1}{2}}\zeta_2. \tag{6.4}$$

The solution correct to order $\nu^{\frac{1}{2}}$ in the vicinity of the leading edge is therefore

$$\mathbf{v} = U\mathbf{i}+\operatorname{grad}\phi_1+\mathbf{v}',$$

where ϕ_1 is given in §4, $\mathbf{v}'$ by (6.2)–(6.4), and $\mathbf{i}$ is a unit vector in the direction of the incident stream.

7. The flow near the side edge, excluding the corner region

The flow near the side edge is determined by equations (3.19)–(3.22). The first component of (3.20) can be solved independently of the others since, as can be justified *a posteriori*, $\partial\phi'/\partial x$ is negligible to order $\nu^{\frac{1}{2}}$. Furthermore, when

$$z/x \to 0, \quad \partial\phi_1/\partial x \to 0$$

for the quarter-plane whilst for a more general leading edge $\partial\phi_1/\partial x \to b(x)$, where $b(x)$ is a function of x which can be determined. We shall for simplicity confine attention to the quarter-plane though the more general solution can be obtained if desired. Hence we have to solve

$$U\frac{\partial u'}{\partial x} = \nu\left(\frac{\partial^2 u'}{\partial y^2}+\frac{\partial^2 u'}{\partial z^2}\right), \tag{7.1}$$

subject to the condition $u' = -U$ at the quarter-plane and $u' \to 0$ at infinity. This is the problem already solved by Howarth (1950) and has a solution

$$\frac{u'}{U} = -\operatorname{erfc}\eta+\frac{1}{2^{\frac{1}{2}}\pi^{\frac{3}{2}}}\int_\lambda^\infty\left[\left(\frac{v}{v-\eta}\right)^{\frac{1}{2}}-\left(\frac{v}{v+\eta}\right)^{\frac{1}{2}}\right]e^{-\frac{1}{2}v^2}K_{\frac{1}{4}}(\tfrac{1}{2}v^2)\,dv$$

when $z > 0$, and

$$\frac{u'}{U} = -\frac{1}{2^{\frac{1}{2}}\pi^{\frac{3}{2}}}\int_\lambda^\infty\left[\left(\frac{v}{v-\eta}\right)^{\frac{1}{2}}+\left(\frac{v}{v+\eta}\right)^{\frac{1}{2}}\right]e^{-\frac{1}{2}v^2}K_{\frac{1}{4}}(\tfrac{1}{2}v^2)\,dv$$

when $z < 0$, where as before

$$\eta = \frac{y}{2}\left(\frac{U}{\nu x}\right)^{\frac{1}{2}}, \quad \lambda = \frac{1}{2}\left[\frac{(y^2+z^2)\,U}{\nu x}\right]^{\frac{1}{2}} \tag{7.2}$$

and $K_{\frac{1}{4}}(x)$ is the Bessel function denoted in this way by Watson. The skin friction is given by

$$\tau = \mu\left[\frac{\partial u}{\partial y}\right]_0 = \mu U\left(\frac{U}{\nu x}\right)^{\frac{1}{2}}\left[\frac{1}{\pi^{\frac{1}{2}}} + \frac{1}{(2\pi)^{\frac{3}{2}}}\int_\lambda^\infty e^{-\frac{1}{2}v^2} K_{\frac{1}{4}}(\tfrac{1}{2}v^2)\frac{dv}{v}\right]. \tag{7.3}$$

This is, however, not the most convenient form for our present purpose. Let us write

$$Y = y\left(\frac{U}{\nu}\right)^{\frac{1}{2}}, \quad Z = z\left(\frac{U}{\nu}\right)^{\frac{1}{2}}, \quad u' = U\bar{u}, \quad v' = (\nu U)^{\frac{1}{2}}\bar{v},$$

$$w' = (\nu U)^{\frac{1}{2}}\bar{w}, \quad \phi_1 = \nu f, \quad \psi = \nu g, \tag{7.4}$$

and introduce the Laplace transforms with parameter s^2 with respect to x. We shall denote by $\mathfrak{u}, \mathfrak{v}, \mathfrak{w}, \mathfrak{f}, \mathfrak{g}$ the transforms of $\bar{u}, \bar{v}, \bar{w}, f, g$, respectively. Then since $\bar{u}, \bar{v}, \bar{w} = 0$ at $x = 0$,

$$s^2\mathfrak{u} = \frac{\partial^2\mathfrak{u}}{\partial Y^2} + \frac{\partial^2\mathfrak{u}}{\partial Z^2}, \tag{7.5}$$

$$s^2\mathfrak{v} = \frac{\partial^2\mathfrak{v}}{\partial Y^2} + \frac{\partial^2\mathfrak{v}}{\partial Z^2}, \tag{7.6}$$

$$s^2\mathfrak{w} = \frac{\partial^2\mathfrak{w}}{\partial Y^2} + \frac{\partial^2\mathfrak{w}}{\partial Z^2}, \tag{7.7}$$

$$s^2\mathfrak{u} + \frac{\partial\mathfrak{v}}{\partial Y} + \frac{\partial\mathfrak{w}}{\partial Z} = 0. \tag{7.8}$$

We shall solve (7.5) subject to the conditions

$$\left.\begin{aligned} \mathfrak{u} &= -\frac{1}{s^2}e^{-s\alpha Z} \quad \text{at} \quad Y = 0,\ Z > 0, \\ \frac{\partial\mathfrak{u}}{\partial Y} &= 0 \quad \text{at} \quad Y = 0,\ Z < 0, \end{aligned}\right\} \tag{7.9}$$

where $\alpha > 0$ and then we shall subsequently take the limit as $\alpha \to 0$ to obtain the solution of our problem.

To this end put

$$\mathfrak{u} = \frac{1}{2\pi}\int_{-\infty}^{\infty} \chi(\omega)\exp\{-is\omega Z - s(\omega^2+1)^{\frac{1}{2}}\, Y\}\, d\omega. \tag{7.10}$$

This form* satisfies (7.5) and, in view of the second condition in (7.9), $(\omega^2+1)^{\frac{1}{2}}\chi(\omega)$ is regular in the upper half-plane $\mathrm{Im}(\omega) > k_1$ for some k_1. Hence if we use suffixes + and − to denote, respectively, functions regular in the upper and lower half-planes we may put

$$\chi(\omega)(\omega^2+1)^{\frac{1}{2}} = \Upsilon_+(\omega). \tag{7.11}$$

However, from the first condition of (7.9)

$$\chi(\omega) = -\frac{i}{s^2(\omega + i\alpha)} + \chi_-(\omega). \tag{7.12}$$

* Since the variable χ defined in (4.7) does not appear in the remainder of the analysis no confusion arises from the introduction of the function $\chi(\omega)$, with a different meaning, in (7.10) et seq.

Therefore

$$\frac{\Upsilon_+(\omega)}{(\omega+i)^{\frac{1}{2}}}+\frac{i(-i\alpha-i)^{\frac{1}{2}}}{s^2(\omega+i\alpha)}=\chi_-(\omega)(\omega-i)^{\frac{1}{2}}-\frac{i}{s^2}\left[\frac{(\omega-i)^{\frac{1}{2}}-(-i\alpha-i)^{\frac{1}{2}}}{\omega+i\alpha}\right]. \tag{7.13}$$

If we assume for the moment that Υ_+ is regular for $\mathrm{Im}(\omega) > -\alpha$ and $\chi_-(\omega)$ is regular for $\mathrm{Im}(\omega) < 1$, then the two sides of (7.13) are equal and regular in the strip $1 > \mathrm{Im}(\omega) > -\alpha$. Hence they must be regular everywhere and therefore constant. In view of the integrable singularity in the skin friction at $Y = Z = 0$, this constant is zero. Hence

$$\chi(\omega)=-\frac{i(-i\alpha-i)^{\frac{1}{2}}}{s^2(\omega+i\alpha)(\omega-i)^{\frac{1}{2}}}. \tag{7.14}$$

The proof is completed by noting that with this form Υ_+ and χ_- are in fact regular in the regions in which they were originally assumed to be. Equations (7.10) and (7.14) are equivalent to (7.2).

Next, to deal with $\mathfrak{v}$ and $\mathfrak{w}$ we shall write

$$\mathfrak{v}=\frac{1}{2\pi}\int_{-\infty}^{\infty}V(\omega)\exp\{-is\omega Z-s(\omega^2+1)^{\frac{1}{2}}Y\}\,d\omega+\frac{\partial\mathfrak{h}}{\partial Z}, \tag{7.15}$$

$$\mathfrak{w}=\frac{1}{2\pi}\int_{-\infty}^{\infty}W(\omega)\exp\{-is\omega Z-s(\omega^2+1)^{\frac{1}{2}}Y\}\,d\omega-\frac{\partial\mathfrak{h}}{\partial Y}, \tag{7.16}$$

where

$$s^2\mathfrak{h}=\frac{\partial^2\mathfrak{h}}{\partial Y^2}+\frac{\partial^2\mathfrak{h}}{\partial Z^2} \tag{7.17}$$

and

$$-s(\omega^2+1)^{\frac{1}{2}}V(\omega)-is\omega W(\omega)+s^2\chi(\omega)=0. \tag{7.18}$$

Equations (7.6)–(7.8) are thereby satisfied and subject to (7.18) $V(\omega)$ and $W(\omega)$ can be chosen for convenience in view of the presence of $\mathfrak{h}$ in (7.15) and (7.16).

The boundary conditions on $\mathfrak{v}$ and $\mathfrak{w}$ are

$$\mathfrak{v}+\frac{\partial\mathfrak{f}}{\partial Y}+\frac{\partial\mathfrak{g}}{\partial Z}=0=\mathfrak{w}+\frac{\partial\mathfrak{f}}{\partial Z}-\frac{\partial\mathfrak{g}}{\partial Y} \tag{7.19}$$

on $Y = 0$, $Z > 0$

and

$$\mathfrak{v}+\frac{\partial\mathfrak{f}}{\partial Y}+\frac{\partial\mathfrak{g}}{\partial Z}=0=\frac{\partial\mathfrak{w}}{\partial Y}+\frac{\partial^2\mathfrak{f}}{\partial Y\partial Z}-\frac{\partial^2\mathfrak{g}}{\partial Y^2} \tag{7.20}$$

on $Y = 0$, $Z < 0$. We may note that on $Y = 0$, $Z > 0$

$$\frac{\partial\mathfrak{f}}{\partial Y}=\frac{1}{s}, \tag{7.21}$$

$$\frac{\partial\mathfrak{f}}{\partial Z}=\frac{1}{\pi s}\left[\log sZ+\gamma+\tfrac{1}{2}\log\frac{s^2\nu}{4U}\right], \tag{7.22}$$

whilst on $Y = 0$, $Z < 0$

$$\frac{\partial\mathfrak{f}}{\partial Y}=0,\quad \frac{\partial^2\mathfrak{f}}{\partial Y\partial Z}=0. \tag{7.23}$$

Furthermore since the pressure p is related to $(\partial/\partial x)(\phi_1+\phi')$, we must have $\partial\mathfrak{g}/\partial Z$ and $\partial^2\mathfrak{g}/\partial Z^2$ both vanishing on $Y = 0$, $Z < 0$ so that we can take $\mathfrak{g} = 0$ without loss there. Hence our boundary conditions become

$$\mathfrak{v}+\frac{\partial\mathfrak{g}}{\partial Z}+\frac{1}{s}=0, \tag{7.24}$$

$$\mathfrak{w}-\frac{\partial\mathfrak{g}}{\partial Y}+\frac{1}{\pi s}\left[\log sZ+\gamma+\tfrac{1}{2}\log\frac{s^2\nu}{4U}\right]=0 \tag{7.25}$$

on $Y = 0$, $Z > 0$, and

$$\mathfrak{v} = 0, \quad \frac{\partial \mathfrak{w}}{\partial Y} = 0 \tag{7.26}$$

on $Y = 0$, $Z < 0$. We shall replace (7.24) by

$$\mathfrak{v} + \frac{\partial \mathfrak{g}}{\partial Z} + \frac{1}{s} e^{-sxZ} = 0 \tag{7.27}$$

and ultimately let $\alpha \to 0$.

If now we choose

$$V(\omega) = -\frac{i}{s(\omega + i\alpha)} \tag{7.28}$$

so that

$$\left.\begin{aligned} \frac{1}{2\pi s}\int_{-\infty}^{\infty}\left(-\frac{i}{\omega+i\alpha}\right)e^{-is\omega Z}\,d\omega &= -\frac{1}{s}e^{-\alpha sZ} \quad (Z>0)\\ &= 0 \qquad\qquad\quad (Z<0) \end{aligned}\right\} \tag{7.29}$$

the boundary condition (7.27) then becomes

$$\frac{\partial}{\partial Z}(\mathfrak{g} + \mathfrak{h}) = 0 \tag{7.30}$$

for $Y = 0$, $Z > 0$.

Further, with the choice of $V(\omega)$ in (7.28) we have from (7.17)

$$W(\omega) = \frac{(\omega^2+1)^{\frac{1}{2}}}{s\omega(\omega+i\alpha)} - \frac{(-i\alpha - i)^{\frac{1}{2}}}{s\omega(\omega+i\alpha)(\omega-i)^{\frac{1}{2}}}, \tag{7.31}$$

where we shall imagine the contour indented to pass above the origin in the ω-plane. It follows that the contribution from W to $\partial \mathfrak{w}/\partial Y$ when $Y = 0$, $Z < 0$ is itself zero. Hence the boundary condition $\partial \mathfrak{w}/\partial Y = 0$ when $Y = 0$, $Z < 0$ is equivalent to $\partial^2 \mathfrak{h}/\partial Y^2 = 0$ and since $\partial^2 \mathfrak{h}/\partial Z^2$ vanishes this is equivalent to $\mathfrak{h} = 0$. Therefore the boundary conditions take on the simple form

(i) on $Y = 0$, $Z < 0$, $\mathfrak{g} = \mathfrak{h} = 0$; (7.32)

(ii) on $Y = 0$, $Z > 0$, $\mathfrak{g} + \mathfrak{h} = 0$

and

$$\left.\begin{aligned} \frac{\partial}{\partial Y}(\mathfrak{g}+\mathfrak{h}) = \frac{1}{\pi s}[\log sZ + C] + \frac{1}{2\pi}\int_{-\infty}^{\infty}\frac{e^{-is\omega Z}}{\omega(\omega+i\alpha)s}\left\{(\omega^2+1)^{\frac{1}{2}} - \frac{(-i\alpha-i)^{\frac{1}{2}}}{(\omega-i)^{\frac{1}{2}}}\right\}d\omega, \end{aligned}\right\} \tag{7.33}$$

where $C = \gamma + \frac{1}{2}\log s^2\nu/4U$. An equivalent form is, in the limit $\alpha \to 0$,

$$\frac{\partial}{\partial Y}(\mathfrak{g}+\mathfrak{h}) = \frac{1}{\pi s}\left[\log sZ + \frac{\pi}{2} + C\right]e^{-sxZ} + \frac{1}{2\pi s}\int_{-\infty}^{\infty}\frac{e^{-is\omega Z}}{\omega(\omega+i\alpha)}\{(\omega^2+1)^{\frac{1}{2}} - 1\}\,d\omega. \tag{7.34}$$

It is now convenient to assume that $\mathfrak{g}$ satisfies the more general equation

$$\frac{\partial^2 \mathfrak{g}}{\partial Y^2} + \frac{\partial^2 \mathfrak{g}}{\partial Z^2} = q^2 s^2 \mathfrak{g}, \tag{7.35}$$

where $q > \alpha > 0$ and q will be made to tend to zero after α. This form then ensures that the appropriate functions are regular on the real axis and the principle of analytic continuation can then be applied.

To determine $\mathfrak{g}$, $\mathfrak{h}$ we show that a solution can be found by putting, in $Y > 0$,

$$\mathfrak{g} = -\frac{1}{2\pi s^2}\int_{-\infty}^{\infty} \Theta_+(\omega)\exp\{-s[i\omega Z + (\omega^2+q^2)^{\frac{1}{2}}\,Y]\}\,d\omega, \tag{7.36}$$

$$\mathfrak{h} = \frac{1}{2\pi s^2}\int_{-\infty}^{\infty} \Theta_+(\omega)\exp\{-s[i\omega Z + (\omega^2+1)^{\frac{1}{2}}\,Y]\}\,d\omega, \tag{7.37}$$

where $\Theta_+(\omega)$ is regular in the upper half-plane and we shall, as with (7.31), ultimately indent the contour to pass above the origin. The differential equations are thereby satisfied and so are the conditions on $Y = 0$, $Z < 0$, and the condition $\mathfrak{g}+\mathfrak{h} = 0$ on $Y = 0$, $Z > 0$. Hence we shall have a solution provided the remaining condition on $Y = 0$, $Z > 0$ is satisfied, that is, provided

$$\Theta_+(\omega)\,N(\omega) = -\frac{1}{\omega(\omega+i\alpha)}\,[(\omega^2+1)^{\frac{1}{2}}-1] - \frac{i}{\pi(\omega+i\alpha)}\,[C' - \log(\alpha - i\omega)] + T_-(\omega), \tag{7.38}$$

where

$$N(\omega) = (\omega^2+1)^{\frac{1}{2}} - (\omega^2+q^2)^{\frac{1}{2}}, \tag{7.39}$$

$$C' = \frac{\pi}{2} + C - \gamma = \frac{\pi}{2} + \tfrac{1}{2}\log\frac{s^2\nu}{4U} \tag{7.40}$$

and $T_-(\omega)$ is some function of ω regular in the lower half-plane.

It is shown in Appendix B that

$$\Theta_+(\omega) = -\frac{1}{\omega^2}\left[1 - \frac{1}{N_+(\omega)}\right] - \frac{iD}{\pi\omega N_+(\omega)}, \tag{7.41}$$

where $N_+(\omega)$ is determined in Appendix A, and

$$D = \frac{\pi}{2} + \tfrac{1}{2}\log\frac{s^2\nu}{16U} - 1. \tag{7.42}$$

The forms for $\mathfrak{g}$ and $\mathfrak{h}$ in (7.36) and (7.37) are thus determined. The cross-flow velocities are then obtained from (7.15) and (7.16) by adding the potential flow contributions $\partial\mathfrak{g}/\partial Z$ and $-\partial\mathfrak{g}/\partial Y$, respectively, interpreting and finally adding the flow associated with the original potential ϕ_1, obtained in §4.

The most interesting results are those giving the skin friction on the quarter-plane itself and the velocity when $y = 0$, $z < 0$. We shall henceforward confine our attention to these aspects of the velocity field.

8. The skin friction near the side edge

The component parallel to the main stream of the skin friction in the neighbourhood of $z = 0$ has already been determined by Howarth (equation (7.2) above); here we shall obtain its component parallel to the leading edge. We take $\alpha = 0$, $q = 0$ and note that the potential flow ϕ_1 makes no contribution to the skin friction. The contribution from $\mathfrak{g}$ to w, namely $-\partial\mathfrak{g}/\partial Y$, has to be added to (7.16) and hence the contributions to $(\partial w/\partial Y)_0$ from $\mathfrak{g}$ and $\mathfrak{h}$ amount to

$$-(\partial^2/\partial Y^2)(\mathfrak{g}+\mathfrak{h}).$$

Since $\mathfrak{g}$ satisfies Laplace's equation and $\mathfrak{h}$ satisfies (7.17) and $(\mathfrak{g}+\mathfrak{h})$ vanishes on the plate (and therefore so does $(\partial^2/\partial Z^2)(\mathfrak{g}+\mathfrak{h})$) the contributions from $\mathfrak{g}$ and $\mathfrak{h}$ amount to $s^2\mathfrak{h}$, simply. Hence

$$\left(\frac{\partial w}{\partial Y}\right)_{Y=0+} = -\frac{1}{2\pi}\int_{-\infty}^{\infty} e^{-is\omega Z}\left\{\Theta_+(\omega)+\frac{\omega^2+1}{\omega^2}-\frac{(-i)^{\frac{1}{2}}}{\omega^2}(\omega+i)^{\frac{1}{2}}\right\}d\omega, \tag{8.1}$$

where, as explained previously, the contour of integration is the real axis, indented at the origin into the upper half-plane. If $Z<0$ the integral vanishes. When $Z>0$, the contribution from the last two terms of (8·1) is

$$-\frac{1}{2}+\frac{1}{\pi}\int_1^{\infty}\frac{(t-1)^{\frac{1}{2}}}{t^2}e^{-stZ}\,dt. \tag{8.2}$$

Using (7.41) and (A. 12), the first term in (8.1) can be written as

$$-\frac{1}{2\pi}\int_{-\infty}^{\infty} e^{-is\omega Z}\left[-\frac{1}{\omega^2}\left\{1-\frac{1}{N_+(\omega)}+\frac{i\omega}{\pi}\log\left(-\frac{i\omega}{2e}\right)\right\}-\frac{iD}{\pi\omega N_+(\omega)}+\frac{i}{\pi\omega}\log\left(-\frac{i\omega}{2e}\right)\right]d\omega \tag{8.3}$$

of which the last term integrates to

$$\frac{1}{\pi}\left(\gamma+\log\frac{sZ}{2e}\right). \tag{8.4}$$

Hence

$$\left(\frac{\partial w}{\partial Y}\right)_{Y=0+} = -\frac{1}{2}+\frac{1}{\pi}\left(\gamma+\log\frac{sZ}{2e}\right)+\frac{D}{\pi}$$
$$+\frac{1}{\pi^2}\int_0^{\infty}dt\,e^{-stZ}\left\{\frac{tD-\pi}{tN_-(-it)}+\frac{\pi}{t}\right\}+\frac{1}{\pi}\int_1^{\infty}\frac{e^{-stZ}\,dt}{t^2}\left[\frac{(tD-\pi)(t^2-1)^{\frac{1}{2}}}{\pi N_-(-it)}+(t-1)^{\frac{1}{2}}\right]. \tag{8.5}$$

In inverting (8.5) to get $(\partial w/\partial y)_{y=0+}$ it is convenient to note that the inverse transformation of

$$e^{-stZ} \quad \text{is} \quad \frac{\zeta t}{x\pi^{\frac{1}{2}}}e^{-\zeta^2t^2}, \quad \text{where} \quad \zeta=\frac{Z}{2x^{\frac{1}{2}}}=\frac{z}{2}\left(\frac{U}{\nu x}\right)^{\frac{1}{2}}, \tag{8.6}$$

and of

$$\log\frac{16U}{s^2\nu}e^{-stZ} \quad \text{is} \quad \frac{\zeta t}{x\pi^{\frac{1}{2}}}e^{-\zeta^2t^2}\left[\log\frac{16Ux}{\nu}+g(\zeta t)\right], \tag{8.7}$$

where

$$g(\tau)=\frac{2}{\pi^{\frac{1}{2}}}\int_0^{\infty}e^{-v^2}dv\left\{\frac{1}{v^2+\tau^2}-\log(v^2+\tau^2)\right\}.$$

Using these results it then follows that

$$\frac{\pi x}{U\mu}\left[\mu\frac{\partial w}{\partial y}\right]_{y=0+,\,z>0} = -\frac{1}{2}+\frac{\zeta}{\pi^{\frac{1}{2}}}\int_0^{\infty}t\,e^{-\zeta^2t^2}Q(t,\zeta,x)\,dt$$
$$+\frac{\zeta}{\pi^{\frac{1}{2}}}\int_1^{\infty}e^{-\zeta^2t^2}\left\{\frac{(t-1)^{\frac{1}{2}}}{t}+(t^2-1)^{\frac{1}{2}}Q(t,\zeta,x)\right\}dt, \tag{8.8}$$

where

$$2\pi N_-(-it)\,Q(t,\zeta,x)=-\log\frac{16Ux}{\nu}-g(\zeta t)-2+\pi-\frac{2\pi}{t}. \tag{8.9}$$

It is worth noting that this component of skin friction is of much more complicated form than that for the component parallel to the main stream. The complication arises principally from the presence of the term $\log(16Ux/\nu)$ in (8.9) and means, for example, that the cross-flow does not possess the similarity properties of the main stream component.

In particular, when ζ is large

$$\mu\left[\frac{\partial w}{\partial y}\right]_{y=0+,z>0} = -\frac{\mu U}{\pi x}\left\{1-\frac{1}{2\pi^{\frac{1}{2}}\zeta}\left(\log\frac{z}{8x}+\frac{\pi}{2}\right)+O\left(\frac{\log\zeta}{\zeta}\right)^2\right\}, \tag{8.10}$$

in conformity with (5.8).

When ζ is small

$$\mu\left[\frac{\partial w}{\partial y}\right]_{y=0+,z>0} = -\frac{1}{2\pi^{\frac{1}{2}}(-\frac{3}{4})!}\left(\frac{\mu U}{\pi x\zeta^{\frac{1}{2}}}\right)\left[\log\frac{16Ux}{\nu}+2-\pi-\frac{\{(-\frac{3}{4})!\}'}{(-\frac{3}{4})!}\right]. \tag{8.11}$$

9. Flow in the plane $y = 0$, $z < 0$

In a similar way the velocity distribution in $y = 0, z < 0$ may be found. It can be verified that when ζ is large

$$w \to \left(\frac{U\nu}{\pi^3 x}\right)^{\frac{1}{2}}\log\left|\frac{z}{8x}\right| \tag{9.1}$$

in conformity with (4.15), whilst near $\zeta = 0$ we find

$$w \sim -\frac{2}{(-\frac{3}{4})!}\left(\frac{U\nu\zeta}{\pi^3 x}\right)^{\frac{1}{2}}\left[\log\frac{16Ux}{\nu}+2-\pi-\frac{\{(-\frac{3}{4})!\}'}{(-\frac{3}{4})!}\right].$$

10. Discussion

In the previous sections, expressions correct to order $\nu^{\frac{1}{2}}$ when ν is small have been obtained on the basis of Oseen's equations for the velocity distribution at all points in the fluid except those near the corner of the plate.

The $O(1)$ effect arises, as might be expected from a Blasius-type boundary layer—the primary boundary layer—and produces a frictional stress of order $\nu^{\frac{1}{2}}$ in the direction of the incident stream. What emerges from our calculations is that the modification to this flow arising from the side edge is not confined to the vicinity of that edge. Continuity considerations demand an outflow from the primary boundary layer and the potential flow thereby engendered, which is $O(\nu^{\frac{1}{2}})$, gives rise to a secondary boundary layer in which there are velocity components parallel to each edge. These components give rise to stresses of order ν parallel to each edge.

The primary and secondary boundary layers together with the potential flow give velocities correct to order $\nu^{\frac{1}{2}}$ except for local regions near both edges. The flow near the leading edge can be obtained by the same method (and virtually the same analysis) as that employed by Carrier & Lewis (1949) for the two-dimensional problem and doesn't call for any special comment here.

In the side-edge region the flow component in the direction of the main stream is determined by the same equations as Howarth solved for the time-variable flow engendered by a semi-infinite plane with a straight edge started to move

parallel to the edge. It gives rise to an additional stress of order ν in the direction of the main stream. Hence, in addition to the primary stress, the stress in the direction of the main stream is made up of two quite separate components, the one a direct edge effect local to the edge, the other arising from the secondary boundary layer and significant over much of the plate. Both are of order ν. Howarth's application of Rayleigh's argument to his time-variable problem as a means of obtaining information about the steady problem of the quarter-plane discussed in this paper is therefore incomplete. His argument gives quite correctly the local effect of the edge, but does not take into consideration the widespread effect arising from the secondary boundary layer.

The cross-flow components in the side-edge zone have two features of interest. First of all they depend for their determination, through appropriate boundary conditions, on the potential flow originating from the primary boundary layer and in particular on its behaviour near the side edge. (The component of this potential flow in the direction of the main flow vanishes as the edge is approached and so does not influence the velocity component in the direction of the main flow in this zone.) An important consequence is that if the quarter infinite plate is replaced by another lamina also having $y = z = 0$ as a side edge but otherwise with a different perimeter, the cross-flow in the side-edge zone will also be different. Secondly, in this zone the component of the flow in the direction of the main flow is a function of

$$\eta = \frac{y}{2}\left(\frac{U}{\nu x}\right)^{\frac{1}{2}}, \quad \zeta = \frac{z}{2}\left(\frac{U}{\nu x}\right)^{\frac{1}{2}}$$

only, but the cross-flow components v, w are such that $x^{\frac{1}{2}}v$ and $x^{\frac{1}{2}}w$, in addition to depending on η and ζ, depend also on $\log Ux/\nu$ and this fact considerably complicates the solution.

Of course the use of Oseen's equations simplifies the problem very appreciably and it is interesting to speculate on the effects to be found with the Navier–Stokes equations. The non-linear character of these latter equations implies a much more complicated coupling between the various equations than is the case in our analysis. However, it is possible to draw certain conclusions. We shall, as here, have a primary boundary layer and the outflow from it will engender a potential flow which will be identical, apart from a numerical factor, with that in §4. This will give rise to a secondary boundary layer of a form similar to §5, except that now there is some coupling between the components in the u and w directions through the equation of continuity. The difference is most marked at small values of z/x.

However, the greatest divergences from our analysis are to be expected in the side-edge zone. The coupling there is particularly strong, all three components being interdependent. Thus in particular the component in the direction of the main flow, which in the Oseen formulation was obtained independently of the cross-flow, can no longer be obtained without reference to the cross-flow and therefore to the potential flow. Since, as has already been pointed out, the potential flows for laminae having the same side edge but different leading edges differ in the vicinity of the side edge, the behaviour in the side-edge zone of the component in the direction of the main flow can be longer therefore be considered

as a purely local effect. In addition to its dependence on η and ζ a direct dependence on x is also to be expected.

A consideration of the form of the solution near the side edge also shows that this region cannot be $O(\nu^{\frac{1}{2}})$ in thickness. For if it were, while the viscous terms would be $O(1)$, the inertia terms of the Navier–Stokes equation would be $O(\log \nu^{-1})$, since w is $O(\nu^{\frac{1}{2}} \log \nu^{-1})$ near $y = z = 0$. In the limit $\nu \to 0$ the viscous terms would then be negligible in comparison with the inertia terms and so could not balance them as is required. It is hoped to consider this point in a later paper.

Appendix A

The determination of $N_-(\omega)$ and $N_+(\omega)$

In the strip $-q < \operatorname{Im}\omega < q$,

$$N(\omega) = (\omega^2+1)^{\frac{1}{2}} - (\omega^2+q^2)^{\frac{1}{2}} \tag{A.1}$$

is regular and non-vanishing. Hence using Cauchy's theorem we may write $N(\omega) = N_+(\omega)/N_-(\omega)$ where N_+ and N_- are regular in the upper and lower half-planes respectively and are given by (see, for example, Carrier & Di Prima (1956))

$$\frac{N'(\omega)}{N(\omega)} = \frac{N'_+(\omega)}{N_+(\omega)} - \frac{N'_-(\omega)}{N_-(\omega)} = -\frac{1}{2\pi i}\int_C \frac{\xi\, d\xi}{(\xi^2+1)^{\frac{1}{2}}(\xi^2+q^2)^{\frac{1}{2}}(\xi-\omega)}, \tag{A.2}$$

where C consists of two lines C_1, C_2 parallel to the real axis lying in $-q < \operatorname{Im}\xi < q$ and enclosing ω. Thus we may write

$$\frac{N'_-(\omega)}{N_-(\omega)} = -\frac{1}{2\pi i}\int_{C_2} \frac{\xi\, d\xi}{(\xi^2+1)^{\frac{1}{2}}(\xi^2+q^2)^{\frac{1}{2}}(\xi-\omega)} \tag{A.3}$$

taking C_2 to be above C_1 and the integration to be in the direction $\operatorname{Re}\xi$ increasing since both sides are regular in $\operatorname{Im}\omega < q$. Similarly

$$\frac{N'_+(\omega)}{N_+(\omega)} = -\frac{1}{2\pi i}\int_{C_1} \frac{\xi\, d\xi}{(\xi^2+1)^{\frac{1}{2}}(\xi^2+q^2)^{\frac{1}{2}}(\xi-\omega)}. \tag{A.4}$$

The contour C_2 may now be deformed into the two sides of the straight line joining $\xi = iq$ to $\xi = i$, whence

$$\frac{N'_-(\omega)}{N_-(\omega)} = -\frac{1}{\pi i}\int_q^1 \frac{t\, dt}{(t+i\omega)(1-t^2)^{\frac{1}{2}}(t^2-q^2)^{\frac{1}{2}}}. \tag{A.5}$$

The properties of $N_-(\omega)$ follow by integration on choosing $N_-(0) = 1$, so that $N_+(0) = 1-q$.

The behaviour of $N_-(\omega)$ near $\omega = 0$ if q is small but not zero can be obtained by noting that from A. 5

$$\frac{N'_-(0)}{N_-(0)} = -\frac{1}{\pi i}\int_q^1 \frac{dt}{(1-t^2)^{\frac{1}{2}}(t^2-q^2)^{\frac{1}{2}}} = -\frac{1}{\pi i}\log\frac{4}{q} + O(q). \tag{A.6}$$

Hence we have for ω small

$$N_-(\omega) = 1 + \frac{i\omega}{\pi}\log\frac{4}{q} \tag{A.7}$$

approximately, if $0 \leqslant \omega \ll q \ll 1$, with a corresponding expression for $N_+(\omega)$.

Next we shall need the behaviour of $N_-(\omega)$ in the limit $q \to 0$. Then

$$\frac{N'_-(\omega)}{N_-(\omega)} = -\frac{1}{\pi i}\int_0^1 \frac{dt}{(t+i\omega)(1-t^2)^{\frac{1}{2}}}. \tag{A.8}$$

Hence $$\log N_-(\omega) = \frac{1}{\pi i}\int_0^\omega \frac{1}{\sqrt{(1+\omega^2)}} \log\left[-i\left(\frac{\sqrt{(1+\omega^2)}-1}{\omega}\right)\right]. \tag{A. 9}$$

Thus, when ω is small

$$\log N_-(\omega) = \frac{1}{\pi i}\int_0^\omega \log\left(-\frac{i\omega}{2}\right) d\omega$$

$$= \frac{\omega}{\pi i}\log\left(-\frac{\omega i}{2e}\right),$$

so that $$N_-(\omega) = 1 - \frac{\omega i}{\pi}\log\left(-\frac{\omega i}{2e}\right) \tag{A. 10}$$

when ω is small.

When ω is large it is convenient to integrate A. 8 under the integral sign to give

$$\log N_-(\omega) = +\frac{1}{\pi}\int_0^1 \frac{\log(t+i\omega) - \log t}{(1-t^2)^{\frac{1}{2}}}\, dt$$

$$= \tfrac{1}{2}\log i\omega - \frac{1}{\pi}\int_0^{\pi/2} \log\sin\theta\, d\theta + \frac{1}{\pi i\omega} + O\left(\frac{1}{\omega^2}\right) \tag{A. 11}$$

so that $$N_-(\omega) = (2i\omega)^{\frac{1}{2}} + \frac{1}{\pi}\left(\frac{2}{i\omega}\right)^{\frac{1}{2}} + O(\omega^{-\frac{3}{2}}) \tag{A. 12}$$

when ω is large.

The corresponding results for $N_+(\omega)$ follow immediately from (A. 10) and (A. 12).

Appendix B

The determination of $\Theta_+(\omega)$

The purpose of this appendix is to apply the Wiener–Hopf technique to the determination of $\Theta_+(\omega)$ in equation (7.38).

We can write this equation, with the help of Appendix A, in the form

$$\Theta_+(\omega)\, N_+(\omega) = \sum_{r=1}^{9} J_r, \tag{B. 1}$$

where $$J_1 = -\left(\frac{N_+(\omega) - N_+(0)}{\omega(\omega + i\alpha)}\right), \tag{B. 2}$$

$$J_2 = \left(\frac{1-q}{i\alpha}\right)\left(\frac{N_-(\omega) - N_-(0)}{\omega}\right), \tag{B. 3}$$

$$J_3 = -\left(\frac{1-q}{i\alpha}\right)\left(\frac{N_-(\omega) - N_-(-i\alpha)}{\omega + i\alpha}\right), \tag{B. 4}$$

$$J_4 = \left(\frac{1-q}{i\alpha}\right)\left(\frac{N_-(0) - N_-(-i\alpha)}{\omega + i\alpha}\right), \tag{B. 5}$$

$$J_5 = -\frac{iN_-(-i\alpha)}{\pi(\omega + i\alpha)}(C' - \log(\alpha - i\omega)), \tag{B. 6}$$

$$J_6 = -\left(\frac{N_-(-i\alpha)}{\omega(\omega + i\alpha)}\right)[(\omega^2+q^2)^{\frac{1}{2}} - q], \tag{B. 7}$$

$$J_7 = -\frac{iC'}{\pi(\omega + i\alpha)}[N_-(\omega) - N_-(-i\alpha)], \tag{B. 8}$$

$$J_8 = \frac{i}{\pi}\left[\frac{N_-(\omega) - N_-(-i\alpha)}{\omega + i\alpha}\right]\left[\log(\alpha - i\omega) + \frac{i\pi}{\omega}[(\omega^2+q^2)^{\frac{1}{2}} - q]\right], \tag{B. 9}$$

$$J_9 = T_-(\omega)\, N_-(\omega). \tag{B. 10}$$

We notice at once that J_1, J_4, J_5 are regular in the upper half-plane $\operatorname{Im}\omega > -\alpha$ and J_2, J_3, J_7 are regular in the lower half-plane $\operatorname{Im}\omega < q$. Moreover, J_6 and J_8 can be split into parts J_{6+} and J_{8+} regular in the upper half-plane and J_{6-} and J_{8-} regular in the lower half-plane. Hence, if we assume that $\Theta_+(\omega)\,N_+(\omega)$ is regular in $\operatorname{Im}\omega > -\alpha$ and $T_-(\omega)\,N_-(\omega)$ is regular in $\operatorname{Im}\omega < q$ we can rewrite (B. 1) in the form

$$\Theta_+(\omega)\,N_+(\omega) - J_1 - J_4 - J_5 - J_{6+} - J_{8+} = J_2 + J_3 + J_{6-} + J_7 + J_{8-} + J_9$$

in which the two sides are regular in different overlapping halves of the ω-plane. Hence, both must be regular everywhere and constant; we can complete the proof by noting that with these forms $\Theta_+(\omega)\,N_+(\omega)$ and $T_-(\omega)\,N_-(\omega)$ are in fact regular in the regions in which they were assumed to be. From a consideration of the properties of $\Theta_+(\omega)$ when ω is large it follows that the constant is zero.

Hence we have

$$\Theta_+(\omega)\,N_+(\omega) = J_1 + J_4 + J_5 + J_{6+} + J_{8+}. \tag{B. 11}$$

For $\omega \neq 0$, we can now conveniently take the limit $\alpha \to 0$ though we shall retain q as a small parameter. Then we have immediately

$$J_1 = -\frac{N_+(\omega) - N_+(0)}{\omega^2}, \tag{B. 12}$$

$$J_4 = \frac{(1-q)}{i\pi\omega}\left\{\log\frac{q}{4} + O(q)\right\}, \tag{B. 13}$$

$$J_5 = -\frac{iN_-(0)}{\pi\omega}\,(C' - \log(-i\omega)). \tag{B. 14}$$

To calculate J_{6+} and J_{8+} we must use the same techniques as in Appendix A. Thus, since

$$J_6 = -\frac{N_-(0)}{\omega^2}\,[(\omega^2+q^2)^{\frac{1}{2}} - q], \tag{B. 15}$$

$$J_{6+} = -\frac{N_-(0)}{2\pi i}\int_{C_1}\frac{d\zeta}{\zeta^2}\,\frac{[(\zeta^2+q^2)^{\frac{1}{2}} - q]}{\zeta - \omega}, \tag{B. 16}$$

where C_1 is a contour starting at $-\infty$, ending at $+\infty$ and crossing the imaginary axis in the interval $(-iq, 0)$. This contour can be deformed into the sides of the negative imaginary axis from infinity to $-iq$ where it is indented.

Hence
$$J_{6+} = -\frac{N_-(0)}{\pi}\int_0^{\frac{1}{2}\pi}\frac{\sin^2\theta\,d\theta}{(q - i\omega\cos\theta)} \tag{B. 17}$$

$$= +\frac{N_-(0)}{\pi}\left\{\frac{i}{\omega^2}\sqrt{(q^2+\omega^2)}\log\frac{\omega - \sqrt{(\omega^2+q^2)}}{iq} - \frac{1}{i\omega} + \frac{q\pi}{2\omega^2}\right\}. \tag{B. 18}$$

Thus
$$J_{6+} = \frac{N_-(0)}{\pi i\omega}\left\{-1 + \log\frac{2}{q} + \log(-i\omega) + O(q)\right\} \tag{B. 19}$$

when $q \ll \omega$.

Next.
$$J_{8+} = \frac{i}{\pi}\int_{C_1}\frac{\{N_-(\zeta) - N_-(0)\}}{\zeta(\zeta - \omega)}\left\{\log(-i\zeta) + \frac{i\pi}{\zeta}\,[(\zeta^2+q^2)^{\frac{1}{2}} - q]\right\}d\zeta \tag{B. 20}$$

and deforming the contour into the two sides of the negative axis indented at $-iq$ we find that

$$\pi J_{8+} = I_1 + I_2,$$

$$I_1 = \int_0^q \left[\frac{N_-(-it) - N_-(0)}{t(t-i\omega)}\right] dt,$$

$$I_2 = \int_q^\infty \left[\frac{N_-(-it) - N_-(0)}{t(t-i\omega)}\right]\left[1 - \frac{(t^2-q^2)^{\frac{1}{2}}}{t}\right] dt.$$

Now in I_2 we can split the range of integration into (q, ϵ), (ϵ, ∞) where $q \ll \epsilon \ll 1$. Then in the range (ϵ, ∞)

$$\int_\epsilon^\infty \left|\frac{N_-(it) - N_-(0)}{t(t-i\omega)}\right|\left|1 - \frac{(t^2-q^2)^{\frac{1}{2}}}{t}\right| dt < \int_\epsilon^\infty \left|\frac{N_-(it) - N_-(0)}{t^3(t-i\omega)}\right| q^2\, dt = O(q^2).$$

The contribution to I_2 from the remaining range is equal to

$$\int_1^{\epsilon/q} \frac{[N_-(iqT) - N_-(0)]}{(qT - i\omega)\,T}\left[1 - \frac{(T^2-1)^{\frac{1}{2}}}{T}\right] dT = \int_1^{\epsilon/q} \frac{(qT/\pi)\log(4/q)}{T(qT-i\omega)}\left[1 - \frac{(T^2-1)^{\frac{1}{2}}}{T}\right] dT$$

in view of the restrictions on ϵ.

Also $$I_1 = \int_0^1 \left[\frac{N_-(iqT) - N_-(0)}{(qT - i\omega)\,T}\right] dT = \int_0^1 \frac{(qT/\pi)\log(4/q)}{T(qT-i\omega)}\, dT.$$

Therefore when $q \ll \omega$

$$J_{8+} = O(q \log q). \tag{B. 21}$$

The results of Appendix A together with equations (B. 11), (B. 12), (B. 13), (B. 14), (B. 18) and (B. 21) then serve to determine $\Theta_+(\omega)$. In the limit $\alpha \to 0$, $q \to 0$ equations (B. 11), (B. 12), (B. 13), (B. 19) and (B. 21) then show that

$$\Theta_+(\omega) = -\frac{1}{\omega^2}\left[1 - \frac{1}{N_+(\omega)}\right] - \frac{iD}{\pi\omega N_+(\omega)}, \tag{B. 22}$$

where $N_+(\omega)$ is as determined in Appendix A with $q = 0$ and $D = C' - 1 - \log 2$.

As it stands the behaviour of (B. 22) near $\omega = 0$ is apparently a source of difficulty. However, this may be avoided by noting that since $\Theta_+(\omega)$ is regular in the upper half-plane, $\operatorname{Im}\omega > 0$, the contours in (7.36), (7.37) and those dependent on them may, as already anticipated, be indented to pass above the origin and the integrations performed in standard fashion.

REFERENCES

Carrier, G. F. 1946 *Quart. J. Appl. Math.* **4**, 367–70.

Carrier, G. F. & Di Prima, R. C. 1956 *J. Math. Phys.* **35**, 359–83.

Carrier, G. F. & Lewis, J. A. 1949 *Quart. J. Appl. Math.* **7**, 228–33.

Howarth, L. 1950 *Proc. Camb. Phil. Soc.* **46**, 127–40.

Kaplun, S. 1954 *J. Appl. Math. Phys.* **5**, 111–35.

Latta, G. E. 1951 Thesis, Calif. Inst. of Technology.

Rayleigh, Lord 1911 *Phil. Mag.* (6) **21**, 697–711.

Sowerby, L. 1958 *Quart. J. Mech. Appl. Math.* **11**, 290–301.

The time-dependent magnetohydrodynamic flow past a flat plate

By G. F. CARRIER AND H. P. GREENSPAN
Pierce Hall, Harvard University

(Received 17 April 1959)

Two time-dependent magnetohydrodynamic flow problems are discussed. In Part I we consider the situation in which a semi-infinite flat plate is moved impulsively in its own plane into an electrically conducting viscous fluid. The ambient magnetic field has the same direction as the motion of the plate; it is found that when $\mu H_0^2/\rho U_0^2 < 1$, the flow pattern approaches asymptotically the steady flow found earlier (Greenspan & Carrier 1959). When $\mu H_0^2/\rho U_0^2 > 1$, the asymptotic state is one in which the fluid accompanies the plate in a rigid body motion as was anticipated in the earlier work.

In Part II, an infinite plate is moved impulsively in its own plane in the presence of an ambient magnetic field which is perpendicular to the plane of the plate. It is shown that the problem is not uniquely set until one specifies what three-dimensional problem reduces in the limit to the two-dimensional problem so defined. The answers in the conceptually acceptable limit case investigated here (the plate being a pipe of very large radius) have an asymmetry which at first sight is unexpected.

PART I. THE SEMI-INFINITE PLATE PROBLEM

1. Introduction

A recent paper (Greenspan & Carrier 1959) reports a study of the steady flow of a viscous, incompressible, electrically conducting fluid past a flat plate in the presence of a magnetic field. The unexpected result of that investigation which aroused our interest in the transient problem states that a steady flow with uniform velocity far from the plate can exist only when the ambient fluid speed is greater than the Alfven speed based on the ambient magnetic field (i.e. only when $\rho U_0^2/\mu H_0^2 > 1$). Here, we report the results of a study of the transient problem wherein the motion starts from rest at time zero. Specifically, we formulate the transient problem, linearize it using the modified Oseen technique, solve the linearized problem in a formal way, and, using approximation methods, find a relatively simple description of the flow which is valid for large time. The results are consistent with those of the steady-flow problem and no further surprises appear. The investigation, therefore, may be of more interest as an example of a generally applicable technique for extracting simple quantitative approximate descriptions of phenomena whose precise description is impeded by the details of a non-elementary 'Wiener-Hopf problem'.

2. The flow problem

The fundamental laws governing the flow of a conducting fluid in a magnetic field are Maxwell's equations and the conservation of mass and momentum. When the fluid is viscous and the speed is everywhere small compared to c (the speed of light), these equations take the form

$$\left.\begin{aligned} \mathbf{v}_{t'}(\mathbf{v}.\operatorname{grad})\,\mathbf{v} = \rho^{-1}\operatorname{grad} p = \mu\rho^{-1}(\mathbf{j}\times\mathbf{H}) + \nu\Delta\mathbf{v}, \\ \operatorname{div}\mathbf{v} = 0, \\ \operatorname{curl}\mathbf{H} = \mathbf{j}, \quad \operatorname{div}\mathbf{H} = 0, \\ \operatorname{curl}\mathbf{E} = -\mathbf{H}_{t'}, \quad \operatorname{div}\mathbf{E} = 0, \\ \mathbf{j} = \sigma(\mathbf{E} + \mu\mathbf{v}\times\mathbf{H}). \end{aligned}\right\} \tag{2.1}$$

Here $\mathbf{v}$ is the particle velocity, $\mathbf{H}$ the magnetic field, $\mathbf{E}$ the electric field, $\mathbf{j}$ the current density, σ the electrical conductivity, μ the permeability of the fluid, ρ the mass density, p the pressure and ν the kinematic viscosity.

We consider here the flow of such a fluid past the semi-infinite plate lying in $y = 0, x > 0$. The ambient magnetic field of intensity H_0 is uniform and is parallel to the x-axis. The plate is given a velocity U_0 in the negative x-direction at time zero and we wish to describe the ensuing flow field. If we regard this problem as the limit as $R \to \infty$ of another problem in which the plate is replaced by a pipe of radius R, the symmetry is such that no field quantities depend on the z co-ordinate. Note, however, that the current $\mathbf{j}$ and the electric field $\mathbf{E}$ will be directed in the z direction. The introduction of the vector potentials $\mathbf{v} = U_0 \operatorname{curl}\mathbf{k}\psi(x, y, t)$ and $\mathbf{H} = H_0 \operatorname{curl}\mathbf{k}\,A(x, y, t)$ then allows us to simplify equations (2.1) to the form

$$\Delta\Delta\psi - \psi_y\Delta\psi_x + \psi_x\Delta\psi_y - \Delta\psi_t + \beta(A_y\Delta A_x - A_x\Delta A_y) = 0, \tag{2.2}$$

$$\Delta A - \epsilon(\psi_y A_x + A_t - \psi_x A_y) = 0. \tag{2.3}$$

In the foregoing $x = U_0 x'/\nu$, $y = U_0 y'/\nu$, $t = U_0^2 t'/\nu$, x', y', t', are the physical co-ordinates, $\rho = \mu H_0^2/\rho U_0^2$, $\epsilon = \mu\nu\sigma$, Δ is the Laplace operator in x, y, and all differential operations are taken with regard to the x, y, t co-ordinate system.

Equations (2.2) and (2.3) indicate that ψ and A are governed by a balance of diffusive and convective transport; it is known (Carrier & Lewis 1949; Greenspan & Carrier 1959), that in such problems the 'convective coefficients' ψ_y, ψ_x, A_y, A_x of (2.2) can be replaced by appropriately chosen averages. One rationalizes this by noting, for example, that the net convective effect in (2.2) of the terms $\psi_y\Delta\psi_x - \psi_x\Delta\psi_y \equiv u\Omega_x + v\Omega_y$ (where u, v is the velocity and Ω the vorticity) may be equivalent to a uniform horizontal convection at speed cU_0 where $0 < c < 1$. In the classical viscous-flow-past-a-flat-plate problem the choice $c = 0{\cdot}35$ gives remarkably accurate results. The character of the results is not affected by the choice of c, although the numbers which emerge do depend on c. Since our objective here is to determine the nature of the flow and its dependence on σ, μ, H_0, etc., we will not optimize the choice of these averages but will merely replace ψ_y and A_y in (2.2) and (2.3) by unity and replace ψ_x and A_x in (2.2) by zero. With this 'averaging' of the convective effects, (2.2) and (2.3) become

$$\Delta\Delta\psi - \Delta(\psi_x + \psi_t - \beta A_x) = 0, \tag{2.4}$$

$$\Delta A - \epsilon(A_x + A_t - \psi_x) = 0. \tag{2.5}$$

Note that any other choice for the averages of ψ_y, ψ_x, etc., would lead to equations which transform to (2.4) and (2.5) when the co-ordinates are scaled differently. This assures us that the nature of the results cannot be different for different choices of these quantities.

In view of the symmetry of the problem the boundary conditions require that $\psi(x,0,t) = A(x,0,t) = 0$, $\psi_y(x,0,t) = S(t)$ when $x > 0$, $\psi(x,y,t)$ and $A(x,y,t) \to 0$ as $\mathrm{Im}\,(x+iy)^{\frac{1}{2}} \to \infty$, and that $\psi_{yyy}(x,y,t)$ and $A_y(x,y,t)$ be continuous at $y = 0$.

If we define the Fourier–Laplace transforms of the potentials by

$$\overline{\psi}(\xi,\eta,s) = \int_0^\infty dt \int_{-\infty}^{\infty}\int_{-\infty}^{\infty} e^{-i(\xi x+\eta y)-st}\,\psi(x,y,t)\,dx\,dy, \tag{2.6}$$

the conventional transformation of (2.4) and (2.5) yields

$$(\eta^2+\xi^2)\,[\{\eta^2+(\xi^2+i\xi+s)\}\,\overline{\psi}-i\beta\xi\bar{A}] = i\eta\bar{f}(\xi,s), \tag{2.7}$$

$$[\eta^2+\xi^2+\epsilon(i\xi+s)]\,\bar{A}-i\epsilon\xi\overline{\psi} = 0, \tag{2.8}$$

where $f(x,t)$ (whose transform in x and t is $\bar{f}$) is given by

$$f = \psi_{yy}(x,0+,t)-\psi_{yy}(x,0-,t).$$

We solve (2.7) and (2.8) to obtain

$$\overline{\psi}(\xi,\eta,s) = \frac{i\eta\bar{f}(\xi,s)\,[\xi^2+\eta^2+\epsilon(i\xi+s)]}{\{(\xi^2+\eta^2+i\xi+s)\,(\xi^2+\eta^2+\epsilon[i\xi+s])+\beta\epsilon\xi^2\}\,(\xi^2+\eta^2)}, \tag{2.9}$$

and we define

$$\psi^*(\xi,y,s) = \tfrac{1}{2}\pi)\int_{-\infty}^{\infty} e^{i\eta y}\,\overline{\psi}(\xi,\eta,s)\,d\eta. \tag{2.10}$$

Thus, ψ^* is the transform in x and t only of $\psi(x,y,t)$. If we perform the integration of (2.10), we obtain†

$$\begin{aligned}-2\psi^*(\xi,y,s) = \bar{f}(\xi,s)\,\{&(\eta_3^2-\xi^2)\,(\eta^2-\eta_2^2)\,e^{-|\xi|\,|y|}+(\eta_3^2-\eta^2)\,(\eta_2^2-\xi^2)\,e^{-\eta|y|}\\&+(\eta_3^2-\eta_2^2)\,(\xi^2-\eta^2)\,e^{-\eta_3|y|}\}\,[(\eta_1^2-\eta_2^2)\,(\eta_1^2-\xi^2)\,(\eta_2^2-\xi^2)]^{-1},\end{aligned} \tag{2.11}$$

where $\eta_3^2 = \xi^2+i\xi+s$ and $2\eta_1^2$,

$$2\eta_2^2 = 2\xi^2+(1+\epsilon)\,(i\xi+s)\pm[(1-\epsilon)^2\,(i\xi+s)^2+\beta\epsilon(i\xi)^2]^{\frac{1}{2}}.$$

In particular,

$$\begin{aligned}2\psi_y^*(\xi,0,s) = \bar{f}\{&|\xi|\,(\eta_3^2-\xi^2)\,(\eta_1^2-\eta_2^2)+\eta_1(\eta_3^2-\eta_1^2)\,(\eta_2^2-\xi^2)\\&+\eta_2(\eta_3^2-\eta_2^2)\,(\xi^2-\eta^2)\}\,[(\eta_1^2-\eta_2^2)\,(\eta_1^2-\xi^2)\,(\eta_2^2-\xi^2)] = \bar{f}\bar{K}(\xi,s).\end{aligned} \tag{2.12}$$

When $\epsilon = 1$, (2.12) reduces to

$$\begin{aligned}2\psi_y^*(\xi,0,s)\big|_{\epsilon=1} &= -\tfrac{1}{2}\bar{f}\,[\{|\xi|+[\xi^2+i(1+\beta)\,\xi+s]^{\frac{1}{2}}\}^{-1}+\{|\xi|+[\xi^2+i(1-\beta)\,\xi-s]^{\frac{1}{2}}\}^{-1}]\\&= -\bar{f}\bar{K}_1(\xi,s);\end{aligned} \tag{2.13}$$

and when $\epsilon \to \infty$ (infinite conductivity)

$$2\psi_y^*(\xi,0,s) \to -\bar{f}[|\xi|+[\xi^2+i\xi+s-\beta\xi^2/(i\xi+s)]^{\frac{1}{2}}]^{-1} = -\bar{f}\bar{K}_\infty(\xi,s). \tag{2.14}$$

Equations (2.13) and (2.14) define $\bar{K}_1$ and $\bar{K}_\infty$.

† This calculation reduces to the evaluation of some residues.

The function $\bar{f}(\xi)$ of (2.12) can be found, in principle, by computing $\overline{K}_+(\xi, s)$ and $\overline{K}_-(\xi, s)$, the two factors of $\overline{K}(\xi, s)$ which are analytic functions of ξ in overlapping upper and lower half planes.† Such factors exist provided $|\xi|$ is replaced by $\sqrt{(\xi^2 + m^2)}$ and the limit $m \to 0$ is taken subsequently. Since $\psi_y(x, 0, t)$ is unity for $x > 0$, $t > 0$, and is not known for $x < 0$, $t > 0$, we may write

$$\psi_y(x, 0, t) = S(t)\, S(x) + V(x, t), \tag{2.15}$$

where V is zero when either $t < 0$ or $x > 0$. It follows that

$$\psi_y^*(\xi, 0, s) = (i\xi s)^{-1} + \overline{V}(\xi, s),$$

where $\overline{V}$ is analytic in ξ in some upper half plane whenever $s > 0$. Equation (2.12) can now be written

$$2([i\xi s]^{-1} + V) = \bar{f}\overline{K}_+\overline{K}_-. \tag{2.16}$$

The usual arguments of the Wiener–Hopf method lead to the result

$$\bar{f} = 2/[\overline{K}_+(0, s)\, \overline{K}_-(\xi, s)\, i\xi s], \tag{2.17}$$

and the inversion of $\bar{f}$ over ξ and s completes the calculation of $f(x, t)$. Since f is twice the skin friction on each side of the plate, the character of the flow field can be inferred directly; if more details are wanted, $\psi^*(\xi, y, s)$ as defined in (2.11) must be inverted to obtain $\psi(x, y, t)$. The calculation alluded to here is not very useful because $\overline{K}_+$ and $\overline{K}_-$ are such exceedingly messy functions that no relatively straightforward description of $f(x, t)$ can be so obtained. Since our objective is an interpretable description we shall obtain one at a minor sacrifice in accuracy. Equation (2.12) as well as its special forms (2.13) and (2.14) are each equivalent to an integral equation

$$\psi_y^*(x, 0, s) = \int_0^\infty f^*(x', s)\, K(x - x', s)\, dx', \tag{2.18}$$

where ψ_y^* and f^* are the transforms of ψ_y and f with regard to t only and K is the function whose x transform is $\overline{K}(\xi, s)$. If the kernel $K(x, s)$ of (2.18) is replaced by a suitable substitute kernel, $N(x, s)$, the solution of the so modified integral equation cannot differ markedly from that of (2.18). In particular, if $N(x, s)$ and $K(x, s)$ have the same area, $\int_0^\infty K(x, s)\, dx$, the same first moment, $\int_0^\infty xK(x, s)\, dx$, the same singularity at $x = 0$, and if $K(x, s)/N(x, s)$ tends uniformly to unity as $s \to 0$ the solutions of these integral equations will have identical gross features for $t \gg 1$. A more comprehensive argument on this point will be published elsewhere.‡ It is simpler to choose the substitute kernel, N, for special cases first; when $\beta \leqslant 1$, the case $\epsilon = 1$ is an especially convenient one. A suitable choice for $N(x, s)$ is best described in terms of $\overline{N}(\xi, s)$; in fact, that $\overline{N}(\xi, s)$ for which each of the foregoing considerations is met and which is easily factored§ is given by

$$2\overline{N}(\xi, s) = (1 - i\alpha\xi)^{-\frac{1}{2}}[\{s + i(1+\beta)\,\xi\}^{-\frac{1}{2}} + \{s + i(1-\beta)\,\xi\}^{\frac{1}{2}}], \tag{2.19}$$

where

$$\alpha = [(1+\beta)^{-\frac{1}{2}} + (1-\beta)^{-\frac{1}{2}}]^2.$$

† The details of the Wiener–Hopf process are deliberately omitted here but may be found, for example, in Greenspan & Carrier, 1959.

‡ The original suggestion that this substitution is useful is due to Koiter (1954). The method of choosing the kernel is that of Carrier (1959).

§ N would have no advantage over K if it were not easily factored.

Equation (2.17) now gives

$$\bar{f} = 2[\{s+i(1+\sqrt{\beta})\,\xi\}^{-\frac{1}{2}} + \{s+i(1-\sqrt{\beta})\,\xi\}^{-\frac{1}{2}}]\,i\xi s \tag{2.20}$$

and this can be inverted explicitly to obtain

$$\begin{aligned} f(x,t) = {} & \frac{2(1+\beta)}{\beta}\{\sqrt{[(1-\beta)/\pi x]}\,S[(1-\sqrt{\beta})\,t-x] + 1/\sqrt{(\pi t)}\,S[x-(1-\sqrt{\beta})\,t]\} \\ & \frac{-2(1-\beta)}{\beta}\{\sqrt{[(1+\beta)/\pi x]}S\,[(1+\sqrt{\beta})\,t-x] + (\pi t)^{-\frac{1}{2}}\,S[x-(1+\sqrt{\beta})\,t]\} \\ & -(1/\beta\sqrt{\pi}\,t^{\frac{3}{2}})\,\{[x-(1-\sqrt{\beta})\,t]\,S[x-(1-\sqrt{\beta})\,t] \\ & -[x-(1+\sqrt{\beta})\,t]\,S[x-(1+\sqrt{\beta})\,t]\}. \end{aligned} \tag{2.21}$$

Simply stated, (2.21) implies that: For $0 < x < (1-\sqrt{\beta})\,t$ the skin friction is precisely that of the steady-state problem; further downstream, for $x > (1+\sqrt{\beta})\,t$ in fact, the skin friction is that which an infinite plate would experience. In $(1-\sqrt{\beta})\,t < x < (1+\sqrt{\beta})\,t$ a smooth transition occurs. Note that when $\beta < 1$, both Alfven waves (the one going with the fluid and that going against the fluid) go downstream relative to the plate. Behind the slower one the steady state prevails and ahead of the faster the fluid does not know the plate has a front edge. These statements would be mildly modified by the diffusive effects that are suppressed by our substitution of N for K.

The corresponding approximations can be written down for all ϵ. The results are intrinsically the same as those for $\epsilon = 1$; in $x < (1-\sqrt{\beta})\,t$ the steady flow prevails, in $x > (1+\sqrt{\beta})\,t$ the infinite plate flow occurs. Since **v** and **H** are precisely parallel in the infinite plate problem, **H** plays no role in determining the flow field in $x > (1+\sqrt{\beta})\,t$. In $(1-\sqrt{\beta})\,t < x < (1+\sqrt{\beta})\,t$ the foregoing regions are joined smoothly.

When $\beta > 1$, an Alfven wave can travel upstream relative to the plate and the phenomenon is very different from that associated with $\beta < 1$. In this instance the situation in which $\epsilon \to \infty$ provides the simplest example. The K_∞ of (2.14) is replaced by

$$\bar{N}_\infty = \{(i\xi+s)/[i\xi+s/(1-\sqrt{\beta})]\,[i\xi+s/(1+\sqrt{\beta})]\,[1-\beta-4i\xi]\}^{\frac{1}{2}}. \tag{2.22}$$

When $\beta < 1$, this substitution is consistent with the foregoing results, but when $\beta > 1$, $\bar{N}_+$ becomes $i\xi + s(1-\sqrt{\beta})^{-\frac{1}{2}}$ instead of $[1-\beta-4i\xi]^{-\frac{1}{2}}$, its value when $\beta < 1$. In this case $\bar{f}(\xi, s)$ is given by

$$\bar{f} = 2[\{s/(1-\sqrt{\beta})\}\,\{i\xi+s/(1+\sqrt{\beta})\}\,(1-\beta 4i\xi)/(i\xi+s)]^{\frac{1}{2}}/i\xi s. \tag{2.23}$$

The function $f(x,t)$ obtained by inverting $\bar{f}$ tends to zero at a rate governed by the factor $t^{-\frac{1}{2}}$. Thus, the prediction that the only steady flow for $\beta > 1$ is one in which the fluid and plate undergo a rigid body motion, is substantiated.

Again the same type of approximation can be chosen for all ϵ and the same result emerges. That is, $f \to 0$ like $t^{-\frac{1}{2}}$ for all ϵ. Note that if $f \to 0$ as $t \to \infty$, $\psi_y(x,y,t)$ must tend to -1 for all x, y as $t \to \infty$.

Part II. Rayleigh Motion in a Magnetic Field

3. Introduction

One of the classical problems of viscous fluid theory whose study has aided our understanding of the dynamics of such fluids is that in which an infinitely extended thin plate is immersed in an unbounded viscous fluid and, at time zero, is suddenly given a constant velocity in its own plane. There are many magneto-hydrodynamic extensions of this problem which can be defined; one of these which is informative and which provides a few surprises is the following.

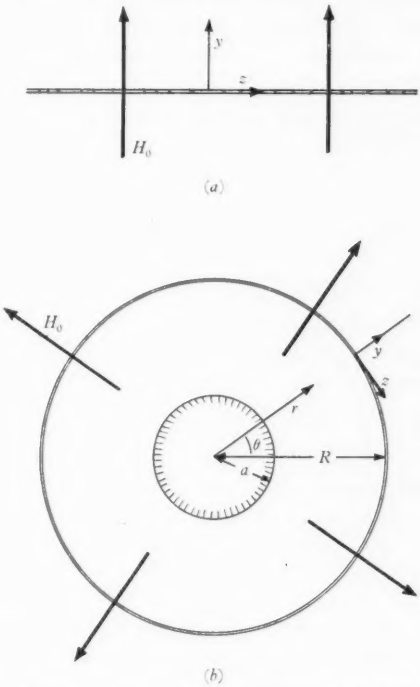

Figure 1. The geometry of the cylindrical problem and its limit, the plate problem.

Let there be a uniform ambient magnetic field perpendicular to the plane of the plate and let the geometry be considered as the limit as $R \to \infty$ of a situation wherein a pipe of radius R is exposed to such an ambient magnetic field and receives a step-function axial velocity at time zero. These geometries and the co-ordinate systems to be used are shown in figure 1. The use of this particular limiting process allows us to specify that the field quantities are dependent only on the time and on r, the co-ordinate perpendicular to the plate. In particular, since no electric charge can accumulate because of the axial symmetry, the electric field intensity, $\mathbf{E}$, must become zero when the steady state has been achieved (i.e. after t has been allowed to become infinite). If this problem is solved for the geometry of figure 1*a*, an answer can be obtained, but after taking the limit $t \to \infty$ it is readily

seen that the velocity distribution is of the form $A + Be^{-b|y|}$, where A, B and b, depend on the physical parameters of the problem, $\mathbf{E}$ is not zero, and the solution is not interpretable in terms of the postulated problem. This solution corresponds, in fact, to a situation in which charge is allowed to accumulate in a very artificial manner. It appears then, that one must solve the cylindrical problem and investigate, carefully, the behaviour as $R \to \infty$. Since the solution to the cylindrical problem contains the description of the solution of the plate problem mentioned above, we shall not develop the plate solution separately. Specifically, then, we shall treat the geometry of figure 1*b* where the solid core of radius a is fixed in space and has conductivity σ_1 and permeability μ_1; the fluid in the annular region $a < r < R$ is identical with that in $r > R$ and has conductivity σ, permeability μ, kinematic viscosity ν, and density ρ; the indefinitely thin solid sheet at R, whose electrical properties do not influence the problem, has the motion $US(t)$ in the axial direction. The fluid is at rest, $\mathbf{E}$ is zero and $\mathbf{H} = \hat{r}H_0R/r$ until time zero. The ambient magnetic field adopted here could not be produced precisely in an experiment but neither could the uniform fields of infinite extent which we postulate in other problems whose study improves our understanding of these magneto-hydrodynamic phenomena.

4. Analysis of the cylindrical problem

The physical laws governing the phenomenon in $r > R$ are again given by (2.1). We introduce cylindrical co-ordinates r, θ, z, and define the following dimensionless quantities,

$$\eta = Ur/\nu, \quad \tau = U^2t/\nu, \quad \mathbf{H} = H_0[\hat{\mathbf{r}}(R/r) + \hat{\mathbf{z}}h], \quad \mathbf{E} = \mu H_0 U\phi\hat{\boldsymbol{\theta}}, \quad \mathbf{v} = Uu\hat{\mathbf{z}},$$
$$k = RU/\nu, \quad b = aU/\nu, \quad \beta = \mu H_0^2/\rho U^2, \quad \epsilon = \mu\nu\sigma.$$

The equations then become

$$(\eta u_\eta)_\eta + \beta k h_\eta - \eta u_\tau = 0, \tag{4.1}$$
$$\eta h_\eta + \epsilon k u + \epsilon\eta\phi = 0, \tag{4.2}$$
$$(\eta\phi)_\eta + \eta h_\tau = 0. \tag{4.3}$$

In the core, since the properties are different from those of the fluid and since the velocity is zero, we have, instead of (4.2) and (4.3),

$$(\eta h_\eta)_\eta - \lambda\eta h_\tau = 0, \tag{4.4}$$

and

$$\phi = -(\sigma/\sigma_1)h_\eta, \tag{4.5}$$

where

$$\lambda = \mu_1\sigma_1/\mu\sigma.$$

The solutions of (4.1), (4.2) and (4.3) are elementary only when $\epsilon = 1$. For other ϵ, the behaviour of the system is different only in detail; we shall indicate the nature of this distinction later, but will develop only the case $\epsilon = 1$.

With $\epsilon = 1$ then, the Laplace transforms of the solutions of (4.1), (4.2) and (4.3), which vanish as $\eta \to \infty$ can be represented in the form

$$\bar{u}(\eta, s) = A(\eta/k)^m K_m(\eta\sqrt{s}) + B(\eta/k)^{-m} K_m(\eta\sqrt{s}), \tag{4.6}$$
$$\bar{h}(\eta, s) = -A(\eta/k)^m K_m(\eta\sqrt{s}) + B(\eta/k)^{-m} K_m(\eta\sqrt{s}), \tag{4.7}$$
$$\bar{\phi}(\eta, s) = -\bar{h}_\eta - k\bar{u}/\eta, \tag{4.8}$$

where $m = k\sqrt{\beta}/2$.

In the annular region, $b < \eta < k$, the fields are given by (4.8) and by

$$\bar{u}(\eta, s) = C(\eta/k)^m K_m(\eta\sqrt{s}) + D(\eta/k)^m I_m(\eta\sqrt{s}) + E(\eta/k)^{-m} K_m(\eta\sqrt{s}) + F(\eta/k)^{-m} I_m(\eta\sqrt{s}), \quad (4.9)$$

$$\bar{h}(\eta, s) = -C(\eta/k)^m K_m(\eta\sqrt{s}) - D(\eta/k)^m I_m(\eta\sqrt{s}) + E(\eta/k)^{-m} K_m(\eta\sqrt{s}) + F(\eta/k)^{-m} I_m(\eta\sqrt{s}). \quad (4.10)$$

In the core:
$$\bar{h} = GI_0(\eta\sqrt{[\lambda s]}), \quad (4.11)$$

and
$$\bar{\phi} = -\sqrt{(\omega s)}\, GI_1[\eta\sqrt{(\lambda s)}], \quad (4.12)$$

where $\omega = \sigma\mu_1/\sigma_1\mu$. The boundary conditions require that

$$\bar{u}(k+, s) = 1/s, \quad \bar{h}(k+, s) = \bar{h}(k-, s), \quad \bar{\phi}(k+, s) = \bar{\phi}(k-, s),$$

$$\bar{u}(k+, s) = \bar{u}(k-, s), \quad \bar{u}(b, s) = 0, \quad \bar{h}(b+, s) = \bar{h}(b-, s), \quad \bar{\phi}(b+, s) = \bar{\phi}(b-, s).$$

Using (4.6) to (4.11) inclusive, these boundary conditions become, in matrix form (with unchanged order),

$$M_{ij} A_j = \delta_{i1} s^{-1}, \quad (4.13)$$

where A_i is the vector $(A, B, \ldots, G)$ and M_{ij} is the following matrix.

$$\begin{matrix}
K_m(k\sqrt{s}) & K_m(k\sqrt{s}) & 0 & 0 & 0 & 0 & 0 \\
K_m(k\sqrt{s}) & K_m(k\sqrt{s}) & K_m(k\sqrt{s}) & I_m(k\sqrt{s}) & -K_m(k\sqrt{s}) & -I_m(k\sqrt{s}) & 0 \\
K_{m-1}(k\sqrt{s}) & -K_{m+1}(k\sqrt{s}) & -K_{m-1}(k\sqrt{s}) & I_{m-1}(k\sqrt{s}) & K_{m+1}(k\sqrt{s}) & I_{m+1}(k\sqrt{s}) & 0 \\
K_m(k\sqrt{s}) & -K_m(k\sqrt{s}) & K_m(k\sqrt{s}) & I_m(k\sqrt{s}) & K_m(k\sqrt{s}) & I_m(k\sqrt{s}) & 0 \\
0 & 0 & \left(\frac{b}{k}\right)^m K_m(b\sqrt{s}) & \left(\frac{b}{k}\right)^m I_m(b\sqrt{s}) & \left(\frac{b}{k}\right)^{-m} K_m(b\sqrt{s}) & \left(\frac{b}{k}\right)^{-m} I_m(b\sqrt{s}) & 0 \\
0 & 0 & -\left(\frac{b}{k}\right)^m K_m(b\sqrt{s}) & -\left(\frac{b}{k}\right)^m I_m(b\sqrt{s}) & \left(\frac{b}{k}\right)^{-m} K_m(b\sqrt{s}) & \left(\frac{b}{k}\right)^{-m} I_m(b\sqrt{s}) & -2\sqrt{\beta} I_0(b\sqrt{s}) \\
0 & 0 & \left(\frac{b}{k}\right)^m K_{m-1}(b\sqrt{s}) & -\left(\frac{b}{k}\right)^m I_{m-1}(b\sqrt{s}) & -\left(\frac{b}{k}\right)^{-m} K_{m+1}(b\sqrt{s}) & \left(\frac{b}{k}\right)^{-m} I_{m+1}(b\sqrt{s}) & -2\sqrt{\beta}\sqrt{\omega} I_1(b\sqrt{s})
\end{matrix}$$

It is especially convenient to represent each of the field quantities by the ratio of two determinants. In particular, the velocity in the outer fluid is given by

$$\bar{u}(\eta, s) = M^*/M, \quad (4.14)$$

where M is the determinant of M_{ij} and M^* is the same determinant with the first row replaced by the entries $[s^{-1}(\eta/k)^m K_m(\eta\sqrt{s}), s^{-1}(\eta/k)^{-m} K_m(\eta\sqrt{s}), 0, 0, 0, 0]$. The numerator determinant for the velocity in the annulus would have a top row in which the third to sixth entries inclusive are $1/s$ times the factors of C, D, E, F, in (4.9). Equally simple forms obtain for each of the other quantities of interest. However, the useful information can all be deduced for (4.14). It is evident that the direct inversion of M^*/M would be very difficult; it is therefore profitable to consider the behaviour of M^*/M for very large k. To do this we divide the columns of both M^* and M by M_{11}, M_{12}, M_{23}, M_{24}, $-M_{25}$, $-M_{26}$, M_{27}, respectively. We then examine each entry and replace it by its limit as $k \to \infty$ only if that limit is valid for *all* non-negative s. It is especially important to avoid replacement when the limit sequence $s \to 0$, $k \to \infty$, provides a different result from that of the sequence $k \to \infty$, $s \to 0$. The significance of this is more easily understood when the results have been obtained.

Fortunately, asymptotic representations of $K_m(z)$ and $I_m(z)$, valid for large m

and for *all* real non-negative z are readily available and we can list the pertinent information. In particular (with $\eta = k+y$, $y \ll k$, $b \ll k$),

$$\frac{K_m[(k+y)\sqrt{s}]}{K_m(k\sqrt{s})} \sim \exp\{-y(s+\tfrac{1}{4}\beta)^{\frac{1}{2}}\},$$

$$(b/k)^m \frac{K_m(b\sqrt{s})}{K_m(k\sqrt{s})} \sim (1+4s/\beta)^{\frac{1}{4}} \times \exp(-m[\log\{\tfrac{1}{2}+\tfrac{1}{2}(1+4s/\beta)^{\frac{1}{2}}\}+1-(1+4s/\beta)^{\frac{1}{2}}]) \equiv g(m,s),$$

$$(b/k)^{-m}\frac{I_m(b\sqrt{s})}{I_m(k\sqrt{s})} \sim g(-m,s),$$

$$\frac{K_{m+1}(k\sqrt{s})}{K_m(k\sqrt{s})} \sim \frac{(4s/\beta)^{\frac{1}{2}}}{1+(1+4s/\beta)^{\frac{1}{2}}} = f(s),$$

$$\frac{K_{m-1}(k\sqrt{s})}{K_m(k\sqrt{s})} \sim 1/f(s).$$

The use of these allows us to evaluate (4.14) and obtain

$$u(\eta,s) = \frac{T}{s}\exp\{-y[(s+\tfrac{1}{4}\beta)^{\frac{1}{2}}-\tfrac{1}{2}\beta^{\frac{1}{2}}]\}$$

where

$$T = \left[1-\frac{(1-e^{-\sqrt{\beta}\,y})(f^2+1)}{2-(f^2+1)\,g(-m,s)/g(m,s)}\right].$$

For real non-negative s, T can be expanded to give

$$T = 1-\frac{1}{2}\left\{\sum_{n=0}^{\infty}[(f^2+1)\,g(-m,s)/2g(m,s)]^n\right\}(1-e^{-y\sqrt{\beta}})(f^2+1)$$

$$= \tfrac{1}{2}(1+e^{-y\sqrt{\beta}})-\tfrac{1}{2}(1-e^{-y\sqrt{\beta}})\sum_{n=1}^{\infty}[\tfrac{1}{2}g(-m,s)/g(m,s)]^n + Q(\eta,s).$$

Here $Q(\eta,s)$ is essentially linear in s for small s.

This series can be inverted term by term and the first term is precisely

$$u_0(\eta,\tau) = \tfrac{1}{4}(1+e^{-y\sqrt{\beta}})\left[\operatorname{erfc}\left(\frac{y-\tau\sqrt{\beta}}{2\sqrt{\tau}}\right)+e^{y\sqrt{\beta}}\operatorname{erfc}\left(\frac{y+\tau\sqrt{\beta}}{2\sqrt{\tau}}\right)\right].$$

The subsequent terms are most readily estimated (with great accuracy for large 'time' τ) by the method of steepest descent. For example, the next term is

$$u_1(\eta,\tau) = \frac{(1-e^{-y\sqrt{\beta}})}{8\pi}\int_{-i\infty}^{i\infty}\exp[s\tau-(y+k)\{(s+\tfrac{1}{4}\beta)^{\frac{1}{2}}-\tfrac{1}{2}\beta^{\frac{1}{2}}\}+O(ks^2)]\,s^{-1}\,ds.$$

When the saddle point of the exponent lies to the right of the origin, the integral is of order $\tau^{-\frac{1}{2}}$; when it lies to the left of the origin the integral is of order unity. Furthermore, for $\tau\sqrt{\beta} = y+k$ the saddle point is at the origin, thus, the mid-point of the transition lies at $y+k = \tau\sqrt{\beta}$. In fact,

$$u_1(k+y,\tau) \sim \tfrac{1}{8}(1-e^{-y\sqrt{\beta}})\operatorname{erfc}\left(\frac{y+k-\tau\sqrt{\beta}}{2\sqrt{\tau}}\right).$$

Thus, like u_0, this term represents a wave whose propagation speed c (in dimensional form) is the Alfven speed; however, this wave has an apparent starting time which is $t_1 = R/c$ (i.e. $\tau_1 = k/\sqrt{\beta}$). This is precisely the time required for the transmission of a wave from the pipe to the origin and back to the pipe.† Thus, the u_1 term represents a wave which has reflected from the core after initiation at

† Note that the time to travel from $r=0$ to $r=R$ in the ambient field $H = H_0R/r$ is exactly half the time required to go the same distance in a uniform field H_0.

the pipe and has arrived late at y. The next term in the series will give another wave, whose history involves transmission to the core, reflexion back to the pipe, a return to the core, and finally transmission to y. This term is just half as big as u_1 and, in fact, all subsequent terms decrease in size as a geometric series. The contribution of Q is quite different since the integrand associated with Q is not singular at the origin or anywhere on the imaginary axis of the s-plane. There can be no contributions of the foregoing type and, in fact, Q merely yields shape corrections to the u_n. Each of these corrections tends to zero as $t \to \infty$ (see figure 2).

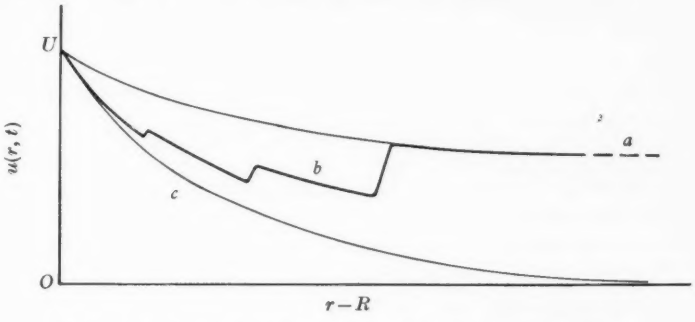

FIGURE 2. Curve a, $u_0(r, \infty)$; curve b, $u(r, t)$; curve c, $u(r, \infty)$.

If we had let $k \to \infty$ with $s \neq 0$ in the $g(m, s)$ terms, we would have obtained $u \equiv u_0$. From a physical viewpoint this means that we would have suppressed the reflexions from the core; such a suppression would imply that we had not solved a cylindrical problem, but had studied some more artificial situation. In fact, u_0 is the solution one obtains by a direct attack on the flat plate problem discussed in the introduction. Note that $2u_0(y, \infty) = 1 + e^{-y\sqrt{\beta}}$ and that $u_0 \to \frac{1}{2}$ as $y \to \infty$; it follows that $\mathbf{E}(y, \infty)$ cannot be zero and direct calculation of $\mathbf{E}$ confirms this.

On the other hand, if we let $t \to \infty$ first, the rigorous inversion of $\bar{u}$ gives

$$u(\eta, \infty) = e^{-y\sqrt{\beta}}.$$

Thus, the velocity vanishes far from the plate, $\mathbf{E}$ *can* be zero, and no physical requirements are violated.

When $\epsilon \neq 1$, the analysis is more difficult. However, the nature of the result can be deduced by noting that the first wave to arrive at a position y in the cylindrical problem would be very closely related to the direct solution of the flat plate problem for the same ϵ. This flat plate solution describes a wave which differs from that of the $\epsilon = 1$ case in that the velocity u_0 behind the wave front has the form

$$u_0 \sim a + (1-s)\, e^{-\gamma y},$$

where $a = \sqrt{\epsilon}/(1+\sqrt{\epsilon})$, $\gamma = \sqrt{(\epsilon\beta)}$.

In the cylindrical problem, the first reflexion will replace part of the first term of U_0 by a further $e^{-\gamma y}$ contribution and the entire wave sequence will lead to a velocity distribution (for large R)

$$u(\eta, \infty) \sim e^{-\gamma y}.$$

The quantitative description of these waves could be obtained by appealing directly to asymptotic techniques for solving (4.1) to (4.3) for large k; however, it is not clear that the further clarification so achieved would justify the labour involved.

Perhaps the most useful lesson to be drawn from the foregoing is the reminder that the replacement of conceptually acceptable three-dimensional problems by more tractable two-dimensional ones must be carefully justified. The specification of the manner in which current paths are closed and the implications regarding the induced fields must be consistent with the formulation of the two-dimensional problem.

REFERENCES

Carrier, G. F. 1959 A useful approximation procedure for Wiener–Hopf problems. *J. Appl. Phys.* (in the Press).

Carrier, G. F. & Lewis, J. A. 1949 Some remarks on the flat plate boundary layer. *Quart. Appl. Math.* **7**, 228.

Greenspan, H. P. & Carrier, G. F. 1959 The magneto-hydrodynamic flow past a flat plate. *J. Fluid Mech.* **6**, 77.

Koiter, W. T. 1954 Approximate solution of Wiener–Hopf type integral equations with applications, I. General theory. *Proc. K. Akad. Wet. Amst.* B, **57**, 558.

Forced small-amplitude water waves: a comparison of theory and experiment

By F. URSELL
Faculty of Mathematics, University of Cambridge

R. G. DEAN AND Y. S. YU
Hydrodynamics Laboratory, Massachusetts Institute of Technology

(Received 22 April 1959)

This paper describes an attempt to verify experimentally the wavemaker theory for a piston-type wavemaker. The theory is based upon the usual assumptions of classical hydrodynamics, i.e. that the fluid is inviscid, of uniform density, that motion starts from rest, and that non-linear terms are neglected. If the water depth, wavelength, wave period, and wavemaker stroke (of a harmonically oscillating wavemaker) are known, then the wavemaker theory predicts the wave motion everywhere, and in particular the wave height a few depths away from the wavemaker.

The experiments were conducted in a 100 ft. wave channel, and the wave-height envelope was measured with a combination hook-and-point gauge. A plane beach (sloping 1:15) to absorb the wave energy was located at the far end of the channel. The amplitude-reflexion coefficient was usually less than 10%. Unless this reflexion effect is corrected for, it imposes one of the most serious limitations upon experimental accuracy. In the analysis of the present set of measurements, the reflexion effect is taken into account.

The first series of tests was concerned with verifying the wavemaker theory for waves of small steepness ($0{\cdot}002 \leqslant H/L \leqslant 0{\cdot}03$). For this range of wave steepnesses, the measured wave heights were found to be on the average 3·4% below the height predicted by theory. The experimental error, as measured by the scatter about a line 3·4% below the theory, was of the order of 3%. The systematic deviation of 3·4% is believed to be partly due to finite-amplitude effects and possibly to imperfections in the wavemaker motion.

The second series of tests was concerned with determining the effects of finite amplitude. For the range of wave steepnesses $0{\cdot}045 \leqslant H/L \leqslant 0{\cdot}048$, the measured wave heights were found to be on the average 10% below the heights predicted from the small-amplitude theory. The experimental error was again of the order of 3%.

It is considered that these measurements confirm the validity of the small-amplitude wave theory. No confirmation of this accuracy has hitherto been given for forced motions.

1. Introduction

Some years ago, a group of engineers working at the Laboratoire Neyrpic at Grenoble published an account of a simple experiment (Neyrpic 1952) which gave results incompatible with the predictions of the mathematical theory of water waves, and which suggested that this theory was physically inadequate or even irrelevant. Even before this, the evidence for the theory had appeared incomplete and unsatisfactory. In the Neyrpic experiment, a paddle wavemaker (i.e. a plate hinged at the bottom of a wave channel) was given a small harmonic motion about a vertical mean position, and the wave height at some distance down the channel was measured; this was then compared with the theory of Havelock (1929), who had calculated the motion on the assumptions of classical hydrodynamics (see §§ 2, 3 below). It was found that the measured wave height was consistently about 30 % below the theoretical wave height. The assumptions of the theory seemed to be satisfied to a close approximation (see the papers by Suquet (1951) and Biésel & Suquet (1951) of the Laboratoire Neyrpic). The Neyrpic group was unable to make a more detailed study, and no explanation has since been given of the discrepancy.

Another attempted verification of theoretical wave-height predictions has been made by Cooper & Longuet-Higgins (1951), who investigated reflexion from a partially immersed vertical barrier by measuring the unsteady state before the secondary incident wave (see § 4.1 below) had travelled back from the wavemaker. This unsteady state persisted for so many periods that it could be treated as a steady state with little loss of accuracy. The measured reflexion coefficient was always lower than the theoretical; the discrepancy tended to decrease as the depth of immersion of the lower edge of the barrier was increased, but was still of the order of 10 % when the depth of immersion was one-third of the wavelength. It was suggested that part of this energy loss occurred near the lower edge of the barrier where an eddying motion with separation was observed.

On the other hand, many experiments on particle orbits, frequencies, and velocities have verified the theoretical predictions (see also § 2 below); in these experiments the orbits were correlated only with the local *measured* wave height. The suggestion might be made on the evidence of the Neyrpic experiments that the theory predicts correctly everything except wave heights (and presumably forces), to which a reduction factor of 0·7 to 0·9 should be applied. By what physical mechanism can a large part of the energy input be lost? Is the same correction factor required in all engineering applications? These and similar questions seemed sufficiently important to warrant an experimental study, which is described in the present paper.

The present experiment, like the Neyrpic experiment, is concerned with the investigation of a wavemaker; however, the results of this investigation agree well with the theoretical predictions of wave heights. We are unable to suggest a convincing reason for the discrepancy found by the Neyrpic group. The present experiment provides some physical verification for the wave-height predictions of the mathematical theory.

2. Small-amplitude waves: theory and experiment

The greater part of the mathematical theory of water waves is based on the following assumptions:

(1) Density variations and viscosity in the fluid are neglected. Then the motion, if originally started from rest, is irrotational and can be described by a velocity potential.

(2) Non-linear terms in the equations of motion are neglected; this seems reasonable if the amplitude of motion is sufficiently small. The mathematical difficulties are greatly increased when non-linear or viscous effects are included, and comparatively little is known about these.

Accounts of the linearized theory are given in most text-books on hydrodynamics (e.g. see Lamb 1932, Chapters 8 and 9). Recent developments are described by Stoker (1957). Many experiments have been made to check the linearized theory, but (as already noted in § 1) these are concerned with regular wave trains or with frequencies and velocities rather than with wave heights or forces. To mention just a few investigations, wave velocities and particle orbits have been measured by the Beach Erosion Board (1941) and more accurately by Suquet & Wallet (1953), and were found to agree with theory within the experimental error of a few per cent. Suquet & Wallet found that the wave profiles agreed well with the non-linear theory. The mean drift velocity of particles (mass transport), however, differed considerably in some shallow-water experiments. This discrepancy has been observed in detail (Bagnold 1947) and explained as a consequence of viscosity (Longuet-Higgins 1953); it is, however, a non-linear effect. The theory has also been confirmed for frequencies, e.g. for resonance frequencies of edge waves by Ursell (1952) and for stability under vertical oscillatory accelerations where a curve of neutral stability was successfully predicted by Benjamin & Ursell (1954). The discrepancy was within the experimental error of a few per cent. The frequency of free oscillation in a vessel has been verified to within a few per cent by Case & Parkinson (1957). On a much larger scale, the group velocity of ocean swell has been found to agree with theory by Barber & Ursell (1948).

In the theory, viscosity has been neglected; this is not always realistic, particularly when flow separation takes place. However, similar difficulties arise in model experiments as well as in the theory. To fix ideas, let us consider a floating body placed in waves. What is the interaction between the body and the waves? What are the forces on the body? Such questions are conventionally treated by a model experiment in the laboratory where forces and velocities can be measured. The problem is, how to derive from these the full-scale forces and velocities. For it is only when viscosity can be neglected that simple Froude scaling is appropriate. Sometimes more complex scaling procedures are used, e.g. in the measurement of ship drag it is customary to separate the force somewhat arbitrarily into viscous and wave-drag components which are scaled according to the Reynolds and Froude laws respectively. By this method, full-scale and model tests are found to correlate quite reasonably. A similar procedure has been used to analyse wave forces on vertical fixed piles. The agreement is best when viscous effects are small.

In addition to these difficulties of principle, model tests suffer from experimental errors which can be large. There are therefore definite advantages in studying problems theoretically, and to try to find at least the non-viscous effects from the mathematical theory; this is perhaps as accurate as the traditional experimental method. But before the results of the theory can be used with any confidence, the relevance of the theory must be established by careful experiments; in particular, the Neyrpic experiment, which seems to be incompatible with the theory, requires further study.

3. Wavemaker theory

The Neyrpic experiment was carried out with a paddle wavemaker, while the present study was made with a piston wavemaker. The relevant theory has long been known (Havelock 1929), and in its general form applies to both of these and to a much wider class of wavemakers. The general form of the wavemaker theory will be presented first, from which the special cases of piston and paddle wavemakers are obtained by substituting the appropriate boundary conditions.

Let us consider two-dimensional small-amplitude waves, which are generated in a semi-infinite channel ($0 \leqslant x < \infty$, $0 \leqslant y \leqslant h$) of constant depth h by giving a simple-harmonic motion to a moving partition oscillating about $x = 0$; the co-ordinate y is chosen to increase with depth. The amplitude of motion of the partition is assumed to be so small that the equations can be linearized, and the partition is assumed to remain nearly vertical. To this approximation, the horizontal fluid velocity on $x = 0$ is equal to the horizontal component of the velocity of the partition.

Viscosity and surface tension are neglected, and the simple-harmonic wave motion is described by a velocity potential $\phi(x, y, t)$ which satisfies (see Lamb 1932, § 227)

$$\frac{\partial^2\phi}{\partial x^2} + \frac{\partial^2\phi}{\partial y^2} = 0 \quad \text{in the region} \quad 0 \leqslant x < \infty, \quad 0 \leqslant y \leqslant h, \tag{3.1}$$

with the boundary conditions

$$\frac{\partial\phi}{\partial y} = 0 \quad \text{on} \quad y = h, \tag{3.2}$$

$$\sigma^2\phi + g\frac{\partial\phi}{\partial y} = 0 \quad \text{on} \quad y = 0, \tag{3.3}$$

$$\frac{\partial\phi}{\partial x} = U(y)\sin\sigma t \quad \text{on} \quad x = 0, \tag{3.4}$$

and also the following boundary condition at infinity:

$$\text{as} \quad x \to \infty, \quad \phi(x, y, t) \to \textit{a progressive wave travelling in the positive } x\textit{-direction.} \tag{3.5}$$

Here $2\pi/\sigma$ is the period, g is the acceleration of gravity and $U(y)$ is the prescribed horizontal velocity on the wavemaker. The condition (3.3) expresses the constancy of pressure on the free surface; the *radiation condition* (3.5) is valid in a semi-infinite channel, or in a finite channel when there is complete absorption

by the beach, but is not exactly satisfied when the absorption is incomplete. According to Havelock, the potential is of the form:

$$\phi(x,y,t) = A_0 \cosh k_0(h-y)\cos(k_0 x - \sigma t) + \sin\sigma t \sum_{n=1}^{\infty} A_n e^{-k_n x}\cos k_n(h-y), \tag{3.6}$$

where k_0 is the real positive root of $\sigma^2 = gk\tanh kh$, and $k_1, k_2, \ldots$, are the real positive roots of $\sigma^2 = -gk\tan kh$. It can be shown that $(n-\frac{1}{2})\pi < k_n h < n\pi$, whence $k_n h > \frac{1}{2}\pi$ for all n, and so the terms under the summation in (3.6) are negligible at a distance of about $3h$ from the wavemaker. The constants $A_0, A_1, A_2, \ldots$ are to be chosen to satisfy equation (3.4); thus, from (3.6), it follows that

$$U(y) = A_0 k_0 \cosh k_0(h-y) - \sum_{n=1}^{\infty} A_n k_n \cos k_n(h-y), \tag{3.7}$$

where the functions on the right of (3.7) form a complete orthogonal set, and so

$$\int_0^h U(y)\cosh k_0(h-y)\,dy = A_0 k_0 \int_0^h \cosh^2 k_0(h-y)\,dy,$$

$$\int_0^h U(y)\cos k_n(h-y)\,dy = -A_n k_n \int_0^h \cos^2 k_n(h-y)\,dy.$$

In particular, the wave profile at infinity is (Lamb, § 227)

$$\frac{1}{g}\left(\frac{\partial\phi}{\partial t}\right)_{y=0} = \frac{\sigma A_0}{g}\cosh k_0 h \sin(k_0 x - \sigma t) = \frac{\sigma}{gk_0}\cosh k_0 h \sin(k_0 x - \sigma t)\frac{\int_0^h U(y)\cosh k_0(h-y)\,dy}{\int_0^h \cosh^2 k_0(h-y)\,dy}. \tag{3.8}$$

For a *piston wavemaker*, $U(y) = \text{constant} = \frac{1}{2}S\sigma$, where S is the stroke of the wavemaker, and thus

$$\frac{H}{S} = \frac{\text{wave height}}{\text{wavemaker stroke}} = \frac{\sigma^2\cosh k_0 h}{gk_0}\frac{\int_0^h \cosh k_0(h-y)\,dy}{\int_0^h \cosh^2 k_0(h-y)\,dy} = \frac{2(\cosh 2k_0 h - 1)}{\sinh 2k_0 h + 2k_0 h}, \tag{3.9}$$

since $\sigma^2 = gk_0\tanh k_0 h$. In these expressions H is the wave height at a distance (say $x > 3h$) from the wavemaker, and $2\pi/k_0$ is the wave length at a distance from the wavemaker.

For a *paddle wavemaker* hinged at the bottom, we have $U(y) = \frac{1}{2}S\sigma\{1-(y/h)\}$, and hence

$$\frac{H}{S} = \frac{\sigma^2\cosh k_0 h}{gk_0}\frac{\int_0^h \{1-(y/h)\}\cosh k_0(h-y)\,dy}{\int_0^h \cosh^2 k_0(h-y)\,dy} = \frac{4\sinh k_0 h}{k_0 h}\frac{k_0 h\sinh k_0 h - \cosh k_0 h + 1}{\sinh 2k_0 h + 2k_0 h}. \tag{3.10}$$

Equation (3.10) has been derived and discussed by Biésel & Suquet (1951) and by Suquet (1951) and tested experimentally by the Neyrpic engineers. The present investigation was made on the piston wavemaker (for which equation (3.9) is appropriate) at the Hydrodynamics Laboratory of the Massachusetts Institute of Technology.

4. Effects not included in the simple theory

4.1. *Reflexion from the beach*

In § 3 it was assumed that the wave channel is infinitely long, or that the absorption of wave energy is complete. In practice it is incomplete (the amplitude reflexion coefficient is at least a few per cent., e.g. see Greslou & Mahe (1954)), and unless it is corrected for, it is one of the most serious limitations on experimental accuracy. Let us consider how the steady state is initially set up. When the wavemaker is first set in motion, a progressive wave train (primary incident wave) travels towards the beach. There it is partially reflected (primary reflected wave); the reflected amplitude is usually only a small fraction of the incident amplitude. The primary reflected wave is reflected (almost completely) from the wavemaker, as a secondary incident wave; this is reflected from the beach as a secondary reflected wave; and so on. The higher reflexions have progressively smaller amplitudes, and the steady state is almost attained after a few reflexions. Thus, if the reflexion is 10 % or less, the secondary reflected wave is at most 1 % of the primary incident wave, and is usually negligible. This description in terms of wave trains is valid only at a distance from the wavemaker and the beach (see equation (3.6) for the end effect near the wavemaker); thus, in this middle region, the motion consists of an incident wave train (the sum of the primary, secondary, etc., incident waves) and a reflected wave train (the sum of the primary, secondary, etc., reflected waves). However, the relative phases of primary, secondary and higher-order waves depend on the effective length of the channel and are unknown. It will be noted that the final incident wave is not given by the theory of § 3, which actually predicts the primary incident wave. It is the primary wave which must be obtained from the measurements. If the radiation condition is dropped and a standing wave now included, the potential valid except near the beach and satisfying all conditions of § 3 except (3.5) is

$$\begin{aligned}\phi(x,y,t) = {} & A_0 \cosh k_0(h-y)\,[\cos(k_0 x-\sigma t)+2\epsilon\cos k_0 x\cos(\sigma t+\delta)] \\ & +\sin\sigma t\sum_{n=1}^{\infty} A_n\, e^{-k_n x}\cos k_n(h-y) \\ & +\textit{negligible end effects from the beach}, \qquad (4.1)\end{aligned}$$

where the coefficients A_n $(n = 0, 1, \ldots)$ are the same as in § 3, and ϵ and δ are unknown parameters depending on beach characteristics and length of channel.

The wave profile is (in an obvious notation) of the form

$$\zeta \sim \sin(k_0 x-\sigma t)-2\alpha\epsilon\cos k_0 x\sin(\sigma t+\delta). \qquad (4.2)$$

This involves the assumption that at the wavemaker the reflexion is complete. From the description at the beginning of this section it is easily seen that ϵ is

nearly equal to the reflexion coefficient when ϵ is small. (The reflexion coefficient is by definition the amplitude ratio of the primary reflected wave to the primary incident wave, and also of the total reflected wave to the total incident wave.) The amplitude α of (4.2) is to be compared with the half-stroke $\frac{1}{2}H$ given by (3.9). It will now be shown how α can be derived from measurements of the wave profile. An obvious method is to measure the wave height at points where $\cos k_0 x = 0$, i.e. where $x = (\frac{1}{2}m + \frac{1}{4})$ wavelengths from the wavemaker (and not too near to the wavemaker or the beach). It has been found that this method does not lead to very consistent results, perhaps because of slight irregularities in the motion of the wavemaker, and another method of analysis has been used which depends on mean values rather than on values at one point. The amplitude of oscillation a at a distance x from the wavemaker is seen (from (4.2)) to be given by

$$a^2 = \alpha^2[1 + 2\epsilon\cos\delta + 2\epsilon\cos(2k_0x + \delta) + 2\epsilon^2\cos 2k_0x + 2\epsilon^2],$$

and when ϵ is small

$$a = \alpha[1 + \epsilon\cos(2k_0x + \delta) + \epsilon\cos\delta + O(\epsilon^2)]. \tag{4.3}$$

Thus the wave amplitude varies sinusoidally from point to point, between $a_{\max}$ and $a_{\min}$, where

$$a_{\max} = (1 + \epsilon + \epsilon\cos\delta),$$
$$a_{\min} = (1 - \epsilon + \epsilon\cos\delta).$$

It is found that the reflexion coefficient ϵ_r is given by

$$\epsilon_r = \frac{a_{\max} - a_{\min}}{a_{\max} + a_{\min}} = \frac{\epsilon}{1 + \epsilon\cos\delta} = \epsilon + O(\epsilon^2). \tag{4.4}$$

Equation (4.3) predicts that the sinusoidal variation of amplitude along the channel has a wavelength equal to half the wavelength of the incident wave; if measurements show such a variation, then ϵ_r can be obtained. The averaged position of the maxima and minima gives an estimate for δ. Once ϵ (assuming $\epsilon \doteqdot \epsilon_r$) and δ are known, an estimate for α is found by averaging the amplitude over half a wavelength. From equation (4.3), we have

$$a_{\text{av}} = \alpha[1 + \epsilon\cos\delta + O(\epsilon^2)], \tag{4.5}$$

whence

$$\alpha = \frac{a_{\text{av}}}{1 + \epsilon\cos\delta} \tag{4.6}$$

or, less accurately,

$$\alpha = a_{\text{av}} \quad \text{if} \quad \epsilon \text{ is small.} \tag{4.7}$$

It is the result calculated from equation (4.6) which is to be compared with the theoretical prediction (equation (3.9)) with $H = 2\alpha$.

4.2. *Attenuation*

The analysis in terms of an incident and a standing wave (equation (4.2)) is not strictly appropriate when viscosity is taken into account. Viscosity causes a slight attenuation of the wave height as the incident wave travels from the wavemaker towards the beach and as the reflected wave travels from the beach towards the wavemaker. The theoretical estimate is due to Hunt (1952) who calculated the dissipation of energy in the boundary layers on the side-walls and on the bottom of the channel, making plausible assumptions. It would be expected that

boundary layers account for most of the dissipation. If the amplitude attenuation is adequately described by a damping factor $\exp(-K'x)$, it is found that, for a progressive wave train,

$$K' = \frac{2k_0}{b}\left(\frac{\nu}{2\sigma}\right)^{\frac{1}{2}}\left(\frac{k_0 b + \sinh 2k_0 h}{2k_0 h + \sinh 2k_0 h}\right), \tag{4.8}$$

where b is the width of the channel, ν is the kinematic viscosity, and the other symbols are defined in § 3. This leads to values of K' of the order of 5×10^{-4} ft.$^{-1}$, for which this effect is just measurable in the M.I.T. wave channel.

4.3. *Higher harmonics*

The motion of the wavemaker is not quite simple harmonic; the second harmonic may be of the order of 5 %, too large to be neglected. However, the third and higher harmonics will be assumed to be negligible. The motion at a fixed point is then approximately of the form

$$f(t, \epsilon') = \alpha' \cos \sigma t + \alpha' \epsilon' \cos(2\sigma t + \delta'), \tag{4.9}$$

where α' is the local amplitude that is to be found, δ' is a constant but unknown phase angle, and ϵ' is a number much smaller than unity (ϵ'^2 is negligible when compared with unity). It will be shown that the difference between the maximum and minimum values of f is

$$f_{\max} - f_{\min} = 2\alpha'\{1 + O(\epsilon')^2\}, \tag{4.10}$$

involving only second and higher powers of ϵ'. Therefore this measurement is sufficient for our purpose.

To prove equation (4.10), denote by $t_{\max}(\epsilon')$ and $t_{\min}(\epsilon')$ the times at which $f(t, \epsilon')$ attains its maximum and minimum, respectively. These times depend on ϵ'. Clearly in any one cycle $t_{\max}(0) - t_{\min}(0) = \pi/\sigma$. Consider

$$[f\{t_{\max}(\epsilon'), \epsilon'\} - f\{t_{\min}(\epsilon'), \epsilon'\}].$$

This is a function of ϵ' which can be expanded in powers of ϵ'. The coefficient of ϵ' is

$$\frac{\partial f}{\partial t}(t_{\max}, \epsilon')\frac{dt_{\max}}{d\epsilon'} + \frac{\partial f}{\partial \epsilon'}(t_{\max}, \epsilon') - \frac{\partial f}{\partial t}(t_{\min}, \epsilon')\frac{dt_{\min}}{d\epsilon'} - \frac{\partial f}{\partial \epsilon'}(t_{\min}, \epsilon')$$

evaluated at $\epsilon' = 0$. Clearly

$$\frac{\partial f}{\partial t}(t_{\max}, \epsilon') = \frac{\partial f}{\partial t}(t_{\min}, \epsilon') = 0,$$

and so the coefficient is

$$\alpha' \cos(2\sigma t_{\max} + \delta') - \alpha' \cos(2\sigma t_{\min} + \delta'),$$

and this vanishes when $\epsilon' = 0$, since $2\sigma t_{\max}$ and $2\sigma t_{\min}$ then differ by 2π. Thus the coefficient of ϵ' in $f\{t_{\max}(\epsilon'), \epsilon'\} - f\{t_{\min}(\epsilon'), \epsilon'\}$ vanishes, and the power series is

$$f_{\max} - f_{\min} = 2\alpha'\{1 + O(\epsilon')^2\},$$

as previously stated in equation (4.10).

4.4. *Non-linear effects*

The object of the present investigation is to test the validity of the linearized theory, and accordingly no correction need be made for non-linear effects. Actually, since there is as yet no non-linear wavemaker theory, these corrections could not have been included even if we had wished to do so.

5. Experimental apparatus

The wave channel in which the experiments were conducted is of rectangular cross-section with glass sides and bottom and is 3 ft. deep, $2\frac{1}{2}$ ft. wide and approximately 100 ft. long (see figure 1). A piston-type wavemaker was used to

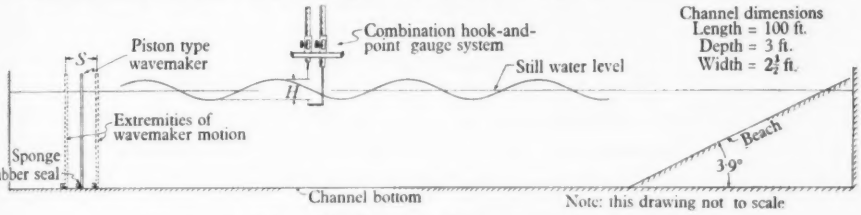

FIGURE 1. Schematic diagram of experimental equipment.

generate the waves. A beach with a slope of 1:15 at the far end of the channel from the wavemaker was used for the absorption of wave energy. A combination hook-and-point gauge was used for the measurement of the waves. These components are described in the following paragraphs.

5.1. *The wavemaker*

The wavemaker is a smooth aluminium plate oriented perpendicular to the axis of the channel and oscillates in a direction parallel to the axis of the channel. There is a small clearance of approximately $\frac{1}{4}$ in. between the edges of the wavemaker and the side-walls and bottom of the channel which was closed by an adjustable sponge rubber seal, thereby reducing the leakage around the edges of the wavemaker.

The motion of the wavemaker is controlled by a hydraulic (oil) servomechanism system. The shaft of a double-acting cylinder is connected directly to a carriage by which the wavemaker is supported. Flow of oil under pressure into and out of the two chambers of the double-acting cylinder drives the wavemaker and is metered by a valve, the output of which is prescribed by a rotating cam acting through a mechanical leverage system, magnifying the input from the cam. The linear displacement of the wavemaker with time is designed to be the same (except for a scale factor) as the angular variation of the distance from the surface of the cam to the rotational axis of the cam. By use of different cams, each with a different control surface, the motion of the wavemaker can, in principle, be given any desired periodic form, but in practice the response was imperfect. To test the theory described in § 3 the motion of the wavemaker was desired to be simple harmonic. Actually, we found at the beginning of the investigation that

with a simple harmonic cam the wavemaker motion was far from simple harmonic, but consisted of short steps rather than a smooth and continuous curve. This effect was noted particularly at the lower frequencies. Tests showed that it was due to friction in the seals of the hydraulic piston and could be reduced by continuously rotating the shaft of the piston. Further improvement was sometimes achieved by trial-and-error adjustment of the valves controlling the oil pressures in the hydraulic system. The motion of the wavemaker was then nearly simple harmonic with the second harmonic not exceeding 5 % of the fundamental and the third harmonic being presumably much smaller. (In our analysis of the measurements, the second harmonic is in effect eliminated, see § 4.3 above.) To obtain a simple-harmonic wave motion, other investigators have used wave filters (e.g. Biésel 1948); however, since a wave filter involves viscous dissipation, it could not have been used in this investigation which attempts to verify an inviscid theory.

The stroke of the wavemaker can be varied from 0·01 to 2 ft. by changing the length of the lever arm which transmits the motion of the cam to the valve. The periodicity can be varied from 0·7 sec to arbitrarily long periods by changing the rotational speed of the cam. A more detailed description of the wavemaker is given by Ippen & Eagleson (1955).

5.2. *The beach*

The beach is of plane, impermeable, varnished material, with a small gap (about $\frac{1}{4}$ in.) between the beach edges and the walls of the flume through which seepage could occur. The slope of the beach is 3·9 degrees. It was found that in most cases the reflected wave heights was less than 10 % of the incident wave height (see § 7.1 below). This compares favourably with the efficiency of other known absorbers, e.g. see Greslou & Mahe (1954) and Herbich (1956).

5.3. *Combination hook-and-point gauge*

This was used for the measurement of wave height. It is an adaptation of a well-known method for the measurement of water-surface elevations which are steady (i.e. time-independent) or varying very slowly. In the final version of the gauge, the hook and point were on the same base, but could be adjusted independently. The hook and point portions of the gauge were used to indicate the trough and crest elevations, respectively. The difference between these levels can be shown to be independent of any second-harmonic component which may be present (see § 4.3).

The tip of the hook gauge was made of wire of small diameter (0·06 in.), and there was no noticeable flow disturbance due to the tip for most waves used in this test. Both the hook and point portions of the gauge were attached to graduated staffs equipped with an adjusting knob and a vernier graduated to read displacements of the staff to the nearest 0·1 mm. The gauges were mounted with their tips in a vertical line and were both attached to a movable carriage which could be rolled on top of the channel to any longitudinal position along the channel and could be clamped rigidly in position for the measurement of a wave height. A source of light, mounted on the opposite side of the channel from the

observer, caused a reflected light pattern on the water surface and was useful in determining when the hook and point tip made contact with the water surface. When the hook or point gauge just touched the water surface, the curvature of the water surface at this point changed abruptly, thereby interrupting the reflected light pattern at this point. It is estimated that each gauge could be read with a maximum error of 0·1 mm. In many cases the unsteadiness of the water surface was of the same order, and to allow for it the elevation of the crest (similarly of the trough) was defined as the elevation at which the gauge made contact with half the crests (or troughs). For high waves, the higher particle velocities at the trough position caused ripples near the tip of the hook gauge and increased the uncertainty involved in the adjustment of the hook gauge elevation.

In order to obtain a measurement of wave height, it is necessary to know the difference in the two vernier readings when the tips of the two gauges are at the same elevation. This was obtained from readings at a still water surface. Since both gauges are on the same base, this difference is independent of the location of the gauge system along the channel.

At first a capacity-wire gauge was used for wave measurement, and this was estimated to have an absolute error of about 2 mm (this agrees with the estimate of Tucker & Charnock (1955)). An absolute error of this magnitude is too large for our present purposes; for the size of waves used in this study (1–5 cm) the error would range approximately from 4–20 %. This gauge is also described in detail by Ippen & Eagleson (1955).

An inherent disadvantage of the hook-and-point gauge is that only the wave height is obtained, while the capacity-wire gauge gives a continuous measurement of the water surface elevation; however, the absolute error associated with the hook-and-point gauge is much less than that associated with the capacity-wire gauge. Since we were concerned mainly with small-amplitude waves, where the error is limited by the absolute error of the gauge, we adopted the hook-and-point gauge and were content to regard the measurements of wave height (rather than of complete profiles) as a sufficient experimental check on the theory.

6. Methods of measurement

The theory of § 3 predicts a relation (equation (3.9)) between the ratio

$$\frac{\text{wave height at a distance from the wavemaker}}{\text{stroke of wavemaker}} = \frac{H}{S} \tag{6.1}$$

and the ratio

$$\frac{2\pi \times \text{water depth}}{\text{wave length}} = \frac{2\pi h}{L}. \tag{6.2}$$

It is this relation that was tested in the present set of experiments, with the aim of verifying the theory. For this purpose, it is necessary to measure the following variables: (1) water depth, (2) wavemaker stroke, (3) wavelength, (4) wave height.

6.1. *Water depth*

The water depth was measured directly (in ft.) with a wooden scale immersed through the still water surface. For the range of depths involved, the error in

measured depth was less than 2 %. The resulting error in the ratio (6.1) due to a 2 % error in the ratio (6.2) is equal to or less than 2 % (actually much less for short waves).

6.2. *Wavemaker stroke*

The wavemaker stroke was measured (in cm) by fixing a pointer on the wavemaker carriage. Directly behind the pointer, a metre stick was fixed to a stationary support, and so the relative positions of the extremities of motion could be

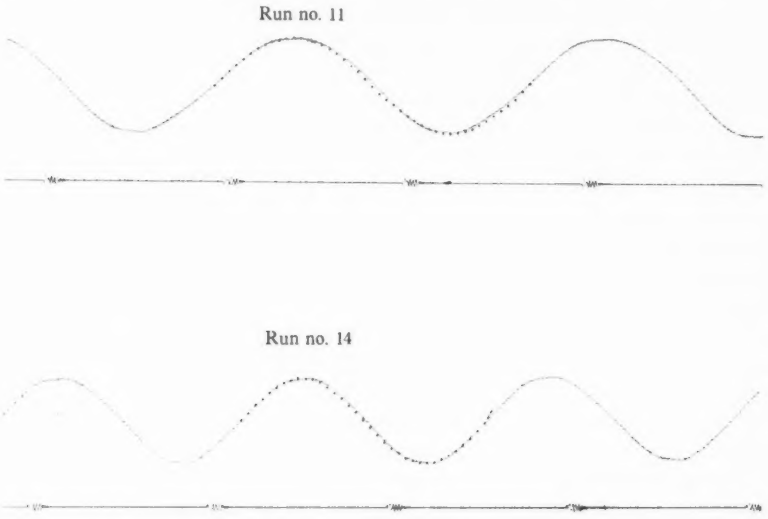

FIGURE 2. Sample of wavemaker motion (continuous line) compared with sine curve (dotted line).

measured visually. Attempts by different observers to reproduce the readings resulted in a maximum difference in the measured stroke of 0·2 mm. The resulting maximum proportional error is 2 % for the range of strokes used in this investigation. A sample of the form of the wavemaker motion was also measured for each run by using a mechanical linkage to convert the translational displacement of the wavemaker into a small angular displacement. A variable rotary capacitor converted the angular displacement into an electrical signal which was recorded by a commercial Sanborn Model 150 oscilloscope. No significant non-linear effects were introduced by this method of conversion of the translation motion into an angular displacement. (See figure 2 for a comparison of measured wavemaker motion with simple harmonic motion.)

7. Measurement of effects not included in the simple theory

The present section describes measurements of effects not included in the simple wavemaker theory, some of which have been discussed in § 4: (1) the incident wave is partially reflected from the sloping beach, see § 4.1; (2) the wave height is attenuated because of viscous dissipation, see § 4.2 where a theoretical

expression for the attenuation coefficient was presented; (3) the waves may not be strictly two-dimensional; there may be transverse reflexions and transverse slopes of the water surface.

7.1. *Measurement of reflexion from the beach*

As explained in § 4.1, partial reflexion of the incident wave from the beach causes a partial standing wave system within the channel such that the wave height is not the same at all locations along the channel, but oscillates about

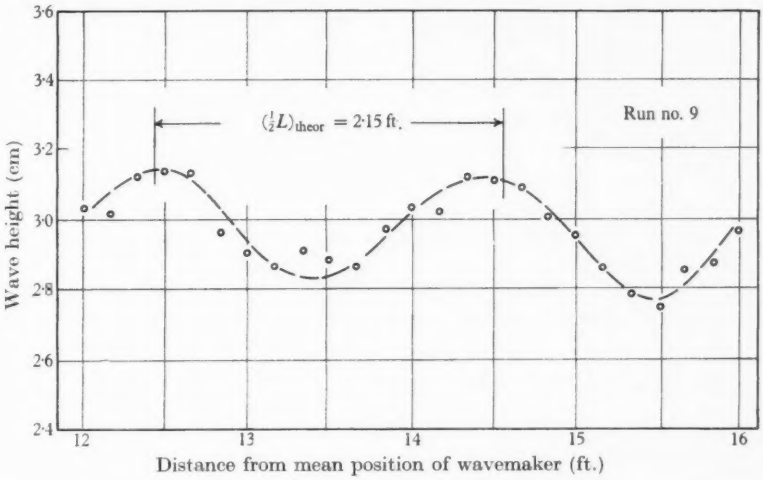

FIGURE 3. Measurement of wave height against distance. (Wavelength calculated from frequency by small-amplitude theory.)

a mean value, the wavelength of the oscillation being $\frac{1}{2}L$. Figure 2 shows one experimental measurement of wave-height variation with distance, showing the expected reflexion effect. If the maximum and minimum values of the wave-height envelope (figure 3) are denoted by $H_{\max}$ and $H_{\min}$, respectively, then the amplitude reflexion coefficient of the beach ϵ_r defined as the ratio of the reflected wave height to the incident wave height, may be expressed in the form (see also equation (4.4)

$$\epsilon_r = \frac{H_r}{H_i} = \frac{H_{\max} - H_{\min}}{H_{\max} + H_{\min}}. \tag{7.1}$$

Reflexion coefficients were calculated from the measurements wherever the variation of wave height with distance was of the form to be expected from the simple reflexion theory. In several cases, the wave height variation with distance was not of wavelength $\frac{1}{2}L$, and there is some evidence that this may be due to transverse effects (see § 7.3 below). The reflexion coefficients are plotted against deep-water wave steepness, H_0/L_0 in figure 4, and are seen to be mostly of the order of 10 % or less. The mechanism of wave reflexion by a sloping beach is not yet understood. A formula for the reflexion coefficient has been given by Miche (1951) which seems to predict the right order of magnitude, although it does not

claim to represent the physical processes correctly. Miche's formula is also shown in figure 4. Miche first considers a standing wave on an impermeable beach of constant small slope β. The slope of the water surface at the shore line varies between a maximum (positive) and a minimum (negative) value which are (according to the linear theory) proportional to the deep-water steepness H_0/L_0. Miche defines a critical deep-water standing-wave steepness $(2H_0/L_0)_{\text{crit}}$, for which the maximum water surface slope at the beach is formally equal to the

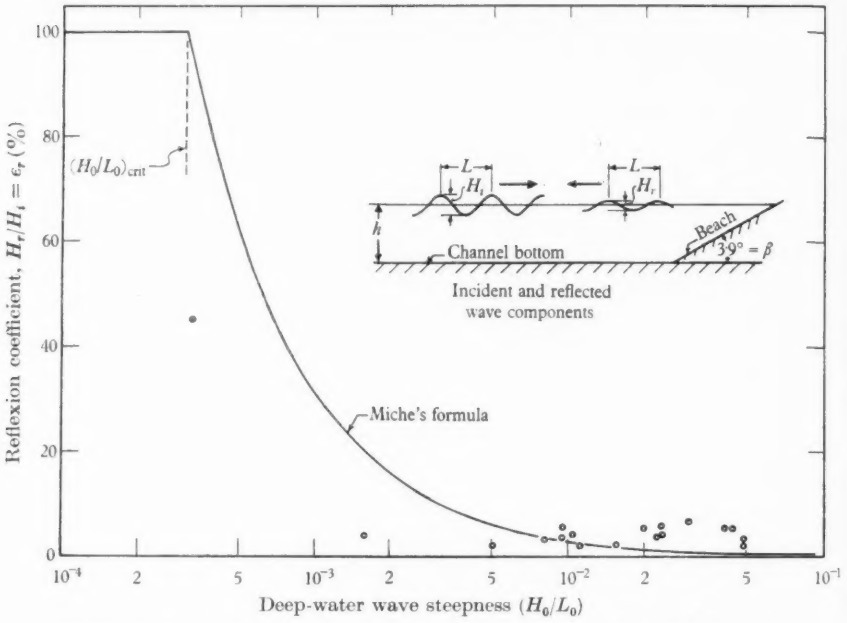

FIGURE 4. Comparison of measured reflexion coefficients with Miche's formula for a plane smooth beach.

slope of the beach β (actually, the linear theory is not applicable here). The corresponding deep-water progressive-wave steepness for a beach of small slope β is

$$(H_0/L_0)_{\text{crit}} = \sqrt{\left(\frac{2\beta}{\pi}\right)} \frac{\sin^2 \beta}{\pi}. \tag{7.2}$$

Miche further suggests that the reflexion coefficient ϵ_r, the progressive wave deep-water steepness H_0/L_0, and the *critical* progressive wave deep-water steepness $(H_0/L_0)_{\text{crit}}$ are related by

$$\epsilon_r = 1 \quad \text{for} \quad H_0/L_0 \leqslant (H_0/L_0)_{\text{crit}}, \tag{7.3}$$

$$\epsilon_r = \frac{(H_0/L_0)_{\text{crit}}}{H_0/L_0} \quad \text{for} \quad H_0/L_0 \geqslant (H_0/L_0)_{\text{crit}}. \tag{7.4}$$

Miche also modifies his formulas with an empirical coefficient to take into account the effect of roughness. While the arguments leading to equations (7.3) and (7.4)

seem to lack a real physical basis, the predictions agree quite well (at least in order of magnitude) with the measurements; see also Herbich (1956) for other measurements of reflexion.

7.2. *Attenuation*

Assume that the reduction in wave height (mainly due to viscous effects) as the wave progresses down the channel can be described by

$$H_2 = H_1 e^{-K'(x_2 - x_1)},$$

where H_2 and H_1 are the wave heights at stations x_2 and x_1 respectively, and K' is the 'attenuation coefficient' with the dimensions of reciprocal length. A theoretical expression for the attenuation coefficient was presented in § 4.2 (equation (4.8)). Two measurements of the attenuation coefficient were made by measuring the wave height (averaged over a half wavelength) at two stations

Run no.	H_1 (Station 14)* (cm)	H_2 (Station 51) (cm)	h (ft.)	T (sec)	L (ft.)	K'_{meas} (ft.$^{-1}$)	K'_{theor} (ft.$^{-1}$)
17	2·20	2·17	1·67	1·273	7·38	0·00038	0·00064
18	2·62	2·55	2·31	0·927	4·39	0·00070	0·00098

* Note. Stations are measured (in feet) from the mean position of the wavemaker with: $b = 2{\cdot}5$ ft., and $\nu = 1 \times 10^{-5}$ ft.^{2}/sec.

TABLE 1. Comparison of measured and theoretical attenuation coefficients

37 ft. apart along the channel (see Table 1), and it was found that the decrease in wave height over the constant-depth portion of the channel was so small (about 0·5 mm) as to be comparable with the absolute error. The conclusion is that, if the wave height is measured within 10 or 20 ft. of the wavemaker, the wave can be considered unattenuated for practical purposes. The wave characteristics and the values of the measured and theoretical attenuation coefficients are shown in Table 1.

The measured and theoretical attenuation coefficients are in better agreement than could have been expected when the small difference in wave height between the two stations is considered; particularly since the probable error in the measurement of H_1 and H_2 is of the same order as the difference of H_1 and H_2. It is interesting to note that some investigators (e.g. Benjamin & Ursell 1954, and Case & Parkinson 1957) had previously found measured attenuation coefficients which were greater than predicted by theory. One possible explanation for measured attenuation coefficients greater than theoretical predictions is that experiments performed on a small scale may include surface dissipation effects not included in the theory.

7.3. *Three-dimensional variations*

If all the generative and dissipative forces acting on the wave system were uniform across the channel, then no variation of wave height along the transverse dimension of the channel would be expected. In some cases effects were observed

which may be due to the following three-dimensional causes: (1) Symmetric or asymmetric seepage past the edges of the wavemaker, or similar seepage between the edges of the beach and the side-walls of the channel. (2) Dissipation along the walls of the channel. (3) Breaking, or backflow after breaking, of a wave which is not uniform across the channel. (4) Three-dimensional instabilities (see Schuler 1933). These effects were usually too small to be measurable; however, in some instances the variation of wave height with distance was not even approximately of the simple form (wave length $\frac{1}{2}L$) predicted in § 4.1, but wavelengths of $\frac{1}{4}L$ and $\frac{1}{2}L$ were also prominent. When this occurred, the wave motion was seen to be three-dimensional, although the reasons are not understood. A measurement of wave height *across* the channel for one of these cases showed the wave height varying approximately antisymmetrically about the centre of the channel. The difference in wave height at the two sides of the channel was of the order of 1 mm. Simple averaging of the wave height over a distance of $\frac{1}{2}L$ on the centre line of the channel was used to reduce three-dimensional effects, as well as reflexion effects. This averaging process also tends to reduce any higher harmonics in the wave height which may be introduced by higher harmonics in the motion of the wavemaker.

8. Test of wavemaker theory; discussion and conclusions

In order to test the theory for a piston wavemaker, the measured wave height was compared with the theoretical wave height as predicted by equation (3.9). In order to check the theory, it is necessary to measure wave height H, wave period $2\pi/\sigma$, water depth h, and wavemaker stroke S. Of these, the wave height cannot be found from a single measurement; the wave height was measured over a distance of at least $\frac{1}{2}L$, and the primary incident wave height, $H = 2\alpha$, was deduced by the analysis described in § 4.1. (There were six runs where the height variation was not even approximately of the form given by equation (4.3); see the discussion of § 7.3. In these cases, only a crude average over $\frac{1}{2}L$ was taken.) From the wave period $2\pi/\sigma$, the wavelength $2\pi/k_0$ was calculated by use of the formula $\sigma^2 = gk_0 \tanh k_0 h$; then the ratios H/S and $k_0 h$ were calculated. According to the theory, they should be related by equation (3.9).

The measurements were first made for small wave steepnesses

$$(0{\cdot}002 \leqslant H/L \leqslant 0{\cdot}03)$$

to test the validity of the small amplitude theory. The comparison with theory is shown in figure 5.

Each experimental point assigns a value of H/S to a value of $k_0 h$; for the same value of $k_0 h$ a theoretical value of H/S can be calculated, and the difference between this and the experimental value may be defined as the deviation between theory and experiment. Thus, for every point a percentage deviation is obtained. The deviation for the small wave steepnesses is found to be 5 %; however, much of this comes from a single measurement for which the percentage deviation is 32 % and the reflexion coefficient is 45 % (which is in any case too high for the correction of § 4.1 to be applicable). If this measurement is henceforth neglected, the average percentage deviation is 3·4 % below the theoretical curve. The scatter

about a mean curve drawn 3·4 % below the theoretical curve is of the order of 3 %, and this is a reasonable estimate for the experimental error since the errors in measurement of wave height, wavelength, water depth, and wavemaker stroke have each been estimated to be of the order of 2 %. Another source of scatter should be mentioned at this point. According to equation (4.3), the variation of wave height with distance should be sinusoidal. Actually, it is found that the envelope though smooth is not exactly of the predicted form. In particular,

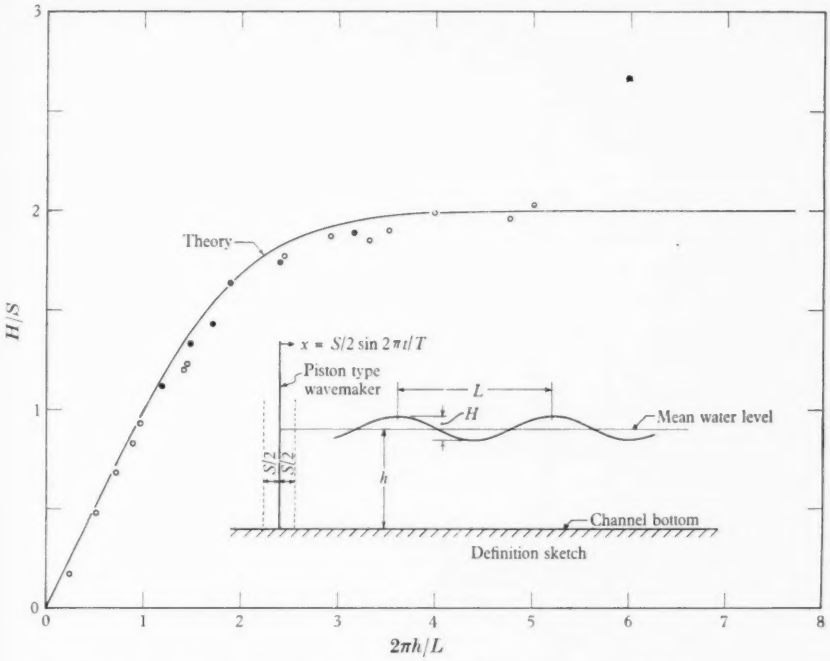

FIGURE 5. Test of wavemaker theory for small wave-steepnesses. ○, Experiments corrected for reflexion; ●, experiments not corrected for reflexion.

H_{max} and H_{min} do not repeat exactly at successive maxima and minima of the wave-height envelope. If the analysis of § 4.1 is, nevertheless, applied, there is an uncertainty in the wave height, leading to a scatter. If the mean uncertainty is defined as one-half the average of the differences of successive maxima plus one-half the average of the differences of successive minima divided by the average wave height, the mean percentage uncertainty is found to be of the order of 3 %. The reason for H_{max} and H_{min} not exactly repeating is not understood, although it is felt that it may be a result of interference with transverse reflexions.

The deviation between theory and experiment is measured by the systematic mean deviation of 3·4 %. This small deviation between theory and experiment may be partly explained by two effects, each tending to cause deviations in the observed direction. These are (i) leakage past the wavemaker, and (ii) finite-amplitude effects (see the next paragraph). Further improvements in equipment,

measuring technique and analysis would probably lead to even better agreement with theory, for sufficiently low waves.

To test the limitation which finite-amplitude effects place on the range of validity of the small-amplitude theory, measurements were also made on steeper waves ($0{\cdot}045 \leqslant H/L \leqslant 0{\cdot}048$). The comparison of these measurements with small amplitude theory is shown in figure 6. The mean deviation is 10 % below the theoretical curve; the mean scatter of the experimental results about a curve 10 % below the theoretical curve is again of the order of 3 %. The systematic deviation of 10 % is evidence that the effect of finite amplitude is to cause the

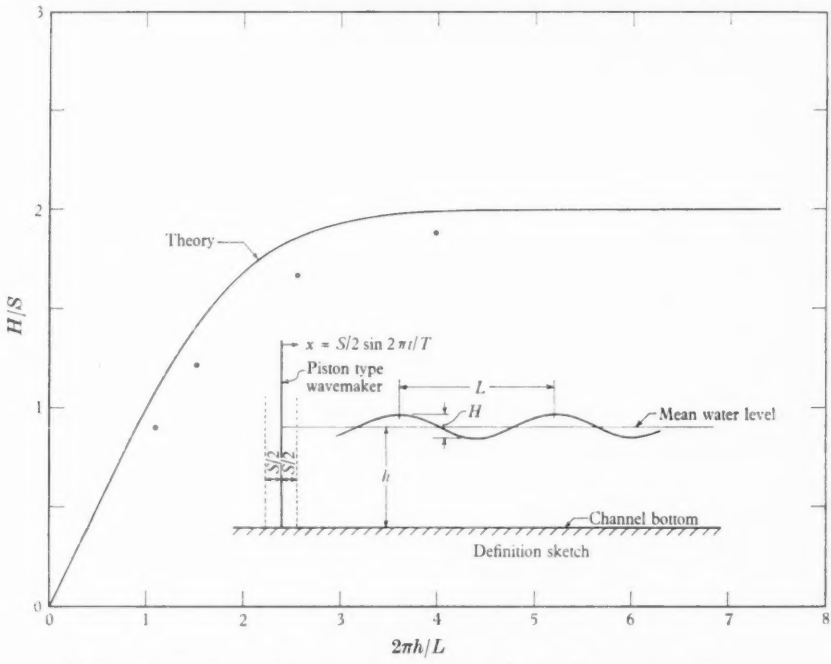

FIGURE 6. Deviation from wavemaker theory due to finite wave steepness. (All points are corrected for reflexion.)

wave height to be less than predicted by small amplitude theory. The larger reduction, however, observed in the Neyrpic experiments can only be partly attributed to finite-amplitude effects.

Two measurements of attenuation coefficients were made, and these were found to agree in order of magnitude with the theoretical predictions. In order to check the theory (based on a laminar boundary layer) with greater accuracy, it would be necessary to have a channel with a larger ratio of wetted area to cross-sectional area; at the same time the size of the equipment must be large enough to avoid surface tension effects.

The main limitation to experimental accuracy lies in the lack of a really efficient energy absorber. This study utilized a beach of small slope (3·9°) with a resulting amplitude reflexion coefficient less than 10 % in most cases. The reflexion was

allowed for in the analysis; however, the possible error would be reduced and the analysis simplified if a more efficient absorber could be found.

No explanation can be given for the rather large systematic deviation between theory and experiments found in the earlier Neyrpic experiment on a paddle wavemaker. The systematic deviation found in the present set of experiments on

no. of run	H (cm)	S (cm)	h (ft.)	T (sec)	$\frac{2\pi h}{L}$	$(H/S)_{\text{meas}}$	$(H/S)_{\text{theor}}$	ϵ_r (%)	(H_0/L_0)	Uncertainty in H/S (%)
1	2·67	5·66	2·01	3·23	0·51	0·48	0·51	4·1	0·00157	+
2	4·07	4·93	2·01	1·68	0·89	0·83	0·88	4·2	0·0103	+
3*	3·63	2·22	2·01	1·17	1·89	1·64	1·62	—	0·0170	—
4	2·56	1·37	2·01	0·92	2·92	1·87	1·92	2·1	0·0110	+
5*	1·77	1·34	2·19	1·42	1·49	1·33	1·37	—	0·00608	—
6	2·13	1·05	2·40	0·77	5·01	2·03	2·00	4·3	0·0230	2
7	2·01	1·03	2·40	0·79	4·76	1·96	2·00	3·9	0·0220	7
8	3·33	1·67	2·40	0·86	3·99	1·99	1·99	6·9	0·0293	6
9	2·88	1·51	2·40	0·92	3·52	1·90	1·97	5·9	0·0230	3
10*	2·71	1·56	2·40	1·12	2·40	1·74	1·82	—	0·0142	—
11*	2·03	1·82	2·40	1·73	1·19	1·12	1·15	—	0·00472	—
12*	2·40	1·68	2·40	1·36	1·71	1·43	1·52	—	0·00887	—
13	2·77	1·56	2·40	1·11	2·44	1·77	1·82	2·4	0·0153	0
14	2·10	2·25	1·58	1·63	0·97	0·93	0·97	2·1	0·00500	5
15	1·40	2·06	1·57	2·09	0·72	0·68	0·70	5·7	0·00957	1
16	0·81	4·80	0·63	3·67	0·24	0·17	0·25	45·1	0·00326	20
17	2·26	1·88	1·67	1·27	1·42	1·20	1·32	3·6	0·00944	2
18	2·72	1·45	2·31	0·93	3·31	1·85	1·96	5·7	0·0197	3
19	1·84	1·50	1·67	1·25	1·45	1·23	1·33	3·3	0·00799	1
20*	2·00	1·06	2·28	0·94	3·16	1·89	1·94	—	0·0145	—
21	4·77	2·54	2·00	0·79	3·98	1·88	1·99	2·2	0·0488	1
22	5·25	3·15	1·50	0·85	2·55	1·67	1·85	3·6	0·0485	3
23	5·47	4·50	1·00	0·95	1·51	1·22	1·39	5·4	0·0439	2
24	5·14	5·73	0·66	0·96	1·09	0·90	1·05	5·5	0·0409	2

Note:

(*a*) Runs 1 to 20 are for low wave-steepnesses ($0{\cdot}002 \leqslant H/L \leqslant 0{\cdot}03$).

(*b*) Runs 21 through 24 are for high wave-steepnesses ($0{\cdot}045 \leqslant H/L \leqslant 0{\cdot}048$).

(*c*) Values of H and H/S are corrected for reflexion effects except in those runs marked with superscript *, where the wave height envelope was not of the expected form. Values of ϵ_r and the 'uncertainty' were not calculated for these runs.

(*d*) Runs marked * are runs where only one maximum and minimum was obtained in the wave height envelope; therefore, the uncertainty could not be calculated.

Table 2. Summary of results

a piston wavemaker is much less. It is felt that the theory is also correct for paddle wavemakers (for small amplitude waves) and that the deviation found by the Neyrpic group can only be explained as the result of reflexion or of effects not accounted for in the theory (i.e. possibly leakage about the edges of the wavemaker, motion of the wavemaker which was not simple harmonic, or other effects).

The experiments constitute a close verification of the small-amplitude wave theory as applied to the simple case of a piston wavemaker, and provide evidence,

for the first time, that this theory may be used with confidence to calculate wave amplitudes (and probably also forces) in more complex cases where experimental verification is not available.

A summary of all measurements and calculations, for the present set of experiments on a piston wavemaker, is presented in Table 2.

This investigation was carried out at the Hydrodynamics Laboratory of the Department of Civil and Sanitary Engineering at the Massachusetts Institute of Technology and was sponsored by the Office of Naval Research, United States Department of the Navy under Contract no. Nonr–1841 (44).

REFERENCES

Bagnold, R. A. 1947 *Inst. Civil Engng*, **27**, 447–69.

Barber, N. F. & Ursell, F. 1948 *Phil. Trans.* A, **240**, 527–60.

Beach Erosion Board 1941 *Beach Erosion Board Technical Memorandum No.* 1.

Benjamin, T. B. & Ursell, F. 1954 *Proc. Roy. Soc.* A, **225**, 505–15.

Biésel, F. 1948 *Houille blanche*, **3**, 276–84.

Biésel, F. & Suquet, F. 1951 *Houille blanche*, **6**, 475–96, 723–37.

Case, K. M. & Parkinson, W. C. 1957 *J. Fluid Mech.* **2**, 172–84.

Cooper, R. I. B. & Longuet-Higgins, M. S. 1951 *Proc. Roy. Soc.* A, **206**, 425–35.

Greslou, L. & Mahe, Y. 1954 *Proc. Fifth Congr. Coastal Engineering, Grenoble*, pp. 68–84.

Havelock, T. H. 1929 *Phil. Mag.*, Series 7, **8**, 569–76.

Herbich, J. B. 1956 *Saint Anthony Falls Hydraulic Lab. Project Rep.* no. 44, Minneapolis.

Hunt, J. N. 1952 *Houille blanche*, **7**, 836–42.

Ippen, A. T. & Eagleson, P. S. 1955 *M.I.T. Hydrodynamics Laboratory Tech. Rep.* no. 18, 35–46.

Lamb, H. 1932 *Hydrodynamics*, 6th ed. Cambridge University Press.

Longuet-Higgins, M. S. 1953 *Phil. Trans.* A, **903**, 535–81.

Miche, A. 1951 *Ann. Ponts et Chauss.* **121**, 285–319.

Neyrpic 1952 *Houille blanche*, **8**, 779–801.

Schuler, M. 1933 *Zeit. angew. Math. Mech.* **13**, 443–6.

Stoker, J. J. 1957 *Water Waves.* New York: Interscience.

Suquet, F. 1951 *Houille blanche*, **6**, 475–96, 723–737.

Suquet, F. & Wallet, A. 1953 *Proc. Int. Hydraulics Convention, Minneapolis*, pp. 173–91.

Tucker, M. J. & Charnock, H. 1955 *Proc. Fifth Congr. Coastal Engineering, Grenoble*, pp. 177–87.

Ursell, F. 1952 *Proc. Roy. Soc.* A, **214**, 79–97.

The stability and transition of a two-dimensional jet

By HIROSHI SATO
Aeronautical Research Institute, University of Tokyo, Japan

(Received 23 April 1959)

A study was made of the transition of a two-dimensional jet. In the region where laminar flow becomes unstable, two kinds of sinusoidal velocity fluctuation have been found; one is symmetrical and the other is anti-symmetrical with respect to the centre line of the jet. The fluctuations grow exponentially at first and develop into turbulence without being accompanied by abrupt bursts or turbulent spots.

The response characteristics of laminar jets to artificial external excitation were investigated in detail by using sound as an exciting agent. The effect of excitation was seen to be most remarkable when the frequency of excitation coincides with that of self-excited sinusoidal fluctuations.

Numerical solutions of equation of small disturbances superposed on laminar flow were obtained assuming the Reynolds number as infinity. Theoretical eigenvalues and eigenfunctions are in good agreement with experimental results, thus verifying the existence of a region of linear disturbance in the two-dimensional jet.

1. Introduction

Theoretical investigations of the stability of boundary-layer-type flows are usually based on the assumption of a small disturbance. The fundamental equation is the well-known Orr–Sommerfeld equation, which has been solved under various boundary conditions.

In 1943, Schubauer & Skramstad (1948) verified the stability theory of laminar flow by their experiment on the boundary layer along a flat plate. The frequency, wave-number, amplification rate and amplitude function were in good agreement with theoretical predictions given by Tollmien, Schlichting and others. Since then, there has been little doubt concerning the validity of linearized theory, at least in the early stage of transition from laminar to turbulent flow.

Besides the boundary layer on a solid wall, there is another group of boundary layers. They are so-called 'free boundary layers', such as jets, wakes, separated layers, etc., in which the solid boundaries are absent in the flow field. The stability characteristics of free boundary layers are rather different from those of flows with a solid wall. The main reason for the difference seems to lie in the existence of a point of inflexion in the mean-velocity distribution of free boundary layers.

The laminar two-dimensional jet issued from a narrow slit was first investigated by Andrade (1939) using water. He found that when the Reynolds number was small, the observed mean-velocity distribution was in agreement with the theoretical 'similarity' solution. It was also pointed out that the jet became

unstable when the Reynolds number exceeded a certain value of the order of 10. The patterns of velocity fluctuations in a two-dimensional jet were clarified by the work of Brown (1935) in connexion with the sensitivity of jets to sound. His smoke pictures show vortex streets just like those observed in the wake of a cylinder. It was Savic (1941) who obtained an exact solution of the Orr–Sommerfeld equation for the two-dimensional jet. Although his solution was limited to the case of infinite Reynolds number, the wavelength and wave velocity of the oscillations were in good agreement with Brown's experimental results. Savic's comparison is, however, far from complete, because Brown did not give the mean-velocity distribution and Savic assumed that the observed pattern corresponded to neutrally stable fluctuations. More detailed numerical calculations of the wave-number and propagation velocity for various sets of the amplification rate of small oscillations were reported by Lessen & Fox (1955) in the case of infinite Reynolds number. Recently, Tatsumi & Kakutani (1958) have given the neutral curve for a wide range of Reynolds number. The present investigation was undertaken with the intention of comparing the experimental results with those existing theories. The first part of this paper gives measurements of the mean and fluctuating components of velocity in the transition region of two-dimensional jet. The next part describes some numerical solutions of the Orr–Sommerfeld equation, which were carried out after the above-mentioned theoretical work had been found unsatisfactory for comparison with the experiments, since the mean-velocity distribution assumed in the existing theories was not realized experimentally. In the final part, both experimental and theoretical results are compared, and the general features of transition of free boundary layers are discussed.

It was not intended to determine the critical Reynolds number for instability, since a completely different set of equipment was necessary for it. Experimental results for an air-jet at extremely low Reynolds number will be reported in the near future.

2. Experimental arrangement

2.1. *Two-dimensional jet*

The experiment was conducted on a jet issued from a rectangular slit. The general layout is shown in figure 1. The flow is accelerated from a settling chamber, passes through a parallel two-dimensional channel, and issues from a slit as a two-dimensional jet. The width $2h$ and the length l of the parallel channel were changed over five different sets of values in order to cover a wide range of Reynolds number as well as mean-velocity distribution at the slit. The breadth of the slit was 40 cm in all cases. The five combinations of width and length of channel used are tabulated in table 1. Detailed measurements were made using the combination of values denoted by SLIT 4·4 mm S and SLIT 6 mm L in table 1.

Air was supplied by an axial blower which was driven by a direct-current motor. The maximum wind-speed at the centre of the slit was 25 m/sec. Special care was taken to reduce disturbances at the test section. Velocity fluctuations were reduced by the use of a large settling chamber and damping screens. The ratio of the areas of settling chamber and two-dimensional channel was 67 for SLIT 6 mm L, for example, which was exceptionally large compared with the

contraction ratio of conventional wind-tunnels. The residual turbulence level at the slit was below 0·1%. Acoustic noise was also carefully reduced. The noise level at the test section was approximately 47 decibels, no predominant frequency component was found in the noise. Slight draught from windows and breeze due to the circulation of air inside the laboratory also tended to cause early transition of the jet. They were weak in the present experiments, but their effects were observed as a slow velocity fluctuation at the outer edge of the jet. The two-dimensional character of the jet was found to be satisfactory by checking the mean-velocity distribution.

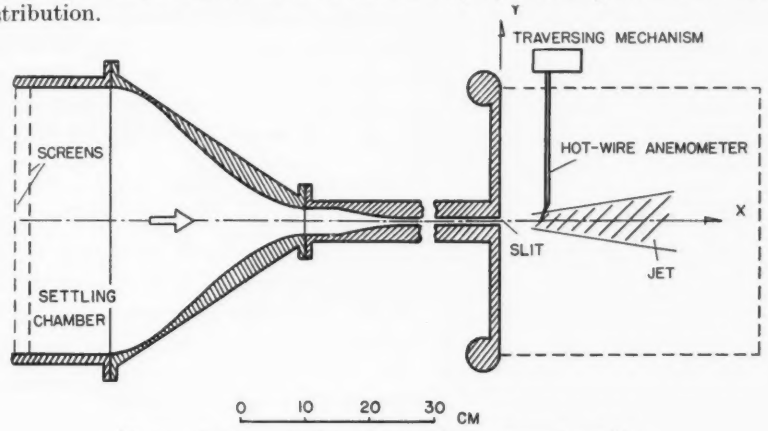

FIGURE 1. Layout of experimental two-dimensional jet.

Notation for experimental conditions	Width $2h$ (mm)	Length of channel l (mm)	Aspect ratio
SLIT 40 mm S	40	300	10
SLIT 10 mm S	10	300	40
SLIT 4·4 mm S	4·4	300	91
SLIT 10 mm L	10	1100	40
SLIT 6 mm L	6	1100	67

TABLE 1. Dimensions of channel and slit. The aspect ratio is the ratio of breadth to width of slit.

2.2. *Hot-wire equipment*

Hot-wire anemometers were exclusively used for measurements of both mean and fluctuating velocities. At first, a fine Pitot tube was used for the mean-velocity measurements. But when a large error was found due to the static-pressure variations across the layer and large inclination of flow in the transition region, all the data obtained by the Pitot tube were discarded.

Mean-velocity surveys by hot-wire were made for U and V, the longitudinal and transverse velocities (respective to the X- and Y-directions), while for the velocity fluctuations only the longitudinal component u was measured except in a few special cases. For the anemometers, use was made of 10% rhodium

platinum wire, 5μ in diameter and about 1·5 mm in length. Care was taken to prevent vibration of the wire. Characteristics of hot-wire anemometer at extremely low speed had previously been investigated in detail by the present author (1957); the calibration curve down to 20 cm/sec had been established, and errors occurring in the measurements in highly turbulent stream had been estimated. These results were fully utilized in the present investigation.

A full account of the electronic equipment may be found in a paper by Sato *et al.* (1954). The overall frequency response of hot-wire and amplifiers was flat from 20 to 20,000 c/s, provided the compensation was properly adjusted.

The hot-wire anemometers were traversed in the X- and Y-directions with micrometer screws. Accuracy of Y-positioning at different X-stations was approximately 0·1 mm, while relative position at the same X-station was read to within 0·01 mm by a precision dial-gauge. The accuracy of X-positioning was about 0·1 mm.

2.3. *Artificial excitations*

For the artificial excitation of fluctuations in the flow, use was made of a 10 W loudspeaker placed facing the test section. The intensity of sound was uniform throughout the test section and no noticeable resonance effect was detected in the frequency range from 30 to 800 c/s. The influence of the angle of incidence of the sound to the flow was very slight, but the direction of the sound was made perpendicular to the flow direction. The maximum intensity of sound from the loudspeaker was about 100 decibels including the background noise.

It was not attempted to determine the absolute intensity of sound exactly since the background noise changed from day to day and it was impossible to measure accurately the intensity of sound in the stream.

3. Experimental results

In this section, experimental data are presented without discussion. The comparison of experiment with theoretical results is deferred until § 5.

It should first of all be noted that the transition phenomenon was very unstable, that is, it was easily affected by various kinds of outside condition, for example, acoustic noise, draught, vibration, etc. In fact, the natural transition takes place as a result of the amplification of extremely small outside disturbances. These small disturbances change day by day and lie beyond our control. In spite of the careful arrangements described in § 2, the flow field in the transition region sometimes showed poor reproducibility. For this reason, an experimental accuracy of 10 % was the best attainable for certain measurements, while for most parts of the present experiments errors were expected to be of the order of 5 %.

3.1. *Natural transition*

The mean-velocity distribution in the laminar region of a jet depends on the condition upstream, that is, on the velocity distribution at the slit. When the length of channel l is long enough compared to the width $2h$ of the slit, the mean-velocity distribution at the slit is parabolic. On the other hand, when l is not large, the boundary layer on the wall of the channel is not thick enough to cover the whole cross-section; therefore the velocity distribution has a flat part at

the central region. Schlichting (1934) showed that the velocity distribution in the inlet region of laminar two-dimensional channel flow depends on a non-dimensional parameter $\nu l/h^2U_{00}$, where ν is kinematic viscosity and U_{00} is the velocity at the centre of the slit. Measured mean-velocity distributions at the slit for various combinations of l, h and U_{00} were in good agreement with Schlichting's calculations.

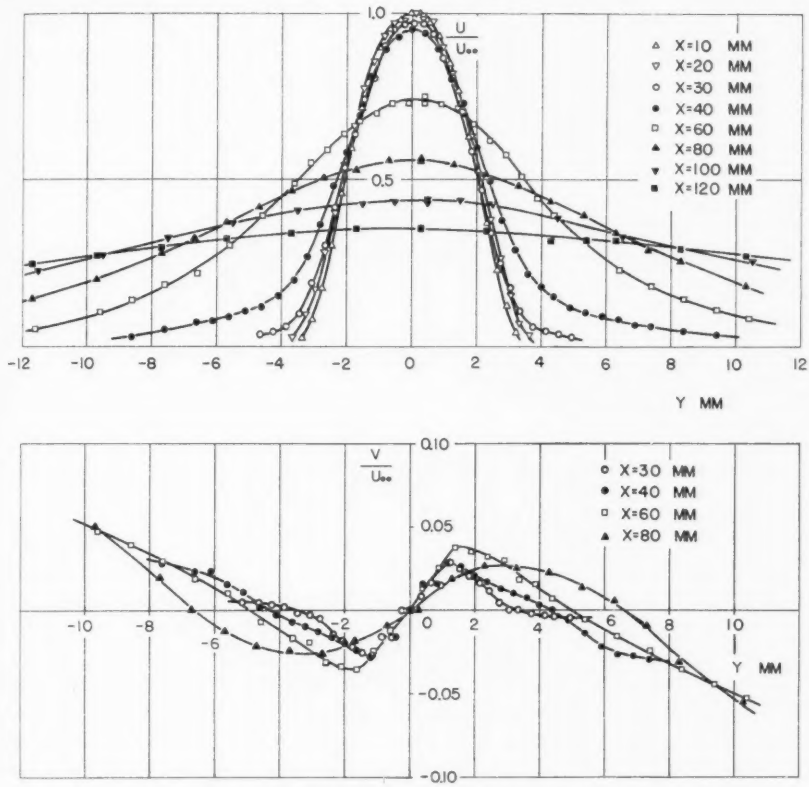

FIGURE 2. Mean-velocity distribution. SLIT 6 mm L, $U_{00} = 10{\cdot}0$ m/sec. X is measured from the slit.

Figure 2 shows an example of mean-velocity distribution for SLIT 6 mm L, $U_{00} = 10{\cdot}0$ m/sec and $\nu l/h^2U_{00} = 0{\cdot}18$. In this case, the distribution at the slit is approximately parabolic. The variation of mean-velocity distribution with respect to the distance downstream is described as follows.

Before transition takes place, the change of distribution is gradual, except at the outer region of the jet, where the increase of velocity is very great due to the sudden change of boundary conditions there. At the central part, velocity changes quite little. At about 3 to 8 times of total width of channel downstream from the slit, depending on the initial distribution, the variation of distribution becomes very marked, that is, a large decrease of central velocity and rapid broadening

of the jet takes place. Further downstream, the mean-velocity distribution becomes similar, regardless of the initial velocity distributions.

In the same figure, the distribution of lateral mean velocity is also shown. The magnitude of V is rather small compared with U, except at the edge of jet. This fact justifies the neglect of V in the theoretical treatment.

The above-mentioned general trend is more clearly demonstrated in figures 3 and 4. In figure 3, the half breadth b (i.e. the distance from the centre line to the point where U/U_0 is 0·5, U_0 being the mean velocity at the centre line) is plotted against $X/2h$. It is shown that the development of breadth is gradual at first and becomes directly proportional to $X/2h$ as the distance downstream increases. The

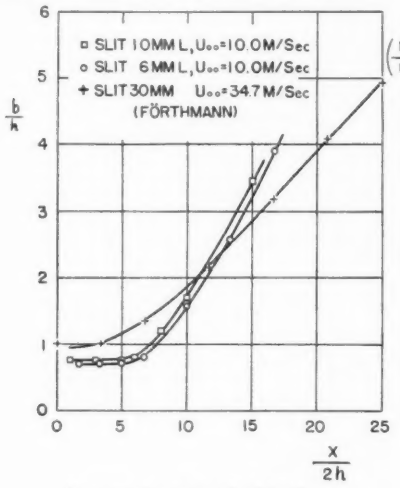

FIGURE 3. Spread of half breadth b of jet.

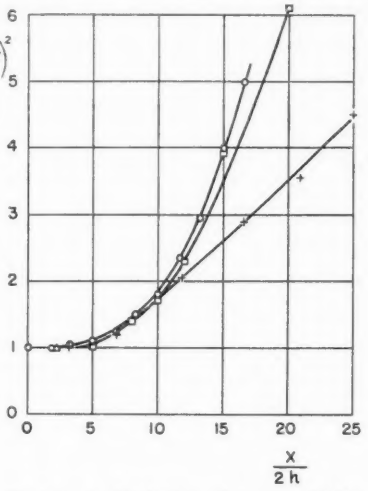

FIGURE 4. Variation of mean velocity on the centre line of jet.

experimental data of Förthmann (1934) are added. They show a tendency similar to the present results. In figure 4, the centre-line velocity U_0 is plotted in the form $(U_{00}/U_0)^2$ against $X/2h$. When $X/2h$ is small, U_0 stays approximately constant. As $X/2h$ increases, $(U_{00}/U_0)^2$ begins to increase and tends to become proportional to $X/2h$ when the distance downstream increases further. These linear relations seem to be characteristic of turbulent jet. The point of sharp rise of b/h or $(U_{00}/U_0)^2$ may correspond to the 'transition point'. The definition of the transition point is, however, quite arbitrary and the change from laminar to turbulent flow never takes place at a 'point'.

Figure 5 (plate 1) is a reproduction of oscillographic records of u-fluctuations at a small distance downstream from the slit. The wave-forms are nearly sinusoidal, higher frequency corresponding to higher wind-speed. At first, it was questioned that this regular pattern might be possibly caused by vibrations of the hot-wire anemometer or some kind of acoustical resonance in the channel. The former possibility was soon ruled out, since the change of hot-wire support caused no change in fluctuation patterns. The possibility of a resonance phenomenon was investigated by a small microphone. No distinct frequency component was found in the sound

at the test section and settling chamber. It was confirmed that transition of the jet is initiated by sinusoidal velocity fluctuations, which are weak at first and then amplified as the distance downstream increases. This was expected in view of the experiments on separated layers conducted by the present author (1956), because essential features of transition seem to be identical for both separated layer and jet. A remarkable difference, however, exists between the two. In the jet, two

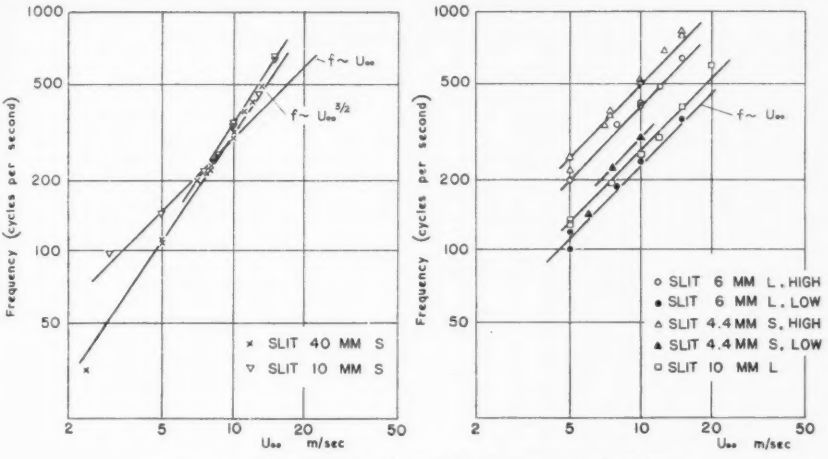

FIGURE 6. Frequency of sinusoidal velocity fluctuations plotted against central velocity at the slit U_{00}.

modes of fluctuation are found. They are different in frequency as well as in phase relation. Fluctuations shown in figure 5(A) are at higher frequency and are symmetrical with respect to the centre-line, while fluctuations shown in figure 5(B) are at lower frequency and are anti-symmetrical. In the separated layer, only one mode of fluctuation exists. The relative intensity of two modes of fluctuation is strongly dependent on the mean-velocity distribution. When $\nu l/h^2 U_{00}$ is large at the slit, i.e. the velocity distribution is nearly parabolic, the anti-symmetrical fluctuation prevails. On the other hand, when $\nu l/h^2 U_{00}$ is small, the anti-symmetrical fluctuation is not observed.

In figure 6, the fluctuation frequency is plotted against wind-speed. When the slit is wide, the frequency is approximately proportional to the $\frac{3}{2}$ power of wind-speed, as in the case of a pure separated layer (Sato 1956). A similar relation between frequency and wind-speed was found by Wehrmann & Wille (1957) for a circular jet. On the other hand, when the slit is narrow, as shown in the right half of the figure, the frequency is proportional to the wind-speed. These facts suggest that the frequency depends on the thickness of the shear layer rather than the width of the slit. When the slit is narrow, the velocity distribution at the slit is parabolic, and then the thickness of shear layer does not depend on the wind-speed; while for the wider slit, the thickness of shear layer is inversely proportional to the square root of wind-speed as in the case of a separated layer. This may explain the difference in the relation between frequency and wind-speed for different sizes of slit.

Simultaneous records of u-fluctuations at two different points separated in the X-direction revealed that the sinusoidal fluctuation is a progressive wave in the X-direction.

Figure 7 shows the energy spectrum of the u-fluctuations in the region where sinusoidal fluctuations are found. The scale of the ordinate is chosen arbitrarily, but the relative magnitude of two curves is represented correctly. At $Y = 0$, there is a single peak corresponding to the symmetrical fluctuations; while at $Y = 2$ mm, two peaks are observed at high and low frequencies.

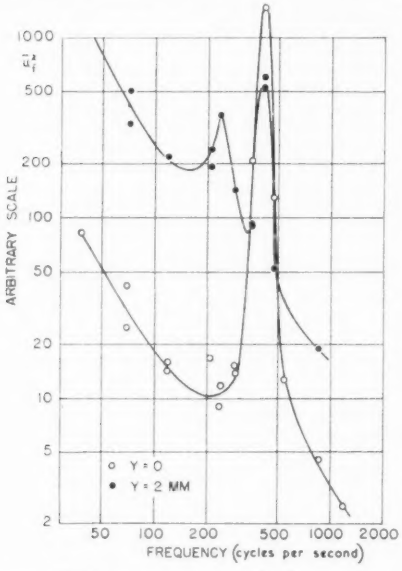

FIGURE 7. Energy spectrum of u-fluctuations. SLIT 6 mm L, $U_{00} = 10{\cdot}0$ m/sec, $X = 30$ mm.

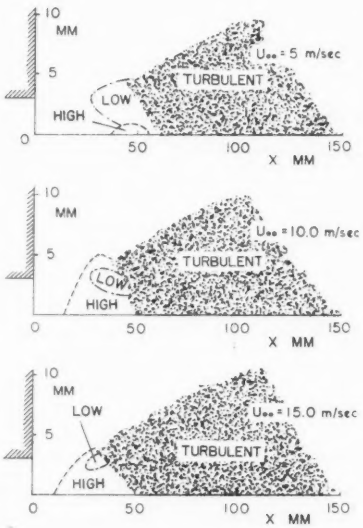

FIGURE 8. Map of patterns of u-fluctuations. SLIT 6 mm L.

After the existence of sinusoidal fluctuation was confirmed, a complete survey of the u-fluctuations was made in the transition region. Results of detailed observations of patterns of u-fluctuation are summarized in figure 8 as a map of various fluctuation patterns. Inside regions denoted by *HIGH* or *LOW*, sinusoidal fluctuations of high frequency (symmetrical) or low frequency (anti-symmetrical) are observed. It is shown that the extent of the region where there are two types of sinusoidal fluctuation depends on wind-speed—or more precisely, on mean-velocity distribution.

Wave-forms of the u-fluctuations at various X- and Y-positions are reproduced as figure 9 (plate 2). No marked bursts of turbulence are found in the wave-form. Development from sinusoidal into irregular fluctuation is gradual. Some intermittent bursts are observed only at the outer edge of the turbulent jet.

The distribution of the u-fluctuations is shown in figure 10, with SLIT 6 mm L and $U_{00} = 10{\cdot}0$ m/sec. The distribution is almost similar when X is small, and positions of peaks in the distribution approximately coincide with positions of maximum gradient in mean-velocity distribution. As the distance downstream

increases, values at peak and bottom become closer. The root-mean-square intensity, expressed as a ratio to U_{00}, reaches its maximum at about $X = 80$ mm and then decreases gradually. This is more clearly shown in figure 11, in which the

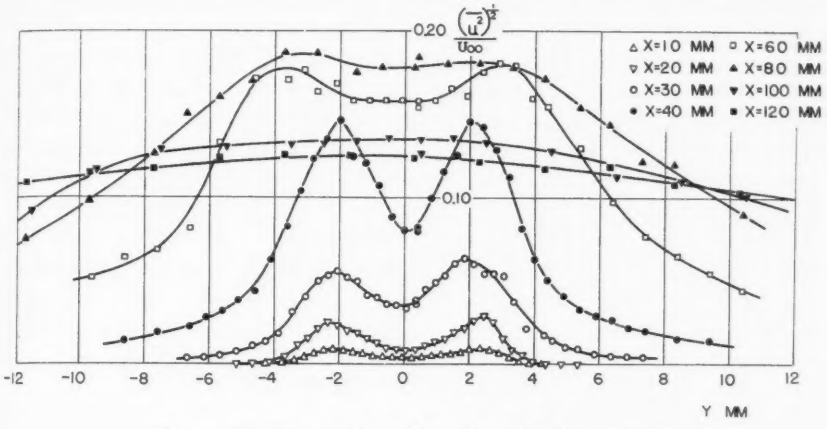

FIGURE 10. Distribution of intensity of u-fluctuations.
SLIT 6 mm L. $U_{00} = 10{\cdot}0$ m/sec.

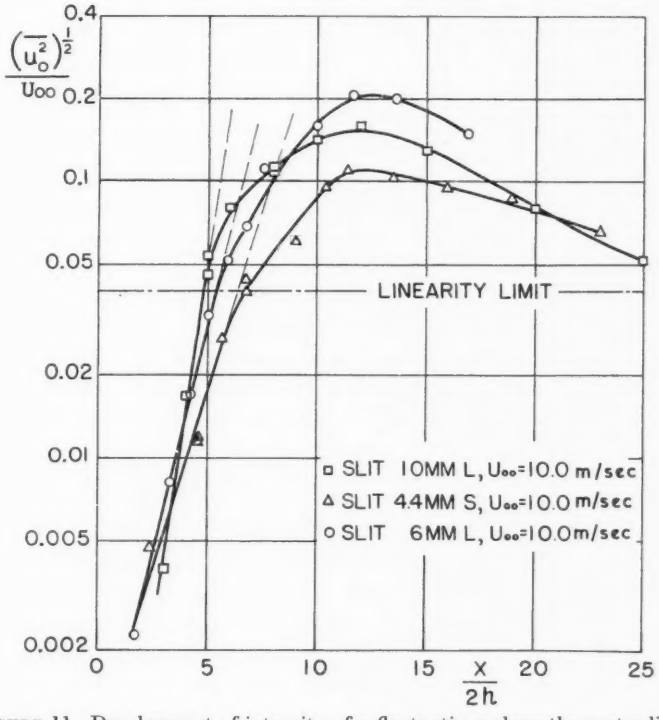

FIGURE 11. Development of intensity of u-fluctuations along the centre line in a logarithmic plot.

intensity on the centre line is plotted against $X/2h$. Three curves for three different sizes of slit indicate an identical general trend. In the logarithmic plot, the intensity on the centre line increases linearly, in other words, grows exponentially when $X/2h$ is small. When the intensity reaches approximately 0·04, the rate of growth becomes less and the maximum value appears at about $X/2h = 12$. This general trend suggests the possibility of classifying fluctuation field into two parts. Points on the X-axis where $(\overline{u^2})^{\frac{1}{2}}/U_{00} = 0{\cdot}04$—denoted as *LINEARITY LIMIT*—distinguish the region of exponential growth from non-exponential region. It is worth while to note that the point where the sharp increase of breadth of the jet takes place approximately coincides with the above-mentioned dividing point.

3.2. *Excited transition of jet*

The sound from the loudspeaker proved to be satisfactory as a means of artificial excitation. It had, however, some shortcomings. First, the sound could not be focused, so the excitation was distributed over the flow field. And

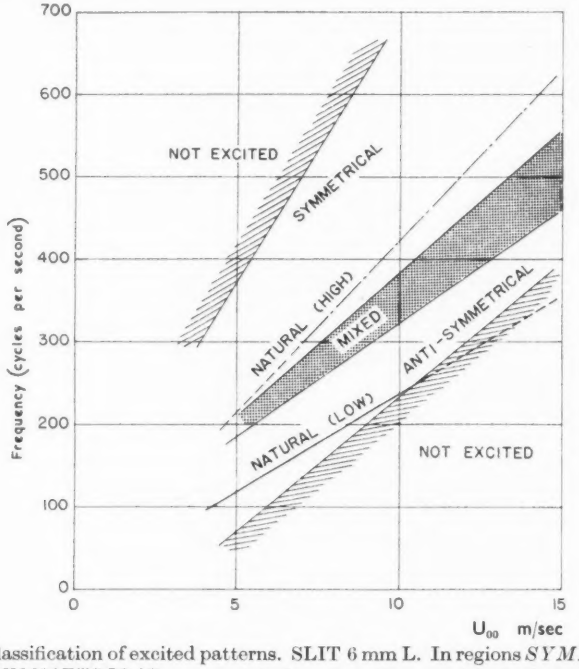

FIGURE 13. Classification of excited patterns. SLIT 6 mm L. In regions *SYMMETRICAL* and *ANTI-SYMMETRICAL*, symmetrical and anti-symmetrical sinusoidal velocity fluctuations are induced, respectively.

moreover, the relation between intensity of sound and velocity fluctuation is not fully understood in shear flows. Schubauer & Skramstad (1948) have pointed out that the effect of reflexion of sound from the tunnel wall can be fatal to a quantitative experiment. Fortunately, in the case of a jet, the flow field is open, and no effects of reflexion and resonance were found.

Before quantitative data are presented, some illustrative records of u-fluctuations are shown in figures 12 to 15. Figure 12 (plate 3) shows the effect of excitation on the u-fluctuations. Definite effects are found when the frequency of excitation is 390 or 420 c/s. In these cases, the frequency of induced velocity fluctuation is the same as that of the incoming sound. On the other hand, for lower (290 c/s) frequencies, the effect of excitation is hardly observed. It is thus confirmed that the rate of amplification strongly depends on the frequency of excitation. Results of systematic observations on this point are shown in figure 13. The limit of excitation, though it cannot be rigorously defined, varies approximately linearly with the wind-speed. In the region denoted by *MIXED*, both symmetrical and anti-symmetrical fluctuations are possible. Fluctuations excited by sound of higher frequency are symmetrical, while those by lower frequency are anti-symmetrical. Simultaneous records at $Y = 0$ and 2 mm with artificial excitations are reproduced as figure 14 (plate 3). With excitation of lower frequency (300 c/s), the amplitude of fluctuation is nearly zero at $Y = 0$, and with higher frequency (510 c/s), the fluctuation vanishes at $Y = 2$ mm.

The symmetricity of excited fluctuation is more clearly shown by the Lissajous figures in figure 15 (plate 4). Without excitation, the symmetrical fluctuation at high frequency is accompanied with anti-symmetrical fluctuation at low frequency. With excitations of 240 c/s and 330 c/s, the two signals are in adverse phase. At 330 c/s, the Lissajous figure is somewhat curved. With excitation at 420 c/s, the fluctuation is purely symmetrical, and at 600 c/s, the two modes are mixed. The figures at $Y = 2$ mm and 4 mm are completely different. Signals with excitation at 240 c/s are in the same phase and those excited at 420 c/s are almost in adverse phase.

It is apparent that there is a selective mechanism governing the two modes of fluctuation according to the frequency of excitation.

Effects of excitation on the mean velocity and intensity of fluctuation are shown in figures 16 to 18. It is noticed that the effect of excitation depends on its intensity. The background acoustic noise is around 47 decibels, and the following measurements were made with a sound intensity about 85 decibels including background noise. When the intensity of excitation is small, the effect is small, and at about 85 decibels the effect reaches its maximum and no longer increases with the increased intensity of excitation.

As shown in figure 16, effects on the mean velocity are not remarkable except at the outer part of jet. The increase of mean velocity there may be due to the increased intensity of fluctuation by excitation as shown in figure 17, which demonstrates the lateral distribution of intensity of fluctuation with and without excitations. The effect is remarkable again at 420 c/s. With this frequency, the wave-form of fluctuation is purely sinusoidal in the whole region of Y. The irregular slow fluctuation at the outer part of jet is suppressed, and a sinusoidal wave-form is observed even at $Y = 4$ mm. The phase inversion exists at about $Y = 3$ mm. With excitation at 330 c/s, which frequency is inside the region denoted by *MIXED* in figure 13, the intensity of fluctuation increases without changing the form of distribution. On the development of fluctuation along the centre line, effect of excitation is remarkable again when the frequency of sound

coincides with that of self-excited velocity fluctuation. This fact is conceivable since in a natural transition a sinusoidal fluctuation is supposed to be the disturbance which receives the maximum amplification. In figure 18, the intensity

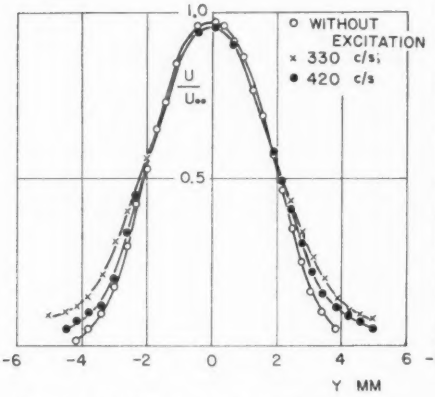

FIGURE 16. Effect of excitation on mean-velocity distribution. SLIT 6 mm L, $U_{00} = 10{\cdot}0$ m/sec, $X = 30$ mm.

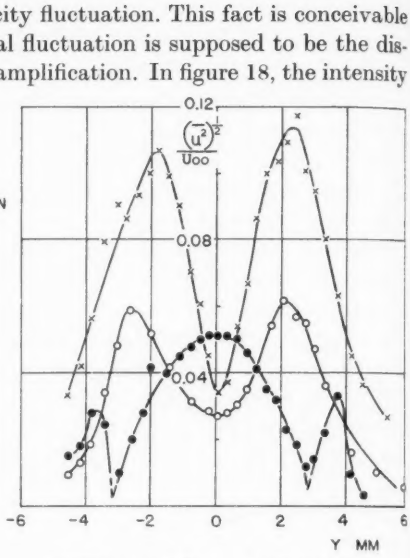

FIGURE 17. Effect of excitation on intensity of u-fluctuations. SLIT 6 mm L, $U_{00} = 10{\cdot}0$ m/sec, $X = 30$ mm.

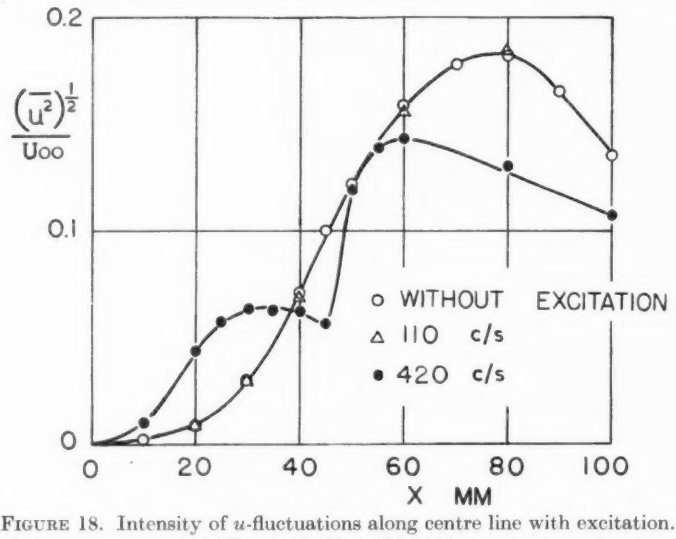

FIGURE 18. Intensity of u-fluctuations along centre line with excitation. SLIT 6 mm L, $U_{00} = 10{\cdot}0$ m/sec.

of fluctuation with excitation at 420 c/s has two maxima along the centre line. With excitation at 110 c/s, the effect of excitation is hardly recognized.

Distributions of spectral components of the u-fluctuations are shown in figure 19 in which $(\overline{u_f^2})^{\frac{1}{2}}$ is the root-mean-square value of spectral components. The maximum value of $(\overline{u_f^2})^{\frac{1}{2}}$ is taken as unity. In the upper two curves, the 180-degree

phase shift is observed at $Y = 0$, and with excitation at 330 c/s, another phase inversion is probable at $Y = 3{\cdot}3$ mm. In the case of a filter setting at 420 c/s, no excitation was applied because the intensity of the component at 420 c/s is rather large even without excitation. A large phase shift seems to take place at about $Y = 3$ mm.

The development of spectral components on the X-axis is shown in figure 20. The scale of the ordinate is taken arbitrarily for components of different frequency,

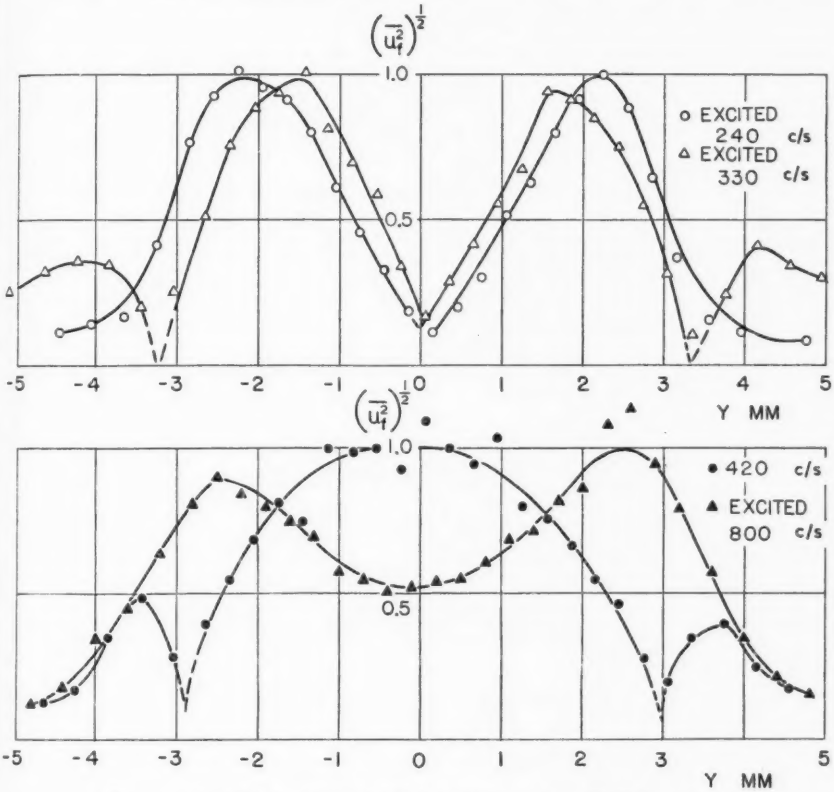

FIGURE 19. Distributions of spectral components. SLIT 6 mm L, $U_{00} = 10{\cdot}0$ m/sec, $X = 30$ mm.

while for the same frequency, the relative magnitude is correctly expressed. The intensity grows exponentially until it reaches the *LINEARITY LIMIT* which was explained above. Generally speaking, the growth rate deviates from being exponential earlier due to the presence of excitation. This is remarkably shown at the frequency 420 c/s. The exponential growth in this case is maintained only until $X = 20$ mm. From the gradient of each curve, the rate of amplification was calculated.

The damped fluctuation is not found in figure 20. In order to observe the damped fluctuation, the initial disturbance must be fairly large. Sound cannot

produce such a large disturbance at a specified point in the flow. In figure 21, the ratio of spectral components with and without excitation is plotted against frequency. The neutral frequency is determined as the point where the ratio becomes unity. Arrows under abscissa indicate the theoretical predictions which are described in detail in the next section.

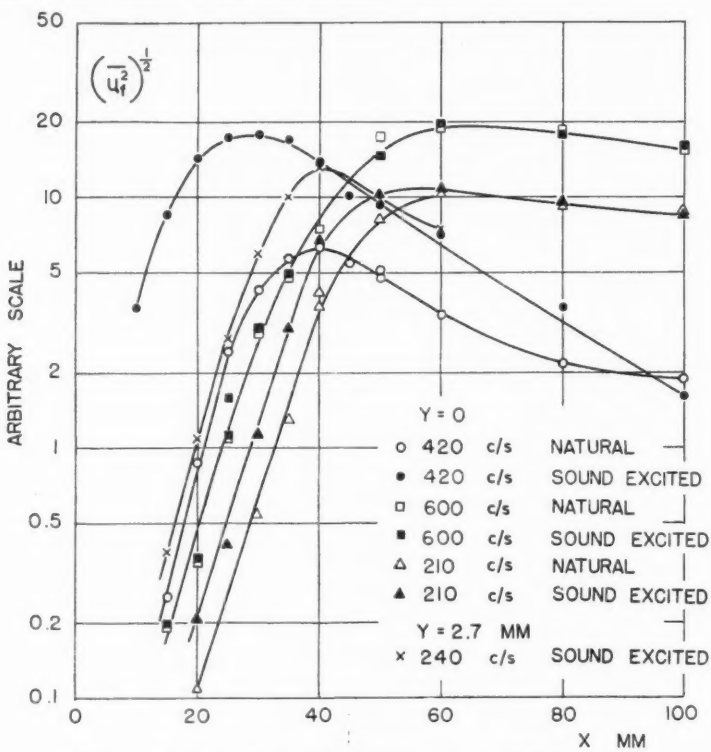

FIGURE 20. Growth of spectral components. SLIT 6 mm L, $U_{00} = 10{\cdot}0$ m/sec.

4. Theoretical considerations

The theoretical results on stability of two-dimensional jet obtained by Savic (1941) and others are found to be inadequate for the comparison with the present experiment, the main reason being the disagreement between the mean-velocity distribution assumed theoretically and the experimental one. In the theoretical work conducted so far, the basic flow was assumed to have the form $\mathrm{sech}^2 y$. This is the similarity solution for a fully developed laminar jet, but the transition usually takes place before this similarity distribution is established. This distribution may be realized before transition only when the Reynolds number is extremely low. The present experiments were made in the region of fairly high Reynolds number.

The work by Tatsumi & Kakutani (1958) shows that in the jet the wave-number of neutral oscillation varies little with Reynolds number if it is fairly

high. From this fact, we expect that the stability characteristics at high Reynolds number may well be approximated by those at infinite Reynolds number. Therefore, in this section Reynolds number is assumed infinity. Calculations are based on the Orr–Sommerfeld equation with various kinds of mean-velocity distribution which approximate the distribution obtained experimentally.

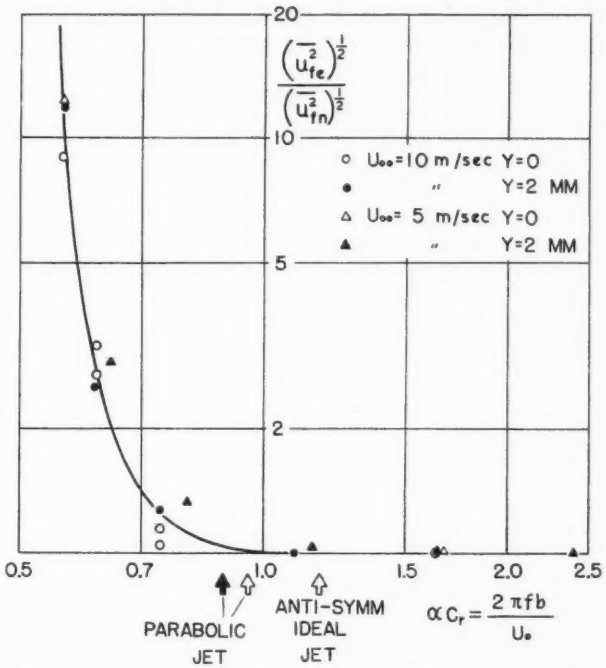

FIGURE 21. Determination of frequency of neutral oscillation. SLIT 6 mm L. $(\overline{u_{fe}^2})^{\frac{1}{2}}$ and $(\overline{u_{fn}^2})^{\frac{1}{2}}$ denote root-mean-square values of the components of frequency f with and without artificial excitation respectively.

4.1. *Mean-velocity distributions*

The mean-velocity distribution in the channel is characterized by a non-dimensional parameter $\nu l/h^2 U_{00}$ as mentioned before. The velocity distribution in a laminar jet is determined by the distribution at the exit of the channel and is, therefore, also characterized by $\nu l/h^2 U_{00}$. As far as the jet remains laminar, the velocity distribution may approach to the similarity distribution of the form $\mathrm{sech}^2 y$.

From the above considerations, the following expression for the velocity distribution seems reasonable:

$$\frac{U}{U_0} = \left[1 + sky^2\left(\frac{2-y^2-y^4}{1+ky^6}\right)\right]\mathrm{sech}^2 ay, \tag{1}$$

in which y is the lateral distance non-dimensionalized by the half-breadth b, k and s are parameters which characterize the distribution and $a = 0{\cdot}88136$ is a constant.

Expression (1) was obtained from purely geometrical considerations. The

second term in the bracket is the modification from the similarity distribution and is chosen to make the best fit to the experimental distribution. At the central part of jet, expression (1) should approximate the velocity distribution in the inlet region of the channel. The parameter s is chosen as 0·7 to obtain the best fit at large y.

Four typical distributions used for the calculations are shown in figure 22. Parameters for each distribution are tabulated in table 2.

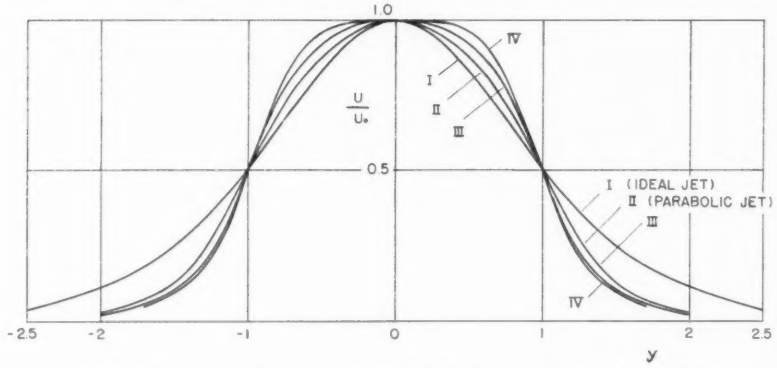

FIGURE 22. Theoretical mean-velocity distributions in jet used as basic flows for the calculation of small disturbances.

Notation	k	s	$U''(0)/U(0)$	Corresponding vl/h^2U_{00}	θ/b	Named
I	0	—	−1·5536	—	0·375	Ideal jet
II	0·1977	0·7	−1·0000	∞	0·255	Parabolic jet
III	0·3821	0·7	−0·4837	0·043	0·220	—
IV	0·5549	0·7	0	0·024	0·196	—

TABLE 2. Mean-velocity distributions used for the calculation of small disturbances.

4.2. *Disturbance equations*

The procedure of calculation presented here is one commonly employed. The basic flow is two-dimensional and is assumed to be a function of y only. The lateral velocity V is neglected. The disturbance velocities u and v are assumed to be functions only of x and y and of time. Quantities in the equations of motion and continuity are made non-dimensional by taking the half-breadth b and central velocity U_0 as units, these being assumed not to vary with x in the following theory.

Since u and v are small, the disturbance equations are linearized as the Orr–Sommerfeld equation, that is,

$$\left(\frac{U}{U_0}-c\right)(\phi''-\alpha^2\phi)-\frac{U''}{U_0}\phi=\frac{1}{i\alpha R}(\phi^{\mathrm{iv}}-2\alpha^2\phi''+\alpha^4\phi) \tag{2}$$

in which primes mean differentiation with respect to y. The function ϕ is defined as follows: if u and v are expressed in terms of a stream function ψ as

$$u=\partial\psi/\partial y, \quad v=-\partial\psi/\partial x,$$

then ψ is written as

$$\psi = \phi(y)\exp[i\alpha(x-ct)]. \tag{3}$$

Here α is the wave-number and c is usually complex in the form $c = c_r + ic_i$, in which c_r is the propagation velocity and c_i is a measure of the rate of amplification of disturbances.

When the Reynolds number $R = bU_0/\nu$ is very large, we have approximately

$$\left(\frac{U}{U_0}-c\right)(\phi''-\alpha^2\phi)-\frac{U''}{U_0}\phi = 0. \tag{4}$$

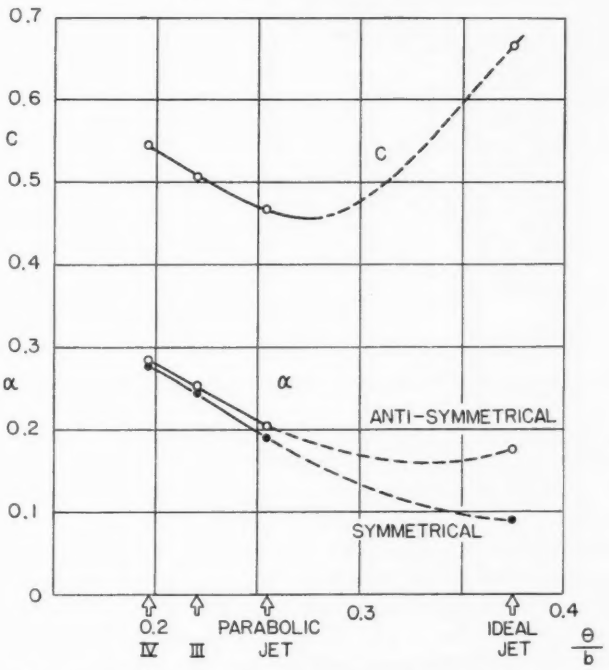

FIGURE 23. Propagation velocity c and wave-number α of neutral oscillations for various kinds of mean-velocity distribution.

The justification for using equation (4) in place of (2) is based on the fact that the stability characteristics of jet-type flows are insensitive to Reynolds number if it is high, in contrast with the case of flow with solid boundaries.

The solution of equation (4) was obtained by numerical integrations using the Runge–Kutta procedure.

4.3. *Neutral oscillations*

If $c_i = 0$, the disturbance is neither amplified nor damped. For the neutral oscillation, it is known that when the basic flow has an inflexion point in the velocity distribution, the propagation velocity c_r is equal to the mean velocity at the inflexion point. Thus, c_r is easily determined for each mean-velocity distribution from I to IV.

Boundary conditions for determining α and ϕ are, because of the symmetricity of basic flow,

$$\text{at} \quad y = \pm\infty, \quad \phi, \phi' \quad \text{are bounded;}$$

$$\text{at} \quad y = 0, \begin{cases} \phi = 0, & \phi' = 1 \quad \text{for symmetrical disturbances,} \\ \phi = 1, & \phi' = 0 \quad \text{for anti-symmetrical disturbances.} \end{cases}$$

The numerical integration was started at $y = 0$ and proceeded along the real axis, and was repeated until the boundary condition at large y was satisfied.

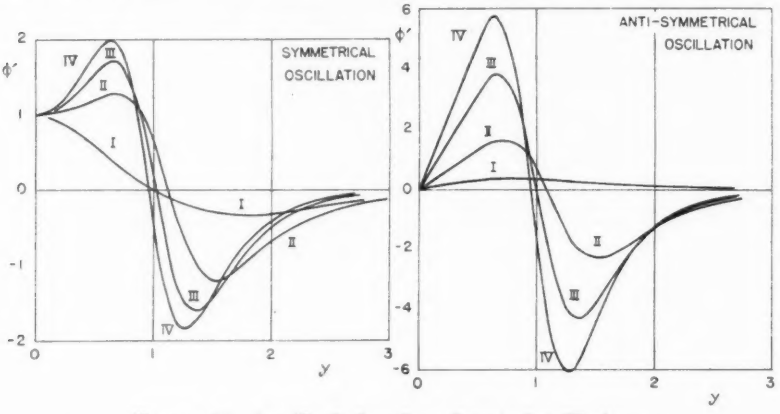

FIGURE 24. Amplitude function of neutral oscillations.

In figure 23, the propagation velocity and wave-number are plotted against θ/b, in which θ is the momentum thickness defined by

$$\theta = \int_0^\infty \frac{U}{U_0}\left(1 - \frac{U}{U_0}\right) dY .$$

θ/b is a form parameter which expresses the flatness of the mean-velocity distribution. θ/b is 0·375 for ideal jet and zero if the thickness of shear layer is zero compared with the breadth of jet. When θ/b is small, α is nearly the same for symmetrical and anti-symmetrical oscillations.

Figure 24 shows the calculated amplitude function ϕ' which expresses the u-fluctuation. The change of sign means a phase reversal at the point.

4.4. *Amplified oscillations*

When $c_i > 0$, the disturbance is amplified. Variables in equation (4) are complex and eigenvalues α, c_i and c_r are unknown. Equation (4) is separated into real and imaginary parts and integrated along the real axis with appropriate boundary conditions.

Figure 25 shows the values of α and c_i as a function of c_r on the parabolic jet (distribution II). Small circles denote calculated values. A great difference is seen for different mean-velocity distributions.

Before we compare these theoretical results with experiment, we have to make a transformation of time axis and X-axis by the relation

$$x = c_r t,$$

since the flow is stationary and the disturbance is amplified when it travels in the X-direction. Thus the spatial rate of amplification is $\alpha c_i/c_r$ instead of c_i.

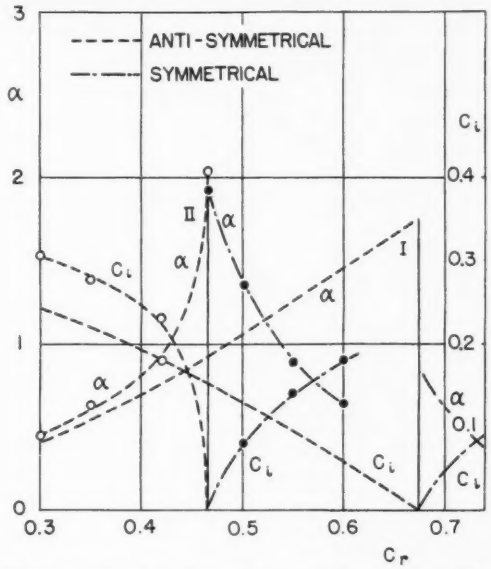

FIGURE 25. Wave-number α and amplification rate c_i of amplified oscillations.

5. Discussion

5.1. *Mean-velocity distribution*

The non-dimensional plot of mean-velocity distribution is shown in figure 26 in which $\nu l/h^2U_{00} = 0{\cdot}18$. It is apparent that for small values of X, the distribution is well approximated by curve II rather than I. Since, in this case, the sinusoidal velocity fluctuation is observed around $X = 20$ to 30 mm, the ideal jet is apparently not adequate as the basic flow for discussing the nature of small disturbances.

When the value of $\nu l/h^2U_{00}$ is smaller, the mean velocity has a flat distribution at the central core, and distributions III and IV well approximate cases where $\nu l/h^2U_{00} = 0{\cdot}043$ and $0{\cdot}024$, respectively. As a limiting case, when $\nu l/h^2U_{00} = 0$, the jet is really a separated layer.

At this point in the work, it was questioned that this kind of observed mean-velocity distribution might possibly be the result of a particular geometrical shape of slit. Since it seemed possible to change the distribution by modifying the shape of slit, measurements were carried out either making the edge of slit round or attaching small pieces to make the edge of slit sharper. These changes, however, little affected the distribution, and the ideal jet (distribution I) was not realized experimentally. Therefore, we returned to the 90°-edge slit because it is well defined. The reason why Andrade (1939) observed the ideal-jet distribution may have been due to the low Reynolds number in his experiment.

5.2. *Frequency of sinusoidal fluctuations*

The frequency of sinusoidal fluctuations in the jet has no simple relation with wind-speed. Figure 27 is a non-dimensional plot of frequency based on the total width of slit $2h$ and central speed U_{00}. The number $S_j = 2hf/U_{00}$ corresponds to the

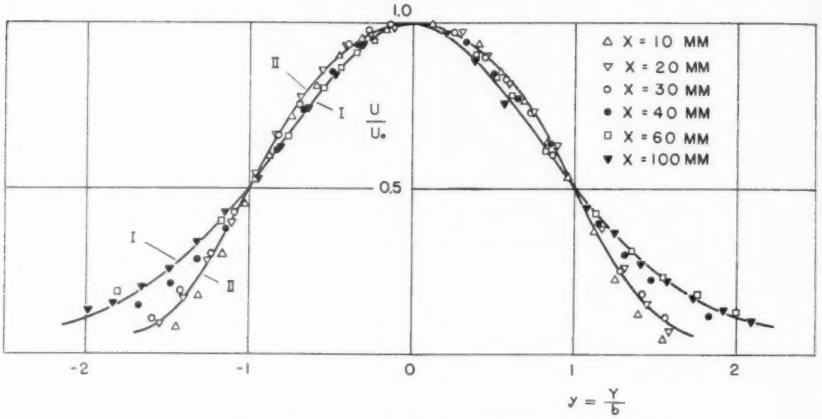

FIGURE 26. Non-dimensional plot of mean-velocity distribution.
SLIT 6 mm L, $U_{00} = 10{\cdot}0$ m/sec.

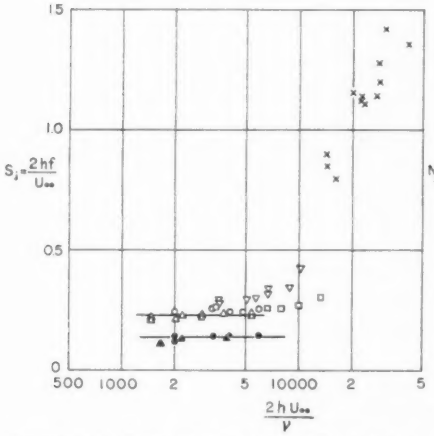

FIGURE 27. Frequency of sinusoidal velocity fluctuations, non-dimensionalized by the total width of slit $2h$.

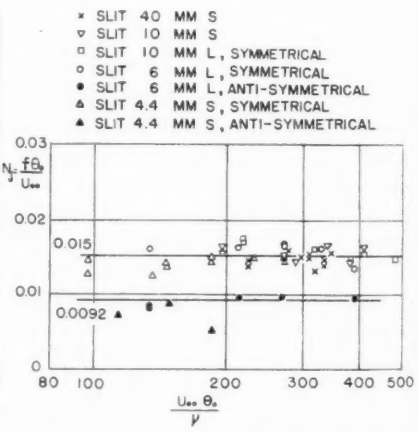

FIGURE 28. Non-dimensional frequency based on the momentum thickness at slit θ_0.

Strouhal number for the wake of a cylinder. Values of S_j for various Reynolds numbers are far from constant, except in the region of small Reynolds number. In the present series of experiments, vl/h^2U_{00} was large when the Reynolds number was small. In the Reynolds number range from 1500 to 8000, the mean-velocity distribution at the slit is parabolic; therefore the characteristic length remains

unchanged with U_{00}. This fact results in the constant value $S_j = 0{\cdot}23$ for symmetrical fluctuations and 0·14 for anti-symmetrical fluctuations.

In order to obtain more general relation between the fluctuation frequency and U_{00}, the momentum thickness of layer is a more suitable characteristic length than the width of slit. In figure 28, a new non-dimensional number $N_j = f\theta_0/U_{00}$ is plotted against the Reynolds number, θ_0 being the momentum thickness in one side at the slit. N_j is almost constant, and moreover it has the same value 0·015 for symmetrical fluctuation of higher frequency as shown in the separated layer (Sato 1956).

5.3. *Comparison with linearized theory*

The comparison of the experimental results with linearized theory is shown in figures 29 to 32. Experimental data used for the comparison are those with large values of $\nu l/h^2U_{00}$.

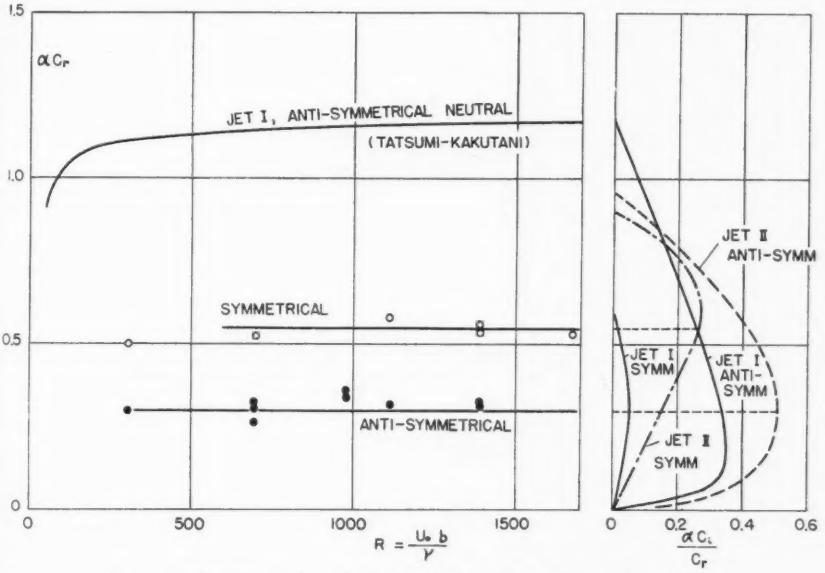

FIGURE 29. Comparison of theoretical and experimental results. Frequency of velocity fluctuation $\alpha c_r = 2\pi f b/U_0$.

Figure 29 shows the comparison of frequency non-dimensionalized by the half-breadth b and central speed U_0. In the right of the figure, theoretical results for the spatial rate of amplification $\alpha c_i/c_r$ at infinite Reynolds number are shown. The observed frequency is expected to correspond to that with maximum rate of amplification. Theoretical results by Lessen & Fox (1955) taking the ideal jet (Jet I) as a basic flow show no correlation with the experimental results. On the other hand, calculations in the preceding section based on the parabolic jet (Jet II) verifies the above statement, namely, that the frequency of sinusoidal fluctuation found in natural transition corresponds to the frequency of the small disturbance which receives maximum spatial rate of amplification theoretically.

The neutral curve given by Tatsumi & Kakutani gives the limit for the existence of amplified fluctuations in the ideal jet.

Figure 30 shows a comparison concerning the propagation velocity of artificially excited sinusoidal fluctuations. Generally speaking, the experimental points are closer to theoretical results for the parabolic jet (Jet II) than those for the ideal jet, and the agreement of both theoretical and experimental results is considered to be satisfactory.

Figure 31 shows the spatial rate of amplification $\alpha c_i/c_r$ plotted against frequency αc_r. For symmetrical fluctuations, experimental values for $\alpha c_i/c_r$ are almost twice and for anti-symmetrical fluctuations 4/5 times the theoretical results for the parabolic jet (Jet II). The reason for this discrepancy may be the slight misfit of assumed mean-velocity distribution, or may be due to the pressure gradient in the region of sinusoidal fluctuations.

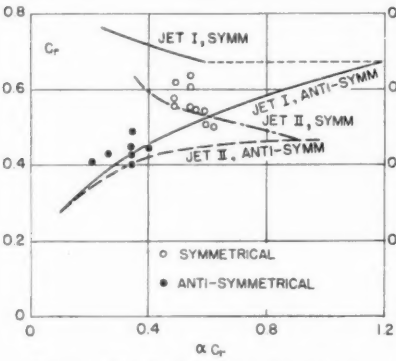

FIGURE 30. Propagation velocity c_r.

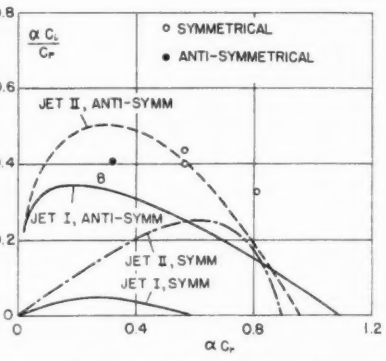

FIGURE 31. Spatial rate of amplification $\alpha c_r/c_i$.

The distribution of amplitude is shown in figure 32, taking the maximum value as unity. The experimental points are root-mean-square values of spectral components of u-fluctuations without artificial excitations. The theoretical curves are those of amplified oscillation based on Jet II with approximately maximum spatial rate of amplification. The agreement between experimental and theoretical results is satisfactory except near $y = 1$ for the symmetrical fluctuation. This disagreement may arise from the slight misfit of assumed basic flow (Jet II) to experimental distribution, because the theoretical amplitude function is extremely sensitive to the mean-velocity distribution as well as its derivatives.

From the preceding discussion, it is concluded that in the two-dimensional jet there is a region in which the velocity fluctuation field is well described by the linearized Navier–Stokes equations. Moreover, considering that the separated layer is an extreme case of a jet, a more general treatment of both flows is possible as shown by the present author (1959).

The regular pattern of sinusoidal fluctuations in a jet suggests a comparison of it with the laminar-boundary-layer oscillations in a boundary layer and the double row of vortices behind a cylinder.

Sinusoidal fluctuations in the free boundary layer seem to be essentially the same as those oscillations found by Schubauer & Skramstad in the boundary layer along a flat plate, except for two remarkable differences. One is the frequency of naturally excited oscillations. In the case of the boundary layer along a plate, the frequency lies on the second branch of the neutral curve as illustrated schematically in figure 33. This is a rather curious situation, because along the

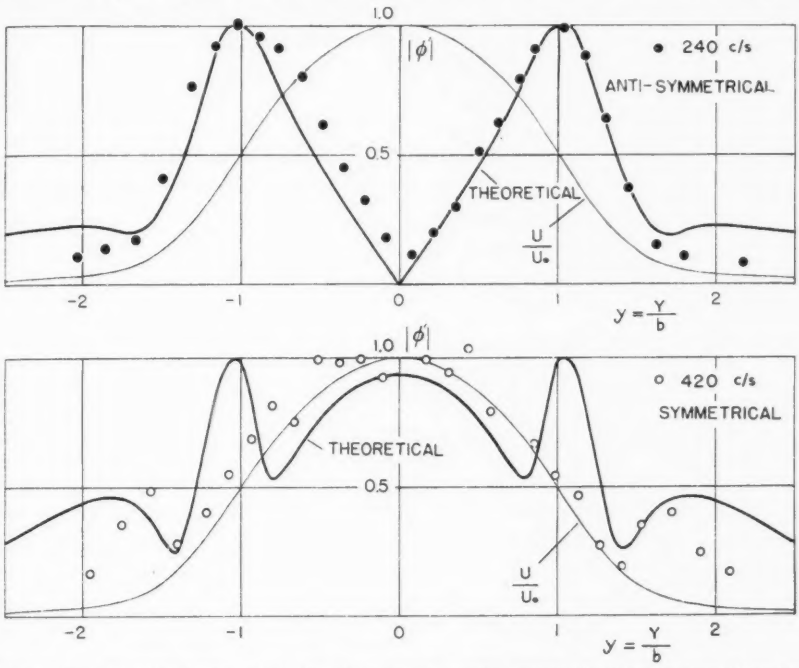

FIGURE 32. Amplitude function. In theoretical results, parabolic distribution (distribution II) is used. For anti-symmetrical fluctuations, $\alpha = 0{\cdot}62$, $c_i = 0{\cdot}28$ and for symmetrical fluctuation, $\alpha = 0{\cdot}88$, $c_i = 0{\cdot}142$.

neutral curve no fluctuation is supposed to be amplified. The explanation for this was given by Schubauer & Skramstad. According to their description, the velocity fluctuation with a definite frequency is amplified along a horizontal line inside the amplified zone in figure 33; and for given Reynolds number R_1, for instance, the frequency which receives maximum amplification lies just inside the amplified zone near branch II. Therefore, the frequency of naturally excited oscillation is found near branch II of the neutral curve.

The situation in the jet is quite different. Since the jet is created by the liberation of channel flow, its history does not begin at $R = 0$. The layer starts suddenly at R_0, for instance, and intensity of sinusoidal fluctuation reaches the *linearity limit* at R_1, which is not so much different from R_0 because of the great rate of amplification in the jet. Therefore, the frequency which receives maximum amplification lies approximately along a line of maximum amplification at R_0 or R_1. In other words, oscillations in the boundary layer along a plate are amplified

over a long history; on the contrary, the fluctuations in a jet are amplified in an instant. This is relevant to the difference in the rate of amplification, which is the second point of difference between these two kinds of fluctuation. The rate of amplification of fluctuations in a jet is roughly 10 times of that in a boundary layer along a plate. The development of velocity fluctuation in the 'non-linear' region may also be influenced by this great difference in the rate of amplification between 'fixed' and free boundary layers.

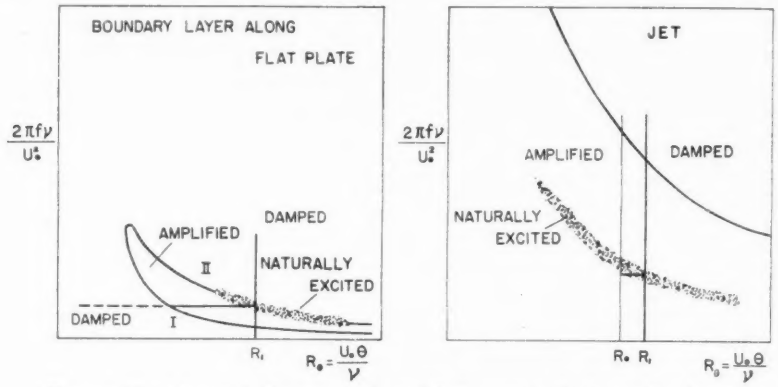

FIGURE 33. Schematic diagrams of amplified zones in the boundary layer along a flat plate and jet.

The vortex street formed in the wake behind a two-dimensional body seems to be essentially different from sinusoidal fluctuations in the jet. When we compare the fluctuations in jet and wake of cylinder we notice, at first, that the energy of sinusoidal fluctuations in the wake is far greater than that in the jet. The maximum root-mean-square intensity $(\overline{u^2})^{\frac{1}{2}}_{\max}/U_0$ of fluctuations in a wake reaches 0·16 according to the measurement by Roshko (1953). The value is approximately 4 times of that found in the jet. It is inconceivable that the fluctuation of such a high intensity as observed in the wake could be treated by linearized theory, unless there is a certain cause which suppresses the non-linear effect.

Another difference between the jet and wake is concerned with the growth of fluctuations. The sinusoidal fluctuation in the wake is usually decaying and no exponential growth has been observed so far. The mechanism of generating sinusoidal fluctuation in the wake is complicated since it seems to be associated with the periodical movement of separation point or stagnation point on the cylinder. At the present stage of knowledge, it seems to be impossible to treat the fluctuations in both jet and wake of a cylinder on a common basis.

5.4. *Transition region*

Generally speaking, the physical process taking place in the transition region of a jet is very similar to that of a separated layer. Especially when the slit is wide, the structure of the transition region of a jet is exactly the same as that of a separated layer. In other words, the shear layer at one side of a jet does not know the existence of the shear layer at the other side. In this case, the mean-

velocity distribution has a wide, flat core at the central part, and the two shear layers from the two sides meet after they become turbulent. In the present experiment, transition of this type is observed when $\nu l/h^2 U_{00}$ is smaller than about 0·015. For larger values of $\nu l/h^2 U_{00}$, the interaction of both shear layers becomes remarkable. Figure 11 shows the development of intensity of velocity fluctuations along the centre line in such a case. The linearity limit is about $(\overline{u_0^2})^{\frac{1}{2}}/U_{00} = 0{\cdot}04$, and the transition point defined by the linearity limit is found at $X/2h \doteqdot 5$–7. The intensity reaches a maximum at about $X/2h = 12$ and begins to decrease thereafter. The structural equilibrium in turbulent jet seems to be accomplished at $X/2h \doteqdot 30$–40.

Two non-dimensional quantities concerning mean velocity, $(U_{00}/U_0)^2$ and b/h, are, roughly speaking, proportional to $X/2h$ in the transition region, although other kinds of expression are also possible from the experimental data (figures 3 and 4). It is interesting to note that the proportionality relations hold in the fully turbulent jet (Townsend 1956). The transition point determined by the spread of jet is in good agreement with that determined by the linearity limit of intensity of u-fluctuations.

From the mean-velocity survey, the mean streamlines were determined experimentally. We notice that the two dividing streamlines—streamlines which start from the edge of the slit—shrink slightly at about $X/2h = 8$, when $U_{00} = 10{\cdot}0$ m/s with SLIT 6 mm L. They, of course, diverge as the distance downstream is further increased. This shrinkage of streamlines means an acceleration of the flow, which results in a decrease of static pressure there. In fact, the static-pressure distribution along the centre line measured under the same conditions shows a minimum at about $X/2h = 8$. The static pressure there is lower than that of the surrounding atmosphere by about 15 % of the dynamic pressure $\frac{1}{2}\rho U_{00}^2$. On the other hand, in the laminar layer and fully turbulent region, the difference of pressure is at most 2 % of the dynamic pressure. These peculiar features of streamlines and static pressure in the transition region might have some relations to the development of velocity fluctuations. But at present detailed relations are not known.

Concerning fluctuation patterns in the transition region of jet, no concrete conclusion is drawn except the non-existence of intermittent burst. The waveform of the u-fluctuations changes gradually from sinusoidal to the irregular pattern which is characteristic of turbulent flow. In the energy spectrum, peaks at definite frequency, which correspond to symmetrical and anti-symmetrical sinusoidal fluctuations, become lower and lower continuously, distributing the energy to other spectral components.

The classification of the transition region as shown in figure 11 is possible also in the case of a boundary layer along a flat plate. Figure 34 is a plot of the maximum intensity of u-fluctuations in each X-station against X. The data were taken from the experiment conducted by Schubauer & Klebanoff (1956) in the boundary layer on a flat plate. The linearity limit is apparently observed at about $(\overline{u^2})^{\frac{1}{2}}_{\max}/U_0 = 0{\cdot}06$. The variation of intermittency factor in the X-direction indicates that the transition point defined by the linearity limit corresponds approximately to the beginning of intermittent bursts. As shown in figure 34, the non-linear region starts at the linearity limit and ends when the intermittency factor

reaches 1. A classification of this kind into linear region, non-linear region and fully turbulent region may be possible for all flows which include transition.

On the possible cause of intermittent burst in the transition region, only conjectures have been made so far by many investigators. In the two-dimensional jet, no intermittent burst was found. The definition of 'burst' itself is so vague that one might call any instantaneous increase of amplitude of fluctuation a 'burst'. Regardless of the difference in definition, the burst in the free boundary layer is, at least, much less remarkable than that observed in the boundary layer

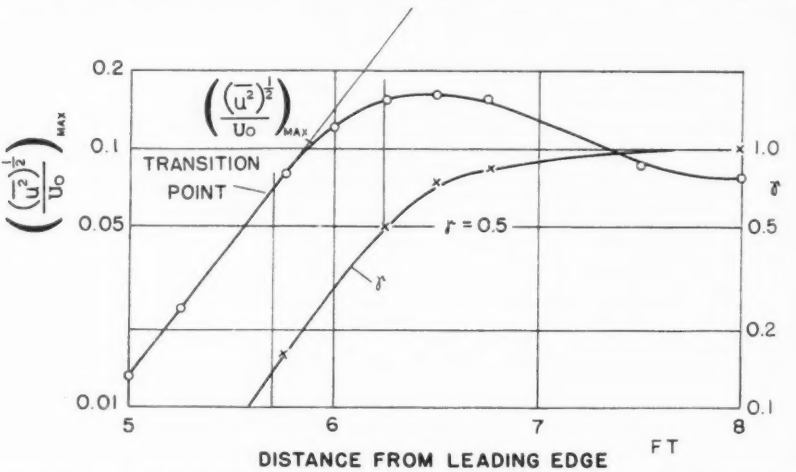

FIGURE 34. Logarithmic plot of maximum intensity of velocity fluctuation in boundary layer along a flat plate. Data after Schubauer & Klebanoff (1956).

on a plate. The reason why there are no bursts in the free boundary layer is not apparent, but it is mentioned with certainty that the generation of a burst is connected with the stability characteristics of the flow as well as with the difference of mean-velocity distribution of laminar and turbulent layers. First, neutral curves, for instance, of a jet and a boundary layer on a flat plate are different, as shown in figure 33. In the boundary layer on a plate, a velocity fluctuation at a certain wave-number is amplified only between the first and second branch of the neutral curve; while in the jet, fluctuation is amplified without limitations.

Concerning the mean-velocity distribution, distributions of laminar and turbulent layers are quite different in a boundary layer on a plate and in pipe flows. Therefore, if the rapid transition between these two states of mean-velocity distribution is required for the energy equilibrium in the layer, the 'fly-back' in mean-velocity distribution can be a cause of intermittent burst. In fact, Rotta (1956) has shown a close relationship between the intermittent burst and mean velocity. The presence of a solid wall in the flow can be another cause of complication in transition. It has various effects on the formation and development of two- or three-dimensional waves or vortices.

When free boundary layers are excited artificially, the above considerations

are enough when the intensity of excitation is low. With increased intensity of excitation, the amplitude of velocity fluctuation 'overshoots' as shown in figure 18. In this case, the velocity fluctuation rearranges itself, possibly by non-linear interactions, until certain equilibrium is reached. The wave-form becomes peculiar when the level of excitation is high.

The quantitative discussion in the transition region is still hardly possible. More systematic and extensive experiments are needed to understand details of Reynolds stresses, pressure fluctuations, dissipation terms and spectral components of u, v and w.

Theoretical investigations should be made parallel with experiments, considering the three-dimensional nature of velocity fluctuations, non-linear terms and viscous dissipation, and using the solution in the linear region as initial condition.

6. Conclusion

From the experimental and theoretical investigations concerning two-dimensional jet, the following conclusions have been obtained:

1. The similar mean-velocity distribution of a laminar jet was not established under the present experimental conditions.

2. When the slit is narrow, the frequency of sinusoidal fluctuations in the jet is almost proportional to the speed of the jet. When the frequency is non-dimensionalized by taking the maximum speed and the momentum thickness of layer as units, it is constant over a wide region of Reynolds number.

3. The sinusoidal fluctuations are similar to the oscillations found in a laminar boundary layer on a flat plate and dissimilar to the double row of vortices in the wake of a cylinder.

4. When the amplitude of sinusoidal fluctuations is not large, it grows exponentially. The frequency, propagation velocity, rate of amplification and amplitude function of fluctuation show good agreement with the predictions of linearized theory.

5. A distinct physical meaning can be given to the 'transition point' by defining it as a point where the growth rate of intensity of velocity fluctuation deviates from being exponential.

6. No intermittent bursts were found in the transition region.

7. The separated layer may be considered as an extreme case of a jet. Both flows belong to the 'jet-type boundary layer'.

The author appreciates the stimulating discussions and advice given throughout the whole course of the investigation by members of the Turbulence Research Group in Japan, which is directed by Professor Itiro Tani. Thanks are extended to Messrs Y. Onda and S. Kyoya who helped to carry out the experimental work, and to Miss M. Nakagawa who assisted in the numerical calculations. This work was financially supported by the Scientific Research Fund of the Ministry of Education of Japan.

REFERENCES

ANDRADE, E. N. DA C. 1939 *Proc. Phys. Soc.* **51**, 784.

BROWN, G. B. 1935 *Proc. Phys. Soc.* **47**, 703.

FÖRTHMANN, E. 1934 *Ingen.-Arch.* **5**, 42.

LESSEN, M. & FOX, J. A. 1955 *50 Jahre Grenzschichtforschung*, p. 122.

ROSHKO, A. 1953 *Nat. Adv. Comm. Aero., Wash., Tech. Note* no. 2913.

ROTTA, J. 1956 *Ingen.-Arch.* **24**, 258.

SATO, H., KOBASHI, Y., IUCHI, M., YAMAMOTO, K. & ONDA, Y. 1954 *Rep. Inst. Sci. Tech. Univ. Tokyo*, **8**, 271.

SATO, H. 1956 *J. Phys. Soc. Japan*, **11**, 702.

SATO, H. 1957 *Rep. Inst. Sci. Tech. Univ. Tokyo*, **11**, 73.

SATO, H. 1959 *Rep. Aero. Res. Inst. Univ. Tokyo* (to be published).

SAVIC, P. 1941 *Phil. Mag.* **32**, 245.

SCHLICHTING, H. 1934 *Z. angew. Math. Mech.* **14**, 368.

SCHUBAUER, G. B. & SKRAMSTAD, H. K. 1948 *Nat. Adv. Comm. Aero., Wash., Rep.* no. 909.

SCHUBAUER, G. B. & KLEBANOFF, P. S. 1956 *Nat. Adv. Comm. Aero., Wash., Rep.* no. 1289.

TATSUMI, T. & KAKUTANI, T. 1958 *J. Fluid Mech.* **4**, 261.

TOWNSEND, A. A. 1956 *The Structure of Turbulent Shear Flow*, p. 192. Cambridge University Press.

WEHRMANN, O. & WILLE, R. 1957 *Proc. Boundary Layer Symposium, Freiburg*, p. 387.

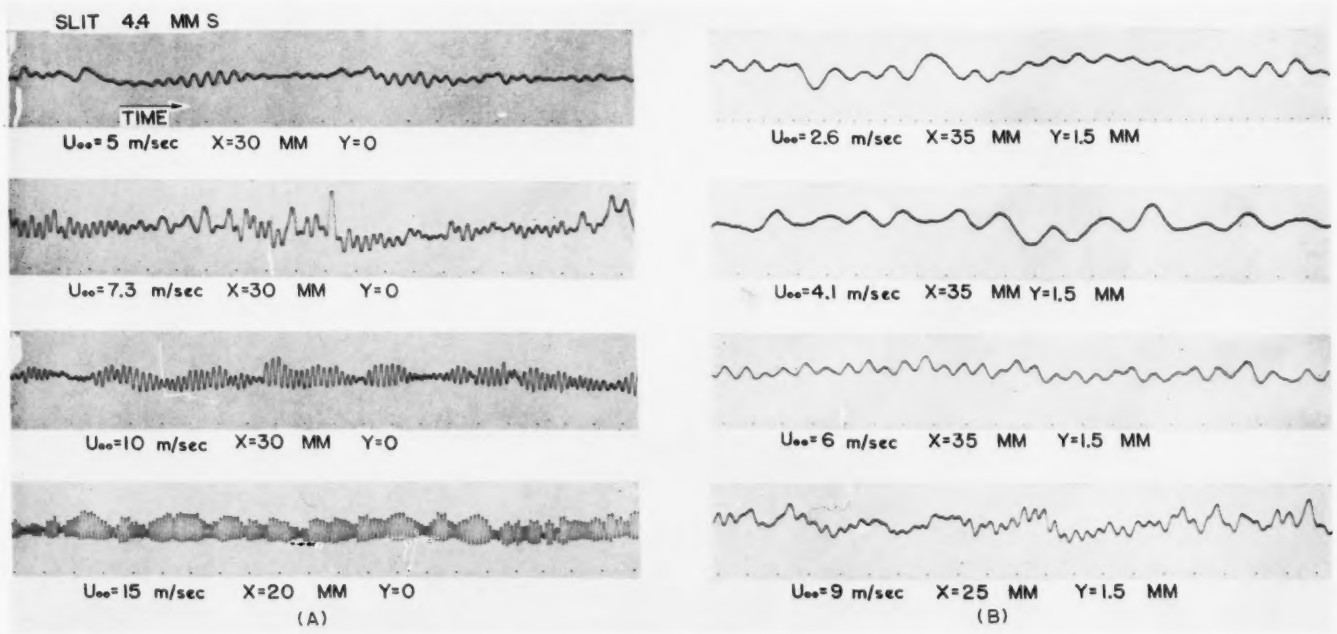
SLIT 4.4 MM S
TIME
U∞=5 m/sec X=30 MM Y=0
U∞=7.3 m/sec X=30 MM Y=0
U∞=10 m/sec X=30 MM Y=0
U∞=15 m/sec X=20 MM Y=0
(A)
U∞=2.6 m/sec X=35 MM Y=1.5 MM
U∞=4.1 m/sec X=35 MM Y=1.5 MM
U∞=6 m/sec X=35 MM Y=1.5 MM
U∞=9 m/sec X=25 MM Y=1.5 MM
(B)

FIGURE 5. Oscillographic records of u-fluctuations. Time interval between dots is 0·01 sec.

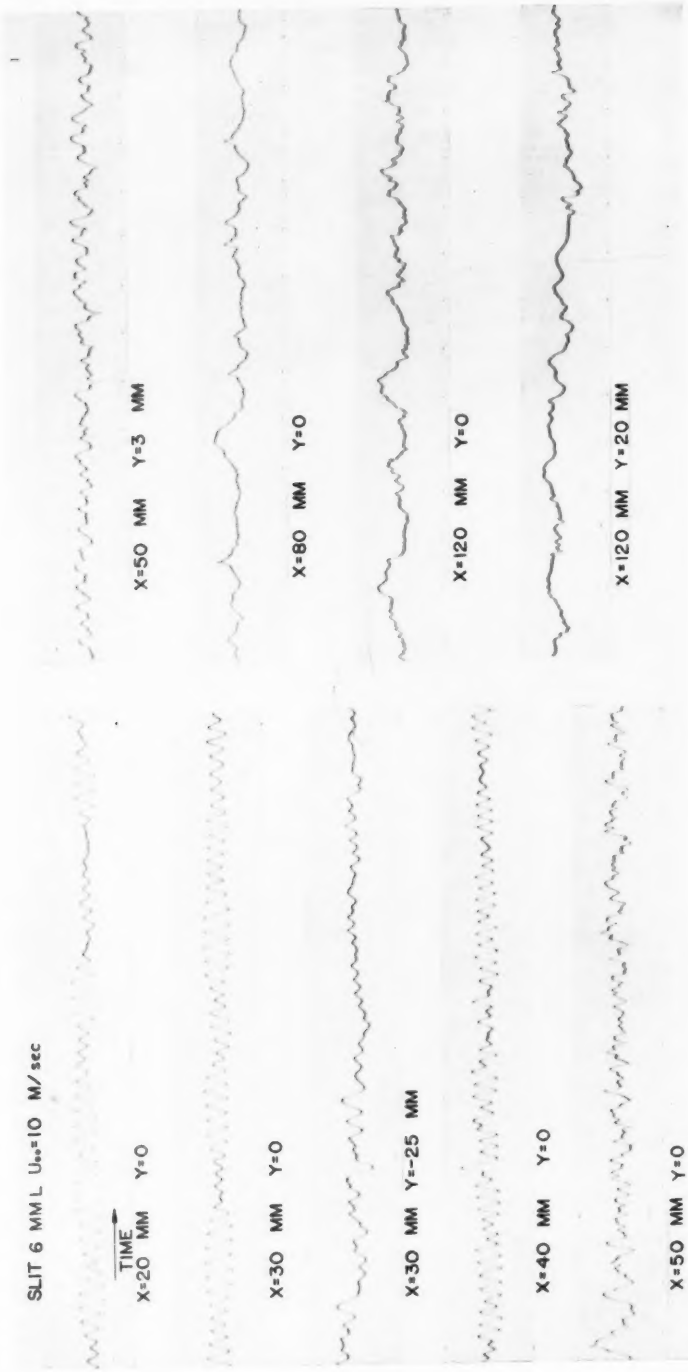

FIGURE 9. Development of u-fluctuations. Time interval between dots is 0·01 sec.

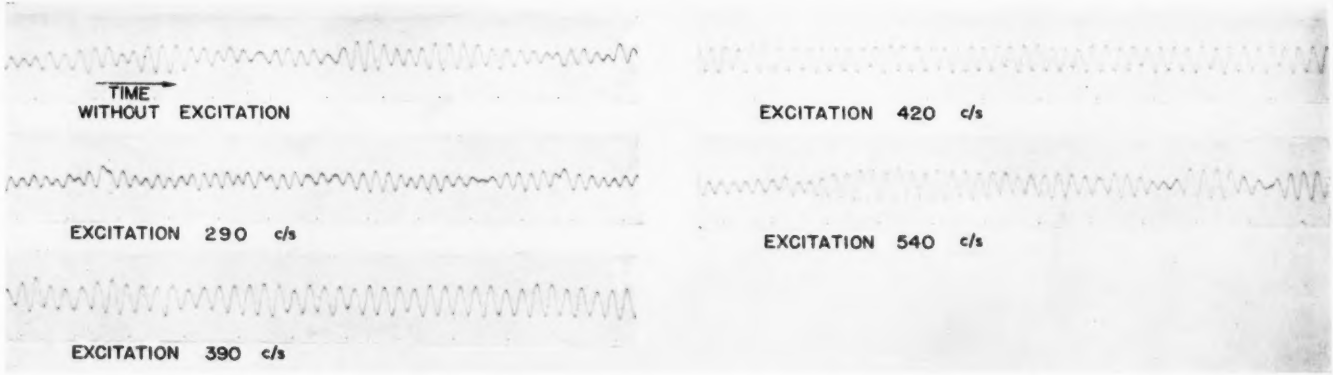

FIGURE 12. Effect of excitation by sound on wave-forms of u-fluctuations. SLIT 6 mm L, $U_{00} = 10{\cdot}0$ m/sec.

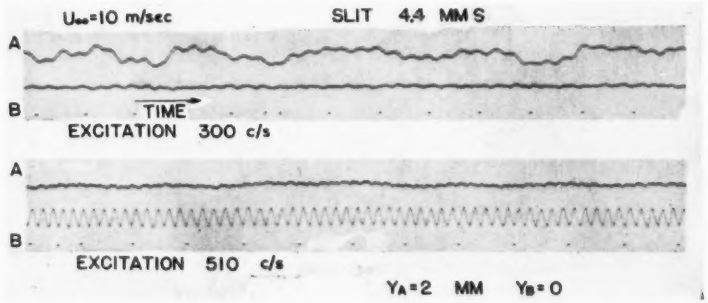

FIGURE 14. Simultaneous records of u-fluctuations at $Y = 0$ and $Y = 2$ mm.
SLIT 4·4 mm S. $U_{00} = 10{\cdot}0$ m/sec, $X = 20$ mm.

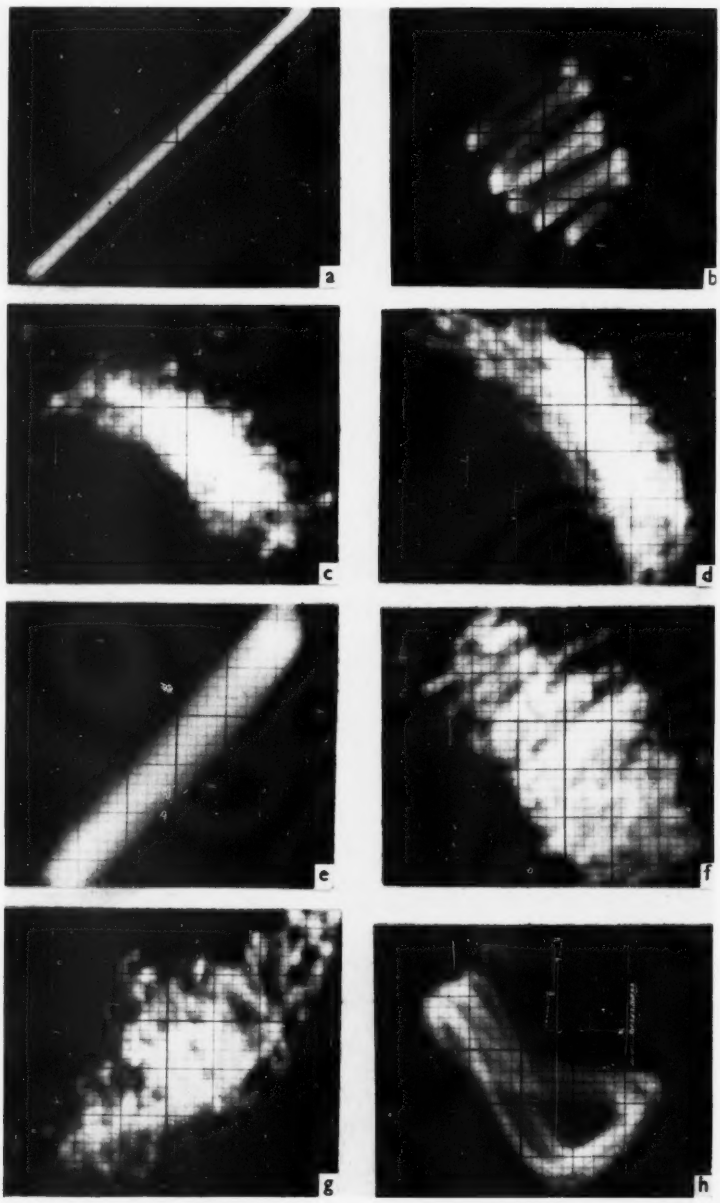

FIGURE 15. Lissajous figures of signals from two hot-wires placed apart in Y-direction. SLIT 6 mm L, $U_{\infty} = 10{\cdot}0$ m/sec, $X = 30$ mm. (*a*) Standard signals in the same phase. (*b*) $Y = \pm 1$ mm, without excitation. (*c*) $Y = \pm 1$ mm, excitation 240 c/s. (*d*) $Y = \pm 1$ mm, excitation 330 c/s. (*e*) $Y = \pm 1$ mm, excitation 420 c/s. (*f*) $Y = \pm 1$ mm, excitation 600 c/s. (*g*) $Y = 2$ mm, 4 mm, excitation 240 c/s. (*h*) $Y = 2$ mm, 4 mm, excitation 420 c/s.

A shallow-liquid theory in magnetohydrodynamics

By L. E. FRAENKEL
Aeronautics Department, Imperial College, London†

(Received 13 March 1959)

The non-linear and linear 'shallow-water' theories, which describe long gravity waves on the free surface of an inviscid liquid, are extended to the case of an electrically conducting liquid on a horizontal bottom, in the presence of a vertical magnetic field. The dish holding the liquid, and the medium outside it, are assumed to be non-conducting. The approximate equations are based on a small ratio of depth to wavelength, on the properties of mercury, and on a moderate magnetic field strength. These equations have a 'magneto-hydraulic' character, for in the shallow liquid layer the horizontal fluid velocity and current density are independent of the vertical co-ordinate.

Some explicit solutions of the linear equations are obtained for plane flows and for axi-symmetric flows in which the velocity vector lies in a vertical, meridional plane. The amplitudes of waves in a dish, and the amplitudes behind wave fronts progressing into undisturbed liquid, are found to be exponentially damped, the mechanical energy associated with a disturbance being dissipated by Joule heating.

The approximate non-linear equations for plane flow are studied by means of characteristic variables, and it appears that, because of the magnetic damping effect, there is less qualitative difference between solutions of the non-linear and linear approximate equations at large times than is the case when the magnetic field is absent. In particular, the characteristic curves depart only a finite distance from their 'undisturbed positions'.

1. Introduction

At the beginning of a general article on the magnetohydrodynamics of liquids, Lehnert (1952) describes some simple experiments made with mercury in a glass dish 20 cm in diameter and about 4 cm in depth. He points out that the surface waves generated by moving a peg in the liquid, or by tapping the dish, 'disappear' when a vertical magnetic field is imposed, and that whereas the liquid appears to have a 'water-like consistence' when there is no field, it 'acts as a thick syrup' when the field is applied.

In the present paper an attempt is made to describe such phenomena theoretically: to this end, stringent approximations have of course to be made. We examine the effect of a vertical magnetic field on long gravity waves in a shallow, inviscid, electrically conducting liquid. The problem is felt to be of

† Most of this work was done while the author was on leave of absence at the Guggenheim Aeronautical Laboratory, California Institute of Technology.

interest because its relative simplicity offers some hope of understanding: the fluid is incompressible and, in the case of mercury, has a substantial and uniform conductivity; the theory for zero magnetic field is well established (Lamb 1932; Stoker 1957); and experiments can be made without excessive difficulty.

The paper is in three parts. In the first, approximate governing equations are found by an order-of-magnitude analysis which is based on a small ratio of depth to wavelength, on the properties of mercury, and on a moderate field strength. As in the case of no magnetic field, two sets of equations are found: a non-linear set, appropriate when the wave amplitude and the depth of the liquid layer are comparable, and a linear set, appropriate when the amplitude is of even smaller order than the depth. With the derivation of these approximations, a simplified physical picture also emerges. To the lowest order, the horizontal components of velocity, electric field, and current density, and the vertical component of the magnetic field, are constant across the liquid layer (as this is traversed vertically); the remaining components vary linearly. To the scale of the field outside, where the material is assumed non-conducting, the liquid appears as a current sheet.

In the second part of the paper, a number of solutions of the linear equations are found; these describe, for plane flow and axial symmetry,† the motion of the free surface in a dish (in terms of modes or standing waves), and the motion due to travelling waves in a layer which is unbounded laterally. In the third part, 'non-linear effects' in plane flow are studied: although even the approximate, non-linear equations are still too difficult to be solved exactly, we obtain some idea of the nature of their solutions by using characteristic co-ordinates.

Theories related to our problem have, of course, been developed by other writers. Lundquist (1952) gave, among much else, a shallow-liquid theory based on infinite electrical conductivity. As he himself observed, and as will be seen below, this assumption is inappropriate to experiments on the laboratory scale. Stewartson (1957) developed a theory to describe some later experiments of Lehnert, and studied the steady viscous flow of mercury resting on a plane, an inner disk of which rotated, while the outer part remained at rest: the magnetic field was assumed to be zero or large.

It has been remarked above that the ordinary non-linear and linear shallow-water theories (Lamb 1932, §§ 187 and 169, respectively, or Stoker 1957, §§ 2.2 and 10.13) are 'well established'. It is certainly true that both theories have a long history, but they appear to remain a subject of dispute among workers of far greater authority than the present writer (see, for example, Stoker 1957, p. 342; Ursell 1953; and Longuet-Higgins 1958). Since these theories form the starting-point of the present paper, however, some discussion of their validity is essential. The relevant parameters are ϵ, the ratio of mean depth to wavelength, and δ, the ratio of amplitude to mean depth. There seems little doubt that if ϵ, measured from the shortest wave in some finite space-time domain, is small (breaking waves, bores, and hydraulic jumps being thus excluded), and δ is $O(1)$, the non-linear theory is a valid first approximation in that domain. If ϵ and δ are both small, the linear shallow-water theory is a valid first approximation. We

† 'Axial symmetry' here means not only symmetry about a (vertical) axis, but also that the velocity vector lies in a meridian plane.

further conclude, from the sources cited above,† that if ϵ and δ are both small, the non-linear approximation is an improvement on the linear one only if ϵ^2/δ is also small, since only then are the additional terms in the approximate non-linear equations larger than the terms neglected in both cases. (If ϵ^2/δ is $O(1)$ or large, the linear shallow-water theory is the more consistent approximation, and improvements upon it take a form different from that of the non-linear shallow-water theory.) There remains the question of bores and breaking waves. In the present paper we follow Lamb (1932, § 187) and Stoker (1957, § 10.6) in incorporating these in the framework of both approximate theories, but we regard this as an empirical procedure, in the nature of mathematical hydraulics, which provides a crude over-all description of the phenomena.

Part I. The Approximate Equations

2. The non-linear approximation

We write Maxwell's and the hydrodynamic equations in terms of the electric field strength $\mathbf{E}$, the magnetic induction $\mathbf{B}$ (which we also call the magnetic field strength), the current density $\mathbf{J}$, and the fluid velocity $\mathbf{V}$; T denotes time, P fluid pressure, ρ density of the liquid, ω charge density, κ dielectric constant, σ electrical conductivity, and μ magnetic permeability. Rationalized M.K.S.Q. units are used. The unit vector $\mathbf{i}_3$ points vertically upwards.

Neglecting displacement and convection currents, and the viscosity of the liquid, we have

$$\nabla \wedge \mathbf{E} = -\frac{\partial \mathbf{B}}{\partial T}, \qquad \nabla . \mathbf{E} = \frac{\omega}{\kappa}, \tag{2.1), (2.2}$$

$$\nabla \wedge \mathbf{B} = \mu \mathbf{J} = \mu\sigma(\mathbf{E} + \mathbf{V} \wedge \mathbf{B}), \quad \nabla . \mathbf{B} = 0, \tag{2.3), (2.4}$$

$$\rho \frac{D\mathbf{V}}{DT} = -\nabla P - \mathbf{i}_3 \rho g + \mathbf{J} \wedge \mathbf{B}, \quad \nabla . \mathbf{V} = 0. \tag{2.5), (2.6}$$

Let (X_1, X_2, X_3) be Cartesian co-ordinates, and consider a flow of conducting liquid bounded by a solid surface $X_3 = 0$, a free surface $X_3 = H(X_1, X_2, T)$, and the vertical wall $\mathscr{D}$ of a dish (which may be at infinity). A vertical magnetic field B_0 is applied, and for simplicity we suppose that this extends throughout space. The medium outside the liquid is assumed to be non-conducting and free of charge (although there may be weak surface charges on the interfaces). The initial disturbance is to be confined to some finite region. The boundary conditions are then as follows.

$$\text{As } \mathbf{X} \to \infty, \qquad \mathbf{B} \to \mathbf{i}_3 B_0, \quad \mathbf{E} \to 0; \tag{2.7a, b}$$

$$\text{on } X_3 = 0, \qquad V_3 = 0; \tag{2.8}$$

$$\text{on } X_3 = H, \qquad P = 0, \quad \frac{\partial H}{\partial T} + V_1 \frac{\partial H}{\partial X_1} + V_2 \frac{\partial H}{\partial X_2} - V_3 = 0. \tag{2.9a, b}$$

Also, the normal component of velocity must vanish on $\mathscr{D}$; and the vector $\mathbf{B}$ and the tangential components of $\mathbf{E}$ must be continuous across the interfaces $X_3 = 0$, H and $\mathscr{D}$, continuity of the tangential components of $\mathbf{B}$ following from the

† Dr Ursell has also been kind enough to show the present writer how the main conclusions of his 1953 paper may be derived much more simply.

requirement of finite current density when the conductivity is finite. (Here we have assumed that the magnetic permeability, μ, is constant throughout the field. If μ is assigned different values in the liquid and outside it, the tangential components of $\mathbf{B}/\mu$ must be continuous: the corresponding changes, in the theory which follows, are easily made.)

We now introduce the small parameter $\epsilon = H_0/L$, where, in the initial conditions, H_0 is a typical depth and L a length characteristic of changes in the horizontal directions, and seek the leading term in the asymptotic expansion of each dependent variable in powers of $\epsilon^{\frac{1}{2}}$. The other parameters of the problem are the magnetic Reynolds number N, and a dimensionless field strength K:

$$N = \mu\sigma L\sqrt{(gL)}, \quad K = \frac{B_0^2\sigma L}{\rho\sqrt{(gL)}}.$$

For mercury $N \doteqdot 4L^{\frac{3}{2}}$ (L in metres): it is therefore assumed that for laboratory experiments $N \leqslant O(1)$. The order of K will be so chosen that the ordinary theory ($B_0^2\sigma = 0$) falls within the range of our approximation: in the momentum equation the magnetic force is not to dominate the gradient of hydrostatic pressure. We therefore assign to the hydrodynamic variables and to the natural time the orders which apply when $B_0^2\sigma = 0$ (see Stoker 1957, § 2.4). Dimensionless variables of $O(1)$ are introduced by

$$\left.\begin{aligned} &\mathbf{X} = (Lx_1, Lx_2, \epsilon^{\alpha}Lx_3), \quad T = \epsilon^{-\frac{1}{2}}\frac{L}{\sqrt{(gL)}}t, \\ &\mathbf{V} = (\epsilon^{\frac{1}{2}}\sqrt{(gL)}\,v_1, \quad \epsilon^{\frac{1}{2}}\sqrt{(gL)}\,v_2, \quad \epsilon^{\frac{3}{2}}\sqrt{(gL)}\,v_3), \quad P = \epsilon\rho gLp, \quad H = \epsilon Lh, \end{aligned}\right\} \tag{2.10}$$

where α is a symbol defined to be 1 inside the liquid layer and 0 outside it. The orders of the electromagnetic variables are determined from the governing equations in the Appendix, and are found to be those in the following scheme:

$$\left.\begin{aligned} &\mathbf{E} = (\epsilon^{\frac{1}{2}}B_0\sqrt{(gL)}\,e_1, \quad \epsilon^{\frac{1}{2}}B_0\sqrt{(gL)}\,e_2, \quad \epsilon^{\alpha+\frac{1}{2}}B_0\sqrt{(gL)}\,e_3), \\ &\mathbf{B} = (\epsilon^{\frac{1}{2}}NB_0b_1, \quad \epsilon^{\frac{1}{2}}NB_0b_2, \quad B_0+\epsilon^{\frac{1}{2}}NB_0b_3), \\ &\mathbf{J} = \left(\epsilon^{\frac{1}{2}}\frac{NB_0}{\mu L}j_1, \quad \epsilon^{\frac{1}{2}}\frac{NB_0}{\mu L}j_2, \quad \epsilon^{\frac{3}{2}}\frac{NB_0}{\mu L}j_3\right). \end{aligned}\right\} \tag{2.11}$$

It is also found necessary to restrict K to be $O(\epsilon^{\frac{1}{2}})$: in place of K we introduce

$$k = \frac{K}{2\epsilon^{\frac{1}{2}}} = \frac{B_0^2\sigma L}{2\rho\sqrt{(gH_0)}} \sim O(1).$$

For mercury and with $\epsilon = 0{\cdot}1$, the following field strengths correspond to $k = 1$:

L (metres)	0·05	0·10	0·15
B_0 (10^4 gauss)	0·35	0·29	0·26

Note that the lowest-order electric field, which is $O(\epsilon^{\frac{1}{2}})$, is not induced by time variations of the magnetic field, which are $O(\epsilon^2)$. As may be seen from the Appendix point (v), and from what follows, the role of this electric field is to conserve the current within the liquid.

The horizontal components of (2.1), (2.3) become

$$-\frac{\partial e_2}{\partial x_3}=0, \quad \frac{\partial e_1}{\partial x_3}=0, \tag{2.12a,b}$$

$$-\frac{\partial b_2}{\partial x_3}=j_1=e_1+v_2, \quad \frac{\partial b_1}{\partial x_3}=j_2=e_2-v_1; \tag{2.13a,b}$$

and the vertical momentum equation reduces, as usual, to

$$0=-\frac{\partial p}{\partial x_3}-1, \quad \text{so that} \quad p=h-x_3,$$

where the boundary condition (2.9a) has been used. The approximate equations which govern the motion of the liquid are then (explanations follow):

$$\frac{\partial h}{\partial t}+\frac{\partial (hv_1)}{\partial x_1}+\frac{\partial (hv_2)}{\partial x_2}=0, \tag{2.14}$$

$$\frac{Dv_1}{Dt}=-\frac{\partial h}{\partial x_1}+2k(e_2-v_1), \quad \frac{Dv_2}{Dt}=-\frac{\partial h}{\partial x_2}-2k(e_1+v_2), \tag{2.15a,b}$$

$$\frac{\partial e_2}{\partial x_1}-\frac{\partial e_1}{\partial x_2}=0, \tag{2.16}$$

$$\frac{\partial}{\partial x_1}\{(e_1+v_2)\,h\}+\frac{\partial}{\partial x_2}\{(e_2-v_1)\,h\}=0. \tag{2.17}$$

In (2.15) the pressure gradient and the **e**-terms are independent of x_3 (see (2.12)), and it is assumed that initially v_1 and v_2 are independent of x_3. Then we may write (2.15) in Lagrangian co-ordinates and integrate with respect to time to show that v_1 and v_2 are independent of x_3 for all time. The continuity equation $\nabla.\mathbf{V}=0$ can now be integrated across the liquid layer to yield (2.14) when the boundary conditions on V_3 are applied. Equation (2.16) is the reduced form of the vertical component of (2.1). Equation (2.17) expresses the conservation of total current within the liquid layer, and may also be derived as follows. In view of the anti-symmetry with respect to x_3 of the outside solution for b_1 and b_2 (see below), and the continuity of these quantities across the interfaces, we may integrate (2.13) to

$$b_1=(e_2-v_1)\,(x_3-\tfrac{1}{2}h), \quad b_2=-(e_1+v_2)\,(x_3-\tfrac{1}{2}h); \tag{2.18a,b}$$

and

$$j_3=e_3=\frac{\partial b_2}{\partial x_1}-\frac{\partial b_1}{\partial x_2} \tag{2.19}$$

in the liquid. Now the continuity of $\mathbf{B}$ across $X_3=0$, H, and $\nabla\wedge\mathbf{B}=0$ outside, require $\mathbf{n}.\mathbf{J}=0$ on $X_3=0$, H, and this condition yields (2.17) on both surfaces.

Equations (2.14) to (2.17) must be solved with appropriate initial conditions and with boundary conditions on $\mathscr{D}$. If suffices n and t denote directions normal and tangential to $\mathscr{D}$, such that '$nt3$' form a right-handed system, we require that

$$v_n=0, \quad e_n+v_t=0 \quad \text{on} \quad \mathscr{D}.$$

To complete the picture of conditions in the liquid we observe that (2.4) reduces to $\partial b_3/\partial x_3=0$; b_3 is thus to be found from the outside solution.

In those special cases (§§ 4, 5) where the dimensionless electric field strength is of higher order than the velocity, the magnetic force in the momentum equation is proportional to the velocity, and is precisely like the quasi-viscous force introduced by Rayleigh (see Lamb 1932, § 242) in his study of the waves caused by application of pressure to the surface of a stream.

Although to our approximation the conduction current is divergence-free, the electric field strength is not: in fact to the lowest order

$$\nabla . \mathbf{E} = -\mathbf{B}_0 . (\nabla \wedge \mathbf{V}),$$

and we shall also have E_3 discontinuous across $X_3 = 0, H$. However, the corresponding charges are $O(\kappa)$—or, in dimensionless form, $O(gL/c^2)$, where c is the velocity of light—and the divergence of conduction current required to create these charges is therefore also $O(\kappa)$, and this is negligible to our approximation.

We now turn to the external problem. To the natural scale L of the outside field the liquid is simply a current sheet, since the boundary conditions on $x_3 = 0-, \epsilon h+$ may be satisfied on $x_3 = 0 \mp$. The field equations reduce to

$$\nabla \wedge \mathbf{b} = 0, \quad \nabla . \mathbf{b} = 0,$$

so that

$$\mathbf{b} = \frac{1}{4\pi} \iint \frac{\mathbf{j}^*(\mathbf{x}') \wedge \mathbf{R}}{R^3} \, dx_1' \, dx_2', \tag{2.20}$$

where

$$\mathbf{j}^* = (j_1 h, j_2 h, 0), \quad \mathbf{R} = \mathbf{i}_1(x_1 - x_1') + \mathbf{i}_2(x_2 - x_2') + \mathbf{i}_3 x_3.$$

To determine the $\mathbf{E}$ field we have to solve another potential problem

$$\nabla \wedge \mathbf{e} = 0, \quad \nabla . \mathbf{e} = 0;$$

here even boundary values of e_1 and e_2 are given on $x_3 = 0 \mp$, and in general we have to solve an integral equation with a source-type kernel.

We shall make no attempt to obtain explicit solutions for these external fields, but shall concentrate on the behaviour of the liquid.

In the ordinary ($k = 0$) non-linear approximation, as expounded by Stoker, the error is a factor $\{1 + O(\epsilon^2)\}$. In our case, inspection of the neglected terms suggests that the error in the hydrodynamic variables is a factor $\{1 + O(\epsilon)\}$. It is true that in the vertical component of (2.3) we retain terms of $O(\epsilon^{\frac{3}{2}})$ and neglect the $\mathbf{V} \wedge \mathbf{B}$ term, which is $O(\epsilon^2)$, but the corresponding neglected force in the momentum equation is only $O(\epsilon^4)$, compared to $O(\epsilon)$ for the lowest-order magnetic force. Moreover, for axi-symmetric and plane flows (§ 5), $\mathbf{V}$ and $\mathbf{B}$ are in the same vertical plane and $\mathbf{V} \wedge \mathbf{B}$ has no vertical component, so that the ratio of neglected to retained terms is $O(\epsilon)$ in all equations.

3. 'Shock waves'; the energy balance

In principle, bores, hydraulic jumps, or shocks (henceforth we shall use the last term) violate the assumptions of the theory, since in their neighbourhood the vertical acceleration is certainly not negligible; but since shocks, idealized to surfaces of discontinuity, have been fitted with some success into the theory for $k = 0$, we shall attempt to incorporate them here also. This is essentially an empirical step. If the governing equations are written, by means of Gauss's and

Stokes's theorems, in an integral form appropriate to a moving 'control surface',† and then applied in the usual way to a small surface enclosing a portion of the shock, the jump conditions are found to be:

(conservation of mass) $$[h(v_n - w_n)] = 0, \tag{3.1}$$

(momentum) $$[\tfrac{1}{2}h^2 + hv_n(v_n - w_n)] = 0, \quad [v_t] = 0, \tag{3.2a, b}$$

(irrotationality of e_1 and e_2) $$[e_t] = 0, \tag{3.3}$$

(conservation of current) $$[h(e_n + v_t)] = 0, \tag{3.4}$$

where horizontal components normal and tangential to the shock are denoted by suffices n and t; '$nt3$' form a right-handed system; w_n denotes the shock velocity; and square brackets denote, for the moment, a jump or discontinuity operator. The hydrodynamic jump conditions are unchanged by the presence of the magnetic field; as usual, energy considerations (below) require that particles cross the shock from a region of smaller to one of larger depth.

The approximate equations (2.12) *et seq.* are not uniformly valid. In their derivation, we have neglected a number of terms which, if retained, would lead to wave-speeds other than $(gH)^{\frac{1}{2}}$, which is the only characteristic speed implicit in our equations. In the case of a wave travelling into still liquid, these neglected effects would propagate disturbance (of a higher order in ϵ) ahead of the wave-front predicted by our theory. The approximate equations give warning of this when the wave-front is a shock: then the tangential current $j_t h$ is discontinuous, so that b_3 is logarithmically singular (cf. a discontinuity in loading in thin aerofoil theory).

We proceed to the energy balance of our approximate system. First, we must write the appropriate Poynting vector, which is, in the liquid,

$$\left.\begin{aligned} \mathbf{S} &= \epsilon^{\frac{1}{2}} \frac{B_0\sqrt{(gL)}}{\mu} \mathbf{e} \wedge \mathbf{B}_0 + \epsilon^2 B_0^2 \sigma g L^2 \mathbf{s}, \\ \text{where} \qquad \mathbf{s} &= \mathbf{i}_1 e_2 b_3 - \mathbf{i}_2 e_1 b_3 - \mathbf{i}_3 (e_1 v_2 - e_2 v_1 + e_1^2 + e_2^2)(x_3 - \tfrac{1}{2}h). \end{aligned}\right\} \tag{3.5}$$

Since $\nabla . (\mathbf{e} \wedge \mathbf{B}_0) = \mathbf{B}_0 . (\nabla \wedge \mathbf{e}) = 0$, the integral of $\mathbf{e} \wedge \mathbf{B}_0$ over a closed surface vanishes. Also, s_1 and s_2 are not significant because their flux is across small surfaces.

Consider now a moving volume of liquid, bounded by a vertical cylinder C, of cross-section A, and containing shocks along a number of vertical surfaces of which C_w is typical. (C_w is not necessarily a closed curve in a plane $x_3 =$ constant.) On C, $\mathbf{n}$ is the outward normal; on C_w, $\mathbf{n}$ points in the direction of the relative fluid velocity, $v_n - w_n > 0$. Suffices $+$ and $-$ refer to values on the downstream and upstream sides of C_w, respectively, and we write $\{h(v_n - w_n)\}_+ = \{h(v_n - w_n)\}_- = m$. To construct the energy equation, we perform the differentiation in

$$\frac{d}{dt} \iint_A (\tfrac{1}{2}h^2 + \tfrac{1}{2}v^2 h)\, dA,$$

† The momentum equation must first be multiplied by h. The integral form of (2.16) is $\int_C \mathbf{e} . d\mathbf{l} = 0$, where $d\mathbf{l}$ is a line element of the horizontal circuit C; the fact that C may be partly in, and partly out of, the liquid causes no difficulty since e_1 and e_2 pass continuously through the liquid and do not change significantly with X_3 in any interval of width $O(\epsilon L)$.

and substitute for $\partial h/\partial t$ from the continuity equation and for $\partial v/\partial t$ from the momentum equation. The result is simplified by introduction of the Poynting vector and the shock equations, and is finally found to be

$$-\int_C \tfrac{1}{2}h^2 v_n\,dl = \frac{d}{dt}\iint_A (\tfrac{1}{2}h^2+\tfrac{1}{2}v^2h)\,dA + \Sigma\int_{C_\sigma}\frac{m(h_+-h_-)^3}{4h_+h_-}\,dl + 2k\iint_A (j^2h+s_3|_{x_3=0}^{h})\,dA. \tag{3.6}$$

Here the left-hand side represents the rate at which the pressures on C are doing work on the volume: on the right there appear the rates of increase of the potential and kinetic energy, of energy dissipation by shocks, of energy dissipation by Joule heating, and of efflux of electromagnetic energy to the external field.

Consider a disturbance initially confined to a finite domain, and choose C outside the wave-front: then the left-hand side of (3.6) vanishes. If we assume that some (or all) of the initial potential and kinetic energy of the disturbance is ultimately dissipated, it is clear that in the ordinary case ($k = 0$) shocks provide the only mechanism for this: in our case other means are available. It therefore seems likely that certain, initially continuous flows, which lead to shocks when $k = 0$, may remain continuous when $k > 0$. In part III it will be shown that this is, in fact, the case.

4. The linear approximation

It has been implicitly assumed so far that the wave amplitude $|H-H_0|_{\max}$ is comparable with the mean depth H_0. We now suppose that the initial conditions introduce a second small parameter

$$\frac{|H-H_0|_{\max}}{H_0} = \delta.$$

Whereas orders with respect to ϵ were written explicitly in (2.10), (2.11), those with respect to δ will be treated implicitly. Like $\partial h/\partial x_1$, the dimensionless velocities v_1, v_2 are now $O(\delta)$, and we write

$$h = 1+\eta(x_1, x_2, t),$$

where η is $O(\delta)$.

In the momentum equation, Dv_1/Dt now reduces to $\partial v_1/\partial t$, and (2.17) reduces to

$$\frac{\partial}{\partial x_1}(e_1+v_2)+\frac{\partial}{\partial x_2}(e_2-v_1) = 0, \tag{4.1}$$

so that the magnetic force in the momentum equation is irrotational, and derivable from a potential. Hence if the vector (v_1, v_2) is irrotational initially (as we assume), it remains so for all time; on the linear theory this is true whether the motion is continuous or not. Then by (2.16) and (4.1)

$$\frac{\partial e_2}{\partial x_1}-\frac{\partial e_1}{\partial x_2} = 0, \quad \frac{\partial e_1}{\partial x_1}+\frac{\partial e_2}{\partial x_2} = 0.$$

If the liquid is unbounded laterally, e_1 and e_2 vanish at infinity, are continuous through the field (by the linearized form of the shock equations), and have no

singularities. Hence $e_1 = e_2 = 0$ (although there will be an electric field to a higher order). Again for axi-symmetric flow, and for certain plane flows (§ 5), the electric field vanishes from the hydrodynamic equations, which are then

$$\frac{\partial \eta}{\partial t} + \frac{\partial v_1}{\partial x_1} + \frac{\partial v_2}{\partial x_2} = 0, \tag{4.2}$$

$$\frac{\partial v_1}{\partial t} = -\frac{\partial \eta}{\partial x_1} - 2kv_1, \quad \frac{\partial v_2}{\partial t} = -\frac{\partial \eta}{\partial x_2} - 2kv_2. \tag{4.3a, b}$$

If the velocity potential ϕ is introduced, such that

$$v_1 = \frac{\partial \phi}{\partial x_1}, \quad v_2 = \frac{\partial \phi}{\partial x_2}, \quad \eta = -\left(\frac{\partial}{\partial t} + 2k\right)\phi, \tag{4.4}$$

the momentum equations are satisfied identically, and the continuity equation becomes

$$\frac{\partial^2 \phi}{\partial x_1^2} + \frac{\partial^2 \phi}{\partial x_2^2} = \frac{\partial^2 \phi}{\partial t^2} + 2k\frac{\partial \phi}{\partial t}, \tag{4.5}$$

which is a form of the telegraph equation.

To obtain the energy balance of the linear approximation (with e_1 and e_2 not necessarily vanishing) we rewrite (3.6) for a fixed vertical cylinder C^* of cross-section A^*; subtract the continuity equation

$$-\int_{C^*} hv_n \, dl = \frac{d}{dt}\iint_{A^*} h \, dA,$$

and, writing $h = 1 + \eta$, neglect terms of $O(\delta^3)$. There results

$$-\int_{C^*} \eta v_n \, dl = \frac{d}{dt}\iint_{A^*} (\tfrac{1}{2}\eta^2 + \tfrac{1}{2}v^2)\, dA + 2k\iint_{A^*} (j^2 + s_3|^1_{x_3=0})\, dA. \tag{4.6}$$

This equation can also be found directly from the linear equations. We observe again that the potential and kinetic energy is continuously dissipated by Joule heating: if C^* is chosen such that $v_n = 0$ there, and if also $e_1 = e_2 = 0$, this is the only effect on the energy within C^*.

5. Plane and axi-symmetric flows

We discuss the plane and axi-symmetric cases together; for this, it is convenient to introduce the symbol β, which is 0 for the former case and 1 for the latter. For the axi-symmetric case, (x_1, x_2, x_3) are identified with cylindrical co-ordinates (r, θ, z), dimensionless as in (2.10). The problems to be considered are those for which $\partial(\quad)/\partial X_2 = 0$, and $V_2 = B_2 = 0$ initially. It then follows from the full equations, (2.1) to (2.6), and from the boundary conditions, that everywhere and for all time

$$V_2 = B_2 = E_1 = E_3 = 0.$$

Currents flow only in the 2-direction.

We now find from (2.1) that, inside and outside the liquid,

$$\frac{\partial e_2}{\partial x_3} = 0, \quad \frac{1}{x_1^\beta}\frac{\partial}{\partial x_1}(x_1^\beta e_2) = 0, \tag{5.1}$$

and if the boundary condition at infinity is used, $e_2 = 0$ everywhere.

But at this stage we must inquire whether these conditions can be simulated in the laboratory. There are no special difficulties associated with the axi-symmetric case (for which $e_2 = 0$ is valid), but we cannot achieve a perfectly 'plane' state of affairs with flow in a channel (even when viscosity is neglected) because the current must flow in closed loops. Probably the best way of obtaining approximately plane flow in a channel is to make the side walls (that is, the walls parallel to $X_2 = 0$) far apart relative to the wavelength L and of highly conducting material, as Hartmann did in his experiments (1937) on plane Poiseuille flow. Even then the electromagnetic field is 'plane' only in a limited region about the central part of the channel, the boundary condition at infinity cannot be invoked, and we must accept an e_2 which is constant in space over the region in question. Its strength is determined by the condition

$$\iint j_2 \, dx_1 \, dx_3 = \int (e_2 - v_1) \, h \, dx_1 = 0 \tag{5.2}$$

for the non-linear theory, with $h \sim 1$ when we linearize. However, this still leads to $e_2 = 0$ if (i) the initial conditions are such that h is an even and v_1 an odd function of x_1, or (ii) the x_1-length of the liquid is much greater than the x_1-length of that part of it which is moving, or (iii) $v_1 h$ is oscillatory such that

$$\int v_1 h \, dx_1 \ll \int h \, dx_1.$$

Again, if the side walls are short-circuited by means of a very good solid conductor, parallel to the x_2-axis and outside the liquid, the electric field e_2 will vanish, while the condition

$$\iint j_2 \, dx_1 \, dx_3 = 0$$

is still satisfied. The contribution to the magnetic field of the current in the solid conductor must, of course, be taken into account.

In what follows we consider only axi-symmetric flows and those plane flows for which the electric field vanishes from the lowest-order hydrodynamic equations. If, as in the axi-symmetric case, the current $\sigma \mathbf{V} \wedge \mathbf{B}$ is exactly parallel to all the insulating boundaries and flows in closed circuits, the electric field is, to the lowest order,

$$\mathbf{E} = (0, \epsilon^2 B_0 \sqrt{(gL)} \, e_2^*, 0),$$

where e_2^* is calculated from the time variation of the magnetic perturbations:

$$\frac{\partial e_2^*}{\partial x_3} = N \frac{\partial b_1}{\partial t}, \quad \frac{1}{x_1^\beta} \frac{\partial}{\partial x_1} (x_1^\beta e_2^*) = -N \frac{\partial b_3}{\partial t}.$$

To the lowest order the current depends only on the velocity, and the magnetic perturbations are found from it, as before.

Part II. Some Linearized Solutions for Plane and Axi-symmetric Flow

6. An initial-value problem

We ask what happens to a given initial elevation $f(x_1)$ of the free surface. More precisely, we consider the following problem for plane flow (x_1, x_2, x_3 being

Cartesian co-ordinates, $\beta = 0$), and axi-symmetric flow (x_1, x_2, x_3 being cylindrical co-ordinates, $\beta = 1$):

$$\frac{1}{x_1^\beta}\frac{\partial}{\partial x_1}\left(x_1^\beta \frac{\partial \phi}{\partial x_1}\right) = \frac{\partial^2 \phi}{\partial t^2} + 2k\frac{\partial \phi}{\partial t}; \tag{6.1}$$

at time $t = 0$,

$$\left.\begin{aligned} \eta &= -\frac{\partial \phi}{\partial t} - 2k\phi = f(x_1), \quad \frac{\partial \eta}{\partial t} = 0, \\ v_1 &= \frac{\partial \phi}{\partial x_1} = 0, \quad \frac{\partial v_1}{\partial t} = -f'(x_1); \end{aligned}\right\} \tag{6.2}$$

at $|x_1| = a$,

$$v_1 = \frac{\partial \eta}{\partial x_1} = 0. \tag{6.3}$$

Waves in a dish of semi-width or radius L ($a = 1$), and in an unbounded fluid ($a \to \infty$) will be considered. In place of x_1 and v_1, we shall now write x and u (when $\beta = 0$) or r and u (when $\beta = 1$).

7. Standing waves in a dish

Here, solutions of two rather elementary eigenvalue problems are required: the method is obvious, and no details of it will be given. In the plane case, to satisfy the requirement of zero total current normal to a flow plane, we specify a disturbance symmetrical about $x = 0$:

$$f(x) = \sum_1^\infty A_n \cos n\pi x \quad (|x| \leqslant 1),$$

where the $n = 0$ term is absent because H_0 is taken to be the mean value of $H(X, 0)$. Then, with $(n^2\pi^2 - k^2)^{\frac{1}{2}} = \omega_n$,

$$\phi = -e^{-kt}\sum_1^\infty A_n \cos n\pi x\, \omega_n^{-1} \sin \omega_n t, \tag{7.1a}$$

$$\eta = e^{-kt}\sum_1^\infty A_n \cos n\pi x \{\cos \omega_n t + k\omega_n^{-1} \sin \omega_n t\}, \tag{7.1b}$$

$$u = e^{-kt}\sum_1^\infty A_n \sin n\pi x\, n\pi\, \omega_n^{-1} \sin \omega_n t, \tag{7.1c}$$

the trigonometric functions of time becoming hyperbolic functions for $k > n\pi$. The effect of increasing field strength, k, upon any single mode, η_n, is precisely like the damping of a mechanical system: at $k = 0$, η_n oscillates harmonically in time; for $0 < k < n\pi$, the frequency is reduced, and the motion is damped; at $k = n\pi$, η_n moves like $e^{-kt}(1 + kt)$; for $k > n\pi$, η_n behaves like

$$\exp\{[-k + (k^2 - n^2\pi^2)^{\frac{1}{2}}]t\};$$

and as $k \to \infty$ (although this is outside the region of validity of our theory), η_n tends not to move.

For the axi-symmetric case, $f(r)$ is expanded in a Dini series (Watson 1944):

$$f(r) = \sum_1^\infty A_n J_0(\lambda_n r) \quad (r \leqslant 1),$$

$$A_n = \frac{2}{J_0^2(\lambda_n)}\int_0^1 f(s)\, J_0(\lambda_n s)\, s\, ds,$$

where λ_n are the positive zeros of J_1, and the $n = 0$ term is absent because H_0 is taken as the mean value of $H(r, 0)$ with respect to horizontal area. Then, with $(\lambda_n^2 - k^2)^{\frac{1}{2}} = \omega_n$,

$$\phi = -e^{-kt} \sum_1^\infty A_n J_0(\lambda_n r)\, \omega_n^{-1} \sin \omega_n t, \tag{7.2a}$$

$$\eta = e^{-kt} \sum_1^\infty A_n J_0(\lambda_n r) \{\cos \omega_n t + k\omega_n^{-1} \sin \omega_n t\}, \tag{7.2b}$$

$$u = e^{-kt} \sum_1^\infty A_n J_1(\lambda_n r)\, \lambda_n \omega_n^{-1} \sin \omega_n t. \tag{7.2c}$$

The shape of the modes is slightly different from that in the plane case; their behaviour with time is precisely the same.

8. Travelling waves in an unbounded liquid

We introduce the Laplace transform

$$\overline{F}(x, p) = p \int_0^\infty e^{-pt} F(x, t)\, dt.$$

In the plane case, with the initial conditions $\partial\phi/\partial t = -f(x)$, and $\phi = 0$ at $t = 0$, the differential equation becomes

$$\frac{d^2\overline{\phi}}{dx^2} - (p^2 + 2kp)\,\overline{\phi} = pf(x), \tag{8.1}$$

and we require that $\overline{\phi} \to 0$ as $|x| \to \infty$. Let $(p^2 + 2kp)^{\frac{1}{2}} = q$; there is a cut from $p = -2k$ to $p = 0$, and q denotes that branch which is positive on the positive real axis. The fundamental solution of (8.1) is

$$g(x; \lambda) = -\frac{e^{-q|x-\lambda|}}{2q};$$

using this, and inverting the transform, we find that

$$\phi = -\frac{1}{2\pi i} \int_{\mathscr{L}} \frac{e^{pt}}{2q}\, dp \int_{-\infty}^{\infty} e^{-q|x-\lambda|} f(\lambda)\, d\lambda, \tag{8.2a}$$

$$= -\tfrac{1}{2} e^{-kt} \int_{x-t}^{x+t} I_0(k\{t^2 - (x-\lambda)^2\}^{\frac{1}{2}})\, f(\lambda)\, d\lambda, \tag{8.2b}$$

where $\mathscr{L}$ denotes the Bromwich path ($c - i\infty$ to $c + i\infty$, $c > 0$, in the present case), I_n is the modified Bessel function of the first kind and order n, and the inversion integral has been evaluated by standard methods (see, for example, van der Pol & Bremmer 1955).

Consider first the simple if unrealistic case of an initial elevation concentrated at the origin such that the raised area of liquid is γ: $f(x) = \gamma\delta^*(x)$, where δ^* is the Dirac function. This will give an indication of the behaviour of more sensible solutions. Then, with U denoting the Heaviside unit function,

$$\phi = -\tfrac{1}{2}\gamma e^{-kt} I_0(k\{t^2 - x^2\}^{\frac{1}{2}})\, U(t - |x|), \tag{8.3a}$$

$$\eta = \tfrac{1}{2}\gamma e^{-kt} \left\{ \delta^*(t - |x|) + \left[\frac{kt}{(t^2 - x^2)^{\frac{1}{2}}} I_1(k\{t^2 - x^2\}^{\frac{1}{2}}) + kI_0(k\{t^2 - x^2\}^{\frac{1}{2}}) \right] U(t - |x|) \right\}, \tag{8.3b}$$

$$u = \tfrac{1}{2}\gamma e^{-kt} \left\{ (\operatorname{sgn} x)\, \delta^*(t - |x|) + \frac{kx}{(t^2 - x^2)^{\frac{1}{2}}} I_1(k\{t^2 - x^2\}^{\frac{1}{2}})\, U(t - |x|) \right\}. \tag{8.3c}$$

Comparing this with the ordinary ($k = 0$) solution, $\eta = (\frac{1}{2}\gamma)\,\delta^*(t-|x|)$, we observe that the surface elevation is exponentially damped near the wave-fronts $|x| = t$, where $I_0 \sim 1$, $I_1 \sim (\frac{1}{2}k)\,(t^2-x^2)^{\frac{1}{2}}$, but that there is also a residual wave between the fronts which decays only slowly near $x = 0$, where $I_0 \sim I_1 \sim e^{kt}\,(2\pi kt)^{-\frac{1}{2}}$.

Such a state of affairs is hardly surprising. We would expect the magnetic force to damp most strongly the high-frequency Fourier components which dominate near the wave-front; on the other hand, continuity requires that $\int_{-\infty}^{\infty} \eta\,dx$ be constant, so that if the elevation is damped near the fronts, it must have compensating values elsewhere.

To examine this effect in more detail, we study the solution due to an initial step, $f(x) = \delta U(-x)$: the flows due to double or multi-steps can be easily constructed from this by superposition. After a little reduction one finds that

$$\eta = \frac{\delta}{2\pi i}\int_{\mathscr{L}} \frac{e^{pt-qx}}{2p}\,dp \quad (x \geqslant 0), \tag{8.4a}$$

$$= \delta - \frac{\delta}{2\pi i}\int_{\mathscr{L}} \frac{e^{pt+qx}}{2p}\,dp \quad (x \leqslant 0), \tag{8.4b}$$

so that $\eta(0,t) = \frac{1}{2}\delta$, and for $x \leqslant 0$, $\eta(x,t) = \delta - \eta(|x|,t)$; hence it is sufficient to study η for $x \geqslant 0$. Also

$$\eta = \frac{\delta\,e^{-kt}}{2}\left(\frac{\partial}{\partial t}+k\right)\int_x^t I_0(k\{t^2-\mu^2\}^{\frac{1}{2}})\,d\mu \quad (0 \leqslant x < t), \tag{8.5}$$

$$u = \frac{\delta\,e^{-kt}}{2}\,I_0(k\{t^2-x^2\}^{\frac{1}{2}}). \tag{8.6}$$

By expanding the integrand of (8.4*a*) in series for p large, or the integrand of (8.5) for $(t-\mu)$ small, one finds that near the wave-front $x = t$,

$$\eta = \frac{\delta\,e^{-kt}}{2}\left\{1+(kt+2)\,k\beta+(k^2t^2+4kt)\frac{k^2\beta^2}{4}+(k^3t^3+6k^2t^2-6kt-24)\frac{k^3\beta^3}{36}+\ldots\right\}, \tag{8.7}$$

where $\beta = \frac{1}{2}(t-x)$. This series may also be rearranged to yield one valid for small times across the whole disturbed region $t > |x|$. By applying the method of steepest descents to (8.4*a*) one finds that, in a region between the wave-front and $x = 0$, where t, $(t^2-x^2)^{\frac{1}{2}}$, and $t-(t^2-x^2)^{\frac{1}{2}}$ are all large,

$$\eta \sim \frac{\delta}{2(2\pi)^{\frac{1}{2}}}\,\frac{\exp\{-kt+k(t^2-x^2)^{\frac{1}{2}}\}}{kt-k(t^2-x^2)^{\frac{1}{2}}}\,\frac{kx}{\{k^2(t^2-x^2)\}^{\frac{1}{4}}}. \tag{8.8}$$

These results suggest the following approximation (which will be useful in part III):

$$\eta = \frac{\delta\,e^{-kt}}{2}\left[e^{kt}-\left\{\frac{3}{2kt}\,(e^{kt}-1-kt-\tfrac{1}{2}k^2t^2)+1+\tfrac{1}{2}kt\right\}kx+\{e^{kt}-1-kt-\tfrac{1}{2}k^2t^2\}\,\frac{x^3}{2t^3}\right]. \tag{8.9}$$

Here a cubic wave profile has been fitted to give the correct values at $x = 0$, $|x| = t$, the correct slope at $|x| = t$, and the correct curvature (zero) at $x = 0$. In figure 1 the values given by (8.9) are compared with values obtained from (8.5) by a careful numerical integration. For $kt = 1, 2$, the 'exact' and approximate curves are indistinguishable in the figure. The equations (8.4*a*) to (8.9), and figure 1, describe the following flow pattern. A compressive discontinuity moves along $x = t$ and an expansive one along $x = -t$ (by 'compressive' we mean that the particles cross from smaller to larger h, by 'expansive', the opposite), the

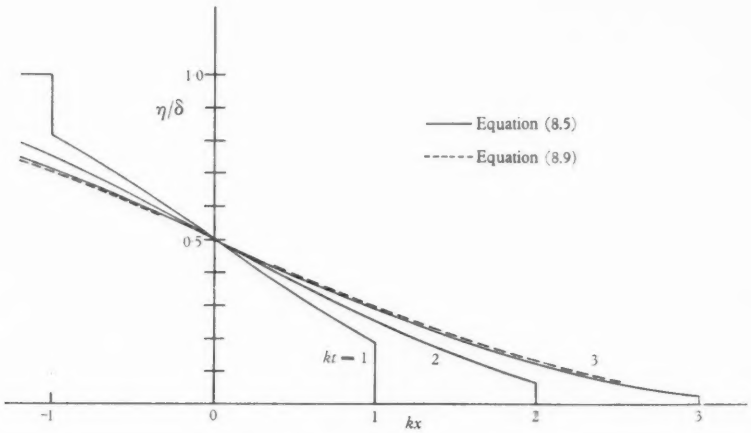

FIGURE 1. Wave profiles due to a step.

heights of both being exponentially damped. The velocity u is positive everywhere, and is similarly damped. Halfway between the fronts, the surface elevation remains $\frac{1}{2}\delta$ and the velocity attains its maximum value, decaying only like $t^{-\frac{1}{2}}$. There is, of course, a continuous transition from the values at the centre to those just inside the wave-fronts.

Figure 2 shows wave profiles resulting from a double step (square wave) $f(x) = \delta U(-x+1) - \delta U(-x-1)$. These pictures, together with equations (8.7) and (8.8), confirm our earlier description of a wave damped at its edges, but tending to maintain a larger elevation near its centre. For the double step, the ordinary theory ($k = 0$) predicts that when $t > 1$, the elevation consists of two portions, in the intervals $t-1 < |x| < t+1$, each of height $\frac{1}{2}\delta$; between them, in $|x| < t-1$, there is no disturbance. In the present case the major part of the elevation remains in $|x| < t-1$.

If the initial surface elevation is sinusoidal everywhere, we recover standing wave solutions like those of § 7, but with arbitrary wave numbers. Thus with $f(x) = \delta e^{i\nu x}$, (8.2*a*) yields

$$\phi = -\delta e^{i\nu x}(\nu^2 - k^2)^{-\frac{1}{2}} e^{-kt} \sin(\{\nu^2 - k^2\}^{\frac{1}{2}} t).$$

Clearly this solution could be made the basis of a more general one by super-

position, but we have thought it more interesting and convenient to proceed from the solution for a pulse, which is the basis of (8.2*b*).

In the axi-symmetric problem, the solution corresponding to (8.2*a*) is

$$\phi = -\frac{1}{2\pi i}\int_{\mathscr{L}} e^{pt}\,dp\left\{K_0(qr)\int_0^r I_0(q\lambda)\,f(\lambda)\,\lambda\,d\lambda + I_0(qr)\int_r^\infty K_0(q\lambda)\,f(\lambda)\,\lambda\,d\lambda\right\}, \tag{8.10}$$

where K_0 is the modified Bessel function of the second kind and order zero (Watson 1944), and a cut is required along the entire negative real axis of the p-plane to make K_0 single-valued.

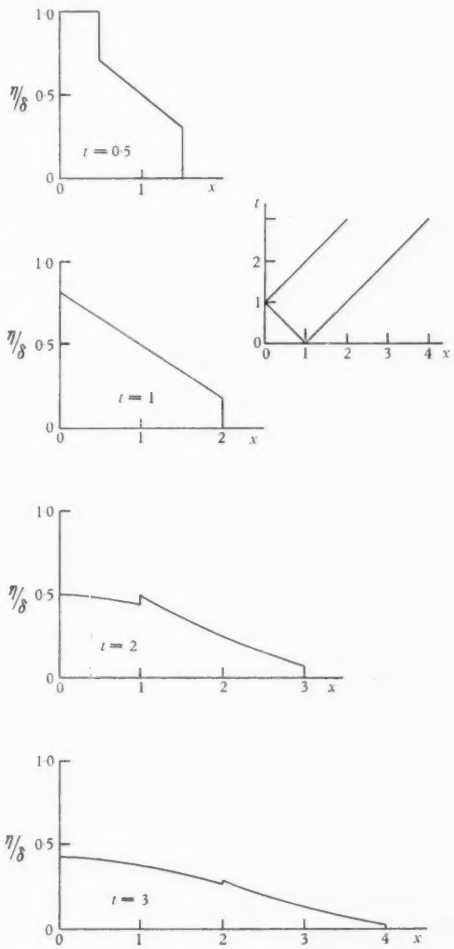

FIGURE 2. Wave profiles due to a double step, $k = 1$. Trajectories of the discontinuities are also shown.

For an initial elevation concentrated at the origin, such that the raised volume is γ, we have $f(r) = \gamma\delta^*(r)/\pi r$, and

$$\phi = -\frac{\gamma}{2\pi}\frac{1}{2\pi i}\int_{\mathscr{L}} e^{pt} K_0(qr)\,dp,$$

$$= -\frac{\gamma}{2\pi}\frac{e^{-kt}\cosh\left(k\{t^2-r^2\}^{\frac{1}{2}}\right)}{(t^2-r^2)^{\frac{1}{2}}}\,U(t-r). \tag{8.11}$$

This solution shows essentially the same properties as the corresponding one for plane flow, (8.3*a*); however, there is now an algebraic singularity (as well as a Dirac pulse in η and u) at the wave-front $r = t$, and the decay of elevation near the origin is slightly more rapid than before ($O(t^{-1})$ instead of $O(t^{-\frac{1}{2}})$).

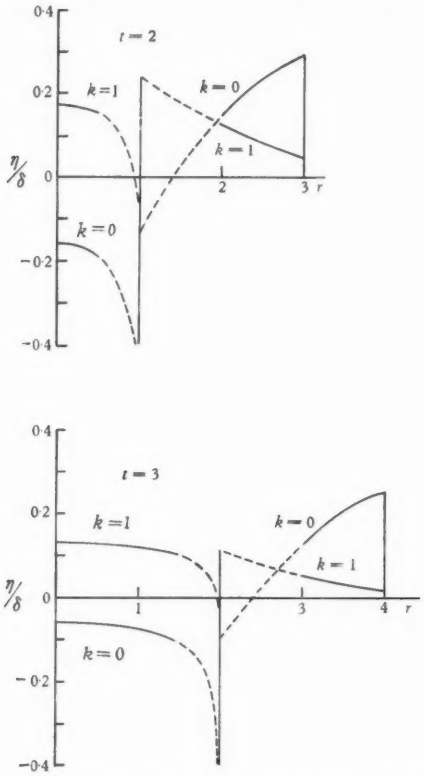

FIGURE 3. Wave profiles due to a cylindrical step.

For a cylindrical step, such that $f(r) = \delta U(1-r)$, the inner integrals of (8.10) may be evaluated, and one can find series for η behind the outgoing ($r = 1+t$) and incoming ($r = 1-t$) wave-fronts. In addition, one can show that immediately behind the reflected wave-front ($r = t-1$)

$$\eta \sim \frac{\delta e^{-kt}}{2\pi r^{\frac{1}{2}}}\log(t-r-1), \tag{8.12}$$

and one can find a series for η in powers of r^2 in the domain $r < t-1$. (The logarithmic singularity is a spurious result of the linearization, but suggestive of large disturbances: Meyer (1948) has studied a similar singularity in a related problem.) These results have been used to construct the wave profiles shown in figure 3. Although the whole profiles are shown, the series used, which were truncated after three terms, are believed to be reliable only for the regions shown by solid curves. The remaining parts of the profiles were constructed from consideration of the singularity behind the reflected wave-front, and from the requirement of continuity that for all time

$$\int_0^\infty \eta\, 2\pi r\, dr = \pi\delta.$$

We observe that for $k = 0$ most of the elevation is carried along behind the outer wave-front, that it decreases inwards, and that inside the reflected wave-front the elevation is negative. On the other hand, for $k = 1$ the elevation is damped behind the outer wave-front and increases inwards. The reflected wave-front is again expansive, but the elevation inside it is predominantly positive; as in the plane case, the wave tends to be 'held together' by the magnetic force.

Part III. Some Non-linear Effects in Plane Flow

9. The approximate equations in characteristic variables

In this final part of the paper, we make attempts to solve the initial-value problem of § 6 for plane flow and a liquid unbounded laterally when the governing field equations are those of our non-linear approximation. Disturbances now move with a variable propagation velocity $(gH)^{\frac{1}{2}}$ relative to the fluid particles (which are themselves moving), and we are particularly interested in the question of whether, according to our approximation, this effect causes shocks to form (waves to break) in fields which are initially continuous. Clearly, there will be two opposing effects: the usual tendency of compressive wavelets to overtake those ahead of them, and thus to form a shock, and the damping effect of the magnetic force on the disturbances immediately behind a wave-front. We also seek to improve the solutions we have obtained for flows whose initial elevation contains steps; where the linearized theory showed compressive and expansive discontinuities moving with speed $(gH_0)^{\frac{1}{2}}$, we try to construct a picture which distinguishes between shocks and centred expansion waves, and which gives an indication of their true velocities. Fortunately, the work of Friedrichs (1948), Lighthill (1949, 1955), Whitham (1952), Lin (1954), and Fox (1955) points the way to the resolution of such questions: we have merely to try to follow, incorporating the effect of the new damping term.

Using suffices to denote partial derivatives, we write the governing equations, namely

$$\left.\begin{aligned} h_t + (uh)_x &= 0, \\ u_t + uu_x + h_x + 2ku &= 0, \end{aligned}\right\} \tag{9.1}$$

in characteristic form:

on C_+

$$\left.\begin{aligned} \frac{x_\alpha}{t_\alpha} &= u + h^{\frac{1}{2}}, \qquad 2(h^{\frac{1}{2}})_\alpha + u_\alpha + 2kut_\alpha = 0, \end{aligned}\right\} \tag{9.2a, b}$$

on C_-

$$\left.\begin{aligned} \frac{x_\beta}{t_\beta} &= u - h^{\frac{1}{2}}, \quad -2(h^{\frac{1}{2}})_\beta + u_\beta + 2kut_\beta = 0. \end{aligned}\right\} \tag{9.3a, b}$$

Here α and β are curvilinear co-ordinates which are defined by (9.2*a*) and (9.3*a*), and we fix their scale by specifying that on $t = 0$, $\alpha = -\beta = \frac{1}{2}x$. With $k > 0$, (9.2) and (9.3) no longer admit 'simple wave' solutions, and we shall have to be content with series expansions of exact solutions. These will be the simplest possible examples of the following two types: (i) wave-front series, in powers of a characteristic co-ordinate measured from a wave-front across which the normal derivatives of u and h are discontinuous, and (ii) small-disturbance series, in which $h(\alpha,\beta)$, $u(\alpha,\beta)$, $x(\alpha,\beta)$, and $t(\alpha,\beta)$ are expanded in powers of the small parameter δ. In connexion with the latter it may be worth reminding the reader that, while we are perfectly free to construct mathematical solutions of the non-linear approximation in powers of δ, the non-linear theory is a better approximation than the linear one only if $\delta \gg \epsilon^2$.

10. Wave-front series

Let the (dimensionless) elevation of the free surface at time $t = 0$ be

$$\left.\begin{aligned} h(x,0) \equiv 1+f(x) &= 1 \quad (x \geqslant 0), \\ &= 1 - Ax + \tfrac{1}{2}Bx^2 + \ldots \quad (x \leqslant 0), \end{aligned}\right\} \tag{10.1}$$

the initial velocity being zero. Discontinuities will be propagated along $\alpha = 0$ and $\beta = 0$. In the region $\beta < 0$, $t \geqslant 0$, the variables are undisturbed, $h = 1$, $u = 0$, $x = \alpha - \beta$, $t = \alpha + \beta$; in the region $\alpha > 0$, $\beta > 0$, all four variables are expanded in Taylor series about $\beta = 0$; and in the region $\alpha < 0$, $t \geqslant 0$, they are expanded in double Taylor series about $\alpha = 0$, $\beta = 0$. This reduces the problem to a series of algebraic and linear ordinary differential equations, with boundary conditions on $t = 0$, $\alpha = 0$, and $\beta = 0$. One finds that for $\alpha > 0$, $\beta > 0$,

$$\left.\begin{aligned} h &= 1 + A\,e^{-k\alpha}\beta + \{A^2(-e^{-2k\alpha} - \tfrac{3}{4}k\alpha\,e^{-k\alpha} + \tfrac{1}{2}e^{-k\alpha}) \\ &\qquad + Ak^2\alpha\,e^{-k\alpha} + 2B\,e^{-k\alpha}\}\tfrac{1}{2}\beta^2 + \ldots, \\ u &= A\,e^{-k\alpha}\beta + \{A^2(-3\,e^{-2k\alpha} - \tfrac{3}{4}k\alpha\,e^{-k\alpha} + 2\,e^{-k\alpha}) \\ &\qquad + Ak(k\alpha\,e^{-k\alpha} - 2e^{-k\alpha}) + 2B\,e^{-k\alpha}\}\tfrac{1}{2}\beta^2 + \ldots, \\ x &= \alpha - \left\{\frac{3A}{4k}(e^{-k\alpha}-1)+1\right\}\beta + \left\{\frac{A^2}{16k}(27\,e^{-2k\alpha} + 9k\alpha\,e^{-k\alpha} - 12\,e^{-k\alpha} - 15)\right. \\ &\qquad \left. + A(-\tfrac{3}{4}k\alpha\,e^{-k\alpha} + \tfrac{1}{2}e^{-k\alpha} + 1) - \frac{3B}{2k}(e^{-k\alpha}-1)\right\}\tfrac{1}{2}\beta^2 + \ldots, \\ t &= \alpha + \left\{\frac{3A}{4k}(e^{-k\alpha}-1)+1\right\}\beta + \left\{\frac{A^2}{16k}(-21\,e^{-2k\alpha} - 9k\alpha\,e^{-k\alpha} + 6\,e^{-k\alpha} + 15)\right. \\ &\qquad \left. + A(\tfrac{3}{4}k\alpha\,e^{-k\alpha} - 1) + \frac{3B}{2k}(e^{-k\alpha}-1)\right\}\tfrac{1}{2}\beta^2 + \ldots. \end{aligned}\right\} \tag{10.2}$$

The main justification for including these rather clumsy expressions here is that they give us a glimpse of the non-linear terms (those in A^2) in an exact solution of equations (9.1). We first observe that the function $t - x$ given by (10.2) is bounded, with $k > 0$ and β bounded, for all α, including $\alpha \to \infty$; whereas for $k = 0$, $t - x \sim O(\alpha)$. Thus with $k > 0$ a characteristic $\beta = \beta^*$ can move only

a finite distance away from its 'undisturbed position' $t-x=2\beta^*$, and the tendency of shocks to form is much reduced. In particular, the derivatives

$$-x_\beta(\alpha,0)=t_\beta(\alpha,0)=1-\frac{3A}{4k}(1-e^{-k\alpha})$$

cannot vanish (which means that at the wave-front characteristics cannot converge, and shocks cannot form), if, and only if,

$$\frac{3A}{4k}<1, \quad \text{i.e. if} \quad \frac{\vartheta\rho}{\sigma B_0^2}\left(\frac{g}{H_0}\right)^{\frac{1}{2}}<\tfrac{2}{3}, \tag{10.3}$$

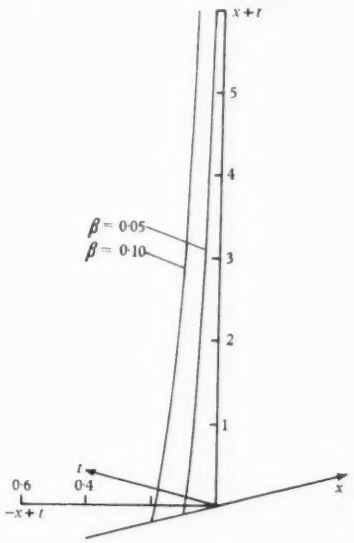

(*a*)

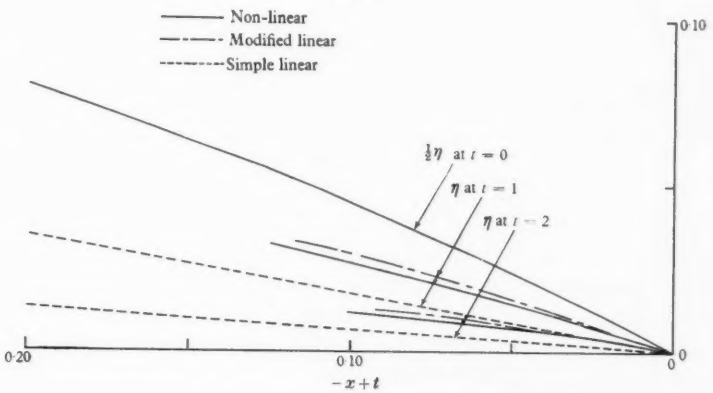

(*b*)

FIGURE 4. (*a*) The paths of the characteristics $\beta=0{\cdot}05$, $0{\cdot}10$; (*b*) the wave profiles near the front of an initially parabolic wave.

where ϑ is the initial wave slope, $-H_X(0-, 0)$, and is positive for a compressive wave-front. Next we observe that if A and B are $O(\delta)$, then in any of the expressions of (10.2) the ratio of second-order (A^2) terms to first-order (A, B) terms is $O(\delta)$ *uniformly* (that is, this ratio is $O(1)$ with respect to α and β for all α and β, including $\alpha \to \infty$), both for $k = 0$ and $k > 0$. This suggests that if we expand solutions in the $\alpha\beta$-plane in powers of δ, then, as in the case $k = 0$, we shall obtain a uniform asymptotic expansion.

Of course, equation (10.2) can also be used for approximate calculations of the leading sectors of flow fields. As an example, we take† $A = 1$, $B = -2$, so that the initial wave profile has the shape, near $X = 0$, of the parabola

$$\frac{H}{H_0} = 1 - \frac{X}{L} - \left(\frac{X}{L}\right)^2 \quad \left(-1 \leqslant \frac{X}{L} \leqslant 0\right),$$

of length L and amplitude $\frac{1}{4}H_0$; we also take $k = 1$, so that the condition (10.3) is satisfied. Figure 4(*a*) shows the characteristics $\beta = 0{\cdot}05$, $0{\cdot}10$, which move forward towards the wave-front, but not sufficiently to form a shock. Figure 4(*b*) shows the leading part of the wave-profile at various times: the appropriate reference quantity at time $t = 0$ is not η, but $\frac{1}{2}\eta$, because the wave splits into forward and backward moving parts. The profiles plotted are (i) the non-linear result of equation (10.2), (ii) the 'modified linear' result, which can be obtained either from (10.2), by neglecting terms in A^2, or by applying the method of § 11 and expanding for β small, and (iii) the 'simple linear' result, which can be obtained either from (10.2), by setting $\alpha \equiv \frac{1}{2}(x+t)$, $\beta \equiv \frac{1}{2}(-x+t)$ and neglecting terms in A^2 in the expressions for h and u, or from equation (8.2). All these results are, of course, only asymptotic for $\beta \to 0$ and are shown only for $\beta \leqslant 0{\cdot}10$.

The forward movement of the characteristics lessens the decay of wave-slope with time predicted by the simple linear theory, and the modified linear theory of § 11, which takes the shift of characteristics into account, yields much more accurate results than the simple one. Of course, the good agreement between non-linear and modified linear results is to be expected in the present case, since their difference occurs only in the curvature (β^2) terms of (10.2).

11. Small-disturbance series

We now consider series of the form

$$h - 1 = \delta\eta_1(\alpha, \beta) + \ldots, \quad u = \delta u_1(\alpha, \beta) + \ldots, \tag{11.1a, b}$$

$$x = \alpha - \beta + \delta x_1(\alpha, \beta) + \ldots, \quad t = \alpha + \beta + \delta t_1(\alpha, \beta) + \ldots, \tag{11.2a, b}$$

and assume, for reasons which follow, that such expansions are uniformly asymptotic series in the $\alpha\beta$-plane. For the case $k = 0$, in which the series for $h^{\frac{1}{2}}$ and u terminate after the terms of $O(\delta)$, Fox (1955) has shown that the infinite series for x, t are not only uniformly asymptotic, but actually converge for quite substantial values of the initial disturbances: it seems unlikely that the inclusion of a damping term should alter this result. Some slight evidence for our assumption has also been obtained in the previous section. Finally, we refer to the work

† Note that taking $|A| = 1$ merely defines L to be $H_0/|\vartheta|$.

of Whitham (1952), in which a number of results obtained by essentially the same hypothesis are checked against more exact solutions.

Substituting (11.1*a*, *b*) and (11.2*b*) into the 'flow equations' (9.2*b*), (9.3*b*), we find that η_1 and u_1 both satisfy

$$F_{\alpha\beta}+k(F_\alpha+F_\beta)=0, \tag{11.3}$$

and this is the linearized equation,

$$F_{xx}-F_{tt}-2kF_t=0,$$

with $x=\alpha-\beta$ and $t=\alpha+\beta$. Accordingly, η_1 and u_1 are simply the linearized solutions of part II with $x+t$ replaced by 2α and $-x+t$ replaced by 2β, but our viewpoint is now quite different. Whereas $x+t$ and $-x+t$ are Cartesian coordinates in the xt-plane, α and β are to be regarded as variables constant on a characteristic: the essential difference lies in the $O(\delta)$ terms of (11.2), which are to be included in the first approximation.

Substituting (11.2*a*, *b*) into the 'direction equations' (9.2*a*), (9.3*a*), we now find that

$$x_{1\alpha}-t_{1\alpha}=\tfrac{1}{2}\eta_1+u_1,$$
$$x_{1\beta}+t_{1\beta}=-\tfrac{1}{2}\eta_1+u_1,$$

so that, in view of the boundary conditions $x_1=0$, $t_1=0$ on $\beta=-\alpha$,

$$x_1-t_1=\int_{-\beta}^{\alpha}\{\tfrac{1}{2}\eta_1(\alpha',\beta)+u_1(\alpha',\beta)\}\,d\alpha', \tag{11.4a}$$

$$x_1+t_1=\int_{-\alpha}^{\beta}\{-\tfrac{1}{2}\eta_1(\alpha,\beta')+u_1(\alpha,\beta')\}\,d\beta'. \tag{11.4b}$$

Since η_1 and u_1 are known, these are, in principle, known functions.

Consider the initial-value problem studied previously: we now write $f(x)\equiv\delta f_1(x)$ for the initial surface elevation. We ask whether shocks can form from an initially continuous surface elevation; that is, whether the Jacobian

$$J\equiv x_\alpha t_\beta-x_\beta t_\alpha=2+\delta(x_{1\alpha}+t_{1\beta}-x_{1\beta}+t_{1\alpha})+\ldots$$

can vanish somewhere in the field. Now it can be shown, by straightforward if lengthy calculations, that if $f_1(x)$ is continuous and its derivative is bounded, such that $|f_1(x)|<M$, $|f_1'(x)|<N$ for all x, then with $\alpha+\beta=\tau\,(\geqslant 0)$,

$$\left.\begin{aligned}|x_{1\alpha}+t_{1\alpha}-x_{1\beta}+t_{1\beta}| &< M(3-2e^{-k\tau})+\frac{3N}{2k}(1-e^{-k\tau})(3-e^{-k\tau}),\\ &\leqslant 3M+\frac{9N}{2k}.\end{aligned}\right\} \tag{11.5}$$

Hence with $k>0$ the first-order term in the Jacobian remains $O(\delta)$ for all τ (whereas with $k=0$ this term is $O(\delta\tau)$), and by the assumption of uniformly asymptotic series, the higher-order terms behave similarly. According to the first-order theory and quite crude estimates, therefore, shocks will not occur if

$$\delta\left(\frac{3M}{2}+\frac{9N}{4k}\right)\leqslant 1. \tag{11.6}$$

We proceed to the case where the initial surface elevation is discontinuous: the discontinuities are assumed to be separated by distances greater than $O(\delta)$. Then the linearized solutions η_1 and u_1 are discontinuous across certain characteristics: let $\beta = \beta^*$ be such a characteristic. By (11.4*a*), $\beta = \beta^* -$ and $\beta = \beta^* +$ will be different curves in the xt-plane, and the quantity

$$\delta[x_1 - t_1]_{\beta=\beta^*-}^{\beta^*+} = G(\alpha), \quad \text{say},$$

is a measure of the distance between them. For shocks G is positive, and the domains $\beta < \beta^*$ and $\beta > \beta^*$ overlap in the xt-plane; for centred expansion waves G is negative, and there is a gap between these two domains in the xt-plane (figure 5). Because the jumps in η and u are exponentially damped, however, the width of the overlapping region or gap remains $O(\delta)$ for all α if $k > 0$, whereas for $k = 0$ it is $O(\delta\alpha)$. It then follows from arguments rather similar to those used in another paper (Fraenkel 1959, § 3) that the shock equations are satisfied, to our order of accuracy, if the shock is drawn halfway between the characteristics $\beta = \beta^* -$ and $\beta = \beta^* +$ in the xt-plane, the solutions between the shock and $\beta = \beta^* -$ on the sheet $\beta < \beta^*$, and between $\beta = \beta^* +$ and the shock on the sheet $\beta > \beta^*$, being discarded. The gap corresponding to an expansion fan may be filled, to our approximation, by taking a linear variation of h and u across it.

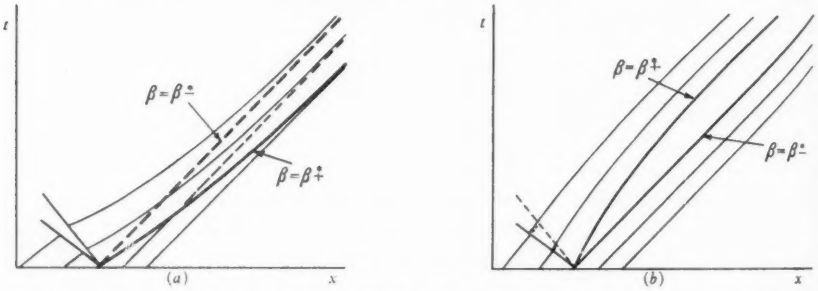

FIGURE 5. (*a*) The 'overlapping region' near a shock, (*b*) the 'gap' produced by a centred expansion wave.

For the initial elevation

$$f(x) = \delta\{1 + O(x)\}\, U(-x),$$

(11.4*a*, *b*) then show, upon elimination of α, that

$$\text{on} \quad \beta = 0-, \ x - t = 0; \quad \text{on} \quad \beta = 0+, \ x - t = \frac{3\delta}{4k}(1 - e^{-kt}) + O(\delta^2). \tag{11.7}$$

Hence for $\delta > 0$ the shock is

$$x - t = \frac{3\delta}{8k}(1 - e^{-kt}) + O(\delta^2), \tag{11.8}$$

while for $\delta < 0$ the equations (11.7) give the boundaries of the expansion fan.

Figure 6 shows the shock and characteristics pattern, according to the present theory, in the problem of a double step considered in part II (with $k = 1$). Here δ has been taken equal to the rather large value 0·4, to make the departure of the characteristics from their undisturbed positions clearly visible. The integrations

of (11.4a, b) to find $\beta = 0{\cdot}5-$ were done numerically, the integrands being given by (8.6) and (8.9) with x and t replaced by $\alpha-\beta-1$ and $\alpha+\beta$; the increments for $\beta = 0{\cdot}5+$, and the equations of the other curves, were found analytically from the equations above. Like figure 4(a), the figure illustrates the convection of disturbances implicit in the characteristic equations.

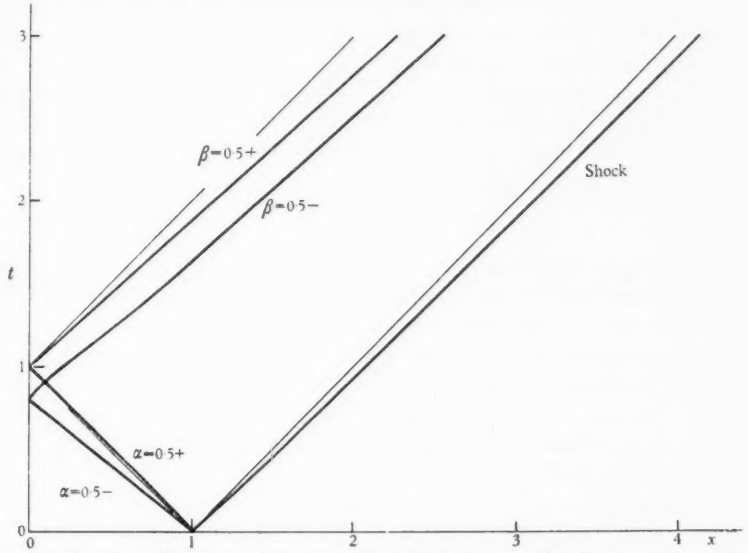

FIGURE 6. Shock and characteristics pattern resulting from a double step; $k = 1$, $\delta = 0{\cdot}4$. The fine lines are the characteristics of the simple linear theory.

Since for $k > 0$ and δ sufficiently small, (i) condition (11.6) is satisfied, so that shocks do not form from initially continuous surface elevations, and (ii) shocks and centred expansion waves depart only a distance $O(\delta)$ from their undisturbed positions, even for large times, we conclude that the linear theory of part II is uniformly valid as an approximation to the non-linear equations for small depth. (These latter, however, are not a uniformly valid approximation to the full equations, as was mentioned in § 3).

12. Concluding remarks

Lehnert's experiments (1952) are only described in a qualitative way in his paper, and a proper comparison with the present theory is therefore not possible. However, the most conspicuous results of the theory, namely the exponential decay of the wave amplitude and fluid velocity in a dish, and of the disturbances immediately behind a wave-front (§§ 7, 8), appear to agree with Lehnert's observation that the waves 'disappear' under the action of a magnetic field. On the other hand, his remark that the fluid 'acts as a thick syrup' in the presence of the field must be treated with caution, for this suggests an effective viscosity, whereas the theory involves a resisting body force proportional to the velocity rather than to its second derivatives.

We have obtained solutions for only the simplest problems, in which the electric field strength is negligible and the current density is simply $\sigma \mathbf{V} \wedge \mathbf{B}_0$ to the lowest order. In this case the most significant effect in the energy balance of the whole flow (equations (3.6) and (4.6)) is the Joule heating, and the decay of disturbances is not surprising. Although solutions have been obtained only for plane and axisymmetric flow, they are believed to be fairly representative of more general situations in a liquid unbounded laterally, for then the electric field still vanishes from the linearized hydrodynamic equations (§ 4).

For general, unsymmetrical waves in a finite dish made of insulating material, the electric field is significant even in the linear approximation, since the normal current must vanish at the vertical wall. In that case the surface elevation still satisfies the equation

$$\frac{\partial^2 \eta}{\partial x_1^2} + \frac{\partial^2 \eta}{\partial x_2^2} = \frac{\partial^2 \eta}{\partial t^2} + 2k \frac{\partial \eta}{\partial t},$$

but the relation of η to the velocity, and the boundary conditions, are less simple than in the cases studied here. In addition, the energy balance involves an exchange of electromagnetic energy between the liquid and the external field. A further investigation of these flows is intended.

There is a certain similarity (first conjectured by H. W. Liepmann) between the wave-front behaviour of the cylindrical waves described in § 8, and that of cylindrical sound pulses propagating into a gas having solid-body rotation and constant temperature (Fraenkel 1959). For zero magnetic field and zero rotation these two problems are, of course, virtually identical. Like the magnetic force of the present paper, the radial pressure gradient of the rotating gas resists the outflow behind the wave-front, and the disturbances there are damped in both cases. However, the analogy is far from complete; the decay of disturbances is like $r^{-\frac{1}{2}} e^{-kr}$ in the magnetic case, and like $r^{-\frac{1}{2}} e^{-k^* r^2}$ in the rotating-gas case (k^* being a constant, the details of which are irrelevant here), and the flow at substantial distances inside the wave-front is quite different in the two problems.

I am indebted to Prof. H. W. Liepmann and to Prof. J. D. Cole for teaching me the elements of magnetohydrodynamics, and for many helpful discussions. This work was partly sponsored by the U.S. Air Force Office of Scientific Research under Contracts AF-18 (600)-383 and AF-49(638)-476.

Appendix. The orders of the electromagnetic variables

Let

$$\left.\begin{aligned} \mathbf{E} &= (\epsilon^q B_0 \sqrt{(gL)}\, e_1,\ \epsilon^q B_0 \sqrt{(gL)}\, e_2,\ \epsilon^l B_0 \sqrt{(gL)}\, e_3), \\ \mathbf{B} &= (\epsilon^m N B_0 b_1,\ \epsilon^m N B_0 b_2,\ B_0 + \epsilon^n N B_0 b_3). \end{aligned}\right\} \tag{A 1}$$

Our object in this Appendix is to select a set of values of q, l, m, n by a *reductio ad absurdum* of all schemes but one. Attention is confined to a liquid unbounded laterally. In view of conditions at the interfaces $X_3 = 0, H$, the orders q, m, n must have the same values inside and outside the liquid; l need not. We shall be concerned only with the lowest-order form of all equations; terms which, on the basis of what has gone before, cannot be among the dominant ones, will be neglected throughout. In each approximation of form $F = \epsilon^v f + \ldots$, $\epsilon^v f$ of course refers to

the first non-vanishing term in the expansion of F. Hence any set of exponents (orders) which leads to any f vanishing everywhere, violates the definition of the ν and is inadmissible.

As before, we use the symbol α, which is 1 for $0 < X_3 < H$, and 0 for $X_3 < 0$ or $X_3 > H$: we shall also refer to these two domains by the words 'inside' and 'outside'. Maxwell's equations now become

$\nabla \wedge \mathbf{E} = -\dfrac{\partial \mathbf{B}}{\partial T}$:

$$\left.\begin{aligned} \epsilon^l \frac{\partial e_3}{\partial x_2} - \epsilon^{q-\alpha} \frac{\partial e_2}{\partial x_3} &= -\epsilon^{m+\frac{1}{2}} N \frac{\partial b_1}{\partial t}, \\ \epsilon^{q-\alpha} \frac{\partial e_1}{\partial x_3} - \epsilon^l \frac{\partial e_3}{\partial x_1} &= -\epsilon^{m+\frac{1}{2}} N \frac{\partial b_2}{\partial t}, \\ \epsilon^q \left(\frac{\partial e_2}{\partial x_1} - \frac{\partial e_1}{\partial x_2} \right) &= -\epsilon^{n+\frac{1}{2}} N \frac{\partial b_3}{\partial t}. \end{aligned}\right\} \qquad (\text{A } 2a, b, c)$$

$\nabla \wedge \mathbf{B} = \mu\sigma(\mathbf{E} + \mathbf{V} \wedge \mathbf{B})$:

$$\left.\begin{aligned} \epsilon^n \frac{\partial b_3}{\partial x_2} - \epsilon^{m-\alpha} \frac{\partial b_2}{\partial x_3} &= \alpha(\epsilon^q e_1 + \epsilon^{\frac{1}{2}} v_2), \\ \epsilon^{m-\alpha} \frac{\partial b_1}{\partial x_3} - \epsilon^n \frac{\partial b_3}{\partial x_1} &= \alpha(\epsilon^q e_2 - \epsilon^{\frac{1}{2}} v_1), \\ \epsilon^m \left(\frac{\partial b_2}{\partial x_1} - \frac{\partial b_1}{\partial x_2} \right) &= \alpha \epsilon^l e_3. \end{aligned}\right\} \qquad (\text{A } 3a, b, c)$$

$\nabla . \mathbf{B} = 0$:

$$\epsilon^m \left(\frac{\partial b_1}{\partial x_1} + \frac{\partial b_2}{\partial x_2} \right) + \epsilon^{n-\alpha} \frac{\partial b_3}{\partial x_3} = 0. \qquad (\text{A } 4)$$

(i) Assume that $n < m$. Then (A 4) reduces to $\partial b_3/\partial x_3 = 0$ inside and outside: b_3 vanishes at $|x_3| = \infty$ and is continuous across $x_3 = 0, h$, therefore $b_3 = 0$. Hence

$$m \leqslant n;$$

and in (A $3a, b$), inside, $\epsilon^n \partial b_3/\partial x_2$, $\epsilon^n \partial b_3/\partial x_1$ are negligible.

(ii) Assume that $m < \frac{3}{2}$ or $q < \frac{1}{2}$. Then the velocity terms in (A $3a, b$) are negligible, and Maxwell's equations and the boundary conditions are satisfied by $\mathbf{b} = 0$, $\mathbf{e} = 0$. Therefore $\quad \frac{3}{2} \leqslant m \leqslant n \quad \text{and} \quad q \geqslant \frac{1}{2}$.

(iii) The vertical momentum equation now reduces to $0 = -\partial p/\partial x_3 - 1$ (provided that K is bounded as $\epsilon \to 0$), so that $p = h - x_3$, and the horizontal pressure gradient is independent of x_3.

(iv) In view of (ii) the horizontal current densities are now represented by

$$\epsilon^q e_1 + \epsilon^{\frac{1}{2}} v_2, \quad \epsilon^q e_2 - \epsilon^{\frac{1}{2}} v_1$$

(although the e_1, e_2 terms may be negligible), and the horizontal momentum equation becomes

$$\frac{Dv_1}{Dt} = -\frac{\partial h}{\partial x_1} + K\epsilon^{-\frac{1}{2}}(\epsilon^{q-\frac{1}{2}} e_2 - v_1), \quad \frac{Dv_2}{Dt} = -\frac{\partial h}{\partial x_2} - K\epsilon^{-\frac{1}{2}}(\epsilon^{q-\frac{1}{2}} e_1 + v_2). \qquad (\text{A } 5a, b)$$

Hence we choose $K \sim O(\epsilon^{\frac{1}{2}})$, in order that the magnetic force shall not dominate the hydrostatic pressure gradient.

If $q > \frac{1}{2}$ the **e**-terms are negligible in (A 5); and if $q = \frac{1}{2}$, (A 2a, b) show, since $l > 0$, $m \geqslant \frac{3}{2}$, that $\partial e_1/\partial x_3 = 0$, $\partial e_2/\partial x_3 = 0$, inside. In either case, it follows from (A 5) that if (v_1, v_2) are independent of x_3 initially, as we assume, then they are so for all time.

(v) Assume that $q > \frac{1}{2}$. Then the magnetic force in (A 5) is proportional to the velocity. Rayleigh introduced such a term (see Lamb 1932, § 242) to represent a quasi-viscous force, and showed that under such a force irrotational flow is maintained, provided that the velocity is continuous; and continuous flows must be included in the approximate theory. For these, then

$$\frac{\partial v_2}{\partial x_1} - \frac{\partial v_1}{\partial x_2} = 0.$$

Also, $m = \frac{3}{2}$, otherwise (A 3a, b) reduce to $v_1 = v_2 = 0$. (A 3a, b) can now be integrated to $\quad b_1 = -v_1 x_3 + f_1(x_1, x_2), \quad b_2 = -v_2 x_3 + f_2(x_1, x_2),$

and the boundary condition $\mathbf{n}.(\nabla \wedge \mathbf{B}) = 0$ on $X_3 = 0, H$, becomes

$$\frac{\partial f_2}{\partial x_1} - \frac{\partial f_1}{\partial x_2} = 0 \quad (\text{on } X_3 = 0), \tag{A 6}$$

$$-\frac{\partial h}{\partial x_1} v_2 + \frac{\partial h}{\partial x_2} v_1 + \left(\frac{\partial f_2}{\partial x_1} - \frac{\partial f_1}{\partial x_2}\right) = 0 \quad (\text{on } X_3 = H). \tag{A 7}$$

Equations (A 5) ($q > \frac{1}{2}$), (A 6), and (A 7), all of which are independent of x_3, then combine to

$$v_2 \frac{Dv_1}{Dt} - v_1 \frac{Dv_2}{Dt} = 0, \quad \text{or} \quad \mathbf{i}_3 . \left(\mathbf{v} \wedge \frac{D\mathbf{v}}{Dt}\right) = 0. \tag{A 8}$$

But v_1 and v_2 are fully determined by the equations of continuity and momentum ($q > \frac{1}{2}$), and the boundary conditions; (A 8) is not, and cannot be, satisfied by a general flow with curved particle paths. Therefore

$$q = \tfrac{1}{2}.$$

(vi) Assume that $m > \frac{3}{2}$. (A 3a, b) reduce to

$$e_1 + v_2 = 0, \quad e_2 - v_1 = 0, \tag{A 9}$$

and the magnetic force vanishes from the hydrodynamic equations. Then if (v_1, v_2) are continuous and initially irrotational

$$\frac{\partial v_2}{\partial x_1} - \frac{\partial v_1}{\partial x_2} = 0 \quad \text{and, by (A 9),} \quad \frac{\partial e_1}{\partial x_1} + \frac{\partial e_2}{\partial x_2} = 0.$$

Further by (A 2c), with $q = \frac{1}{2}$, $n > 0$,

$$\frac{\partial e_2}{\partial x_1} - \frac{\partial e_1}{\partial x_2} = 0.$$

Hence the vector (e_1, e_2) is harmonic, free of singularities and vanishes at infinity, so that $e_1 = e_2 = 0$. But this contradicts (A 9) (and the result $q = \frac{1}{2}$), hence

$$m = \tfrac{3}{2}.$$

(For plane or axi-symmetric flows, in which $q > \frac{1}{2}$, $m = \frac{3}{2}$ also, for otherwise (A 3a, b) reduce to $v_1 = v_2 = 0$.)

(vii) Assume that $n > \frac{3}{2}$. Then, outside, (A 3a, b) reduce to $\partial b_2/\partial x_3 = \partial b_1/\partial x_3 = 0$; b_1 and b_2 vanish at $|x_3| = \infty$, and are continuous across $x_3 = 0, h$; inside, $\partial b_1/\partial x_3$, $\partial b_2/\partial x_3$ are independent of x_3. Hence $b_1 = b_2 = 0$, and therefore

$$n = \tfrac{3}{2}.$$

(viii) It may be recalled that $l = l(\alpha)$. If $l(1) < \frac{3}{2}$, then by (A 3c) $e_3 = 0$ inside, which violates the definition of $l(1)$; if $l(1) > \frac{3}{2}$, then (A 3c) states that $(\partial b_2/\partial x_1) - (\partial b_1/\partial x_2) = 0$, in contradiction of results already established. Hence,

$$l(1) = \tfrac{3}{2}.$$

(ix) If $l(0) < \frac{1}{2}$, (A 2a, b) reduce to $\partial e_3/\partial x_1 = \partial e_3/\partial x_2 = 0$, and since e_3 vanishes for $x_1, x_2 \to \infty$, $e_3 = 0$ outside, which violates the definition of $l(0)$. If $l(0) > \frac{1}{2}$, (A 2a, b) lead to $e_1 = e_2 = 0$ outside, in contradiction of results already established. Hence,

$$l(0) = \tfrac{1}{2}.$$

REFERENCES

Fox, P. A. 1955 Perturbation theory of wave propagation based on the method of characteristics. *J. Math. Phys.* **34**, 133.

Fraenkel, L. E. 1959 A cylindrical sound pulse in a rotating gas. *J. Fluid Mech.* **5**, 637.

Friedrichs, K. O. 1948 Formation and decay of shock waves. *Commun. Pure Appl. Math.* **1**, 211.

Hartmann, J. 1937 Hg-Dynamics I. Theory of the laminar flow of an electrically conductive liquid in a homogeneous magnetic field. *Math.-fys. Medd.* **15**, no. 6.

Lamb, H. 1932 *Hydrodynamics.* Cambridge University Press.

Lehnert, B. 1952 On the behaviour of an electrically conductive liquid in a magnetic field. *Arkiv för Fysik*, **5**, 69.

Lighthill, M. J. 1949 A technique for rendering approximate solutions to physical problems uniformly valid. *Phil. Mag.* (7) **40**, 1179.

Lighthill, M. J. 1955 Article in *General Theory of High Speed Aerodynamics* (ed. W. R. Sears), section E. Princeton University Press.

Lin, C. C. 1954 On a perturbation theory based on the method of characteristics. *J. Math. Phys.* **33**, 117.

Longuet-Higgins, M. S. 1958 Review of Stoker's '*Water Waves*'. *J. Fluid Mech.* **4**, 435.

Lundquist, S. 1952 Studies in magneto-hydrodynamics. *Arkiv för Fysik*, **5**, 297.

Meyer, R. E. 1948 The method of characteristics for problems of compressible flow involving two independent variables, part II. *Quart. J. Mech. Appl. Math.* **1**, 451.

Stewartson, K. 1957 Magnetohydrodynamics of a finite rotating disc. *Quart. J. Mech. Appl. Math.* **10**, 137.

Stoker, J. J. 1957 *Water Waves.* New York: Interscience.

Ursell, F. 1953 The long-wave paradox in the theory of gravity waves. *Proc. Camb. Phil. Soc.* **49**, 685.

Van der Pol, B. & Bremmer, H. 1955 *Operational Calculus.* Cambridge University Press.

Watson, G. N. 1944 *Theory of Bessel Functions.* Cambridge University Press.

Whitham, G. B. 1952 The flow pattern of a supersonic projectile. *Commun. Pure Appl. Math.* **5**, 30.

Steady finite motions of a conducting liquid

By ROBERT R. LONG
School of Engineering, The Johns Hopkins University, Baltimore

(Received 28 April 1959)

In certain cases of steady motion of a conducting fluid in a magnetic field, the primitive equations may be integrated once, yielding a second-order partial differential equation in the stream function. This equation is highly non-linear in general, but for certain choices of basic flow and magnetic fields it is tractable. Several arbitrary functions of integration have to be evaluated to make the analysis useful. This may be done in a region that remains undisturbed. A short discussion is given to suggest a procedure for deciding in a special case whether this undisturbed region is 'upstream' or 'downstream'.

1. Introduction

This paper was suggested by previous work of the author on the mechanics of rotating fluids (Long 1953*a*) and fluids with density stratification (Long 1953*b*). Among other things these papers showed how the primitive equations of motion can be integrated in certain cases to yield a partial differential equation in a single dependent variable analogous to the harmonic equation of potential flow. The procedure used to do this also works in cases of conducting fluids in magnetic fields. We will show this in some detail for the axisymmetric case in the following section. The extension to the plane case is similar and will not be discussed here.

2. Axisymmetric flow

Consider the steady flow of a frictionless, incompressible, conducting fluid of infinite conductivity. If, as is usual, we neglect displacement currents we have the equations (Cowling 1957)

$$-\mathbf{v}\times(\nabla\times\mathbf{v}) = -\nabla\left(\frac{p}{\rho}+\tfrac{1}{2}q^2+\chi\right)-\mathbf{h}\times(\nabla\times\mathbf{h}), \tag{1}$$

$$\nabla.\mathbf{v} = 0, \tag{2}$$

$$\nabla.\mathbf{h} = 0, \tag{3}$$

$$\nabla\times(\mathbf{v}\times\mathbf{h}) = 0, \tag{4}$$

where $\mathbf{v}$ is the fluid velocity vector, p is fluid pressure, ρ is the uniform density, $q = |\mathbf{v}|$ is the speed and χ is the potential of other body forces. We have written $\mathbf{h} = \mathbf{H}\sqrt{(\mu/4\pi\rho)}$, where $\mathbf{H}$ is the magnetic field and μ is the permeability.

We adopt the co-ordinate system of figure 1 and the following additional assumptions:

(1) There is axial symmetry, i.e. all scalars are independent of θ. In particular, if the velocity and magnetic fields are

$$\mathbf{v} = u\mathbf{i} + v\mathbf{j} + w\mathbf{k}, \tag{5}$$

$$\mathbf{h} = f\mathbf{i} + g\mathbf{j} + h\mathbf{k}, \tag{6}$$

the components depend only on r and z.

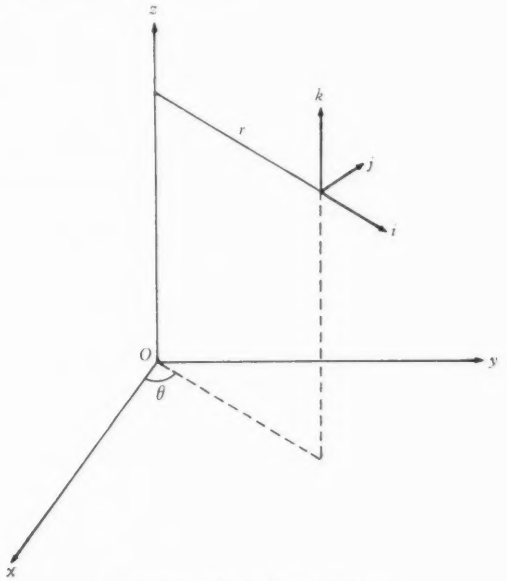

FIGURE 1. Co-ordinate system.

(2) The velocity and magnetic fields are assumed known either at $z \to -\infty$ *or* at $z \to +\infty$. The components u and f of these 'undisturbed fields' are assumed to be zero and, for simplicity, the remaining components depend only on distance from the axis. The question of whether an undisturbed region exists, and if so whether it is 'upstream' or 'downstream' will be discussed only with reference to a special case in the next section.

Equations (2) and (3) can be integrated by introducing two scalar functions $\psi(r, z)$ and $\Lambda(r, z)$, such that

$$ur = -\psi_z, \quad wr = \psi_r, \tag{7}$$

$$fr = -\Lambda_z, \quad hr = \Lambda_r. \tag{8}$$

The three equations in (4) are

$$\frac{\partial}{\partial z}(uh - wf) = 0, \tag{9}$$

$$\frac{\partial}{\partial r}(uhr - wfr) = 0, \tag{10}$$

$$\frac{\partial}{\partial r}(vf - ug) + \frac{\partial}{\partial z}(vh - wg) = 0. \tag{11}$$

Equations (9) and (10) have solution $r(uh-wf) = \text{const}$. The constant is zero, however, since u and f are zero in the undisturbed region. Introducing (8) into $uh-wf=0$, we find

$$\frac{d\Lambda}{dt} = 0, \tag{12}$$

where the material derivative is

$$\frac{d}{dt} = u\frac{\partial}{\partial r} + w\frac{\partial}{\partial z}. \tag{13}$$

Equation (12) may also be written

$$-\psi_z\Lambda_r + \psi_r\Lambda_z = 0, \tag{14}$$

which has the integral

$$\Lambda = \Lambda(\psi). \tag{15}$$

Thus, Λ is constant on the material surfaces $\psi = \text{const}$. Since the latter are stream surfaces, this expresses the well-known principle that magnetic lines move with the fluid in the ideal case of this paper.

Equation (11) may also be integrated. With use of (7) and (8) it takes the form

$$\frac{\partial}{\partial r}\left[\psi_z\frac{g}{r} - \Lambda_z\frac{v}{r}\right] - \frac{\partial}{\partial z}\left[\psi_r\frac{g}{r} - \Lambda_r\frac{v}{r}\right] = 0,$$

or

$$\frac{\partial}{\partial r}\left[\psi_z\left(\frac{g}{r} - \Lambda'\frac{v}{r}\right)\right] - \frac{\partial}{\partial z}\left[\psi_r\left(\frac{g}{r} - \Lambda'\frac{v}{r}\right)\right] = 0, \tag{16}$$

if we use (15) and write $\Lambda' = d\Lambda/d\psi$. Equation (16) is

$$\frac{d}{dt}\left[\frac{g-\Lambda' v}{r}\right] = 0,$$

so that

$$\frac{g-\Lambda' v}{r} = K(\psi), \tag{17}$$

where $K(\psi)$ is an arbitrary function.

Another conserved quantity can be found from the **j**-equation in (1). Since $p/\rho + \frac{1}{2}q^2 + \chi$ is independent of θ, this equation is

$$u\left(v_r + \frac{v}{r}\right) + wv_z - f\left(g_r + \frac{g}{r}\right) - hg_z = 0. \tag{18}$$

The same procedure that led to (17) permits us to integrate this equation. We get

$$vr - \Lambda' gr = L(\psi). \tag{19}$$

The final conservation equation is found by cross-differentiating the remaining two equations in (1) to eliminate $p/\rho + \frac{1}{2}q^2 + \chi$. This vorticity equation is

$$\frac{\partial}{\partial z}\left[-\frac{v}{r}\frac{\partial}{\partial r}(vr) + \frac{g}{r}\frac{\partial}{\partial r}(gr) + w(u_z - w_r) - h(f_z - h_r)\right]$$

$$-\frac{\partial}{\partial r}\left[-\frac{v}{r}\frac{\partial}{\partial z}(vr) + \frac{g}{r}\frac{\partial}{\partial z}(gr) - u(u_z - w_r) + f(f_z - h_r)\right] = 0, \tag{20}$$

or

$$r\frac{d}{dt}\left[\frac{(u_z - w_r) - \Lambda'(f_z - h_r)}{r}\right] - \frac{1}{r^3}\frac{\partial}{\partial z}(vr)^2 + \frac{1}{r^3}\frac{\partial}{\partial z}(gr)^2 = 0. \tag{21}$$

Equations (17) and (19) give us

$$(vr)^2-(gr)^2 = A-Br^4, \tag{22}$$

where A and B are functions of ψ:

$$A = \frac{L^2}{1-\Lambda'^2}, \quad B = \frac{K^2}{1-\Lambda'^2}. \tag{23}$$

Using (22), we get

$$\begin{aligned} -\frac{1}{r^4}\frac{\partial}{\partial z}[(vr)^2-(gr)^2] &= \frac{A'u}{r^3}-B'ur \\ &= \frac{A'}{r^3}\frac{dr}{dt}-B'r\frac{dr}{dt} = -\frac{d}{dt}\left(\frac{A'}{2r^2}+\frac{B'r^2}{2}\right), \end{aligned} \tag{24}$$

and combining (21) and (24), we get

$$-\frac{u_z-w_r-\Lambda'(f_z-h_r)}{r}+\frac{A'}{2r^2}+\frac{B'r^2}{2} = M(\psi). \tag{25}$$

Introducing the stream function ψ, we now get

$$\psi_{zz}+\psi_{rr}-\frac{1}{r}\psi_r-\frac{\Lambda'\Lambda''}{(1-\Lambda'^2)}[(\psi_z)^2+(\psi_r)^2]+\frac{A'}{2(1-\Lambda'^2)}+\frac{B'r^4}{2(1-\Lambda'^2)} = \frac{Mr^2}{(1-\Lambda'^2)}. \tag{26}$$

This is a non-linear differential equation in ψ. The functions $\Lambda(\psi)$, $L(\psi)$, $K(\psi)$, $M(\psi)$ are assumed known (A and B may then be obtained from (23)).

According to our previous assumptions the velocity and magnetic fields in the undisturbed region may be written

$$\mathbf{v}_0 = v_0(r_0)\,\mathbf{j}+w_0(r_0)\,\mathbf{k}, \tag{27}$$

$$\mathbf{h}_0 = g_0(r_0)\,\mathbf{j}+h_0(r_0)\,\mathbf{k}, \tag{28}$$

where the components are functions of $r_0(r,z)$, the distance of the stream surface passing through (r,θ,z) from the axis of symmetry in the undisturbed region. The relation between ψ and the Lagrangian variable r_0 is obtained by integrating

$$w_0 r_0 = \frac{d\psi}{dr_0}, \tag{29}$$

or

$$\psi = \int_0^{r_0} w_0 r_0 dr_0. \tag{30}$$

We may now evaluate all unknown functions of ψ in terms of the known functions of r_0 in (27) and (28). From (8) we get

$$\Lambda = \int_0^{r_0} h_0 r_0 dr_0, \tag{31}$$

$$\Lambda' = \frac{h_0}{w_0}. \tag{32}$$

Equations (17), (19) and (25) show that

$$K = \frac{g_0}{r_0} - \frac{h_0}{w_0}\frac{v_0}{r_0}, \tag{33}$$

$$L = v_0 r_0 - \frac{h_0}{w_0} g_0 r_0, \tag{34}$$

$$M = \frac{1}{r_0}\frac{dw_0}{dr_0}(1-\Lambda'^2) - \Lambda'\Lambda'' w_0^2 + \frac{A'}{2r_0^2} + \frac{B' r_0^2}{2}. \tag{35}$$

These functions and A', B' become known functions of ψ if we eliminate r_0 by using (30).

It is not the purpose of this note to develop applications of the equation (26), but we may point out certain cases in which the equation is tractable:

(1) If the undisturbed conditions are $v_0 = 0$, $w_0 = \text{const.}$, $g_0 = 0$, $h_0 = \text{const.}$, we have the well-known result that the flow is irrotational; thus

$$\psi_{zz} + \psi_{rr} - \frac{1}{r}\psi_r = 0. \tag{36}$$

The magnetic field then does not affect the motion.

(2) In the case $v_0 = \Omega r_0$ (solid rotation), $w_0 = \text{const.}$, $g_0 = 0$, $h_0 = \text{const.}$, we have

$$\Lambda = \tfrac{1}{2}h_0 r_0^2, \quad \psi = \tfrac{1}{2}w_0 r_0^2, \quad K = -\frac{h_0\Omega}{w_0}, \quad L = \Omega r_0^2,$$

so that

$$A = \frac{4\Omega^2\psi^2}{w_0^2[1-(h_0^2/w_0^2)]},$$

$$B = \frac{h_0^2\Omega^2}{w_0^2[1-(h_0^2/w_0^2)]}.$$

Equation (26) is

$$\psi_{zz} + \psi_{rr} - \frac{1}{r}\psi_r + \sigma^2\psi = \tfrac{1}{2}\sigma^2 w_0 r^2 \quad \left(\sigma = \frac{2\Omega}{w_0[1-(h_0^2/w_0^2)]}\right), \tag{37}$$

or, in terms of the perturbed streamfunction ψ' (i.e. $\psi = \frac{1}{2}w_0 r^2 + \psi'$), it takes the neater form

$$\psi'_{zz} + \psi'_{rr} - \frac{1}{r}\psi'_r + \sigma^2\psi' = 0. \tag{38}$$

This is the same as the equation derived by the author for the non-conducting case ($h_0 = 0$). Solutions of interest may be found in ways similar to those in two papers of Long (1955, 1956).

(3) A number of other cases in which equation (26) is linear can be found by a procedure similar to that in a recent paper (Long 1958). This approach will not be developed here.

3. The undisturbed region

If we could have included dissipation in our discussion, we could be sure that the magnetic and flow fields would be undisturbed at sufficient distances from the source of the disturbance. Without dissipation, however, we will frequently have a situation in which steady perturbations can exist at indefinitely great distances

from the source of the disturbance. In subcritical flow of water over an obstacle in a channel, for example, the free surface downstream to infinity is in steady wave motion (Lamb 1932). At sufficiently great distances upstream there is no disturbance. The steady-state theory is incomplete in such cases since the mathematical problem is indeterminate.

Stoker (1953) has shown that in the water-wave case the disappearance of upstream waves occurs even without dissipation if the flow problem is solved from the initial state of rest. On the other hand, Rayleigh (see Lamb 1932) found that indeterminacy of this kind can be removed by introducing a small amount of friction in an artificial way. As the coefficient of friction tends to zero the solution tends to that obtained by the approach of Stoker or by arbitrarily superimposing solutions to wipe out upstream waves. The author has verified that Rayleigh's approach is effective in a case similar to the one in this paper (Long 1955).

We can obtain definite results in the model mentioned in the last section, i.e. a stream of liquid moving at a uniform speed w_0 parallel to the axis, rotating with constant angular velocity Ω, and under a uniform axial magnetic field h_0. If the disturbance is not too large we may suppose that the problem of the undisturbed region may be decided on the basis of linear theory, namely that upstream or downstream conditions will be undisturbed if no energy from the source of disturbance (in the vicinity of $z = 0$) can reach the steady waves which may exist. In the linear case the energy propagation will be at the speed of the group velocity. On the other hand, for large disturbances we recognize that effects that change the basic velocity and magnetic fields may propagate indefinitely in the direction of the assumed undisturbed region. The problem as originally posed would then be overdetermined mathematically. This occurs in the case mentioned above of water flow over an obstacle. If the flow is slow and the obstacle large, a 'blocking' wave propagates upstream, raising the water level and making it impossible to assume that upstream is undisturbed.

The blocking problem is discussed at length in Long (1955) and will not be examined here. The case of small or moderate axisymmetric disturbances leads to a simple and interesting conclusion. If we perturb the basic flow and magnetic fields slightly, we will obtain a spectrum of waves moving in the upstream and downstream directions. If we confine the system to a circular tube of arbitrary radius b, the waves will move at speeds given by (Long 1956)

$$\lambda^2 = \frac{4\pi^2}{[\sigma^2 - (z_n^2/b^2)]}, \tag{39}$$

where λ is wavelength, z_n are the zeros of the Bessel function $J_1(z)$ and σ^2 is now

$$\sigma^2 = \frac{4\Omega^2 c^2}{(c^2 - h_0^2)^2}. \tag{40}$$

The wave-speed or phase velocity is c. These are infinitesimal waves and may be superimposed. The group velocity c_g is

$$\frac{c_g - c}{c} = -\frac{\lambda^2}{c^2}\frac{dc^2}{d\lambda^2}.$$

Solving (39) the phase velocity is

$$c^2 = h_0^2 + \frac{2\Omega^2}{(4\pi^2/\lambda^2) + (z_n^2/b^2)}\left[1 \pm \sqrt{\left\{1 + \frac{h_0^2}{\Omega^2}\left(\frac{4\pi^2}{\lambda^2} + \frac{z_n^2}{b^2}\right)\right\}}\right], \tag{41}$$

so that

$$\frac{c_g - c}{c} = -\frac{8\Omega^2\pi^2}{\lambda^2 c^2\left(\frac{4\pi^2}{\lambda^2} + \frac{z_n^2}{b^2}\right)^2}\left[1 \pm \frac{1 + \frac{h_0^2}{2\Omega^2}\left(\frac{4\pi^2}{\lambda^2} + \frac{z_n^2}{b^2}\right)}{\sqrt{\left\{1 + \frac{h_0^2}{\Omega^2}\left(\frac{4\pi^2}{\lambda^2} + \frac{z_n^2}{b^2}\right)\right\}}}\right].$$

Using (41), we obtain

$$\frac{c_g - c}{c} = \mp \frac{4\pi^2/\lambda^2}{\left(\frac{4\pi^2}{\lambda^2} + \frac{z_n^2}{b^2}\right)\sqrt{\left\{1 + \frac{h_0^2}{\Omega^2}\left(\frac{4\pi^2}{\lambda^2} + \frac{z_n^2}{b^2}\right)\right\}}}. \tag{42}$$

Comparing this with (41) it is seen that waves with speeds $c^2 < h_0^2$ have a group velocity greater than the phase velocity, while those with speeds $c^2 > h_0^2$ have a lower group velocity. In the steady-state problem, if $w_0 > h_0$, waves of the second kind can remain at rest against the current, and these will be found downstream. The undisturbed region will be upstream. However, if $w_0 < h_0$, the standing waves will be upstream and the undisturbed region will be downstream.

We see from (41) that there is both a maximum and minimum wave-speed. If the oncoming stream has a speed outside of these limits, no wave can exist and we would expect the disturbed motion to die out at $z = \pm\infty$. As the current approaches infinity or zero, (37) shows that the motion approaches potential flow.

REFERENCES

Cowling, T. G. 1957 *Magnetohydrodynamics*. New York: Interscience.

Lamb, H. 1932 *Hydrodynamics*, p. 408. New York: Dover.

Long, R. R. 1953*a* *J. Meteorol.* **10**, 197.

Long, R. R. 1953*b* *Tellus*, **5**, 42.

Long, R. R. 1955 *Tellus*, **7**, 341.

Long, R. R. 1956 *Quart. J. Mech. Appl. Math.* **9**, 385.

Long, R. R. 1958 *Quart. J. Roy. Met. Soc.* **84**, 159.

Stoker, J. J. 1953 *Commun. Pure Appl. Math.* **6**, 471.

Free convection in the tilted open thermosyphon

By F. M. LESLIE

Department of Mathematics, University of Manchester

(Received 15 April 1959)

Approximate solutions are found for the fluid flow and heat transfer in a heated cylinder, closed at the bottom and opening at the top into a reservoir of cool fluid, which has been tilted at a small angle to the vertical.

One solution is found for large Rayleigh number when the boundary layer does not fill the tube, and another for small Rayleigh number when the boundary layer fills the tube. In both cases tilting causes a small increase in heat transfer which is proportional to the square of $(l/a)\tan\phi$, where l/a is the length–radius ratio and ϕ the angle of tilt.

1. Introduction

The open thermosyphon consists of a heated vertical cylinder of fluid, closed at the lower end and opening at the top into a reservoir of cool fluid. The fluid is subject to gravity. An annulus of hot fluid at the walls, being less dense, is displaced towards the open end and is replaced by heavier cool fluid moving down the centre of the tube. Thus a circulation is created which transfers heat by convection from the walls of the cylinder to the reservoir.

Holzwarth (1938) suggested that a similar system could be used to cool gas turbine blades. He envisaged a cylindrical cavity in each blade opening into a reservoir of cool fluid in the hub. In this case the external axial acceleration is the centrifugal acceleration, which can be as large as $10^4 g$. Since the system is rotating, there is also a Coriolis acceleration at right angles to the motion of the particles, and hence flow is not quite axially symmetrical.

No attempt had been made to solve this problem theoretically until Lighthill (1953) investigated the action of the thermosyphon in some detail for laminar and turbulent flow. He considered a cylinder whose walls are maintained at a constant temperature, and which had a constant axial acceleration directed towards the lower closed end; and he assumed that the fluid entering the tube along the axis at the open end has the temperature of the reservoir.

In the present paper an attempt is made to extend Lighthill's work by considering the external acceleration to be at a small angle to the axis. Alcock (1951) has pointed out that this problem is similar to that of free convection in rotating turbine blades. The component of the buoyancy force perpendicular to the axis simulates closely the Coriolis force on the moving fluid. The case of Coriolis forces is very difficult to treat, but that of simulated forces can be solved to give a fair estimate of the effect.

Martin (1957) has done experimental work on this problem, using a heated cylinder of fluid closed at the bottom and opening at the top into a reservoir of cool fluid. The external acceleration was gravity, and he investigated the effect of tilting the cylinder from the vertical position. In work so far unpublished, Martin found that, for Rayleigh number $10^{7\cdot25}$, the Nusselt number decreases with increasing angle of inclination to the vertical up to 5°, where it is 90 % of its value for the tube in the vertical position. If the inclination is increased beyond this point, the Nusselt number rises to its initial value by 15° and thereafter to 130 % of this value by 45°. For smaller Rayleigh numbers the initial decrease is smaller, until when the Rayleigh number is $10^{5\cdot25}$ there is no decrease and the Nusselt number increases steadily to 150 % of its initial value at 45°. Martin put forward an explanation for this decrease, which is equivalent to there being an instability at small angles of inclination for larger Rayleigh numbers. He attributed the ensuing rise in heat transfer to an overall decrease in the thickness of the boundary layer which is formed at the walls.

In the present treatment, only laminar flow is considered, and no attempt is made to assess the effects of a breaking down of laminar flow. Attention is given mainly to the flow obtained for large values of Rayleigh number, since a typical value for gas turbine applications is of the order of 10^{10}; however, a solution is also found for small Rayleigh number.

The most important parameter used by Lighthill is $t_1 = (a/l)\,Aa$, where a is the radius of the cylinder and l its length, and Aa is the Rayleigh number based on radius. For large t_1 (> 3400), he found a solution in the form of a rising boundary layer at the walls and a cool descending uniform core in the centre. Because of the complexity of the equations, he used approximate methods of solution based on integrated equations which represent the conservation of mass energy and momentum across a section of the cylinder. For small t_1 (< 311), Lighthill found a similarity solution in which velocity and temperature profiles are similar at different axial positions but vary in magnitude linearly with axial distance.

Solutions of a similar type are found below for the problem of the inclined tube. The boundary-layer thickness is found to decrease, giving an increase in heat transfer, as the inclination of the external acceleration to the axis is increased, which is in agreement with Martin's work. No initial decrease in the Nusselt number is found, however, since the model assumed does not allow for instabilities in the boundary layer in the cylinder due to unstable stratification on the lower side of the tube. This increase in heat transfer varies as the square of $(l/a)\tan\phi$, where ϕ is the angle between the external acceleration and the axis of the cylinder. For large t_1, where the flow is of the boundary-layer type which does not fill the tube, the percentage increase in the Nusselt number is $0{\cdot}17(l/a)^2\tan^2\phi$; and for small t_1, where the boundary layer fills the tube with similarity, this factor is $25(l/a)^2\tan^2\phi$. It is difficult to compare the results obtained in the present paper with those found by Martin in his experiments on account of the initial decrease in the Nusselt number due to another effect. However, there does appear to be qualitative agreement with his results for smaller Rayleigh numbers where there is no initial decrease. They are also supported to some extent by his results for larger angles of inclination at all Rayleigh numbers.

2. The equations of motion

Cylindrical polar co-ordinates (X, R, θ) are used where the X-axis coincides with the axis of the cylinder, the origin being at the closed end and the positive direction towards the open end. The transverse component of body force is directed towards $\theta = 0$. The equations governing the motion are those of conservation of mass, energy and momentum for steady motion; these are respectively

$$\frac{\partial U}{\partial X}+\frac{1}{R}\frac{\partial}{\partial R}(RV)+\frac{1}{R}\frac{\partial W}{\partial \theta}=0, \tag{1}$$

$$U\frac{\partial T}{\partial X}+V\frac{\partial T}{\partial R}+\frac{W}{R}\frac{\partial T}{\partial \theta}=K\left[\frac{1}{R}\frac{\partial}{\partial R}\left(R\frac{\partial T}{\partial R}\right)+\frac{1}{R^2}\frac{\partial^2 T}{\partial \theta^2}+\frac{\partial^2 T}{\partial X^2}\right], \tag{2}$$

$$U\frac{\partial U}{\partial X}+V\frac{\partial U}{\partial R}+\frac{W}{R}\frac{\partial U}{\partial \theta}=-\frac{1}{\rho}\frac{\partial P}{\partial X}-f\cos\phi+\gamma\left[\frac{1}{R}\frac{\partial}{\partial R}\left(R\frac{\partial U}{\partial R}\right)+\frac{1}{R^2}\frac{\partial^2 U}{\partial \theta^2}+\frac{\partial^2 U}{\partial X^2}\right], \tag{3}$$

$$U\frac{\partial V}{\partial X}+V\frac{\partial V}{\partial R}+\frac{W}{R}\frac{\partial V}{\partial \theta}-\frac{W^2}{R}=-\frac{1}{\rho}\frac{\partial P}{\partial R}+f\sin\phi\cos\theta+\gamma\left[\frac{1}{R}\frac{\partial}{\partial R}\left(R\frac{\partial V}{\partial R}\right)+\frac{1}{R^2}\frac{\partial^2 V}{\partial \theta^2}+\frac{\partial^2 V}{\partial X^2}-\frac{V}{R^2}-\frac{2}{R^2}\frac{\partial W}{\partial \theta}\right], \tag{4}$$

$$U\frac{\partial W}{\partial X}+V\frac{\partial W}{\partial R}+\frac{W}{R}\frac{\partial W}{\partial \theta}+\frac{VW}{R}=-\frac{1}{\rho}\frac{1}{R}\frac{\partial P}{\partial \theta}-f\sin\phi\sin\theta+\gamma\left[\frac{1}{R}\frac{\partial}{\partial R}\left(R\frac{\partial W}{\partial R}\right)+\frac{1}{R^2}\frac{\partial^2 W}{\partial \theta^2}+\frac{\partial^2 W}{\partial X^2}-\frac{W}{R^2}+\frac{2}{R^2}\frac{\partial V}{\partial \theta}\right], \tag{5}$$

where U, V, W are components of velocity in the directions of X, R, θ; T is temperature, P pressure, ρ density, f the external acceleration making angle ϕ with the negative direction of the X-axis; and K is the thermal diffusivity and γ the kinematic viscosity.

An equation of state is also required; this is taken to be

$$\frac{1}{\rho}=\frac{1}{\rho_0}(1+\alpha(T-T_0)), \tag{6}$$

where α is the coefficient of cubical expansion and the subscript 0 refers to conditions at the wall.

The boundary conditions are

$$\left.\begin{aligned} U=V=W=0 \quad &\text{at} \quad R=a, \quad \text{or} \quad X=0,\\ T=T_0 \quad &\text{at} \quad R=a, \quad \text{or} \quad X=0,\\ T=T_1 \quad &\text{at} \quad R=0, \qquad\quad X=l, \end{aligned}\right\} \tag{7}$$

where T_0 and T_1 are constant temperatures, T_1 being the temperature of the reservoir, and a, l are the radius and length of the cylinder.

Since either the flow is of the boundary-layer type or the ratio of radius to length is small, second derivatives with respect to X are neglected in comparison with those with respect to R. Large Prandtl number is assumed, and as a result the inertia terms in the momentum equations are neglected. This procedure was adopted by Lighthill and led to an error of 5 % when the Prandtl number was five.

Putting $P = P_1 + p$ where p is due to velocity effects, equations (3) to (5) give, when the velocity is zero,

$$\left.\begin{aligned} \frac{\partial P_1}{\partial X} + \rho_0 f \cos\phi &= 0, \\ \frac{\partial P_1}{\partial R} - \rho_0 f \sin\phi \cos\theta &= 0, \\ R\frac{\partial P_1}{\partial \theta} + \rho_0 f \sin\phi \sin\theta &= 0. \end{aligned}\right\} \tag{8}$$

Thus P_1 is the hydrostatic pressure when the temperature is T_0 throughout. Eliminating P_1 from (3) to (5), and using (8) and then (6), we find

$$-\frac{1}{\rho}\frac{\partial p}{\partial X} + \alpha f \cos\phi\,(T - T_0) + \gamma\left[\frac{1}{R}\frac{\partial}{\partial R}\left(R\frac{\partial U}{\partial R}\right) + \frac{1}{R^2}\frac{\partial^2 U}{\partial \theta^2}\right] = 0, \tag{9}$$

$$-\frac{1}{\rho}\frac{\partial p}{\partial R} - \alpha f \sin\phi\,(T - T_0)\cos\theta + \gamma\left[\frac{1}{R}\frac{\partial}{\partial R}\left(R\frac{\partial V}{\partial R}\right) + \frac{1}{R^2}\frac{\partial^2 V}{\partial \theta^2} - \frac{V}{R^2} - \frac{2}{R^2}\frac{\partial W}{\partial \theta}\right] = 0, \tag{10}$$

$$-\frac{1}{\rho R}\frac{\partial p}{\partial \theta} + \alpha f \sin\phi\,(T - T_0)\sin\theta + \gamma\left[\frac{1}{R}\frac{\partial}{\partial R}\left(R\frac{\partial W}{\partial R}\right) + \frac{1}{R^2}\frac{\partial^2 W}{\partial \theta^2} - \frac{W}{R^2} + \frac{2}{R^2}\frac{\partial V}{\partial \theta}\right] = 0. \tag{11}$$

To reduce equations (1), (2), (9), (10), (11) and boundary equations (7) to non-dimensioned form the following substitutions are made:

$$U = \frac{Kl}{a^2}u^1, \quad V = \frac{K}{a}v^1, \quad W = \frac{K}{a}w^1,$$

$$R = ar, \quad X = lx,$$

$$T - T_0 = -\frac{\gamma K l}{\alpha f a^4 \cos\phi}t^1, \quad p = \frac{\gamma K l}{a^2}p^1.$$

The equations become

$$\frac{\partial u^1}{\partial x} + \frac{1}{r}\frac{\partial}{\partial r}(rv^1) + \frac{1}{r}\frac{\partial w^1}{\partial \theta} = 0, \tag{12}$$

$$u^1\frac{\partial t^1}{\partial x} + v^1\frac{\partial t^1}{\partial r} + \frac{w^1}{r}\frac{\partial t^1}{\partial \theta} = \frac{1}{r}\frac{\partial}{\partial r}\left(r\frac{\partial t^1}{\partial r}\right) + \frac{1}{r^2}\frac{\partial^2 t^1}{\partial \theta^2}, \tag{13}$$

$$-\left(\frac{a}{l}\right)^2\frac{\partial p^1}{\partial x} - t^1 + \frac{1}{r}\frac{\partial}{\partial r}\left(r\frac{\partial u^1}{\partial r}\right) + \frac{1}{r^2}\frac{\partial^2 u^1}{\partial \theta^2} = 0, \tag{14}$$

$$-\frac{\partial p^1}{\partial r} + \epsilon t^1\cos\theta + \frac{1}{r}\frac{\partial}{\partial r}\left(r\frac{\partial v^1}{\partial r}\right) + \frac{1}{r^2}\frac{\partial^2 v^1}{\partial \theta^2} - \frac{v^1}{r^2} - \frac{2}{r^2}\frac{\partial w^1}{\partial \theta} = 0, \tag{15}$$

$$-\frac{1}{r}\frac{\partial p^1}{\partial \theta} - \epsilon t^1\sin\theta + \frac{1}{r}\frac{\partial}{\partial r}\left(r\frac{\partial w^1}{\partial r}\right) + \frac{1}{r^2}\frac{\partial^2 w^1}{\partial \theta^2} - \frac{w^1}{r^2} + \frac{2}{r^2}\frac{\partial v^1}{\partial \theta} = 0, \tag{16}$$

where $\epsilon = (l/a)\tan\phi$. The boundary conditions (7) reduce to

$$\left.\begin{aligned} u^1 = v^1 = w^1 = t^1 = 0 \quad &\text{at} \quad r = 1, \quad \text{or} \quad x = 0, \\ t^1 = t_1 = \alpha f \cos\phi\,(T_0 - T_1)\frac{a^4}{\gamma K l} \quad &\text{at} \quad r = 0, \quad x = 1. \end{aligned}\right\} \tag{17}$$

Since there is symmetry about the plane $\theta = 0$ and the angle ϕ is taken as small, solutions in the form of the leading terms of Fourier series are obtained:

$$u^1 = U + u\cos\theta, \quad v^1 = V + v\cos\theta, \quad w^1 = w\sin\theta,$$
$$p^1 = P + p\cos\theta, \quad t^1 = T + t\cos\theta,$$

where U, V, P, T, and perturbation functions u, v, w, p, t are functions of x, r only. It should be noted that the symbols U, V, P, T, and p have been used earlier with a different meaning.

The boundary conditions (17) become

$$\left.\begin{aligned} U = V = T = 0 \quad &\text{at} \quad r = 1, \quad \text{or} \quad x = 0, \\ T = t_1 \quad &\text{at} \quad x = 1, \quad r = 0, \end{aligned}\right\} \tag{18}$$

and

$$\left.\begin{aligned} u = v = w = t = 0 \quad &\text{at} \quad r = 1, \quad \text{or} \quad x = 0, \\ v + w = 0 \quad &\text{at} \quad r = 0, \\ u = p = t = 0 \quad &\text{at} \quad r = 0. \end{aligned}\right\} \tag{19}$$

This last condition is necessary because of harmonic variation with θ.

Making these substitutions in (12) to (15) and integrating with respect to θ from 0 to 2π to obtain terms independent of θ, we obtain

$$\left.\begin{aligned} \frac{\partial U}{\partial x} + \frac{1}{r}\frac{\partial}{\partial r}(rV) = 0, \qquad &(a) \\ U\frac{\partial T}{\partial x} + V\frac{\partial T}{\partial r} + \frac{1}{2}\left(u\frac{\partial t}{\partial x} + v\frac{\partial t}{\partial r} - w\frac{t}{r}\right) = \frac{1}{r}\frac{\partial}{\partial r}\left(r\frac{\partial T}{\partial r}\right), \qquad &(b) \\ -\left(\frac{a}{l}\right)^2\frac{\partial P}{\partial x} - T + \frac{1}{r}\frac{\partial}{\partial r}\left(r\frac{\partial U}{\partial r}\right) = 0, \qquad &(c) \\ -\frac{\partial P}{\partial r} + \tfrac{1}{2}\epsilon t + \frac{1}{r}\frac{\partial}{\partial r}\left(r\frac{\partial V}{\partial r}\right) - \frac{V}{r^2} = 0. \qquad &(d) \end{aligned}\right\} \tag{20}$$

Here $\frac{1}{2}(u\partial/\partial x + v\partial/\partial r - w/r)t$ and $\frac{1}{2}\epsilon t$ are of the second order of smallness since u, v, w, t are perturbations; if these terms are neglected relative to other terms, equations (20) reduce to those used by Lighthill. He used integrated forms of this reduced set of equations (20) to find approximate solutions for U, T subject to boundary conditions (18). Thus, if $\frac{1}{2}(u\partial/\partial x + v\partial/\partial t - w/r)t$ and $\frac{1}{2}\epsilon t$ are neglected, U, T may be regarded as known functions of x, r for all t_1, and then can be found from Lighthill (1953).

Equations for the perturbation functions are found by substituting for u^1, v^1, w^1, p^1, t^1 in equations (12) to (16): equations (12) to (15) are multiplied by $\cos\theta$ and (16) by $\sin\theta$ and then integrated with respect to θ from 0 to 2π to give

$$\frac{\partial u}{\partial x} + \frac{1}{r}\frac{\partial}{\partial r}(rv) + \frac{w}{r} = 0, \tag{21}$$

$$u\frac{\partial T}{\partial x} + v\frac{\partial T}{\partial r} + U\frac{\partial t}{\partial x} + V\frac{\partial t}{\partial r} = \frac{1}{r}\frac{\partial}{\partial r}\left(r\frac{\partial t}{\partial r}\right) - \frac{t}{r^2}, \tag{22}$$

$$-\left(\frac{a}{l}\right)^2\frac{\partial p}{\partial x} - t + \frac{1}{r}\frac{\partial}{\partial r}\left(r\frac{\partial u}{\partial r}\right) - \frac{u}{r^2} = 0, \tag{23}$$

$$-\frac{\partial p}{\partial r} + \epsilon T + \frac{1}{r}\frac{\partial}{\partial r}\left(r\frac{\partial v}{\partial r}\right) - \frac{2}{r^2}(v + w) = 0, \tag{24}$$

$$\frac{p}{r} - \epsilon T + \frac{1}{r}\frac{\partial}{\partial r}\left(r\frac{\partial w}{\partial r}\right) - \frac{2}{r^2}(r + w) = 0. \tag{25}$$

Eliminating p between equations (24) and (25),

$$r\epsilon\frac{\partial T}{\partial r}-\frac{\partial^2}{\partial r^2}\left(r\frac{\partial w}{\partial r}\right)-\frac{1}{r}\frac{\partial}{\partial r}\left(r\frac{\partial v}{\partial r}\right)+\frac{2}{r}\frac{\partial}{\partial r}(v+w)=0. \tag{26}$$

No attempt is made to solve these equations as they stand because of their complexity. However, they can be expressed as the conservation of mass, energy and momentum (associated with the secondary flow) across a section bounded by the planes θ and $\theta+d\theta$, x and $x+dx$, and $r=1$ by multiplying by r and integrating from 0 to 1 with respect to r, thus

$$\frac{d}{dx}\int_0^1 ru\,dr+\int_0^1 w\,dr=0, \tag{27}$$

$$\frac{d}{dx}\int_0^1 r(uT+Ut)\,dr+\int_0^1 wT\,dr=\left(\frac{\partial t}{\partial r}\right)_{r=1}-\int_0^1\frac{t}{r}\,dr, \tag{28}$$

$$-\int_0^1 rt\,dr+\left(\frac{\partial u}{\partial r}\right)_{r=1}-\int_0^1\frac{u}{r}\,dr=0. \tag{29}$$

In (29) the term containing $\partial p/\partial x$ has been neglected, where p is the perturbation pressure; this appears reasonable physically and can be justified mathematically later. The integrated form of equation (26) is

$$2\epsilon\int_0^1 rT\,dr+\left(\frac{\partial^2 w}{\partial r^2}\right)_{r=1}+\left(\frac{\partial v}{\partial r}\right)_{r=1}=0. \tag{30}$$

The values of equations (21) to (26) at the walls and on the axis are needed to determine the profiles to be used in the similarity solution. These are

$$\left[\frac{1}{r}\frac{\partial}{\partial r}\left(r\frac{\partial t}{\partial r}\right)\right]_{r=1}=0, \tag{31}$$

$$\left[\frac{1}{r}\frac{\partial}{\partial r}\left(r\frac{\partial u}{\partial r}\right)\right]_{r=1}=0, \tag{32}$$

$$\left[\frac{1}{r}\frac{\partial}{\partial r}\left(r\frac{\partial w}{\partial r}\right)\right]+(p)_{r=1}=0, \tag{33}$$

$$\left.\begin{aligned}\left(U\frac{\partial t}{\partial x}+v\frac{\partial T}{\partial r}\right)_{r=0}&=\left[\frac{1}{r}\frac{\partial}{\partial r}\left(r\frac{\partial t}{\partial r}\right)-\frac{t}{r^2}\right]_{r=0},\\ \left[\frac{1}{r}\frac{\partial}{\partial r}\left(r\frac{\partial v}{\partial r}\right)-\frac{2(v+w)}{r^2}\right]_{r=0}+\epsilon(T)_{r=0}-\left(\frac{\partial p}{\partial r}\right)_{r=0}&=0,\\ \left[\frac{1}{r}\frac{\partial}{\partial r}\left(r\frac{\partial w}{\partial r}\right)-\frac{2(v+w)}{r^2}\right]_{r=0}-\epsilon(T)_{r=0}+\left(\frac{p}{r}\right)_{r=0}&=0.\end{aligned}\right\} \tag{34}$$

Simple radial profiles are assumed for velocity and temperature in finding the solution for the boundary layer which does not fill the tube. No attempt is made to satisfy equations (31) to (34), and as a result higher derivatives such as $(\partial^2 w/\partial r^2)_{r=1}$ in (30) cannot be expected to be accurate. It is possible to eliminate this term using equation (33), giving

$$2\epsilon\int_0^1 rT\,dr-\left(\frac{\partial w}{\partial r}\right)_{r=1}+\left(\frac{\partial v}{\partial r}\right)_{r=1}-(p)_{r=1}=0. \tag{35}$$

To eliminate $(p)_{r=1}$, we first integrate (24) with respect to r from 0 to 1:

$$(p)_{r=1} = \epsilon \int_0^1 T\,dr + \left[\frac{\partial v}{\partial r}\right]_0^1 - 2\left(\frac{v+w}{r}\right)_{r=0} - \int_0^1 \frac{1}{r}\frac{\partial v}{\partial r}\,dr - \int_0^1 \frac{2}{r}\frac{\partial w}{\partial r}\,dr,$$

and deduce that

$$2\epsilon \int_0^1 rT\,dr - \epsilon \int_0^1 T\,dr + \left(\frac{\partial v}{\partial r}\right)_{r=0} - \left(\frac{\partial w}{\partial r}\right)_{r=1} + 2\left(\frac{v+w}{r}\right)_{r=0} + \int_0^1 \frac{1}{r}\frac{\partial v}{\partial r}\,dr + 2\int_0^1 \frac{1}{r}\frac{\partial w}{\partial r}\,dr = 0. \quad (36)$$

The Nusselt number (based on radius) is given by

$$N_a = \frac{Qa}{k(T_0 - T_1)\,2\pi l a},$$

where Q is the actual rate of heat transfer from the whole wall surface of the tube and k is the thermal conductivity of the fluid.

Thus

$$N_a = \frac{1}{2\pi l(T_0 - T_1)} \int_0^l \int_0^{2\pi} a\left(\frac{\partial T}{\partial R}\right)_{R=a} dX\,d\theta$$

$$= \frac{1}{2\pi t_1} \int_0^1 \int_0^{2\pi} \left(-\frac{\partial t^1}{\partial r}\right)_{r=1} dx\,d\theta.$$

$$= \frac{1}{t_1} \int_0^1 \left(-\frac{\partial T}{\partial r}\right)_{r=1} dx. \quad (37)$$

Also

$$t_1 = \frac{\alpha f \cos\phi\,(T_0 - T_1)\,a^4}{\gamma K l}$$

$$= \left(\frac{a}{l}\right) A_a,$$

where

$$A_a = \frac{\alpha f \cos\phi\,(T_0 - T_1)\,a^3}{\gamma K}$$

is the Rayleigh number based on radius.

When the effect of the perturbations upon the solution obtained by Lighthill is calculated, several of equations (20) are required in modified form retaining the perturbation terms. With the usual boundary layer assumptions (20*d*) reduces to $\partial P/\partial r = 0$, and, at the wall, (20*c*) becomes

$$-\left(\frac{a}{l}\right)^2 \frac{dP}{dx} + \left[\frac{1}{r}\frac{\partial}{\partial r}\left(r\frac{\partial U}{\partial r}\right)\right]_{r=1} = 0.$$

This equation is used to eliminate P from (20*c*) which is then integrated over a cross-section; thus

$$-\int_0^1 rT\,dr + \frac{1}{2}\left[\frac{\partial U}{\partial r} - \frac{\partial^2 U}{\partial r^2}\right]_{r=1} = 0. \quad (38)$$

When integrated over a cross-section (20*b*) reduces to

$$\frac{d}{dx}\int_0^1 rUT\,dr + \frac{1}{2}\frac{d}{dx}\int_0^1 rut\,dr = \left(\frac{\partial T}{\partial r}\right)_{r=1}. \quad (39)$$

On the axis (20*b*) takes the form

$$\left[U\frac{\partial T}{\partial x}+\frac{1}{2}\left(v\frac{\partial t}{\partial r}-w\frac{t}{r}\right)\right]_{r=0}=\left[\frac{1}{r}\frac{\partial}{\partial r}\left(r\frac{\partial T}{\partial r}\right)\right]_{r=0}. \tag{40}$$

Equations (38) to (40) with the perturbation terms neglected are in the form used by Lighthill.

3. Boundary-layer solution not filling tube

In this section a solution is found in the form of a rising flow in a boundary layer at the walls and a descending flow in a cool uniform core in the centre.

For equations (20) Lighthill assumed the following solution:

$$\left.\begin{aligned} U &= -\phi && (0<r<\beta),\\ &= -\phi\left[1-\left(\frac{r-\beta}{1-\beta}\right)^2(1+\delta(r-1))\right] && (\beta<r<1),\end{aligned}\right\}$$

$$\left.\begin{aligned} T &= t_1 && (0<r<\beta),\\ &= t_1\left[1-\left(\frac{r-\beta}{1-\beta}\right)^2\right] && (\beta<r<1),\end{aligned}\right\}$$

where ϕ, δ, β are functions of x only, which were determined by substitution into the integrated forms of the equations. The solution obtained by Lighthill can be written in the modified form

$$\delta=\frac{6}{\xi^2},\quad \phi=\frac{t_1\xi^3}{18}$$

and

$$\xi=\left(\frac{240}{t_1}\right)^{\frac{1}{4}}x^{\frac{1}{4}},$$

where $\beta=1-\xi$ (i.e. ξ is the boundary-layer thickness) and where higher powers of ξ in the expressions for δ and ϕ have been neglected so that ξ may be expressed in terms of x in manageable form. This procedure is accurate to within 2 or 3 % if t_1 is greater than 10^8.

Radial profiles will be chosen for u, v, w, and t as follows:

$$\left.\begin{aligned} u &= 0 && (0<r<\beta),\\ &= \Phi\frac{(1-r)(r-\beta)^2}{(1-\beta)^3} && (\beta<r<1),\end{aligned}\right\}$$

$$\left.\begin{aligned} v &= \gamma && (0<r<\beta),\\ &= \gamma\left[1-\left(\frac{r-\beta}{1-\beta}\right)^2\right] && (\beta<r<1),\end{aligned}\right\}$$

$$\left.\begin{aligned} w &= -\gamma && (0<r<\beta),\\ &= -\gamma\left[1-\left(\frac{r-\beta}{1-\beta}\right)^2(1+\lambda(r-1))\right] && (\beta<r<1),\end{aligned}\right\}$$

$$\left.\begin{aligned} t &= 0 && (0<r<\beta),\\ &= \Theta\frac{(1-r)(r-\beta)^2}{(1-\beta)^3} && (\beta<r<1),\end{aligned}\right\}$$

where Φ, γ, λ and Θ are functions of x only. It is assumed that the boundary-layer thickness remains independent of θ despite the tilting. Martin (in a paper to be published) found very little variation of boundary-layer thickness with θ in his experiments.

If equations (27), (29), (28), (36) are written in the form of power series in ξ and only the lowest power of ξ is retained in each term, then we have

$$\frac{d}{dx}(\Phi\xi) - \gamma(12 + \lambda\xi^2) = 0.$$

$$12\Phi + \xi^2\Theta = 0,$$

$$\frac{d}{dx}\left[\frac{t_1\Phi\xi}{20} + \frac{t_1\Theta\xi^3}{315}\right] - \gamma t_1\left(1 + \frac{\lambda\xi^2}{20}\right) = -\frac{\Theta}{\xi},$$

$$\gamma\lambda + \frac{\epsilon t_1\xi}{3} = 0.$$

Solving for Φ, Θ, λ and γ to the lowest order in ξ, we find

$$\Phi = -\frac{\epsilon t_1^2\xi^6}{84\times 45}; \quad \Theta = \frac{\epsilon t_1^2\xi^4}{7\times 45};$$

$$\gamma = \frac{\epsilon t_1\xi^3}{54}; \qquad \lambda = -\frac{18}{\xi^2}.$$

Figure 1*a* shows the streamlines in the plane of symmetry ($\theta = 0$) for $t_1 = 10^8$ and $\epsilon = 1$. It can be seen that fluid in the cool uniform core is drawn to one side of the cylinder by the component of external acceleration in that direction. In the boundary layer the fluid tends to flow around the circumference of the cylinder due to this component of the buoyancy force. Figure 1*b*, which shows the projections of the streamlines on to a cross-section of the cylinder, also illustrates the cool fluid moving towards one side of the cylinder.

With these results equation (39) may now be written

$$\frac{d}{dx}\left[\frac{t_1\xi^3}{180} + \frac{\epsilon^2 t_1^{\frac{1}{2}}}{(240)^{\frac{1}{2}}}\frac{256}{27\times 7^3}x^{\frac{11}{4}}\right] = \frac{1}{\xi}, \tag{41}$$

where again only the leading power in ξ is retained in the first term in the bracket. The value of ξ as a function of x quoted above is calculated from this equation where the second term in the bracket (due to perturbations) has been neglected, and hence is accurate only if $\epsilon^2x^2 \ll 13$. To find the effect of the perturbations upon the solution obtained by Lighthill, equation (41) with the perturbation term retained is solved for ξ as a function of x by writing $\xi = (240/t_1)^{\frac{1}{4}}x^{\frac{1}{4}}(1+\eta)$ and neglecting squares and higher powers of η. It is found that $\eta = -0{\cdot}0063\epsilon^2x^2$. If it is noted that, from (37),

$$N_a = 2\int_0^1 \frac{1}{\xi}dx,$$

it follows that the change in the Nusselt number is given by

$$N_a = \frac{8}{3}\left(\frac{t_1}{240}\right)^{\frac{1}{4}}(1 + 0{\cdot}0017\epsilon^2).$$

Thus the secondary flow leads to a percentage increase of $0{\cdot}17\epsilon^2$ in the Nusselt number. It can be seen that the increase in heat transfer is of the second order of small quantities taking the perturbations to be of first order of small quantities. The accuracy claimed for this perturbation solution is in the region of 25 % provided that t_1 is greater than 10^8, ϵ is less than unity, and the Prandtl number is of order 10 or greater.

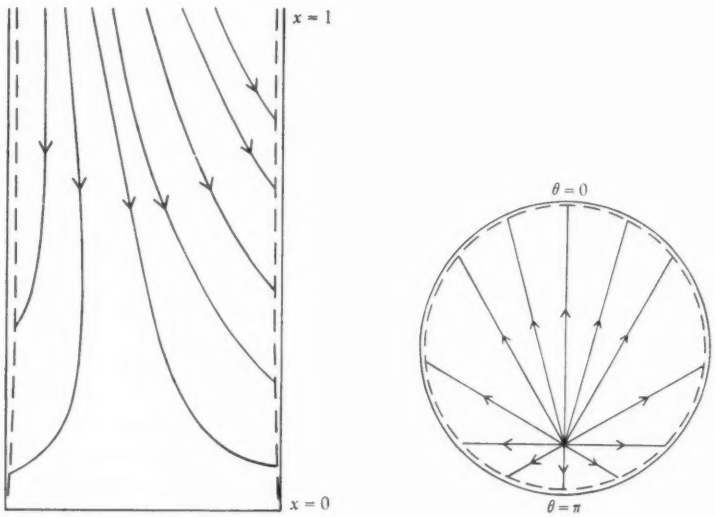

FIGURE 1. (*a*) Sketch of streamlines in plane of symmetry ($\theta = 0$) for $t_1 = 10^8$ and $\epsilon = 1$, i.e. for boundary-layer flow. (*b*) Sketch of projections of streamlines on to a cross-section of the cylinder ($x = 0{\cdot}75$) for $t_1 = 10^8$ and $\epsilon = 1$. – – – Denotes edge of boundary layer.

This calculation was also carried out for the profiles as before except that

$$u = \Phi \frac{(1-r)(r-\beta)}{(1-\beta)^2} \quad (\beta < r < 1),$$

and

$$t = \Theta \frac{(1-r)(r-\beta)}{(1-\beta)^2} \quad (\beta < r < 1).$$

This had the effect of altering Θ, λ, and γ by a factor of 2 approximately. The corresponding value of η was $-0{\cdot}012\epsilon^2 x^2$ and the percentage increase in N_a was $0{\cdot}32\epsilon^2$. This may appear to be rather a large change for the alteration of the profiles but the approximate nature of the solutions must be borne in mind.

Under the conditions of operation of a gas turbine ϵ is of order unity. Hence this calculation suggests that the Coriolis force gives rise to an increase in heat transfer of order 1 % when the flow is laminar.

4. The similarity solution

Lighthill found approximate solutions to equations (20) such that the dependence of U, T on r remains the same although an amplitude factor varies with x, the distance from the bottom of the tube. These solutions are

$$T = t_1 x\left(1-\beta r^2+\frac{(8\beta-9)}{5}r^4+\frac{(4-3\beta)}{5}r^6\right),$$

$$U = -4\beta x(1-6r^2+9r^4-4r^6)-\frac{t_1 x}{24}(r^2-3r^4+2r^6),$$

where the Prandtl number has been assumed infinite. Lighthill found

$$t_1 = 311 \quad \text{and} \quad \beta = 2{\cdot}091.$$

If solutions of a similar type exist for the perturbations then it can be seen from equation (30) that w and v must vary with x and so from (27) that u varies with x^2 and from (29) that t must also vary with x^2. Equations (31), (32), (34) and (30) with boundary conditions (19) are satisfied by

$$u = \lambda x^2 r^4(7-12r^2+5r^4),$$

$$t = \xi x^2 r^4(7-12r^2+5r^4),$$

$$v = x\left[\phi+\left(\frac{2\phi}{3}-\frac{\epsilon t_1}{720}(7\beta+264)\right)r^2+\left(-\frac{5\phi}{3}+\frac{\epsilon t_1}{720}(7\beta+264)\right)r^4\right],$$

$$w = x\left[-\phi+\left(\frac{2\phi}{3}+\frac{\epsilon t_1}{720}(96-7\beta)\right)r^2+\left(\frac{\phi}{3}-\frac{\epsilon t_1}{720}(96-7\beta)\right)r^4\right],$$

where λ, ξ and ϕ are constants to be determined.

From equation (27), we get

$$15\lambda-32\phi+6b = 0,$$

where

$$b = \frac{\epsilon t_1}{720}(96-7\beta).$$

Also from (29),

$$4\xi+105\lambda = 0;$$

and from (28)

$$\lambda t_1\frac{(796-197\beta)}{2800}+\xi\left(\frac{2\beta}{7}+\frac{35}{8}+\frac{t_1}{3360}\right)$$

$$-\phi t_1\frac{(44259-559\beta)}{7\times11\times25\times27}+t_1\frac{26(388-96\beta)}{3\times5\times7\times9\times11} = 0.$$

These equations give

$$\phi = 3{\cdot}7\epsilon, \quad \lambda = -6{\cdot}2\epsilon, \quad \xi = 160\epsilon.$$

Figure 2*a* shows a sketch of the streamlines in the plane of symmetry. It can be seen that there is a tendency for the cool fluid on the axis to be drawn to one side of the cylinder by the component of external acceleration in that direction. Also the hot fluid near the walls is influenced by this component of buoyancy force and at one side moves nearer the wall and at the other moves away from the wall. Figure 2*b*, which shows the projections of the streamlines on to a cross-section of

the cylinder, indicates clearly the fluid moving away from the wall of the cylinder at one side. It also shows the hot fluid moving around the circumference of the cylinder under the influence of the non-axial component of buoyancy force.

After he obtained the profiles stated above for U, T, Lighthill found t_1 and β from (38) and (39) with the perturbation term in (39) omitted. Thus for the values of U, T found by Lighthill to be valid the second term on the left-hand side of (39) must be negligible. However, if this term is retained to find the change in β and

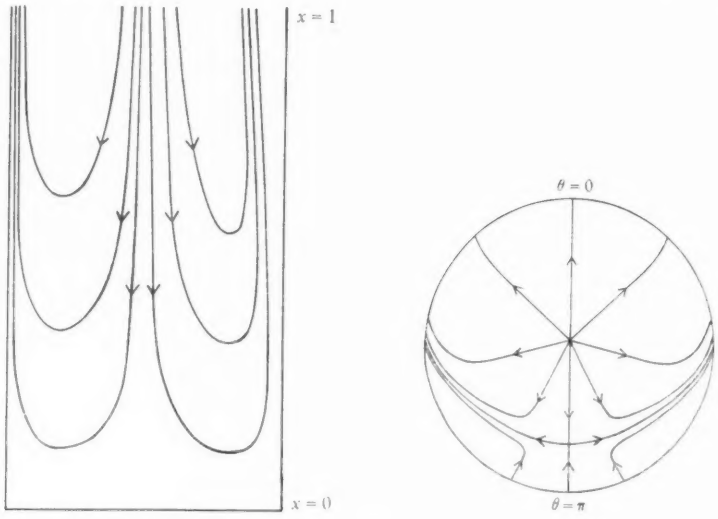

(*a*) (*b*)

FIGURE 2. (*a*) Sketch of streamlines in plane of symmetry ($\theta = 0$) for $t_1 = 311$ and $\epsilon = 0{\cdot}03$, i.e. for similarity flow. (*b*) Sketch of projections of streamlines on to a cross-section of the cylinder ($x = 1{\cdot}0$) for $t_1 = 311$ and $\epsilon = 0{\cdot}03$.

t_1 due to the presence of those perturbations, it can be seen that β and t_1 now depend upon x. Using (40), equations (39) and (38) become

$$\frac{d}{dx}\left[\frac{\beta t_1 x^2(2\beta+9)}{\left(1+\frac{x}{t_1}\frac{dt_1}{dx}\right)105}+\frac{t_1^2x^2}{4200}\frac{13-\beta}{8}\right]$$

$$+\frac{d}{dx}\left[\tfrac{47}{1260}\times 6{\cdot}2\times 160\epsilon^2x^4\right]=\frac{t_1x}{5}(12-4\beta),$$

and

$$t_1\frac{(24+7\beta)}{120}=\frac{48\beta}{\left(1+\frac{x}{t_1}\frac{dt_1}{dx}\right)},$$

where t_1 and β vary with x. The solutions obtained by Lighthill are permissible for U, T if $\epsilon^2x^2 \ll 3$, since then the second term on the left-hand side of (39) is negligible. The two equations are solved to give

$$t_1 = 311(1-0{\cdot}04\epsilon^2x^2), \qquad \beta = 2{\cdot}091-0{\cdot}38\epsilon^2x^2,$$

and thus

$$Na = 0{\cdot}364+0{\cdot}09\epsilon^2.$$

In this case the percentage increase in the Nusselt number is $25\epsilon^2$. The accuracy of the perturbation solution is difficult to assess but cannot be expected to be more than 20 % on account of the approximate methods used.

However, for both ranges of t_1 investigated, it can be seen that there is an increase in heat transfer when the external acceleration makes a small angle with the axis of the cylinder and it appears reasonable to assume that this is so for the complete range of t_1.

My thanks are due to Prof. Lighthill and Mr B. R. Morton for their many helpful suggestions and to Dr B. W. Martin for allowing me to quote results which have not yet been published. I am also indebted to the Sir James Caird's Travelling Scholarship Trust whose grant has made this work possible.

REFERENCES

Alcock, J. F. 1951 *General Discussion on Heat Transfer, Instn Mech. Engrs, Lond.*, section IV, p. 378.

Holzwarth, H. 1938 Die Entwicklung der Holzwarth-Gas Turbine, Holzwarth-Gasturbinen G. m. b. H., Muehlheim-Ruhn.

Lighthill, M. J. 1953 *Quart. J. Mech. Appl. Math.* **6**, 398.

Martin, B. W. & Cresswell, D. J. 1957 *Engineer*, **204**, 926.

Inviscid flow of a reacting mixture of gases around a blunt body

By WILBERT LICK
Pierce Hall, Harvard University, Cambridge, Mass.

(Received 13 April 1959)

A general numerical procedure is described whereby the details of the steady inviscid flow of a mixture of perfect gases about a blunt body, including the effects of finite dissociation and recombination rates, may be calculated. Several numerical examples are calculated in order to apply the numerical procedure to specific cases and also to show the effects of finite reaction times on the flow about a blunt body.

1. Introduction

A considerable amount of effort has been expended recently on the problem of predicting the flow about a blunt body, particularly at high speeds. Almost all of the published papers on this problem have dealt with flow in chemical equilibrium. However, at hypersonic speeds and therefore with high temperatures near the body, the assumption of equilibrium flow becomes questionable. Recent studies (Gunn 1952; Logan 1957; Freeman 1957) have indicated that finite reaction times may have an appreciable effect on the flow properties. A detailed analysis of the non-equilibrium flow is necessary to predict the flow field accurately.

After presenting the fundamental equations and boundary conditions for the inviscid non-heat-conducting flow of a mixture of perfect gases, the present paper describes an inverse method whereby, if the form of the detached shock wave is known or is assumed, the field behind the shock and the corresponding shape of the body may be found. For the continuation of the solution in the supersonic region, a method of characteristics is presented. In order to perform numerical computations, a rough analysis of dissociation and recombination rates is made. The results of several numerical calculations are then presented.

Although the theory and numerical procedure can be easily extended to include finite reaction times for rotation, vibration and ionization, the assumption is made that the rotational and vibrational degrees of freedom are in equilibrium with the translational degrees of freedom, while ionization is neglected. The rate of change of the various components of the gas mixture towards their equilibrium distribution, i.e. towards local thermodynamic equilibrium of the complete system, is governed by dissociation and recombination rate equations. Diffusion of the gases is neglected.

2. Fundamental equations and boundary conditions

For each of the n components of the gas, the equation of state is

$$p_i = \rho_i \frac{R}{M_i} T,$$

where p_i denotes the pressure, ρ_i the density, and M_i the molecular weight of the ith component of the gas. The equation of state for a mixture of perfect gases is obtained by summation and is

$$p = \rho \frac{R}{M} T, \tag{1}$$

where

$$\frac{1}{M} = \sum_i \frac{\rho_i}{\rho} \frac{1}{M_i}.$$

The conservation equations for a gas mixture have been given by Hirschfelder, Curtiss & Bird (1954), Penner (1955), and others. They are presented here in the most convenient form for the present analysis subject to the previous approximations.

For each component of the gas, the continuity equation is

$$\nabla . (\rho_i \mathbf{V}) = \omega_i, \tag{2}$$

where $\mathbf{V}$ is velocity, and ω_i represents the mass rate of production of the component by chemical reaction. By summation over all components of the gas, the overall continuity equation is obtained

$$\nabla . (\rho \mathbf{V}) = 0. \tag{3}$$

By use of the above equation, (2) can be rewritten in the form

$$\frac{D\alpha_i}{Dt} = (\mathbf{V} . \nabla) \alpha_i = \frac{\omega_i}{\rho}, \tag{4}$$

where $\alpha_i = \rho_i / \rho$.

The momentum equation is simply

$$\rho (\mathbf{V} . \nabla) \mathbf{V} + \nabla p = 0. \tag{5}$$

The energy equation is

$$d(h + \tfrac{1}{2}\mathbf{V}^2) = 0, \tag{6}$$

where $h = \sum_i \alpha_i h_i$, and h_i is the enthalpy of each component of the gas, which can be separated into energies due to the active degrees of freedom (translational, rotational and vibrational), the energy of dissociation, and a term p_i / ρ_i: thus

$$h_i = E_{ai} + E_{Di} + \frac{p_i}{\rho_i}.$$

The enthalpy of each component of the gas depends only on the temperature and can be calculated from the equations

$$E_{ai} + \frac{p_i}{\rho_i} = \beta_i \frac{R}{M_i} T,$$

$$E_{Di} = \frac{D_i}{M_i}.$$

The β's are known functions of the temperature, while the dissociation energy D is a constant. By use of the above relations, the energy equation can be written in the two equivalent forms

$$\sum_i \alpha_i \beta_i \frac{R}{M_i} dT + \sum_i \alpha_i \frac{R}{M_i} T\, d\beta_i + \sum_i h_i d\alpha_i + d(\tfrac{1}{2}\mathbf{V}^2) = 0, \tag{7a}$$

$$c_{pa} dT + \sum_i h_i d\alpha_i + d(\tfrac{1}{2}\mathbf{V}^2) = 0, \tag{7b}$$

where $c_{pa} = \sum_i \alpha_i c_{pai}$.

It is assumed that, at a wall, the gas does not interact chemically with the wall, i.e. the wall is non-catalytic. At the solid boundary, the velocity component normal to the wall must be zero; the tangential component is not subject to constraint since the fluid is inviscid.

The boundary conditions at a shock wave can be simplified by resolving the free-stream velocity into components normal and tangential to the shock. The shock transition can then be regarded from a local co-ordinate system moving with a speed equal to the tangential component of velocity. If all the vibrational relaxation distances are very short in comparison with dissociation relaxation distances and in comparison with a typical body dimension, then the properties of the gas immediately after the vibrational degrees of freedom have come to equilibrium and before dissociation has begun may be found by treating the flow by one-dimensional analysis.

The continuity, momentum, and energy equations for one-dimensional flow through a normal shock are, in a usual notation,

$$\rho_\infty v_\infty = \rho_s v_s = c_1, \tag{8}$$

$$p_\infty + \rho_\infty v_\infty^2 = p_s + \rho_s v_s^2 = c_2, \tag{9}$$

$$h_\infty + \tfrac{1}{2} v_\infty^2 = h_s + \tfrac{1}{2} v_s^2 = c_3, \tag{10}$$

where the subscript ∞ refers to free stream conditions in front of the shock and the subscript s refers to conditions immediately behind the shock. Since it is assumed that dissociation has not begun, the enthalpy immediately behind the shock can be written as

$$h_s = \bar{\beta}_s \frac{p_s}{s}, \quad \text{where} \quad \bar{\beta} = \sum_i \alpha_i \frac{M}{M_i} \beta_i.$$

The normal-shock equations plus the equation of state must be solved by an iteration procedure because of the dependence of the β_i's on the temperature and the resulting algebraic complexity of the equations. To accomplish this, the density ρ_s can be found as a function of the temperature, and v_s, p_s, and T_s can be found in terms of ρ_s: thus

$$\rho_s = \frac{\bar{\beta}_s c_2 + \sqrt{\{(\bar{\beta}_s c_2)^2 - 4c_1^2 c_3(\bar{\beta}_s - \tfrac{1}{2})\}}}{2c_3}, \tag{11}$$

$$v_s = \frac{c_1}{\rho_s}, \tag{12}$$

$$p_s = c_2 - \frac{c_1^2}{\rho_s}, \tag{13}$$

$$T_s = \frac{p_s}{\rho_s} \frac{M_s}{R}. \tag{14}$$

Once the free stream conditions are known, c_1, c_2, and c_3 can be calculated. By assuming T_s, $\bar{\beta}_s$ can be calculated and equations (11) to (14) can be solved in succession. The process is continued until the assumed T_s and the T_s calculated from (14) agree to the desired accuracy.

3. Inverse method of axisymmetric flow

The inverse method of finding the body shape and the flow field behind a detached shock when the form of the shock wave is given has been successfully applied by other investigators (Zlotnick & Newman 1957; Van Dyke 1958) to the blunt body problem with the restrictions of equilibrium flow, a perfect gas, and constant specific heats. Although the inverse problem as presented here and by the above authors is a Cauchy problem for elliptic equations and is therefore improperly given, it has been shown that accurate solutions may be found by this method if proper care is taken.

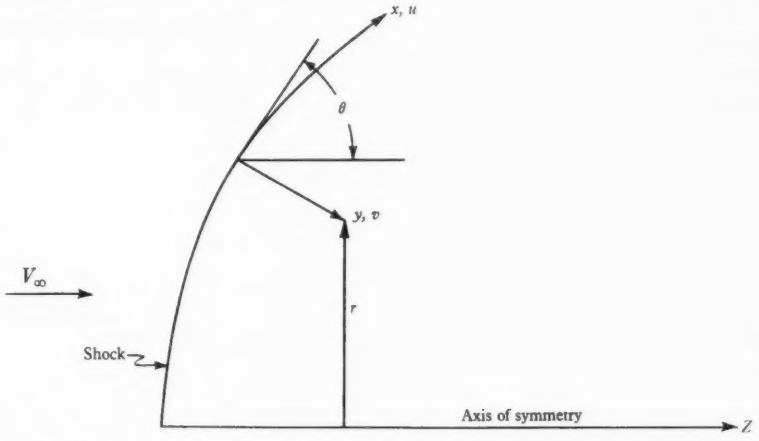

FIGURE 1. Co-ordinate system. Shock radius of curvature at $x = 0$ is R_0.

To simplify the analysis, it is advantageous to choose a natural co-ordinate system which contains the shock wave as one of its surfaces, is applicable to a wide range of shock shapes, and is not restricted to a particular family of curves. Such an orthogonal curvilinear co-ordinate system is shown in figure 1. The origin of the co-ordinate system is taken at the intersection of the shock and the axis of symmetry. Let x be the distance along the shock surface, and let y be the co-ordinate normal to the shock surface. Let u and v be respectively the velocities in the x- and y-directions. Let

$$K = \frac{d\theta}{dx} = -\frac{1}{R},$$

where K is a known function of x for a given shock shape. The local shock radius of curvature is R, and θ is the local angle which the shock makes with the free stream.

The equations of motion, written in the above co-ordinate system, are

$$\frac{u}{1+Ky}\frac{\partial \alpha_i}{\partial x}+v\frac{\partial \alpha_i}{\partial y}=\frac{\omega_i}{\rho}, \tag{15}$$

$$\frac{\partial}{\partial x}[\rho ur]+\frac{\partial}{\partial y}[\rho vr(1+Ky)]=0, \tag{16}$$

$$u\frac{\partial u}{\partial x}+Kuv+(1+Ky)\,v\frac{\partial u}{\partial y}=-\frac{1}{\rho}\frac{\partial p}{\partial x}, \tag{17}$$

$$u\frac{\partial v}{\partial x}+(1+Ky)\,v\frac{\partial v}{\partial y}-Ku^2=-\frac{1+Ky}{\rho}\frac{\partial p}{\partial y}, \tag{18}$$

$$\sum_i \alpha_i\beta_i\frac{R}{M}dT+\sum_i \alpha_i\frac{R}{M_i}Td\beta_i+\sum_i h_i d\alpha_i+d(\tfrac{1}{2}\mathbf{V}^2)=0. \tag{19}$$

The additional relation that is needed is the equation of state

$$p=\rho\frac{R}{M}T, \tag{20}$$

and the reaction rates must also be known.

Algebraic manipulation of the above equations yields the following set of relations for the y-derivatives of α_i, u, v, p, and ρ, where the substitutions

$$K_1=\sum_i \alpha_i\frac{R}{M_i}\beta_i, \quad K_2=\sum_i \alpha_i\frac{R}{M_i}\frac{d\beta_i}{dT}$$

have been made:

$$\frac{\partial \alpha_i}{\partial y}=\frac{1}{v}\left[\frac{\omega_i}{\rho}-\frac{u}{1+Ky}\frac{\partial \alpha_i}{\partial x}\right], \tag{21}$$

$$\frac{\partial u}{\partial y}=\frac{1}{v(1+Ky)}\left[-\frac{1}{\rho}\frac{\partial p}{\partial x}-Kuv-u\frac{\partial u}{\partial x}\right], \tag{22}$$

$$\begin{aligned}\frac{\partial v}{\partial y}\left[\frac{v}{T}+(K_1+K_2T)\left(\frac{1}{v}-\frac{Mv}{RT}\right)\right]&=-\frac{u}{T}\frac{\partial u}{\partial y}-\sum_i\left[\frac{h_i}{T}-(K_1+K_2T)\frac{M}{M_i}\right]\frac{\partial \alpha_i}{\partial y}\\&+\frac{K_1+K_2T}{1+Ky}\left[\frac{M}{RT}\left(u\frac{\partial v}{\partial x}-Ku^2\right)-\frac{1}{v}\left(\frac{\partial u}{\partial x}+\frac{u}{\rho}\frac{\partial \rho}{\partial x}+\frac{u}{r}\frac{\partial r}{\partial x}+vK+(1+Ky)\frac{v}{r}\frac{\partial r}{\partial y}\right)\right],\end{aligned} \tag{23}$$

$$\frac{\partial p}{\partial y}=-\frac{\rho}{1+Ky}\left[u\frac{\partial v}{\partial x}+(1+Ky)\,v\frac{\partial v}{\partial y}-Ku^2\right], \tag{24}$$

$$\frac{\partial \rho}{\partial y}=-\frac{\rho}{v(1+Ky)}\left[(1+Ky)\frac{\partial v}{\partial y}+\frac{\partial u}{\partial x}+\frac{u}{\rho}\frac{\partial \rho}{\partial x}+(1+Ky)\frac{v}{r}\frac{\partial r}{\partial y}+vK+\frac{u}{r}\frac{\partial r}{\partial x}\right]. \tag{25}$$

The boundary conditions at points at equal intervals along the shock can be found by the procedure described previously. The x-derivatives of all dependent variables can then be easily calculated. Once the dependent variables and their x-derivatives are known along the line $y_n = \text{const.}$, the above equations can be solved successively and yield the derivatives in a direction normal to the shock.

The quantities (u, for example) at a station y_{n+1} can then be found, as a first approximation, by linear extrapolation

$$u_{n+1}=u_n+\left(\frac{\partial u}{\partial y}\right)_n\Delta y_{n,n+1},$$

where

$$\Delta y_{n,n+1}=y_{n+1}-y_n.$$

From the equation of state, the temperature is determined. The β_i's, which can be written as simple polynomials dependent on T, can then be calculated. All derivatives of the functions at y_{n+1} are subsequently found in a similar manner. An improved value for the function at y_{n+1} can be evaluated by using the average of the derivatives in the y-direction at stations n and $n+1$ or

$$u_{n+1} = u_n + \frac{\Delta y_{n,n+1}}{2}\left[\left(\frac{\partial u}{\partial y}\right)_n + \left(\frac{\partial u}{\partial y}\right)_{n+1}\right].$$

The iteration procedure is then continued until the desired accuracy is obtained.

The integration proceeds in a direction normal to the shock by applying this method to successive intervals in the y-direction.

The surface of the body is determined by applying a continuity analysis to the flow. The mass flow in the x-direction through the surface $x = x_1$ between the shock and station y_N is

$$\pi\rho_s u_s r_s \Delta y_{0,1} + \pi \sum_1^{N-1} \rho_n u_n r_n (\Delta y_{n-1,n} + \Delta y_{n,n+1}) + \pi\rho_N u_N r_N \Delta y_{N-1,N}.$$

The mass flow through the shock between $x = 0$ and $x = x_1$ is $\pi\rho_\infty V_\infty r_s^2$. The body surface can then be determined by calculating the y-ordinate at which the two mass flows are equated.

4. Method of characteristics

As x increases, the distance from the body to the shock also increases, and a larger number of intervals are required to reach the body by the inverse method causing large errors to develop before the body is reached. A more suitable procedure of extending the solution is by the method of characteristics. The calculations by the inverse method in the supersonic region can also be checked by the method of characteristics. The characteristic equations will be presented for both plane and axisymmetric flows using rectangular Cartesian co-ordinates.

By using the standard techniques, the characteristic equations and directions can be found. The characteristic directions correspond to (1) the streamlines, along which the following characteristic equations apply:

$$u\,dy - v\,dx = 0, \tag{26}$$

$$u\frac{\partial \alpha_i}{\partial x} + v\frac{\partial \alpha_i}{\partial y} = \frac{\omega_i}{\rho}, \tag{27}$$

$$d\left(\frac{V^2}{2}\right) + \frac{1}{\rho}dp = 0, \tag{28}$$

and (2) the Mach lines, along which the following characteristic equations apply:

$$\frac{dy}{dx} = \tan(\theta \pm \alpha), \tag{29}$$

$$\frac{1}{\tan\alpha}\frac{dp}{\rho V^2} \pm d\theta = \frac{a}{V}\delta \pm s\left\{-\frac{\epsilon}{y}\sin\theta - \sum_i \frac{h_i}{V c_{pa} T}\frac{\omega_i}{\rho} + \sum_i \frac{1}{V}\frac{M}{M_i}\frac{\omega_i}{\rho}\right\}, \tag{30}$$

where α is the angle which the Mach lines make with the streamline, a is the 'frozen' speed of sound defined as

$$a^2 = \left(\frac{\partial p}{\partial \rho}\right)_{s,\alpha_i} = \gamma_a \frac{R}{M} T,$$

where γ_a is the ratio of specific heats of the active degrees of freedom, and θ is the angle of flow inclination.

The method of solution by the application of the above characteristic equations is similar in almost all respects to the ordinary methods developed for equilibrium flow except that in addition the rate of change of the n components of the gas along a streamline are to be determined by the n equations (27).

5. Reaction rates

The explicit forms of the terms ω_i which determine the rate of production of the various components of the gas have not yet been discussed. Since air is composed mainly of oxygen and nitrogen and it is assumed that other components have a negligible effect on the reaction rates for oxygen and nitrogen, only the dissociation and recombination rates of these two gases will be treated here. The following presentation is based on Logan's modification of simple collision theory and attempts to account approximately for the effects of the interaction of the internal degrees of freedom during the collision process.

Air is assumed to consist of oxygen and nitrogen atoms and molecules only. The process of dissociation, which involves collisions between a molecule and some other particle, is considered first. Since only simple molecules and atoms are present, the number of pairs of rotational degrees of freedom which are effective in transferring energy during the collision process is assumed to be one.

By considering the molecules in each vibrational state as a separate species, the energy required to dissociate a molecule in its nth vibrational state is then $D - E_n$, where D is the dissociation energy and E_n is the vibrational energy of the nth state. The rate of dissociation for a diatomic molecule considering all vibrational states is given by

$$\frac{dv}{dt} = -\sum_n Z_n \alpha_n \left(\frac{D - E_n}{kT}\right) \exp\left[-\left(\frac{D - E_n}{kT}\right)\right], \tag{31}$$

where v is the number of particles per unit volume, and α_n represents the percentage of molecules in each vibrational state. From statistical mechanics, we have

$$\alpha_n = \alpha_0 \exp\left(-E_n/kT\right),$$

where α_0 is the percentage of molecules in the zeroth vibrational state. Z is the total number of collisions per unit volume and per unit time and is given by

$$Z = \frac{2 v_1 v_2}{\sigma_{12}} d_{12}^2 \left(\frac{2\pi k T}{\mu}\right)^{\frac{1}{2}},$$

where k is Boltzmann's constant, d_{12} is the average diameter and is the reduced mass of the colliding particles, and σ_{12} is a symmetry factor which is equal to one if the colliding particles are of different species and is equal to two if of the same

species. The subscript 1 refers to the molecules under consideration and the subscript 2 refers to all other colliding particles.

The additional assumption is made that all reaction partners are equally effective in causing dissociation. The rate of dissociation for the molecules m can then be written in the form

$$\frac{dv_m}{dt} = -k_d v_m \sum_i v_i, \tag{32}$$

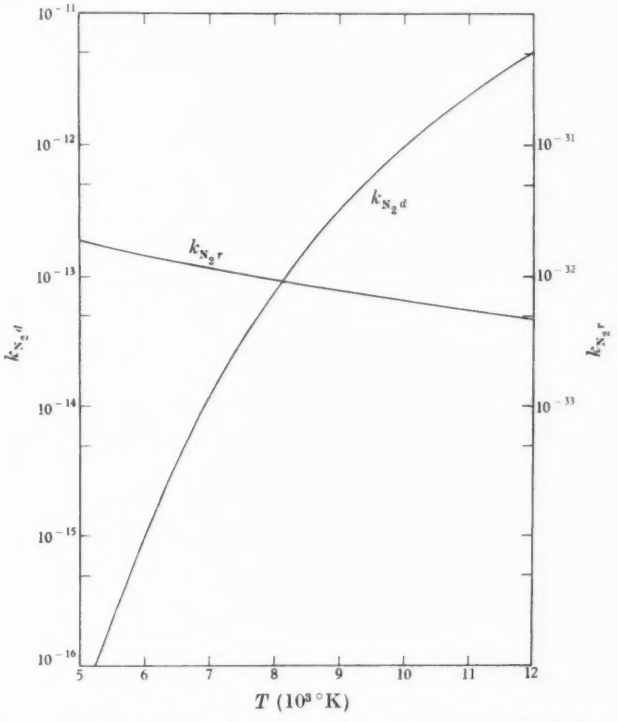

FIGURE 2. Dissociation and recombination rate constants for nitrogen.

where k_d is the dissociation rate constant and is a function of temperature only. The summation is to be taken over all particles i. By equating equations (31) and (32), k_d can be evaluated.

Similarly, for the case of recombination, which requires a three-body collision between two atoms a and another particle i, the rate can be written as

$$\frac{dv_m}{dt} = k_r v_a^2 \sum_i v_i. \tag{33}$$

The recombination rate constant k_r can now be evaluated using equilibrium theory. At equilibrium

$$\frac{dv_m}{dt} = k_r v_a^2 \sum_i v_i - k_d v_m \sum_i v_i = 0.$$

and therefore

$$\frac{k_d}{k_r} = \frac{\nu_a^2}{\nu_m} = K_e, \tag{34}$$

where K_e is the equilibrium constant and is a known function of temperature.

The dissociation and recombination rate constants were evaluated for both nitrogen and oxygen. The results are shown in figures 2 and 3. The variable ω_i is related to the above rate constants by

$$\omega_i = \frac{M_i}{N}\frac{dv_i}{dt},$$

where N is Avagadro's number.

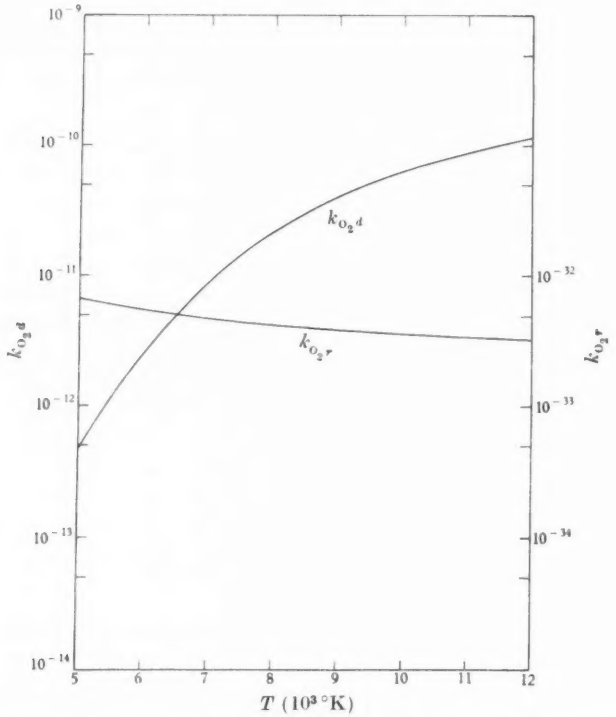

FIGURE 3. Dissociation and recombination rate constants for oxygen.

6. Numerical computations

By using the inverse method, the method of characteristics, and the previously determined dissociation and recombination rates, four numerical examples were calculated for the flow of a gas through a specified shock shape at a Mach number of 14 and for free-stream density and temperature corresponding to the density and temperature of air at an altitude of 100,000 ft. The calculation of the boundary conditions and the inverse method were programmed in floating point on the IBM 650. The flow conditions in the supersonic region calculated by the inverse

method were partially checked and slightly extended by hand computation using the method of characteristics.

The gas treated in the first three examples consisted of a mixture of oxygen and nitrogen in the same ratio to each other as in atmospheric air, an approximation to the real composition of air. To show the effects of non-equilibrium flow, various shock radii were chosen, so that a typical relaxation distance for oxygen dissociation near the stagnation streamline in comparison with the detachment distance was (i) small and the flow was practically in equilibrium throughout, (ii) of the same order of magnitude and the flow was only partially in equilibrium, and (iii) very large and no dissociation or recombination occurred.

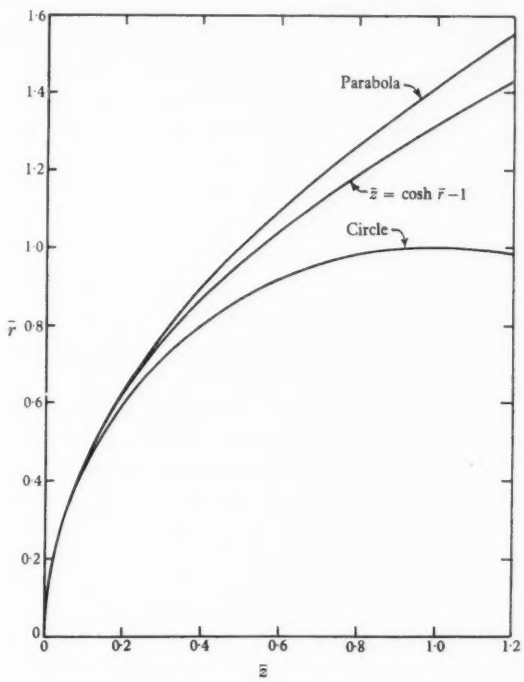

FIGURE 4. Shape of assumed shock.

To demonstrate also the effects of non-equilibrium flow on a pure gas, numerical results were obtained for the flow of pure oxygen for the case (ii) mentioned above.

To begin the computations, the shape of the shock must be specified. Preferably, the assumed shock shape must resemble closely the shocks produced by typical blunt-nosed bodies. For convenience in numerical computations, an analytic shock shape is desired wherein all shock variables dependent on the co-ordinate system such as $d\theta/dx$, $\sin\theta$, $\cos\theta$, and the position variables of the shock, r and z, can be expressed in terms of x, the co-ordinate parallel to the shock surface (see figure 1).

and therefore

$$\frac{k_d}{k_r} = \frac{\nu_a^2}{\nu_m} = K_e, \tag{34}$$

where K_e is the equilibrium constant and is a known function of temperature.

The dissociation and recombination rate constants were evaluated for both nitrogen and oxygen. The results are shown in figures 2 and 3. The variable ω_i is related to the above rate constants by

$$\omega_i = \frac{M_i}{N}\frac{dv_i}{dt},$$

where N is Avagadro's number.

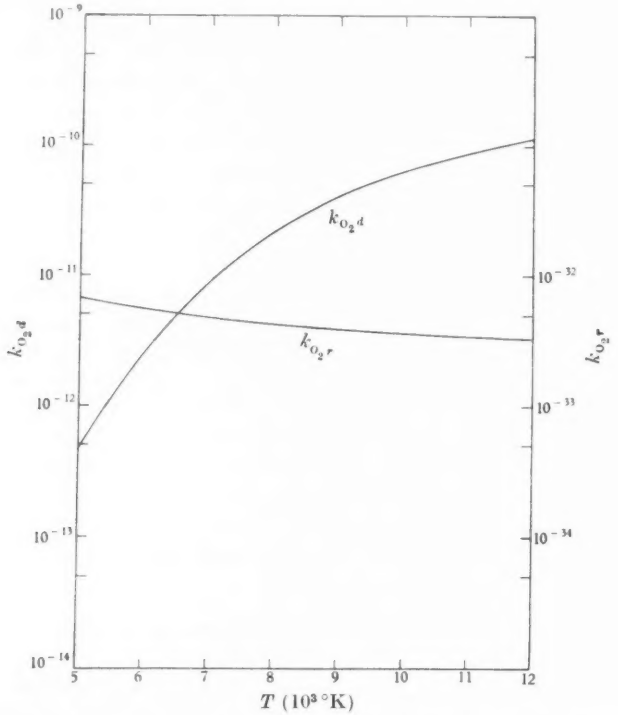

FIGURE 3. Dissociation and recombination rate constants for oxygen.

6. Numerical computations

By using the inverse method, the method of characteristics, and the previously determined dissociation and recombination rates, four numerical examples were calculated for the flow of a gas through a specified shock shape at a Mach number of 14 and for free-stream density and temperature corresponding to the density and temperature of air at an altitude of 100,000 ft. The calculation of the boundary conditions and the inverse method were programmed in floating point on the IBM 650. The flow conditions in the supersonic region calculated by the inverse

method were partially checked and slightly extended by hand computation using the method of characteristics.

The gas treated in the first three examples consisted of a mixture of oxygen and nitrogen in the same ratio to each other as in atmospheric air, an approximation to the real composition of air. To show the effects of non-equilibrium flow, various shock radii were chosen, so that a typical relaxation distance for oxygen dissociation near the stagnation streamline in comparison with the detachment distance was (i) small and the flow was practically in equilibrium throughout, (ii) of the same order of magnitude and the flow was only partially in equilibrium, and (iii) very large and no dissociation or recombination occurred.

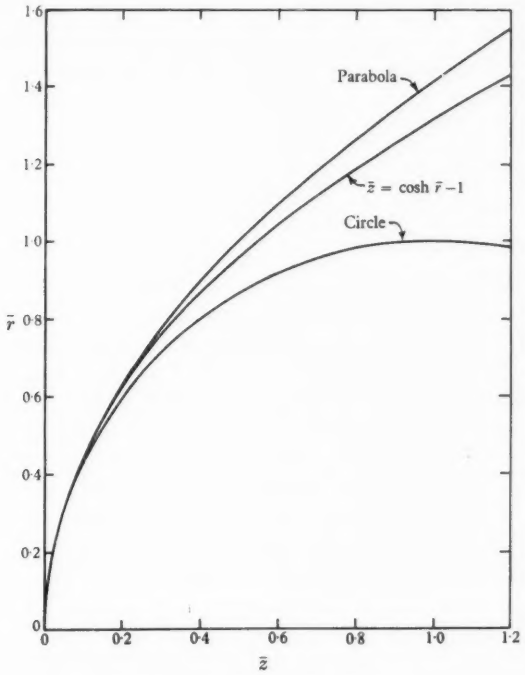

FIGURE 4. Shape of assumed shock.

To demonstrate also the effects of non-equilibrium flow on a pure gas, numerical results were obtained for the flow of pure oxygen for the case (ii) mentioned above.

To begin the computations, the shape of the shock must be specified. Preferably, the assumed shock shape must resemble closely the shocks produced by typical blunt-nosed bodies. For convenience in numerical computations, an analytic shock shape is desired wherein all shock variables dependent on the co-ordinate system such as $d\theta/dx$, $\sin\theta$, $\cos\theta$, and the position variables of the shock, r and z, can be expressed in terms of x, the co-ordinate parallel to the shock surface (see figure 1).

These properties are fulfilled by the curve known as the catenary, which is compared with the parabola and circle in figure 4 and which is given by

$$\bar{z} = \cosh \bar{r} - 1, \tag{36}$$

where the bars denote quantities made non-dimensional with respect to R_0, the radius of curvature of the shock on the axis of symmetry. Of course, the co-ordinate system can be adapted to an almost completely arbitrary shock shape as produced by blunt-nosed bodies including shock shapes with inflexion points.

By using the iteration procedure described previously, the conditions at the shock were calculated at 50 values of $\bar{x}$ at equally spaced intervals $\Delta\bar{x} = 0{\cdot}04$ starting at $\bar{x} = 0{\cdot}02$ in order to avoid, in later computations, the indeterminate forms $(u/r)(\partial r/\partial x)$ and $(v/r)(\partial r/\partial y)$ at $\bar{x} = 0$. After the boundary conditions at the shock have been found, the solution can be continued in the subsonic and slightly supersonic regions by the inverse method and in the supersonic region by the method of characteristics. In these computations, it was found convenient to write the governing equations in terms of the dimensionless quantities

$$\bar{V} = \frac{V}{V_\infty}, \quad \bar{P} = \frac{P}{\rho_\infty V_\infty^2}, \quad \bar{\rho} = \frac{\rho}{\rho_\infty}, \quad \bar{T} = \frac{T}{T_\infty}.$$

7. Results and discussion

In the three problems calculated for air, the free-stream conditions and the shock shape are identical, and therefore the shock boundary conditions are also identical. The differences in the flow quantities in the field are then dependent on a local non-equilibrium parameter χ, which can be shown from the non-dimensional equations to be $(R_0/\rho_\infty V_\infty)(\omega_{O_2}/\bar{\rho})$ or $(R_0/\rho_\infty V_\infty)(\omega_{N_2}/\bar{\rho})$. The parameter R_0/V_∞ is a characteristic time associated with the flow, while either $(\omega_{O_2}/\rho_\infty\bar{\rho})^{-1}$ or $(\omega_{N_2}/\rho_\infty\bar{\rho})^{-1}$ is a characteristic time associated with the non-equilibrium process. χ_{O_2}, evaluated at $x = y = 0$, was chosen to vary over a range from practically equilibrium flow ($\chi_{O_2} = 100$, $R_0 = 10\,\text{cm}$) through partial equilibrium flow ($\chi_{O_2} = 5$, $R_0 = 0{\cdot}5\,\text{cm}$) to frozen dissociation flow ($\chi_{O_2} = \chi_{N_2} = 0$).

From the results of the computations, two regions of the flow field were found to be of particular interest: (1) the region near the axis of symmetry, where the flow behaves similarly to the flow through a normal shock and where the finite dissociation rates have a large influence on the flow properties, and (2) the region of flow expansion around the body near the surface, where the finite recombination rates have a large influence on the flow properties. The variations of α_0, $\bar{V}$, $\bar{p}$, $\bar{\rho}$, and $\bar{T}$ in these two regions for the three examples calculated for air are shown in figures 5 to 14. The variation of α_N for air is not given since in the present problems the dissociation of nitrogen is negligibly small.

Figure 5 presents the distribution of oxygen atoms along the stagnation streamline for $\chi_{O_2} = 100$ and $\chi_{O_2} = 5$. For $\chi = 0$, since the dissociation rate is zero, α_0 is constant and equal to zero throughout the shock layer. It can be seen that for $\chi_{O_2} = 100$, the oxygen dissociation is near equilibrium a short distance from the shock, while for $\chi_{O_2} = 5$, the dissociation is not in equilibrium until the stagnation point is reached. Both cases show the rapid dissociation near the shock due to the high temperatures and the exponential factor in the dissociation rate.

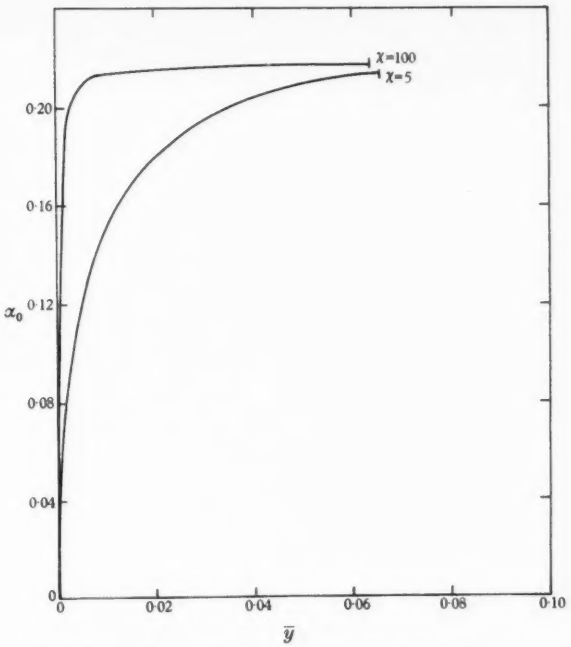

FIGURE 5. Variation of mass fraction of atomic oxygen α_0 along the stagnation streamline.

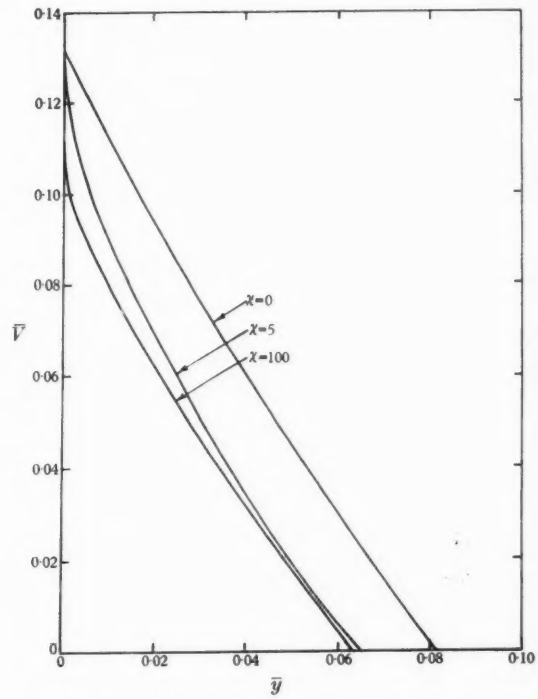

FIGURE 6. Variation of velocity $\bar{V}$ along the stagnation streamline.

The effect of the non-equilibrium is evident in figure 6 showing the variation of $\overline{V}$ along the stagnation streamline. For $\chi_{O_2} = 100$, dissociation causes a rapid decrease in $\overline{V}$ near the shock. The detachment distance can be seen to be approximately 0·064.* For $\chi_{O_2} = 5$, the decrease in the velocity is less abrupt. The detachment distance has increased to approximately 0·066. For $\chi = 0$, little change in gradient of the velocity occurs. The shock detachment distance is approximately 0·081.

The effect of the dissociation on the pressure, density, and temperature is similar to the effect on the velocity as can be seen from figures 7 to 9. Large variations in the flow quantities occur near the shock for $\chi_{O_2} = 100$. For $\chi_{O_2} = 5$, the variations are less rapid but extend to the stagnation point. For $\chi = 0$, the changes in $\overline{p}$, $\overline{\rho}$, and $\overline{T}$ are comparatively very small.

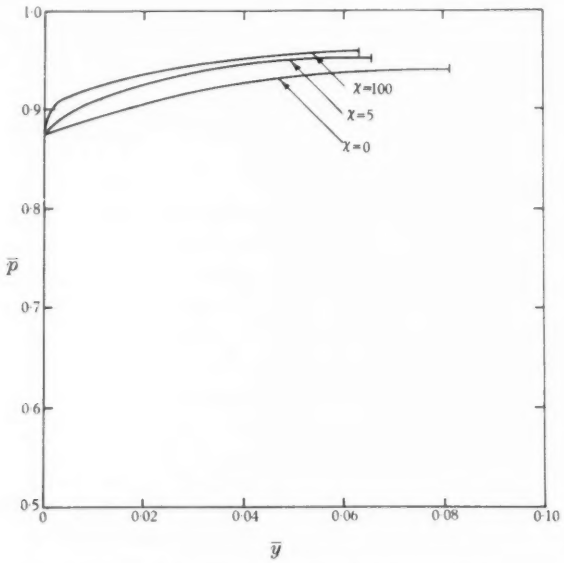

FIGURE 7. Variation of pressure $\overline{p}$ along the stagnation streamline.

Finite reaction rates have little effect on pressure as can be expected from normal shock-wave theory. However, dissociation causes the density to increase greatly, which is the main reason for the decrease in detachment distance as χ increases. The most dramatic effect of dissociation is the temperature drop near the shock due to the absorption of energy by the dissociating molecules offsetting the slight increase in temperature due to compression of the gas near the stagnation point.

* Note that all distances are made non-dimensional with respect to R_0, the radius of curvature of the shock at $\bar{x} = 0$. For detachment distances made non-dimensional with respect to the radius of curvature of the body at $\bar{x} = 0$, the detachment distances as presented here must be multiplied by the ratio of the shock radius of curvature to the body radius of curvature, approximately 1·3 in the present case.

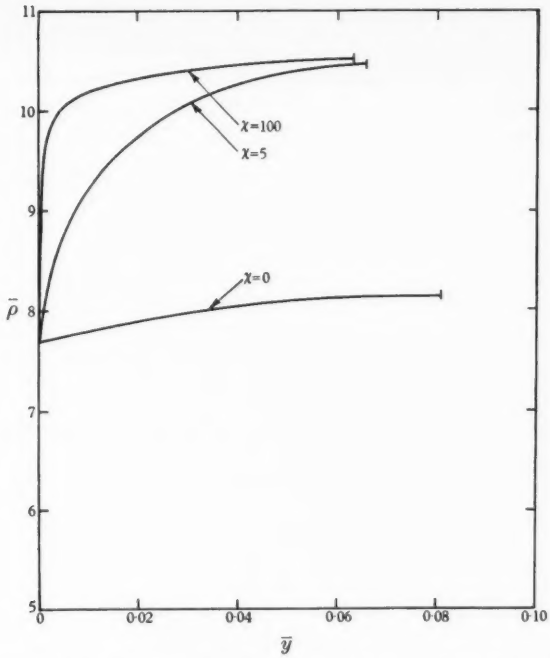

FIGURE 8. Variation of density $\bar{\rho}$ along the stagnation streamline.

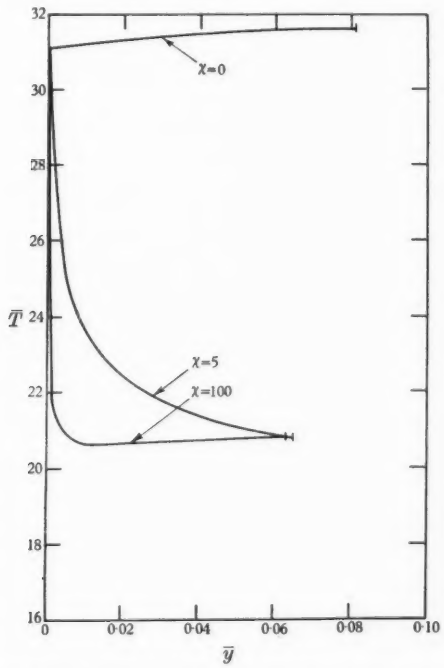

FIGURE 9. Variation of temperature $\bar{T}$ along the stagnation streamline.

The variation of α_0 along the body surface is shown in figure 10. It can be seen that the percentage of oxygen dissociated is slightly higher near the stagnation point for $\chi_{O_2} = 100$ than for $\chi_{O_2} = 5$. However, as $\bar{x}$ increases, the amount of oxygen dissociated soon becomes greater for $\chi_{O_2} = 5$, indicating that the flow is partially frozen as it expands along the body surface.

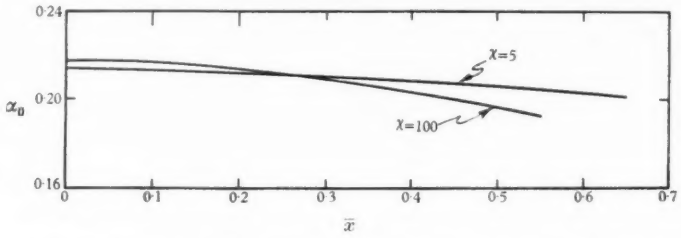

FIGURE 10. Variation of mass fraction of atomic oxygen α_0 along surface of body.

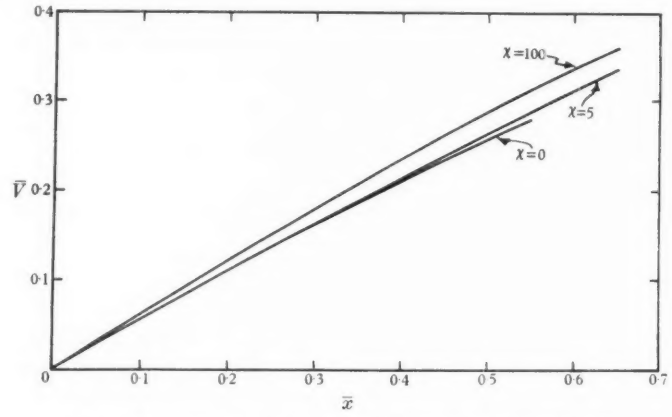

FIGURE 11. Variation of velocity $\bar{V}$ along surface of body.

The effect of the finite recombination rates on $\bar{V}$, $\bar{p}$, $\bar{\rho}$ and $\bar{T}$ on the body surface are shown in figures 11 to 14. There is little effect on the velocity except in the limiting case of frozen flow. It can be seen from figure 12 that, although the pressure at the stagnation point is different for all three bodies, the rate of decrease from this maximum is almost identical. For purposes of comparison, the Newtonian pressure is shown for the case $\chi_{O_2} = 100$. It can be shown that the effect of the non-equilibrium flow is to slightly increase the disagreement between the calculated and Newtonian pressure.

The finite recombination rate causes the density to fall off less rapidly as the gas expands, as can be seen from figure 13. The large differences in temperatures on the three bodies due to dissociation and recombination is shown in figure 14. Also noticeable is the greater rate of decrease in temperature for $\chi_{O_2} = 5$ and $\chi = 0$ due to the fact that in a rapidly expanding flow the recombination rate may be less than necessary to keep the flow in equilibrium. In this circumstance, the inert

degrees of freedom will retain their energy, and the temperature of the active degrees of freedom must decrease more rapidly to compensate for this.

For the fourth calculation, that of pure oxygen, the same shock shape was assumed. Although the free-stream density and temperature were chosen

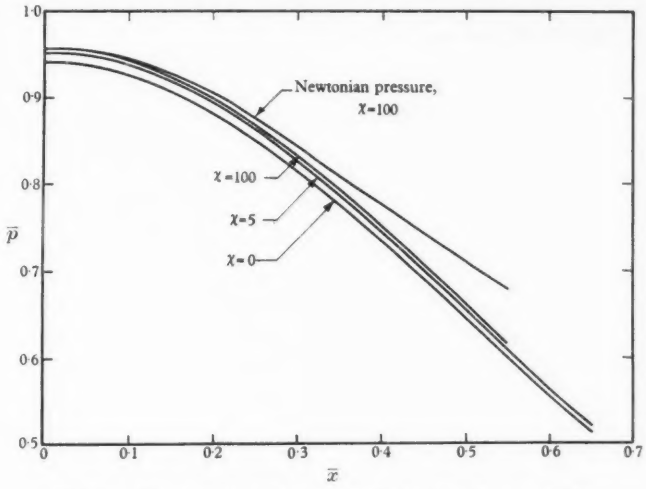

FIGURE 12. Variation of pressure $\bar{p}$ along surface of body.

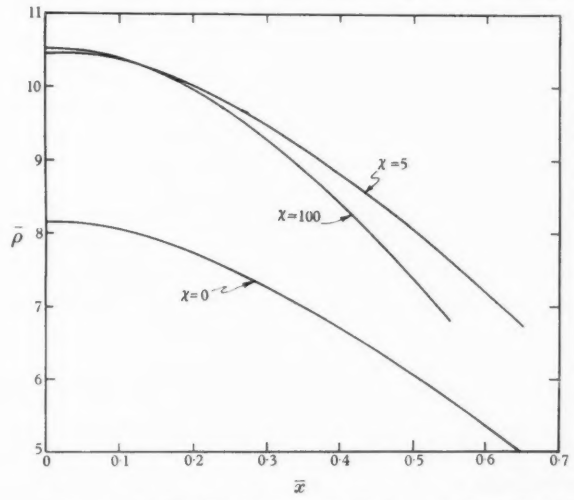

FIGURE 13. Variation of density $\bar{\rho}$ along surface of body.

identical with those in the previous examples, the free-stream pressure was not the same due to a change in the molecular weight of the gas. Therefore the shock boundary conditions were not the same as before. A greater amount of the gas is dissociated in this case than in the previous examples. A correspondingly greater effect on the flow field is expected and does result. Except that the variations are

greater than for air with $\chi_{O_2} = 5$, the shape of the curves and general appearance of the flow fields are similar.

A limitation to the present computational results is the inadequate knowledge of dissociation and recombination rates. A variation in the actual reaction rates from those assumed here of course does not invalidate the present results but does make the results applicable to bodies of different size. Another limitation to the

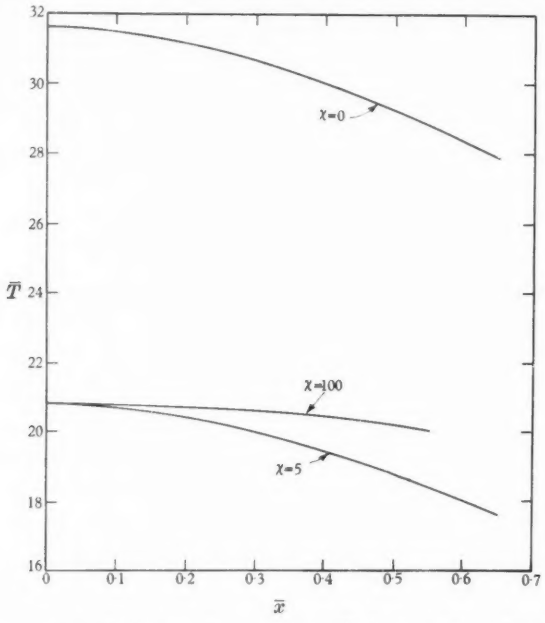

FIGURE 14. Variation of temperature $\bar{T}$ along surface of body.

present results for air is the assumption that air consists of a mixture of oxygen and nitrogen atoms and molecules. No account has been taken of the interaction of oxygen and nitrogen with each other to form NO or other compounds, which may have an effect on the gas properties and especially the reaction rates.

REFERENCES

FREEMAN, N. C. 1957 Dynamics of a dissociating gas. III. Non-equilibrium theory. *NATO Rep.* no. 133.

GUNN, J. C. 1952 Relaxation time effects in gas dynamics, R and M. *A.R.C. Tech. Rep.* no. 2338.

HIRSCHFELDER, J. O., CURTISS, C. F. & BIRD, R. B. 1954 *Molecular Theory of Gases and Liquids.* New York: Wiley.

LOGAN, J. 1957 Relaxation phenomena in hypersonic aerodynamics. *I.A.S. Preprint,* no. 728.

PENNER, S. S. 1955 Chemical reactions in flow systems. *AGARD Rep.* no. 7.

VAN DYKE, M. 1958 The supersonic blunt-body problem—review and extension. *I.A.S. Preprint,* no. 801.

ZLOTNICK & NEWMAN 1957 Theoretical calculation of the flow on blunt-nosed axisymmetrical bodies in a hypersonic stream. *AVCO TR*-2-57-29.

The viscous secondary flow ahead of an infinite cylinder in a uniform parallel shear flow

By ALAR TOOMRE
Mechanics of Fluids Department, University of Manchester

(Received 29 May 1959)

A simple method is presented in this paper for calculating
(*a*) the secondary velocities, and
(*b*) the lateral displacement of total pressure surfaces (i.e. the 'displacement effect')
in the plane of symmetry ahead of an infinitely long cylinder situated normal to a steady, incompressible, slightly viscous shear flow; the cylinder is also perpendicular to the vorticity, which is assumed uniform but small. The method is based on lateral gradients of pressure, these being calculated from the primary flow alone. Profiles of the secondary velocities are obtained at several Reynolds numbers ahead of two specific cylindrical shapes: a circular cylinder, and a flat plate normal to the flow. The displacement effect is derived and, rather surprisingly, is found to be virtually independent of the Reynolds number.

1. Introduction

The inviscid mathematical theory of the secondary flow caused by an infinite cylinder situated perpendicular to a steady, incompressible, weakly sheared parallel flow, and also to the vorticity of that stream, was developed by Lighthill (1956) in a paper titled 'Drift'. He investigated the bending and stretching inflicted upon vortex lines as they are convected around the cylinder by the primary flow along planes perpendicular to the cylinder. Lighthill found a remarkably simple expression for the secondary flow thus induced, which showed that to the order of the approximation involved this flow is entirely parallel to the cylinder, and is independent of the distance along the generators.

When one tries to apply this theory to derive certain results of practical interest, namely, the magnitude of the cross-flow very near the cylinder, and the 'displacement effect', certain shortcomings of the theory become apparent. The 'displacement effect' is the distance by which a curve of pressure measured at holes flush with the upstream face of a cylinder, and plotted against height, would appear shifted—in the direction of decreasing total pressure—from the true total pressure profile of the undisturbed flow. A particular application for this displacement effect arises in determining a non-uniform velocity profile by means of a transverse cylindrical total pressure probe (e.g. Livesey 1956).

The inviscid theory predicts a logarithmically infinite cross-flow velocity on the surface of the cylinder. But actually this velocity reaches a maximum a

short distance away, and of course vanishes at the surface itself because of the no-slip condition. It might be argued that the logarithmic singularity is a mild one, and that even a wild guess of the thickness of the boundary layer of the secondary flow could be used to provide a fair approximation of the actual maximum secondary velocity. This turns out to be true. However, there remains the fact that inviscid theory predicts a displacement effect which is likewise infinite, and it is harder to see any means of adjusting this result so as to give a reasonable estimate. In short, a viscous theory from the outset would be desirable, and the present note is a contribution towards that end.

The physical basis of the current work will be that when the shear is assumed small, the fluid moves almost precisely in a two-dimensional manner along planes imagined drawn perpendicular to the cylinder, although in each of these laminae the upstream velocity is one which is appropriate to that particular value of the ordinate. However, as velocities vary slightly between adjoining planes, not only will the fluid be subjected to stresses which determine its essentially two-dimensional motion, but it will also be subjected to a small lateral pressure gradient which causes a certain amount of cross-flow.

The approximation which 'stacks' these two-dimensional (and, in general, viscous) flows one above the other will be referred to in this paper as the *primary flow*. The term *secondary flow* will denote the first-order correction to the former; it is, in fact, the above cross-flow. We shall assume that higher-order corrections will be much smaller, and shall ignore them. The important thing to bear in mind about this approach is that the secondary velocity is considered to arise from fluid elements being convected with the *known* primary velocities across *known* lateral pressure gradients, determined from the primary flow alone. At the same time, they are also subjected to shear stresses arising from their lateral motion, and must obey boundary conditions.

Although this problem is considerably simpler than trying to solve simultaneous Navier–Stokes equations in three dimensions, in its complete form it still remains an ambitious task. In order to further simplify matters, one might now be tempted to suppose that the boundary layer of the secondary flow is considerably thicker than that of the primary flow, and thus to regard the primary flow as inviscid at least around the forepart of the cylinder. Such an assumption would, unfortunately, be mistaken. The thicknesses of these boundary layers are of the same order because the relevant speeds of convection are the same for both. This means that a complete viscous secondary flow solution will inescapably involve the primary boundary layer; and the computation of that alone is known to be very cumbersome.

For this reason calculations have been carried out in this paper only for the flow in the plane of symmetry that extends upstream from the cylinder. Fortunately, we can obtain useful results there, but with much reduced labour. (As a matter of convenience, we consider only cylinders that are symmetrical, and hence non-lifting, though of otherwise fairly arbitrary shape.) In the plane of symmetry, the geometry and the assumed small uniform shear together permit significant simplifications to be made in the equation of motion for the cross-flow component of velocity. As a result, just an ordinary linear

differential equation has to be solved to obtain the desired secondary flow. The primary flow in this plane is taken to consist of an outer part calculated from ordinary potential flow and matched near the cylinder to Hiemenz's solution for viscous stagnation point flow. To conclude §2, the above methods are used to compute some secondary velocity profiles for two particular cylinders.

The displacement effect is studied in §3, where it is found, to a good first approximation, that this does not depend on the Reynolds number. It is indicated that an intuitively based adjustment of the inviscid theory to find this quantity would have been considerably mistaken. Next, the somewhat unrealistic nature of the assumption of *unbounded* shear flow is discussed in connexion with the displacement effect which would be observed in practice. Finally, two specific examples are again worked out in detail.

2. Secondary flow velocity

Choose a system of right-handed Cartesian co-ordinates as illustrated in figure 1. The velocity far upstream has the components

$$v_x = U_1(y) = U + Ay, \quad v_y = v_z = 0, \tag{1}$$

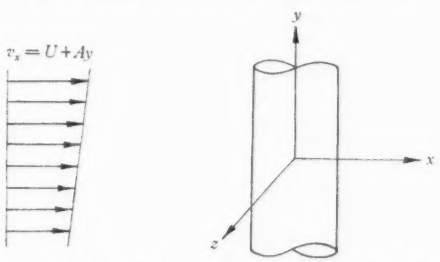

FIGURE 1. Cylinder in shear flow, showing co-ordinate axes.

U and A being constants. It is thus already assumed that the flow is parallel and that the shear can be approximated as uniform. We further require that the latter also be small, or that

$$aA/U_1 \ll 1, \tag{2}$$

where a is a typical dimension of the cylinder. (In the two examples to be treated later, $2a$ = width.) It might also be added, to avoid any possible confusion, that the region of interest does not include $U_1 < 0$.

The first approximation to the actual flow by the primary flow has been mentioned already. It supposes that the actual velocity $\mathbf{v}$ at any point (x, y_0, z) just equals the velocity $\mathbf{v}_1(x, z; y_0)$ that would result from a *uniform* stream of speed $U_1(y_0)$ flowing past the cylinder. Consequently, v_{1x} and v_{1z} must together obey the two-dimensional equations of motion and continuity, and satisfy the boundary conditions $\mathbf{v}_1 = 0$ at the surface, and $\mathbf{v}_1 = (U_1, 0, 0)$ at infinity. However, $v_{1y} = 0$ everywhere. Note that if the Reynolds number R did not vary with the ordinate y, then the following similarity relation would hold exactly:

$$\mathbf{v}_1(x, z; y) = (U + Ay)\,\mathbf{u}(x, z). \tag{3}$$

As it is, R varies slowly, but (3) remains sufficiently exact to be used hereafter.

It becomes evident on closer examination that the primary flow quite accurately depicts the actual motion in the planes perpendicular to the cylinder, but does not do so well as regards the flow parallel to the cylinder. We begin by writing down the equation of motion for v_y:

$$v_x\frac{\partial v_y}{\partial x}+v_y\frac{\partial v_y}{\partial y}+v_z\frac{\partial v_y}{\partial z}=-\frac{1}{\rho}\frac{\partial p}{\partial y}+\nu\nabla^2 v_y. \tag{4}$$

Near the cylinder $\partial p/\partial y$ is generally of the order of $(\partial/\partial y)\,[\frac{1}{2}\rho(U+Ay)^2] = \rho AU_1$. Consequently, v_y is of the order of $\int\frac{1}{\rho v_x}\frac{\partial p}{\partial y}\,dx$ or of $O(aA)$, whereas the primary flow had estimated it as zero. It is interesting that v_y is independent of y to a rough approximation; this can be confirmed by more detailed analysis (e.g. equation (9)). This was also one of Lighthill's conclusions.

On the other hand, if one were to write the dynamical equation for v_x (or for v_z) and in it insert $v_x = v_{1x}$ (or $v_z = v_{1z}$), then a number of terms would at once drop out since they would constitute the two-dimensional equation of motion, leaving only the terms $\nu(\partial^2 v_{1x}/\partial y^2)$ and $v_y(\partial v_{1x}/\partial y)$ (or their analogues). The former is quite negligible because of (3). The latter is of $O(Av_y)$, whereas a typical vanished term such as $v_x(\partial v_x/\partial x)$ would be of $O(U^2/a)$. This suggests that errors in v_x and v_z caused by representing the actual flow by the primary flow alone amount to $UO(aAv_y/U^2) = O(a^2A^2/U)$, or only about (aA/U) times those for v_y.

Of course, a solution must also satisfy the equation of continuity

$$\operatorname{div}\mathbf{v}=0. \tag{5}$$

But since v_{1x} and v_{1z} already obey its two-dimensional equivalent, and since $v_y = O(aA)$ is not a function of y to the first approximation, there is no difficulty on this point. Thus we are now justified in stating that the *secondary* flow consists entirely of motion directed parallel to the cylinder. Only one velocity component, v_y, remains to be computed, whereas $v_x \doteq v_{1x}$ and $v_z \doteq v_{1z}$ are already presumed known as functions of position. In addition, the pressure and thus $\partial p/\partial y$ are already determined from the requirements of the primary flow.

It will be of interest to consider briefly the secondary flow which can be calculated from this approach should the fluid be *inviscid*. In that case, (4) would reduce to

$$v_{1x}\frac{\partial v_y}{\partial x}+v_{1z}\frac{\partial v_y}{\partial z}=-\frac{1}{\rho}\frac{\partial p}{\partial y}, \tag{6}$$

where it has been reasonably assumed that $v_y(\partial v_y/\partial y)$ is negligible. Representing by u the magnitude of the vector $\mathbf{u}$ which was defined by (3), and noting that Bernoulli's equation,

$$p-p_\infty=\tfrac{1}{2}\rho(U_1^2-v_1^2), \tag{7}$$

gives

$$\frac{\partial p}{\partial y}=\rho AU_1(1-u^2), \tag{8}$$

it becomes possible to write this explicit solution of (6):

$$-\frac{v_{y_i}}{aA}=h_i(x)=\int_{s\,(\text{at } x)}^{s_0\,(\text{at } x_0)}\frac{1-u^2(s)}{u(s)}\,ds. \tag{9}$$

The integration is to proceed along a streamline of the primary flow, and $ds = -(1/a)\,(dx^2+dz^2)^{\frac{1}{2}}$. Equation (9) also assumes that $v_y = 0$ at $x = x_0$; the reason why x_0 does not necessarily equal $-\infty$ appears in the last paragraphs of § 3.

It is a simple matter to demonstrate that when $x_0 = -\infty$, (9) agrees exactly with Lighthill's corresponding result (equation (43)), which he obtained from vorticity considerations. The coincidence should cause no surprise, as the methods are, of course, fundamentally related. On the other hand, it does serve as a cross-check to show that the approximations involved are identical. This modest success of the pressure gradient method should, however, not disguise the fact that the vorticity method seems definitely superior for calculating higher-order corrections to the inviscid flow.

After these preliminaries, let us confine our subsequent attention to the viscous problem in that part of the plane of symmetry, $z = 0$, which lies upstream of the cylinder, and where considerable simplifications of (4) are justified. In this plane one omits quite readily the terms $v_y(\partial v_y/\partial y)$ and $v_z(\partial v_y/\partial z)$, the former because $v_y \ll U_1$ and $(\partial v_y/\partial y) = 0$, and the latter because $v_z = 0$ due to symmetry. The term $\nu(\partial^2 v_y/\partial y^2)$ is also thoroughly negligible, again because of $(\partial v_y/\partial y) = 0$. The only omission which calls for lengthier consideration is that of $\nu(\partial^2 v_y/\partial z^2)$. The ratio of this term to the significant viscous term $\nu(\partial^2 v_y/\partial x^2)$ is usually of $O(\delta^2/a^2)$, where δ is the stagnation point boundary layer thickness; thus the approximation

$$\partial^2 v_y/\partial z^2 \ll \partial^2 v_y/\partial x^2 \tag{10}$$

requires an R at least large enough to make $a^2 \gg \delta^2$. However, it should be noted that the word 'usually' presumes that the cylinder is sufficiently blunt-faced. (By way of contrast, a forward-facing wedge, with an only slightly blunted leading edge of radius b, would here require that $b^2 \gg \delta^2$, a more stringent requirement than the previous one.)

Adopting these restrictions, (4) becomes

$$v_{1x}\frac{dv_y}{dx} = -\frac{1}{\rho}\frac{\partial p}{\partial y} + \nu\frac{d^2 v_y}{dx^2} \tag{11}$$

in the plane of symmetry. Together with the boundary conditions

$$v_y(x = x_c) = v_y(x = x_0) = 0, \tag{12}$$

where the subscript c refers to the cylinder surface, this is a well-set problem.

However, rather than trying to solve (11) outright, it is profitable to split up the solution into a viscous inner part and a matching outer part for which the viscous term in (11), if not wholly disregarded, is treated as only a small perturbation. Since δ/a is so small, $\partial p/\partial y$ can be assumed equal to $\rho A U_1$ throughout the entire viscous solution. Moreover, the primary flow can there be approximated by a viscous stagnation point flow against a flat plate for which the Hiemenz solution is well known (Goldstein 1938). On the other hand, a solution already exists for the outer part in the form of (9); although, in order to be more accurate, $u(s)$ might have to be derived from a potential flow around the combined profile of the cylinder and the displacement thickness of the boundary layer and the wake.

For the inner solution, it is best to replace x by the Hiemenz variable

$$\eta = \frac{1}{a}(u'R)^{\frac{1}{2}}(x_c - x). \tag{13}$$

Here u' is the value of $\partial u/\partial s = -(a/U_1)(\partial v_{1x}/\partial x)$ at $x = x_c$ that would arise from inviscid primary flow; and the Reynolds number is given a definite meaning by $R = aU_1/\nu$. Then v_{1x} is

$$v_{1x} = U_1(u'/R)^{\frac{1}{2}} f_1(\eta), \tag{14}$$

$f_1(\eta)$ being a well-tabulated function (see Goldstein 1938, p. 151); also,

$$f_1 \sim \eta - 0{\cdot}6479$$

for large η. Put

$$v_y = -aAh(\eta) = -\frac{aA}{u'}q(\eta). \tag{15}$$

Consequently, (11) transforms into

$$\frac{d^2q}{d\eta^2} + f_1(\eta)\frac{dq}{d\eta} = -1. \tag{16}$$

Putting $f_0(\eta) = \int_0^\eta f_1(\eta')\,d\eta'$, the solution of (16) is

$$\begin{aligned} q(\eta) &= -\int_0^\eta e^{-f_0(\zeta)} \int_0^\zeta e^{+f_0(\zeta')}\,d\zeta'\,d\zeta + K\int_0^\eta e^{-f_0(\zeta)}\,d\zeta \\ &= -q_{\mathrm{I}}(\eta) + Kq_{\mathrm{II}}(\eta). \end{aligned} \tag{17}$$

Here K is an arbitrary constant equal to $\partial q(0)/\partial\eta$; another constant has already been disposed of by the requirement $q(0) = 0$.

The integrals $q_{\mathrm{I}}(\eta)$ and $q_{\mathrm{II}}(\eta)$ were calculated up to $\eta = 6$ numerically. These results are summarized in table 1. Knowing that for large η

$$f_0 \sim \tfrac{1}{2}(\eta - 0{\cdot}6479)^2 + const., \tag{18}$$

η	$q_{\mathrm{I}}(\eta)$	$q_{\mathrm{II}}(\eta)$	η	$q_{\mathrm{I}}(\eta)$	$q_{\mathrm{II}}(\eta)$
0·0	0·000	0·000	3·0	2·261	1·733
0·2	0·020	0·200	3·2	2·369	1·741
0·4	0·080	0·399	3·4	2·465	1·747
0·6	0·178	0·594	3·6	2·551	1·750
0·8	0·312	0·782	3·8	2·629	1·751
1·0	0·476	0·959	4·0	2·700	1·752
1·2	0·663	1·120	4·2	2·765	1·753
1·4	0·867	1·262	4·4	2·826	1·753
1·6	1·077	1·384	4·6	2·883	1·753
1·8	1·286	1·483	4·8	2·936	1·753
2·0	1·487	1·562	5·0	2·986	1·753
2·2	1·674	1·623	5·2	3·034	1·753
2·4	1·846	1·667	5·4	3·079	1·753
2·6	2·001	1·698	5·6	3·123	1·753
2·8	2·139	1·719	5·8	3·164	1·753
3·0	2·261	1·733	6·0	3·204	1·753

TABLE 1

we can calculate that

$$q(\xi) \sim 1{\cdot}753K - 1{\cdot}545 - \ln \xi + \tfrac{1}{2}\xi^{-2} + \tfrac{3}{4}\xi^{-4}\ldots, \tag{19}$$

where ξ denotes $(\eta - 0{\cdot}6479)$, and where the values of the first two constants have been supplied by the numerical integration. It has been pointed out by Mr E. J. Watson that the integral $q_{\mathrm{II}}(\eta)$ is also encountered in the study of the boundary layer on a yawed cylinder.

As regards the outer solution, one might not wish to omit the viscous term in (11) altogether. However, we would still use (9) to compute v_y initially to an inviscid approximation, namely v_{yi}. The first-order viscous correction to this, say $v_{y'}$, would then be calculated from the following adaptation of (11):

$$v_{1x}\frac{dv_{y'}}{dx} = \nu\frac{d^2v_{yi}}{dx^2}, \tag{20}$$

or, more to the point, from the solution of (20) given as

$$-\frac{v_{y'}(x)}{aA} = \frac{1}{R}\left(\frac{1}{u^2(x)} - \ln u(x)\right). \tag{21}$$

By way of illustration, the foregoing analysis is now applied to two specific examples: (i) a circular cylinder (denoted by CC) of radius a, and (ii) a flat plate normal to the stream (FP) of width $2a$. In both cases it is assumed that the primary flow outside the boundary layer is adequately described by the ordinary potential flow around these cylinders. (This constitutes probably the largest single source of error here.) Thus,

$$\text{CC:}\quad u(s) = 1 - s^{-2}; \qquad \text{FP:}\quad u(s) = s(1+s^2)^{-\frac{1}{2}} \tag{22}$$

(Milne-Thomson 1955). In order to facilitate the matching of the inner and outer solutions, it is desirable that $u(s) = 0$ at a distance from the surface equal to the displacement thickness

$$\delta = 0{\cdot}6479a(u'R)^{-\frac{1}{2}}; \tag{23}$$

hence the somewhat artificial definition

$$s = -\frac{1}{a}(x+\delta). \tag{24}$$

Here $x = 0$ at the centres of both cylinders.

Assuming that $v_y = 0$ at $x = -\infty$ for the present, we now insert (22) into (9) and integrate to obtain the approximate inviscid outer solutions

$$\left.\begin{aligned} \text{CC:}\quad -v_{yi}/aA &= \frac{1}{s} + \tfrac{1}{2}\ln\frac{s+1}{s-1}, \\ \text{FP:}\quad -v_{yi}/aA &= \ln\frac{s}{(1+s^2)^{\frac{1}{2}}-1}. \end{aligned}\right\} \tag{25}$$

For small values of ξ, (25) can be expanded as

$$\left.\begin{aligned} \text{CC:}\quad q(\xi) &= 2 + \tfrac{1}{2}\ln(8R) - \ln\xi - \frac{3\xi}{8R} + \frac{15}{32}\frac{\xi^2}{R}\cdots, \\ \text{FP:}\quad q(\xi) &= \ln 2 + \tfrac{1}{2}\ln R - \ln\xi + \frac{\xi^2}{4R}\cdots. \end{aligned}\right\} \tag{26}$$

A viscous correction to be added to (26) is obtained from (21). When ξ is small, it is found for either of the cylinders that this correction is approximately

$$\Delta q(\xi) = \xi^{-2}. \tag{27}$$

Selecting the value of ξ at which the inner and outer solutions are to be matched is somewhat a matter of choice. Here we have decided to equate (19) with the sum of (26) and (27) at $\xi = 5$ for $R = 10^3$, 10^4, 10^5 and 10^6. The resulting secondary velocity profiles are displayed in figure 2.

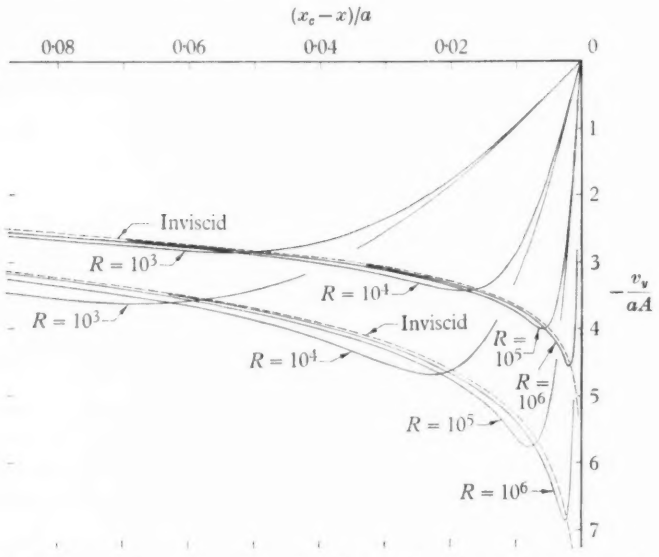

FIGURE 2. Profiles of the viscous secondary flow in the plane of symmetry in front of a circular cylinder (upper curves) and a flat plate (lower curves).

3. Displacement effect

Let us return once more to the equation of motion, which we now write in the following well-known form:

$$\nabla(\tfrac{1}{2}\rho v^2) + \rho \mathbf{w} \times \mathbf{v} = -\nabla p + \mu \nabla^2 \mathbf{v}, \tag{28}$$

where $\mathbf{w} = \operatorname{curl} \mathbf{v}$. Consequently, if p_0 denotes the total pressure $(\frac{1}{2}\rho v^2 + p)$, then

$$\frac{\partial}{\partial x} p_0 + \rho(\mathbf{w} \times \mathbf{v})_x = \mu \nabla^2 \mathbf{v}_x. \tag{29}$$

In the plane of symmetry, $(\mathbf{w} \times \mathbf{v})_x = -w_z v_y$, since $w_y = v_z = 0$. We write approximately, as before,

$$v_x = (U + Ay)\, u(x), \quad \text{and} \quad v_y = -aA\, h(x). \tag{30}$$

Hence

$$w_z = -\frac{\partial v_x}{\partial y} + \frac{\partial v_y}{\partial x} = -A\left\{u(x) + a\frac{\partial}{\partial x} h(x)\right\}. \tag{31}$$

Insert these into (29), and simplify $\nabla^2 v_x$ to $\partial^2 v_x/\partial x^2$, partly by arguments similar to those which accompanied (10) and partly because $\partial^2 v_x/\partial y^2 = 0$ from (3). Then integrate the result with respect to x. This leaves

$$\left[p_0 - \mu\frac{\partial v_x}{\partial x} - \frac{\rho a^2 A^2}{2}h^2(x')\right]_{x_0}^{x_c} = \rho a A^2 \int_{x_0}^{x_c} h(x')\,u(x')\,dx'. \tag{32}$$

Since $\partial v_x(x_0)/\partial x = \partial v_x(x_c)/\partial x = 0$, and $h(x_0) = h(x_c) = 0$, we observe that the total pressure at the surface exceeds the total pressure at the same ordinate far upstream, at $x = x_0$, by the amount

$$\Delta p_0 = \rho a A^2 \int_{x_0}^{x_c} h(x')\,u(x')\,dx'. \tag{33}$$

It is known that the total pressure gradient, $\partial p_0/\partial y$, is $\rho A U_1$, and therefore we conclude that the displacement of the total pressure towards the region of lower pressure is given by

$$\frac{\Delta y}{a} = \frac{aA}{U_1}\int_{s_c}^{s_0} h(s')\,u(s')\,ds'. \tag{34}$$

Here the dimensionless s_0 and s_c correspond to x_0 and x_c, respectively.

It happens that the contribution to this expression from a region extending only a small distance Δx from the surface is roughly of the order of

$$(aA/U_1)\,(\Delta x/a)^2.$$

Since the entire $\Delta y/a = O(aA/U_1)$, (34) can to good accuracy be calculated using the $u(s)$ and $h(s)$ that are given by the inviscid outer solution, omitting the tiny contribution from the inner solution altogether.

Thus, the remarkable thing about the displacement effect as described by (34) is its virtual independence from the Reynolds number. This is hardly what one would have anticipated from inviscid considerations. The displacement of streamlines, and therefore that of constant total pressure loci, from s_0 to some s nearer the cylinder would be given by inviscid theory instead as

$$\frac{\Delta y(s)}{a} = \frac{aA}{U_1}\int_{s}^{s_0} \frac{h(s')}{u(s')}\,ds'. \tag{35}$$

Although (35) is such that† $\lim_{s\to s_c} \Delta y(s) = \infty$, there is no reason to doubt its correctness even for the present case, provided only that s remains sufficiently large to exclude the boundary layer. However, one would have thought that by inserting a lower limit $s = s_c + \delta = s_c + 0{\cdot}6479a(u'R)^{-\frac{1}{2}}$, from (23), one might obtain a rough estimate for $\Delta y/a$, and that this would consequently strongly depend on R. But (34) indicates that this is not so.

The surprising behaviour of the surfaces of constant total pressure occurs entirely in the boundary layer. Here one deduces from (32) that their displacement is in fact larger at any distance $O(\delta)$ from the cylinder than at the surface itself. The decrease in the displacement near the surface as (34) implies, must necessarily be of an amount sufficient just to cancel out any effects of the

† This remains the case even if the h and u obtained from viscous theory are inserted in (35).

Reynolds number. (To make these remarks seem more plausible, recall that in a Poiseuille flow too, a given total pressure surface lies further downstream anywhere in the channel than at the walls.)

A difficulty remains, however, about what to do with the upper limit of (34), s_0, which has so far remained unspecified. The reason why it cannot be chosen equal to ∞ here is that Δy turns out to behave as $\ln s_0$ at large s_0 for any cylinder whose effect at large distances upstream can be approximated by that of a line dipole, i.e. any closed cylinder in inviscid flow. For an unclosed cylinder, such as that formed by a line source, or a closed cylinder with a wake, this behaviour is evident in the secondary velocity itself. In that case Δy grows linearly with s_0 as $s_0 \to \infty$! This handicap seems to be an unavoidable, but not necessarily an erroneous, feature of the theory for an unbounded shear flow containing an infinite cylinder.

It is almost certain, however, that the concept of *unbounded* shear flow is unrealistic at large distances. Not only are actual shear flows usually generated not very far upstream, but also, more importantly, they are in practice either bounded by walls or confined to layers. It seems physically unlikely that these lateral constraints would permit appreciable secondary flow to extend to a distance upstream of more than several times the typical lateral dimension d.

The idea of a cut-off distance x_0 is therefore attractive. For the purposes of calculating the displacement effect, the secondary velocity would be presumed to begin only when the flow reaches $x = x_0 = O(d)$. Lighthill (1957) considered a similar cut-off in connexion with the displacement effect for a source in a bounded shear flow, and in fact derived an integral expression for estimating this distance. It should be possible in principle to extend his methods to our cylinders, by regarding them as composed of suitable arrangements of line sources and sinks. But bearing in mind the complexity of the methods, and that this cut-off distance will generally vary from one streamline to another (even in the simple case of a uniform shear flow in a channel), we will not attempt to calculate x_0 here. It will suffice to remember that this distance depends only on the flow profile and boundaries, and neither on the size nor the shape of the cylinder.

The displacement effects for the circular cylinder and the flat plate are worked out below as functions of the above-mentioned cut-off distance. If we could assume that $u(s)$ is accurately described by the potential flow around these cylinders, we would take $u(s)$ from (22), and $h(s)$ as implied by (25), integrate (34) and so find

$$\left.\begin{aligned} \text{CC:}\quad & \Delta y/a = (aA/U_1)\left(2\ln s_0 + \frac{4}{s_0} - \frac{3}{2s_0^2} + \ldots - 2{\cdot}886\right), \\ \text{FP:}\quad & \Delta y/a = (aA/U_1)\left(\ln s_0 + \frac{1}{s_0} - \frac{1}{6s_0^3} + \ldots - 0{\cdot}693\right). \end{aligned}\right\} \tag{36}$$

To be realistic, though, these bodies have to be considered together with their wakes. Let us represent a wake by a line source through the origin. Consequently the expression for $u(s)$ takes the form

$$u(s) \doteqdot 1 - (C_D/2\pi)\, s^{-1} - (\text{Potential flow terms of } O(s^{-2})). \tag{37}$$

Here C_D denotes the drag coefficient defined as the drag per unit length divided by $\rho U_1^2 a$, and the fact has been used that the displacement thickness of a wake tends to $\frac{1}{2}C_D$ times the cylinder width. Applying equation (37) to (9), we see that the wake must thus contribute to the non-dimensional secondary flow velocity an amount

$$h_{\text{wake}} \doteq (C_D/\pi) \ln (s_0/s) \tag{38}$$

(as long as s remains somewhat larger than unity). From (34) it then follows that this is responsible for displacing the total pressure surfaces by approximately an additional amount

$$\Delta y/a \doteq (aA/U_1)(C_D/\pi)(s_0 - \ln s_0), \tag{39}$$

which must be added to (36) for the combined effect of the cylinder and wake. We observe that when the drag coefficient is of order unity as here, then s_0 need not assume particularly large values before the contribution of the wake to the displacement effect becomes the dominant one. This is the case despite the fact that the fraction of the secondary velocity observed near the cylinder which has been caused by the wake may typically be only, say, a quarter of the total.

It is a pleasure to acknowledge my indebtedness both to Prof. M. J. Lighthill for a number of discussions on this topic and to the Marshall Aid Commemoration Commission for a scholarship.

REFERENCES

GOLDSTEIN, S. (ed.) 1938 *Modern Developments in Fluid Dynamics*, vol. 1. Oxford University Press.

LIGHTHILL, M. J. 1956 *J. Fluid Mech.* **1**, 31.

LIGHTHILL, M. J. 1957 *J. Fluid Mech.* **3**, 113.

LIVESEY, J. L. 1956 *J. Aero. Sci.* **23**, 949.

MILNE-THOMSON, L. M. 1955 *Theoretical Hydrodynamics*, 3rd ed. New York: Macmillan.

REVIEWS

Electromagnetic Phenomena in Cosmical Physics. Edited by B. LEHNERT. Cambridge University Press, 1958. 545 pp. £2. 10*s*.

Magnetohydrodynamics. Edited by R. K. M. LANDSHOFF. Stanford University Press, 1957. 115 pp. $4.00 or £1. 12*s*.

The Plasma in a Magnetic Field. Edited by R. K. M. LANDSHOFF. Stanford University Press, 1958. 130 pp. $4.50.

The Magnetodynamics of Conducting Fluids. Edited by D. BERSHADER. Stanford University Press, 1959. 145 pp. $4.50.

Magnetohydrodynamics, with its partner, plasma physics, is now becoming a fully fledged branch of fluid mechanics. Already it occupies a sizeable fraction of this *Journal*'s space. And yet ten or fifteen years ago it was the concern only of a few astrophysicists and isolated scientists and engineers to whom the unity and ramifications of the new field was barely apparent. It is interesting to speculate why the subject has suddenly undergone an exponential eruption after being so long quiescent. After all, most of the essential facts were known to Faraday's generation. In 1832 Faraday* himself records speculations such as the possibility that motions of the electrically conducting oceans might be responsible for the observed distortions of the earth's magnetic field, and in the same year Ritchie* records how he caused water to move by subjecting it to an electric current perpendicular to a magnetic field and wonders whether this action might be the cause of ocean currents. Here we have the two vital ideas of magnetohydrodynamics, the mutual interactions between the velocity field and the electromagnetic field. One might have expected such giants as Maxwell and Rayleigh to take these ideas up, but for a long time the only activity was the invention of various gadgets to measure pressure, velocity or current or to pump mercury by exploitation of the magnetohydrodynamic interaction. Hints of things to come were the observation of the pinch effect in liquid metals by Hering and Northrup* in 1907 and Larmor's* suggestion of solar dynamo action in 1919, but not until about a century after Faraday did the subject begin to gain adherents, with Cowling exploring the dynamo problem, and Bennett the pinch effect, and Williams and Hartmann making experiments on pipe flow under transverse fields. Although Ferraro, Biermann and others explored the subject a little further, there was still a surprising time lag before the subject really found its feet early in World War II with the advent of Alfvén's waves, characterized by a fully mutual coupling of the magnetic and flow fields. The vital idea that the fluid and field may 'freeze' together was clearly realized at last.

The post-war period has seen the astrophysical and geophysical implications fully appreciated and the early, limited practical applications to liquid metals

* M. Faraday, *Phil. Trans.* (1832), p. 176. W. Ritchie, *Phil. Trans.* (1832), p. 295. E. F. Northrup, *Phys. Rev.* **24**, (1907), p. 474. J. Larmor, *Engineering, Lond.*, **108**, (1919), p. 461.

transcended by the tantalizing prospect of applications to controlled fusion, plasma technology, aeronautics and astronautics.

What then provided the impetus which caused the subject finally to develop? It seems that the major factor was the realization by astronomers that conducting matter and magnetic fields are commonplace in the universe. As van de Hulst remarks in the first volume under review, the observation of unexplained novelties in the cosmos was a great spur to the development of the subject. To astrophysicists goes the credit for taking over the subject from the gadgeteers, and setting it on a respectable formal basis. It has since mellowed in the hands of fluid dynamicists and others who have applied it to laboratory and technical problems, more closely specified than the typical cosmic application.

The subject has not entirely avoided the failing of early fluid mechanics, the cleavage between ideal hydrodynamics and empirical hydraulics, even though such pioneers of the formal subject as Alfvén are experimentalists at heart. There are still very large gaps between observed fact and idealized theory, and still a deplorable tendency for magnetohydrodynamics to be treated as a playground for applied mathematicians. The temptation lies in the fact that, if ordinary fluid mechanics offers infinite scope, its generalization to conducting fluids is at least doubly infinite. It is so easy to find new theoretical problems in the field that one must plead for a self-imposed discipline that only problems with some conceivable relevance to real phenomena be pursued. Only by this means can the present torrent of papers be kept to reasonable proportions.

One sign of adult vigour in the subject is the number of conferences and symposia being devoted to it all over the world, ever since the 1949 I.A.U. meeting in Paris. Notable among these have been the three annual ones sponsored by the Lockheed Missiles and Space Division since 1956. At these latter symposia the topics have in no way been confined to applications to aviation and space flight. In fact there has obviously been considerable effort to make the coverage of topics sufficiently basic and catholic to justify the general titles borne by the published proceedings of these symposia, *Magnetohydrodynamics* (held in 1956), *The Plasma in a Magnetic Field* (held in 1957), and *The Magnetodynamics of Conducting Fluids* (held in 1958). These titles indicate that the books aim to function as primers in the subject, but this is not entirely achieved. Nevertheless, they are welcome additions to a literature in which such few books as exist are predominantly astrophysical in tone. Their chief value lies in the inclusion of one or two authoritative articles. Many of the other contributions were of transient interest only or were abbreviated previews of work which has since been presented more comprehensively in regular journals.

The 6th I.A.U. Symposium, held in Stockholm in 1956, has recently had its lengthy proceedings published in full, thanks to the diligence of B. Lehnert, as a volume entitled *Electromagnetic Phenomena in Cosmical Physics*. In this case the title tends to give a false impression, for many of the papers are of general interest and some even are more relevant to applied science than to the cosmos. Into this last class fall the contributions in German from the Russian fusion delegates. These three papers, incidentally, had already appeared in the regular Russian journals in 1956, and in English in *Journal of Nuclear Energy* in 1957.

In this review it is obviously impossible to comment on more than a few of the papers in these four volumes. In choosing papers for comment here, the obvious principle to adopt is to select work of sustained rather than transient interest (particularly since two of the symposia took place as long ago as 1956) and work of general fluid-mechanical rather than astrophysical significance.

The Stockholm symposium proceedings are split into parts dealing in turn with general, solar, stellar and experimental problems, etc. Several of these parts begin with historical review articles, of which the one by Cowling on solar electrodynamics is particularly noteworthy. Another valuable review is provided by Lehnert, who discusses the practicability of experiments with plasmas or liquid metals with a view chiefly to simulating cosmic phenomena. The conclusion is pessimistic, but, be it noted, the point is that cosmic simulation is all but impossible, not that general magnetohydrodynamic experimentation is futile. Indeed such experiments for their own sake can be very rewarding.

Lehnert and Baños (who extends his work on magnetohydrodynamic waves to fluids with viscosity and thermal conductivity) state energy equations in various rival forms which may tend to cause confusion. One reason for this is that both authors show a strange reluctance to mention entropy and to relate its creation to heat transfer and viscous and ohmic dissipation. One way in which Lehnert's energy equation differs from Baños' version is that it is a purely thermodynamic or material one and does not include magnetic energy. The electrical energy supply to the material is $\mathbf{E}.\mathbf{j}$ in the usual notation. Baños's equation uses the Poynting flux, whose divergence represents the total energy supply to the material and the electromagnetic field. Lehnert's review is confined to cases where kinetic energy and magnetic energy densities are comparable, with the result that a Lundquist number (of the form length multiplied by Alfvén wave velocity divided by diffusivity of field, momentum or heat) becomes the dominant parameter. There are of course many interesting magnetohydrodynamic phenomena where the two energies are not comparable and consequently other dimensionless groups are important.

Schlüter and Åström make useful contributions to plasma theory. Schlüter discusses generalized Ohm's laws for partially and full ionized gases, while Åström examines the effective permeability and permittivity of collision-free plasma in a magnetic field. Some generalization of thermodynamics for this case seems to be called for.

Bostick's entertainingly illustrated contribution to the book consists of a salvo of plasmoids (if that is the appropriate collective noun). Much of the other discharge work described by Pease and the Russians has been overtaken by events, particularly by the great release of information at the 1958 Geneva Conference on peaceful uses of atomic energy. The central mass of the book deals with specifically astrophysical matters, but it ends with a miscellany which includes Sweet on magnetohydrostatic equilibrium, Kaplan on magnetoturbulence and Kopecký on the conductivity of partially ionized gas.

We turn next to the Lockheed Symposium volumes. The first one, *Magnetohydrodynamics*, opens with Kantrowitz and Petschek's valuable classification of domains in plasma physics, presented very clearly in a diagram for the case of

deuterium under a magnetic field whose pressure equals the gas pressure. This is almost the same as setting the Alfvén wave and sound velocities equal. Elsasser and, later in the book, Landshoff, discuss the important dimensionless ratios in magnetohydrodynamics, and Elsasser reproduces some of his work on dynamo action. He uses the unfortunate term 'magnetic viscosity', which since the publication of Hartmann's work has taken on many conflicting meanings. The term diffusivity is to be preferred for all quantities of dimensions L^2/T which measure the rate of diffusion per unit gradient of intensity, whether of magnetic field, momentum, heat, neutrons or anything else. The ratio of the diffusivities for momentum and magnetic field, $\mu\sigma\nu$ (in M.K.S. units), has not yet acquired a name or regular symbol, but certainly deserves them. One possibility, the term *magnetic Prandtl number*, has already been interpreted by Zhigulev as the ratio of the magnetic and *thermal* diffusivities, $\rho C_p/\mu\sigma K$, instead. The quantity $\mu\sigma\nu$ is particularly important in boundary-layer problems (such as the one studied by Carrier and Greenspan in the third Lockheed volume).

Burgers's contribution is to consider the penetration of a shock into plasma at rest in a dipole field. The most interesting section is his simple study of the structure of a plane shock in a relatively poor conductor in which the magnetic diffusity exceeds all others. Rosenbluth concludes this section with his simplified theory of the fast pinch and some discussion of the Boltzmann equation.

The second half of the book deals with experimental work, mostly with shock tubes, apart from Colgate's scantily described experiment on the instability of a shell of liquid sodium accelerated inwards by a magnetic field, and Newcomb's scheme for exciting magnetohydrodynamic waves in plasma contained within a cylindrical tube or wave guide. There is a full description of work with T-tubes by Kolb and by Kash, but the AVCO shock tube work is more fully described elsewhere.

The title of the second Lockheed volume, *The Plasma in a Magnetic Field*, reflects the trend towards plasma physics, although pure magnetohydrodynamics, governed by classical continuum equations, is not entirely excluded. The book is in three parts, of which the first deals with basic plasma physics. In this Chandrasekhar studies single particles and gives a sophisticated theory of adiabatic invariants, while Rosenbluth takes particles by the swarm and investigates the validity of the hydrodynamic approximation for the collision-free case. The second section is a mixed bag, ranging from Colgate's brief but illuminating explanation of the generation of neutrons in unstable pinches to Weibel's fully detailed solution for the case of a plasma column confined by the pressure of electromagnetic waves excited between the plasma and a concentric conductor. Karr gives a thorough account of some of the Los Alamos observations on pinches. The last section is also motley, although interesting. The work described by Blackman and Niblett on shocks produced by an electrodeless discharge has been reported in this and other journals. The next paper is by the home team from Lockheed, Kash *et al.*, and deals with shock-speed measurement. There follows Los Alamos work on shock tubes with axial fields, and the book ends with Liepmann outlining the work of Bleviss and Chester on Couette and Stokes flow, recently published in full elsewhere.

With the third Lockheed volume, *The Magnetodynamics of Conducting Fluids*, Landshoff hands over the editorship of the Lockheed series to Bershader. The change in terminology in the title is not significant; the five words employed are synonymous with 'magnetohydrodynamics'. This volume is in several ways different from its two predecessors. Nearly all the work is theoretical, and most is presented in detail at some length. The continuum approximation is used throughout. The book is more homogeneous, more even in quality than the earlier two. Most of the basic ideas presented are already familiar, however. This is partly due to the fact that, apart from Busemann's contribution, all the papers had received at least limited circulation in whole or part before this Lockheed publication ensured the wide currency that most of them deserve. Typifying this class is Grad's authoritative contribution on the propagation of undamped magnetohydrodynamic waves from localized or point sources in compressible fluids. The only experimental study is that presented by the AVCO contingent, who used a shock tube to generate ionized gas flow past and through a transverse solenoid. Together with the attendant analysis, this constitutes a fine achievement, remarkable for the successful development of flow-visualization techniques appropriate to plasma motions.

Busemann's paper is the most novel and stimulating one, though poorly written. He tackles one of magnetohydrodynamics' major idiosyncrasies, the fact that, given perfect conductivity, compressible fluids can undergo free surface motions, confinement being achieved by surface current sheets. He considers configurations in internal and external aerodynamics where the fluid and fields occupy different regions of space. An example is the well-known case of potential flow past a line of transverse magnetic dipoles. The crucial question as to whether these flows of a perfect conductor have any counterpart in the case of high but finite conductivity is not discussed. An interesting lack of uniqueness occurs in the case of flows past purely magnetic obstacles if the ionization is produced in a bow shock. The fluid has the alternative of flowing un-ionized past the obstacle without any interaction at all.

Cole discusses magnetohydrodynamic shocks generated by a moving piston. Mitchner goes into great detail on one- and two-dimensional flows in the case where the field is transverse and proportional to the density. The Cornell work on linearized theory for gas flows with finite conductivity is surveyed by Resler and McCune. Finally, Carrier and Greenspan give a condensed, approximate version of their work, already published in this *Journal*, on flat-plate boundary layers. The essential mechanics of the flow is well conveyed.

All the four books here reviewed ought to be available to workers in the fields of magnetohydrodynamics and plasma physics, as all four contain a fraction of permanently valuable and fully described work. Needless to say, the definitive text on magnetohydrodynamics still remains to be written, but at the moment it would be premature. Though magnetohydrodynamics has come of age, it is still too youthful and volatile at this stage for such a text to be timely. When truly consolidated text-books begin to emerge, we can reckon that magnetohydrodynamics has become middle-aged and respectable.

J. A. Shercliff

THE QUÉRE TITROMETER

has wide applications in recording physico-chemical processes

The Quére Titrometer is a precision instrument for recording titrations accurately. Equipped with an automatically variable recording table to suit the gradient of the curve, it permits the rate of advance to be reduced when the rate of change increases. Reagent flow is controlled by the table mechanism and by changing the jet of the syringe, the volume being represented by the abscissa of the graph and the state of mixture by the ordinate. The circle method determines accurately the end points of titration. *The circuits permit all kinds of potentiometric titrations and with special attachments it is possible to perform conductimetric or polarised-electrode titrations.*

- ✳ **PHOTOMETRY** The Quére strip photometer attachment is provided with filters and a vacuum type photocell giving accurate and stable readings.
- ✳ **USING A LIQUID MEDIUM** photometric attachment to this Recorder allows any photocolourimetric titration, recording photometric variations instead of equivalent points.
- ✳ **INTEGRATION** The Recorder automatically integrates the curve as it is traced. The results are entered on the axis of the ordinate of the curve by means of an electric pen marking 'tens' and 'units'.
- ✳ **RECORDING TIME FUNCTIONS** The Titrometer is fitted with a zero drift correcting circuit using an automatic potentiometer. To make accurate measurements it is necessary only to check the zero per odically; the instrument itself will then introduce the necessary corrections.

Write for fully illustrated and descriptive leaflet

Tinsley

H. TINSLEY & CO. LTD.

Werndee Hall, South Norwood, London, S.E.25

Telephone ADDiscombe 6046–8

ISP 5719

JOURNAL OF FLUID MECHANICS

Volume 7, Part 1 January 1960

CONTENTS

On the flow past a quarter infinite plate using Oseen's equations
by K. STEWARTSON and L. HOWARTH *page* 1

The time-dependent magnetohydrodynamic flow past a flat plate
by G. F. CARRIER and H. P. GREENSPAN 22

Forced small-amplitude water waves: a comparison of theory and experiment
by F. URSELL, R. G. DEAN and Y. S. YU 33

The stability and transition of a two-dimensional jet
by HIROSHI SATO 53

A shallow-liquid theory in magnetohydrodynamics
by L. E. FRAENKEL 81

Steady finite motions of a conducting liquid
by ROBERT R. LONG 108

Free convection in the tilted open thermosyphon
by F. M. LESLIE 115

Inviscid flow of a reacting mixture of gases around a blunt body
by WILBERT LICK 128

The viscous secondary flow ahead of an infinite cylinder in a uniform parallel shear flow
by ALAR TOOMRE 145

REVIEWS

Electromagnetic Phenomena in Cosmical Physics 156
Magnetohydrodynamics 156
The Plasma in a Magnetic Field 156
The Magnetodynamics of Conducting Fluids 156

Printed in Great Britain at the University Press, Cambridge
(Brooke Crutchley, University Printer)